Experimentele bepaling en wiskundige modellering
van oevereffecten op schepen

Experiment Based Mathematical Modelling of Ship-Bank Interaction

Evert Lataire

Promotor: prof. dr. ir. M. Vantorre
Proefschrift ingediend tot het behalen van de graad van
Doctor in de Ingenieurswetenschappen: Maritieme Techniek

Vakgroep Civiele Techniek
Voorzitter: prof. dr. ir. P. Troch
Faculteit Ingenieurswetenschappen en Architectuur
Academiejaar 2014 - 2015

UNIVERSITEIT
GENT

ISBN 978-90-8578-748-8
NUR 969, 974
Wettelijk depot: D/2014/10.500/94

Wat benodigd is, is pessimisme van het verstand en optimisme van de wil

Antonio Gramsci

Promotor:

prof. dr. ir. Marc Vantorre

President:

prof. dr. ir. Patrick De Baets

Examining Board:

prof. dr. ir. Patrick De Baets

prof. dr. ir. Tom De Mulder

dr. ir. Guillaume Delefortrie

prof. dr. ir. Katrien Eloot

prof. dr. Alexander Härting

prof. dr. ir. Peter Troch

prof. dr. ir. Marc Vantorre

prof. dr. ir. Jan Vierendeels

prof. dr. ir. Michael Woodward

Preface

The presented research was funded by the Flemish Government, Department Mobility and Public Works, and the model tests were executed at Flanders Hydraulics Research (Antwerp, Belgium). The initial research is commissioned by Flanders Hydraulics Research to the Maritime Technology Division of Ghent University to supply scientific support. The study is executed in the frame of the Knowledge Centre Ship Manoeuvring in Shallow and Confined Water (cooperation between Flanders Hydraulics Research and the Maritime Technology Division of Ghent University).

This dissertation is submitted for the degree of *Philosophiæ Doctor* at Ghent University. The author performed his doctoral research as an assistant at Ghent University (2008–2014).

This research project, I could never have succeeded without the aid of many people.

Eerst en vooral wil ik mijn promotor Marc Vantorre bedanken voor de vele mogelijkheden en ondersteuning die hij mij geboden heeft.

The members of the jury I would like to thank for their interest in this work, their critical questions and valuable suggestions.

Daarnaast gaat er ook een woord van dank uit naar mijn scheepsbouwkundige (en één bouwkundige) collega's en ex-collega's; Guillaume, Maxim, Katrien, Jeroen, Stefan, Stijn, Tri, Jan, Manases en Erik welke ik zowel te pas als te onpas kon lastigvallen met inzichten en praktische problemen.

De vele, vele modelproeven uitgevoerd in de sleeptank van het Waterbouwkundig Laboratorium met inbouwen allerhande konden slechts succesvol genoemd worden dankzij de technische vakkennis en hulp van onder andere Luc, Greet en Sam.

Floris dien ik te danken voor zijn diepgravend literatuuronderzoek en Steven voor zijn niet aflatende zoektocht en vondsten van zowel standaard publicaties als ver verborgen grijze literatuur.

Bij de simulatorploeg, Joeri, Kristien en Karel, kon ik vooral terecht voor wiskundige of programmatorische vragen. Bij mijn poging tot het creëren van colourful fluid dynamics kon ik dan weer rekenen op de steun en ervaring van Marilyne en Wim.

Bij een project van deze omvang hoort een aanzienlijke administratieve belasting waarbij ik gelukkig kon rekenen op de hulp en werk van Frans, Ellen en Karine.

Tot slot wil ik mijn vrouw Laike, familie en vrienden danken voor hun oprechte interesse.

U, lezer, wens ik veel leesplezier toe.

I hope you will enjoy the reading.

Ghent, summer 2014,

Evert

Summary

A displacement vessel, as the name suggests, displaces an (enormous) amount of water. In open and unrestricted waters this water can travel relatively unrestricted underneath and along the ship's hull. In restricted and shallow sailing conditions this displaced water is squeezed under and/or along the hull. This tightness results in higher velocities of the water travelling along the hull which also generates a pressure drop around the same hull. This pressure drop acts as a combination of forces and moments on the vessel. These forces/moments are named **bank effects** if generated because of the presence of a bank.

The horizontal forces of the bank effects on a ship are sought for. These three forces are: the bank effects acting in the longitudinal direction and in the lateral direction at the forward and aft perpendicular. The knowledge of bank effects is acquired with an extensive literature study on one hand and with dedicated model tests carried out in different towing tanks on the other. The majority of the utilised model tests is carried out in the shallow water towing tank at Flanders Hydraulics Research in Antwerp, Belgium.

The data set on bank effects consists of more than 8 000 unique model test setups. Eleven different ship models, at a range of draft to water depth ratios, are tested. The captive towing tests are conducted at a range of different forward speeds and propeller actions. The data set contains model tests carried out along twenty five different bank geometries at different lateral positions of the ship from the bank. During the model tests forces, moments and motions are measured on the hull, propeller(s) and rudder(s). These measurements are the input for the analysis of bank effects and the creation of the mathematical model of the three previously mentioned forces in the horizontal plane.

The physical based mathematical model is constructed in such a way that (relative) easy implementation in a ship manoeuvring simulator is possible.

Overall the magnitude of the bank effects: the longitudinal force and both lateral forces (at the fore and aft perpendicular) increase with:

- A higher forward speed of the ship
- A more loaded propeller (higher propeller rate)
- A lower under keel clearance
- A more confined sailing area; steeper banks, smaller distance between port and starboard bank
- The closer the distance between ship and bank

The longitudinal force of the bank effects always acts on the ship as an augmented resistance. The lateral force at the aft perpendicular acts always as an attraction force directed towards the nearest bank. In deep water the lateral force at the forward perpendicular is also an attraction force towards the nearest bank while in very shallow water this force is always a repulsion force directed away from the nearest bank. In between there is a transition from repulsion to attraction which shifts with the forward speed of the ship and relative water depth.

In the mathematical model the thrust delivered by the propeller is transformed into a thrust velocity (the theoretic axial velocity behind the propeller). This velocity is combined with the forward speed of the vessel into an equivalent velocity. This, in turn, is used as input to calculate the Tuck number which takes into account the water depth and blockage (ratio of the cross section area of the ship and fairway). This Tuck number is proportional to the magnitude of longitudinal and lateral forces of the bank effects. For the lateral force at the forward perpendicular an extra function (dependent of the Froude number and relative water depth) is added to cope with the changing sign in the shallow water range.

The position and distance between a ship and random shaped bank is ambiguous. Therefore the weight factor is introduced. This factor is a value between zero and one which exponentially decreases further away from the ship (in both horizontal and vertical direction). The weight factor is integrated over the considered area (cross section at port/starboard, midship section) to achieve a weighted value for that area.

A dimensionless distance to the bank and equivalent blockage is introduced and calculated based upon weighted areas. As such the nuances of a random cross section are taken into account without exaggerating the bathymetry at a distance far away from the ship or without underestimating the bank shape very close to the ship. The lateral forces are inversely proportional to the dimensionless distance to the bank while the magnitude of the longitudinal force is proportional to the square of the equivalent blockage.

The influence width is the (horizontal) distance between a ship and bank where the bank effects are infinitesimally small and can be neglected. When the proximity between the ship and closest bank is greater than the influence width then the ship manoeuvres as sailing in unrestricted (but sometimes shallow) waters. Based upon dedicated model tests carried out in a towing tank it is found that this influence width is proportional to the water depth dependent Froude number.

Although the model tests are carried out with the utmost care and scaled according to Froude's law (common for model tests on ship hydrodynamics) there remains an issue with the boundary layer on ship and bank. This boundary layer is relatively thicker on model scale than at full scale when scaled according to this Froude's law. The lateral force at the aft perpendicular did no longer increase the closer it was towed to the bank when the ship model was towed very close to a (vertical) bank. The same is observed at very shallow water depths. This behaviour is ascribed to the influence of the boundary layer on the lateral force. When the gap between ship and cross section (keel – bottom or ship's side – bank) is

narrower than the boundary layer influence thickness then the viscosity of the water comes into play and overrules the (mainly) non-viscous hydrodynamics generating the bank effects. This boundary layer influence thickness (a formulation is given) is about (relative) two to three times as thick on model scale than at full scale.

Samenvatting

Zoals de naam al doet vermoeden, verplaatst een deplacementschip een (enorme) hoeveelheid water. Dit water kan in open en onbeperkte vaarwaters relatief ongehinderd onder en langs het schip stromen. In ondiepe en/of beperkte vaarwateren wordt dit water echter onder en langs de romp geperst. Deze krapte zorgt er voor dat het water aan een hogere snelheid langs de romp heen zal vloeien, deze hogere snelheid resulteert eveneens in een drukdaling omheen het schip. De verlaagde druk resulteert op zijn beurt in een combinatie van krachten en momenten op het schip. Het zijn deze krachten en momenten die **oevereffecten** worden genoemd wanneer ze veroorzaakt worden door de aanwezigheid van een oever.

De krachten van de oevereffecten die aangrijpen in het horizontale vlak (evenwijdig met het vrije vloeistofoppervlak) zijn diegene waarnaar gezocht wordt. De drie betreffende krachten zijn; de oevereffecten die aangrijpen in de langsrichting van het schip en de krachten die aangrijpen in de dwarsrichting aan de voorste en achterste loodlijn. De kennis van oevereffecten is tot stand gekomen door enerzijds een uitgebreide literatuurstudie en anderzijds door specifieke modelproeven uitgevoerd in verscheidene sleeptanks. De overgrote meerderheid van de modelproeven werden echter uitgevoerd in de ondiep water sleeptank van het Waterbouwkundig Laboratorium te Antwerpen, België.

De gecreëerde database van oevereffecten bevat ruim 8 000 unieke modelproeven. Er werden elf verschillende scheepsmodellen getest bij een variatie van verschillende verhoudingen van de diepgang tot de waterdiepte. De gedwongen sleepproeven zijn uitgevoerd bij een ruim bereik van voorwaartse snelheden en schroefbelastingen. De dataset bevat proeven die werden uitgevoerd langs vijfentwintig verschillende oevervormen

op verschillende laterale afstanden tussen scheepsmodel en oever. Krachten, momenten en verplaatsingen op en van de romp, schroef en roer werden geregistreerd tijdens de proeven. Deze metingen vormen de invoer van de analyse van de oevereffecten en voor de creatie van een wiskundig model van de drie eerder vermelde krachten in het horizontale vlak.

Het voorgestelde wiskundige model is zo samengesteld dat een (relatief) eenvoudige implementatie in een scheepsmanoeuvreer-simulator mogelijk is.

Globaal kan gesteld worden dat de grootte van de oevereffecten: de langskrachten en beide dwarskrachten (aan de voorste en achterste loodlijn) stijgen met:

- Een hogere voorwaartse snelheid van het schip
- Een meer belaste schroef (hogere schroeftoerentallen)
- Kleinere kielspeling
- Een beperktere vaaromgeving; steilere oevers, kleinere afstand tussen bakboord- en stuurboordoever
- Een kleinere afstand dat er bij een oever gevaren wordt

Het aandeel van de oevereffecten in de langsrichting is altijd zodanig dat het schip een verhoogde weerstand ondervindt. De dwarse kracht aan de achterste loodlijn is steeds gericht naar de meest nabije oever. Het achterschip wordt dus naar de oever toe gezogen. De dwarse kracht aan de voorste loodlijn is in diep water tevens een aantrekkingskracht naar de meest nabije oever toe. In heel erg ondiep water is dit echter een afstotende kracht weg van de meest nabije oever. Tussenin is er een overgang van aantrekking naar afstoting. Deze overgangszone varieert met de voorwaartse snelheid van het schip en met de relatieve waterdiepte onder het schip.

De stuwkracht die de schroef levert is in het wiskundig model omgevormd naar een snelheid (de theoretische axiale snelheid van het water achter de schroef). Deze snelheid is gecombineerd met

de voorwaartse snelheid van het schip tot een equivalente snelheid. Deze snelheid wordt dan op gebruikt als invoer voor de berekening van het Tuck getal. Dit Tuck getal houdt rekening met de waterdiepte en de blockage (dit is de verhouding tussen de dwarsdoorsnede van het schip en de vaarweg). Het Tuck getal is evenredig met de grootte van de langs- en dwarskrachten van de oevereffecten. Voor de dwarskracht aan de voorste loodlijn wordt er een extra functie (variërend met de relatieve waterdiepte en voorwaartse snelheid) toegevoegd om met de verandering van het teken bij ondiep water te kunnen omgaan.

De positie en afstand tussen het schip en een grillig gevormde oever zijn niet eenduidig bepaald. Hiervoor werd de gewichtsfactor geïntroduceerd. Deze factor is een waarde tussen nul en één die exponentieel daalt hoe verder (in zowel horizontale als verticale richting) men zich van het schip verwijdert. De gewichtsfactor wordt geïntegreerd over het beschouwde gebied (dwarsdoorsnede aan bak- of stuurboordzijde, dwarsdoorsnede van het schip, enz.) om op die manier een gewogen oppervlakte te bekomen.

Een dimensieloze afstand tot de oever en equivalente blockage (eveneens zonder dimensie) is bekomen op basis van de gewogen oppervlaktes. Op die manier worden de nodige nuances van een dwarsdoorsnede in rekening gebracht zonder de invloed van de bathymetrie veraf te overdrijven of de invloed van de oevervorm dichtbij te onderschatten. De dwarse krachten (zowel voor- als achteraan) zijn omgekeerd evenredig met de dimensieloze oeverafstand en de grootte van de langse kracht staat in verhouding met het kwadraat van de equivalente blockage.

De invloedsbreedte is de (horizontale) afstand tussen schip en oever waarbij de oevereffecten infinitesimaal klein zijn geworden en kunnen verwaarloosd worden. Wanneer de afstand tussen schip en meest nabij gelegen oever groter is dan deze invloedsbreedte, dan manoeuvreert het schip alsof het in onbeperkt (maar soms ook ondiep) water vaart. Specifieke modelproeven hebben tot de

conclusie geleid dat deze invloedsbreedte in verhouding staat tot het waterdiepteafhankelijke Froudegetal.

Ondanks dat de modelproeven met de meeste zorg zijn uitgevoerd en geschaald volgens de schaalwetten van Froude (hetgeen gebruikelijk is voor modelproeven voor scheepshydrodynamica) behoudt men een probleem met de grenslaag op het scheepsmodel en oever. Deze grenslaag is op modelschaal relatief dikker dan op ware grootte wanneer de proeven zijn uitgevoerd volgens de schaalwetten van Froude. De dwarse aantrekkingskracht aangrijpend aan de achterste loodlijn steeg niet langer wanneer het scheepsmodel extreem dicht langs een (verticale) oever gesleept werd. Een gelijkaardig gedrag werd vastgesteld bij extreem lage kielspelingen. Dit gedrag wordt toegeschreven aan de invloed van de grenslaag op deze dwarskracht. Wanneer de afstand tussen schip en omgeving (kiel – bodem of scheepswand – oever) smaller is dan de grenslaag-invloedsdikte dan komt de kleverigheid (viscositeit) van het water in het spel. Deze invloed overheerst dan de voornamelijk niet-viskeuze hydrodynamica welke oevereffecten genereert. Deze grenslaag-invloedsdikte (waarvoor een formule wordt gegeven) is ongeveer twee- tot driemaal dikker (relatief) op modelschaal dan op ware grootte.

Table of Contents

Nomenclature

O_0	[ ]	origin of the earth bound coordinate system
A_0	[m²]	propeller disc area
A_M	[m²]	midship area
A_W	[m²]	waterplane area
a	[m]	half the distance between source and sink of a Rankine oval
B	[m]	breadth of the ship
B_S	[m]	hull spacing (catamaran), distance between hull centre lines
C_B	[ ]	block coefficient
C_M	[ ]	midship coefficient
C_{PR}	[ ]	prismatic coefficient
C_W	[ ]	waterplane coefficient
$d2b$	[ ]	dimensionless distance to bank
D	[m]	propeller diameter
e	[ ]	Euler's number
Fr	[ ]	Froude number
Fr_{crit}	[ ]	critical speed
Fr_{eff}	[ ]	effective Froude number
Fr_h	[ ]	Froude number (water depth dependant)
F_{NR}	[N]	rudder normal force
F_{TR}	[N]	rudder tangential force
g	[m/s²]	gravity constant of the Earth
h	[m]	water depth
h_{avg}	[m]	average water depth of the cross section
h_{min}	[m]	minimal water depth with influence of boundary layer
h_{ship}	[m]	average water depth of the cross section under the ship
K	[Nm]	roll moment
KM	[m]	transverse metacentre above keel
KM_L	[m]	longitudinal metacentre above keel
k	[m⁻¹]	wave number
L	[m]	length
L_{CB}	[m]	longitudinal centre of buoyancy
L_{CF}	[m]	longitudinal centre of flotation
L_{OA}	[m]	length overall
Lpp	[m]	length between perpendiculars

m	[m²/s]	magnitude of the source/sink of a Rankine oval
m	[ ]	blockage ratio
m_{crit}	[ ]	critical blockage ratio
m_{eq}	[ ]	equivalent blockage ratio
m_{lim}	[ ]	equivalent blockage ratio within the influence width
N	[Nm]	yaw moment
n	[rpm]	propeller rate
Q_P	[Nm]	torque on the propeller shaft
Q_R	[Nm]	torque on the rudder stock
R_{OW}	[N]	open water ship resistance
Re	[ ]	Reynolds number
S	[m²]	wetted surface area
T	[m]	draft
T_A	[m]	draft at the aft perpendicular
T_F	[m]	draft at forward perpendicular
T_M	[m]	draft at midship
T_P	[N]	thrust of the propeller
Tu	[ ]	Tuck number
Tu_m	[ ]	Tuck number taking into account blockage ratio
t	[ ]	thrust deduction
U	[m/s]	Undisturbed flow speed
u_0	[m/s]	ship speed component in the x_0-direction
V	[m/s]	forward speed (of the ship)
V_A	[m/s]	advance speed of propeller
V_{CB}	[m]	vertical centre of buoyancy
V_{eq}	[m/s]	equivalent forward speed
V_{eff}	[m/s]	effective forward speed
V_{ship}	[m/s]	forward speed of the vessel
V_T	[m/s]	the axial speed in the flow field behind the propeller induced by the propeller
V_{Tp}	[m/s]	the axial speed in the flow field behind the port side propeller induced by the propeller
V_{Ts}	[m/s]	the axial speed in the flow field behind the starboard side propeller induced by the propeller
V_{Tavg}	[m/s]	average axial speed of starboard and port side propeller
v_0	[m/s]	ship speed component in the y_0-direction
W	[m]	width of the canal section

W_h	[m]	width of the canal section at the bottom (or at water depth h)
W_0	[m]	width of the canal section at the free surface
w	[ ]	weight factor
X	[N]	longitudinal force
X_H	[N]	hull resistance
X_R	[N]	rudder force directed in the ship bound x axis
x	[m]	longitudinal position (from the midship)
x	[m]	longitudinal position from the forward perpendicular (to calculate the Reynolds number)
x_0	[m]	longitudinal earth bound coordinate
Y	[Nm]	sway force
y	[m]	lateral position
y_0	[m]	lateral earth bound coordinate
y_{eq}	[m]	equivalent distance
y_{Infl}	[m]	influence width or horizontal reach of a bank
y_{wall}	[m]	distance between ship and wall
z	[m]	vertical position
z	[m]	sinkage
z_0	[m]	vertical earth bound coordinate
z_h	[m]	height of the submerged platform
z_{VA}	[m]	running sinkage at the aft perpendicular
z_{VF}	[m]	running sinkage at the forward perpendicular
Δ	[N]	displacement force
α	[°]	half the Kelvin wedge
δ	[°]	rudder angle
δ	[m]	boundary layer thickness
δ_{BLI}	[m]	boundary layer influence thickness
$\delta V(x)$	[m/s]	speed difference between the disturbed and undisturbed flow
δV	[m/s]	return flow velocity
ζ	[m]	decrease of the water level in the cross section
λ	[ ]	scale factor
ν	[m²/s]	kinematic viscosity
ξ	[ ]	coefficient of the mathematical model
π	[ ]	mathematical constant pi or $\tau/2$
ρ	[kg/m³]	density of the fluid
τ	[ ]	turn (ratio between circumference and radius of a circle)

χ	[ ]	the 'weight' of a cross section
χ_{ocean}	[ ]	the 'weight' of an infinite large cross section
χ_p	[ ]	the 'weight' of the port side cross section
χ_s	[ ]	the 'weight' of the starboard side cross section
χ_{ship}	[ ]	the 'weight' of the ship section
ψ	[m²/s]	potential flow stream function
ψ	[°]	heading of the ship
Ω	[m²]	canal cross section area
Ω_{lim}	[m²]	canal cross section area within the influence width
Ω_{ship}	[m²]	canal cross section area at the location of the ship
∇	[m³]	displacement volume

Subscripts:

0	earth bound coordinate system
A	at the aft perpendicular
$ANCH$	anchor
$BANK$	induced by the bank(s)
COL	collision
CUR	current
$crit$	critical
eff	effective
eq	equivalent
F	at the forward perpendicular
H	hull
i	number
M	at midship
$MOOR$	mooring
m	model scale
max	maximum
P	propeller
R	rudder
RET	retardation
STS	ship to ship
V	running
s	full scale
z	for the sinkage

Abbreviations:

2D	two dimensional
3D	three dimensional
ACP	Autoridad del Canal de Panamá (Panama Canal Authority)
AIS	Automatic Identification System
CCTV	Closed-circuit television
CEMT	Conférence Européenne des Ministres de Transport (European Conference of Ministries of Transport)
CFD	Computational Fluid Dynamics
DWT	Deadweight
ECDIS	Electronic Chart Display Information System
EFD	Experimental Fluid Dynamics
FFT	Fast Fourier Transform
FHR	Flanders Hydraulics Research
ITTC	International Towing Tank Conference
KGT	Ghent-Terneuzen canal (Kanaal Gent-Terneuzen)
KVLCC2	KRISO Very Large Crude Carrier 2
KRISO	Korea Research Institute of Ships and Ocean Engineering
LCD	Liquid Chrystal Display
LNG	Liquefied Natural Gas
PIANC	Permanent International Association for Navigation Congresses (The World Association for Waterborne Transport Infrastructure)
PMM	Planar Motion Mechanism
QY	Quay, vertical wall
RANSE	Reynolds-Averaged Navier-Stokes Equation
RoPax	Roll-on/roll-off Passenger
RoRo	Roll-on/Roll-off
SP	Surface Piercing bank
SS	Semi submerged bank
SSPA	Statens Skepps Provnings Anstalt
SST	Shear Stress Transport (Menter's turbulence model)
TEU	Twenty feet Equivalent Unit
VLCC	Very Large Crude Carrier
VOF	Volume Of Fluid

Bank Effects

1 INTRODUCTION

Transport of goods over water is among the oldest modes of transport for mankind. Although rather slow compared to other modes (over road, rail or through the air) it is very cost effective for the transport of large amounts of cargo. Ships cross oceans, seas, lakes and rivers and the cargo in all its appearances (bulk, gas, containerised, passengers) is loaded and unloaded from the vessel at the port.

1.1 Motive

1.1.1 Belgian maritime access

There are four sea ports in the Flemish region of Belgium (in alphabetic order): Port of Antwerp (Appendix 11.1), Port of Ghent, Port of Ostend and Port of Zeebrugge (Figure 1.2). Two ports are located at sea (Ostend and Zeebrugge) while the other two are located more inland. The Port of Antwerp is located some 40 nautical miles upstream the mouth of the River Scheldt, the Port of Ghent is connected to open water by the 17 nautical miles manmade canal Ghent–Terneuzen with a lock connection at the estuary of the Western Scheldt in Terneuzen (Netherlands). The approach of the two seaside harbours is not unrestricted but connected to the world with dredged fairways.

A lot of (domestic) transport of goods is carried out by inland vessels (in Belgium 117 million tons in 2013 compared to 261 million tons by seagoing vessels in the same year (Promotie Binnenvaart Vlaanderen 2013) on the dense web of European inland waters. These inland vessels also sail a large fraction of the time in shallow and/or restricted waters.

The restrictions to call a harbour is not only an issue in Belgium but it seen on the access towards harbours all over the world.

The main dimensions of ship sizes have increased dramatically over the last ten years. In Figure 1.1 the largest maximal capacity of a container carrier (expressed as Twenty Feet Equivalent units, TEU) is plotted for the last five decades. A more than exponential increase is observed (dashed line in Figure 1.1). The largest capacity container carrier of 2013, the Maersk Triple E-class (18 270 TEU), carries more than double the amount of the largest capacity container carrier of 2003, *OOCL Shenzhen* (8 063 TEU).

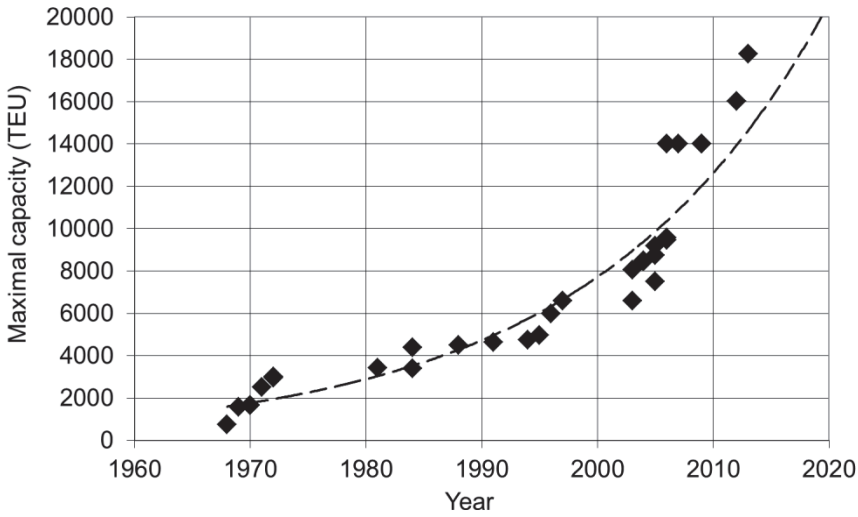

Figure 1.1 increase in container capacity (in TEU) over the last 5 decades

Unfortunately it is not feasible to have the natural rivers or manmade canal increased at the same rate as the ship dimensions. Therefore more vessels sail in more restricted and confined

waters. A rather arbitrary distinction in draft to water depth ratios is published in (PIANC Working group 20; 1992):

- $3.00 < \frac{h}{T}$ deep
- $1.50 < \frac{h}{T} < 3.00$ medium deep
- $1.20 < \frac{h}{T} < 1.50$ shallow
- $1.00 < \frac{h}{T} < 1.20$ very shallow

A more hydrodynamic interpretation of the shallowness of water is reported by (Robbins & Thomas 2013).

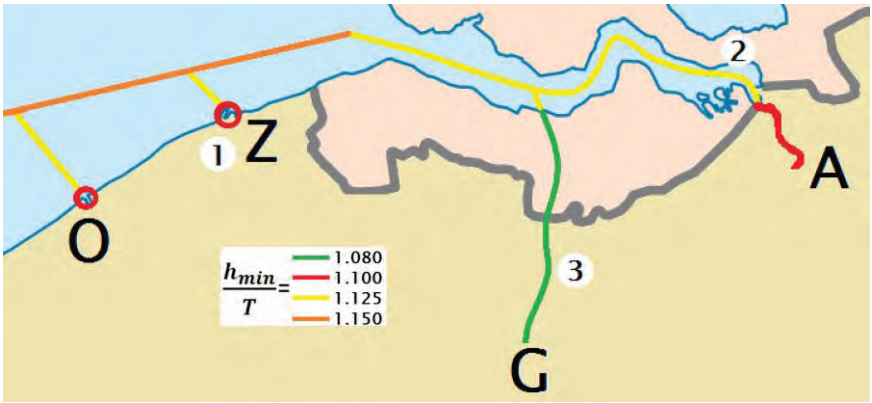

Figure 1.2 the imposed minimal water depth h_{min} (different for LNG-carriers) on the access channels towards the four Flemish sea harbours (A: Antwerp, G: Ghent, O: Ostend, Z: Zeebrugge)

The Flemish authorities (together with the Dutch authorities for the Western Scheldt Estuary) impose deterministic minimal water depth h_{min} to draft T ratios (Table 1.1 and Figure 1.2) depending of cargo type and the area where the ship operates (Vantorre et al. 2014).

h_{min}/T_{max}	Type of cargo	
	Bulk, Containers	**LNG**
Sea	1.150	1.200
Sea approach	1.125	1.200
Outer harbour (within breakwaters)	1.100	1.150
Sea canal (Ghent-Terneuzen)	1.080	-
Scheldt estuary	1.125	-
Upstream River Scheldt	1.100	-

Table 1.1 minimal relative water depths h_{min} imposed by authorities on the approach of a Flemish harbour based upon T_{max}

According to (PIANC Working group 20; 1992) all the approach channels towards Flemish sea ports are classified as very shallow water for the deepest drafted vessels.

In 1933 Flanders Hydraulics Research (FHR) was founded as part of the Antwerp Maritime Services. The original objective was to gain better insight into the impact of dredging works in the navigation channels on tidal currents in the river Scheldt. FHR's first full mission bridge simulator was inaugurated in 1988 and four years later the fully automated Towing Tank for Manoeuvres in Shallow Water (cooperation Flanders Hydraulics Research – Ghent University) ran for the first time. With these facilities (which are updated and extended continuously) an enormous knowledge on shallow water hydrodynamics is acquired.

1.1.2 Shallow water hydrodynamics

Shallow water hydrodynamics have diverse causes and have a different influence on the ship hydrodynamics (ITTC 2002). Overall the hydrodynamic forces will increase with decreasing water depth. The resistance of the vessel, for example, will be larger in shallow water than in deeper water for the same vessel at the same forward speed. Together with the increase of hydrodynamic forces there will be a decrease of manoeuvrability (Eloot et al. 2006). If standard manoeuvring tests are compared in shallow and

in deep water then the turning circles (advance, transfer, tactical diameter, final diameter) will increase the more shallow the water is. For zigzag tests the overshoot angles as well as the yaw rates will be smaller.

The vertical sinkage (known as squat) will increase and be more critical in shallow waters (Lataire et al. 2012). The added mass in shallow water can be the multiple of the added mass of the same vessel sailing in deep water and in some navigation areas there is even interaction between the ship and a muddy bottom (Delefortrie et al. 2004) or with specific constructions (of limited length compared to the ship length) such as bridge pillars. Finally, the course stability of a ship sometimes improves in shallow water (Crane 1979) but in general the manoeuvrability gets worse while the course stability improves with decreasing water depth.

1.1.3 Definition of bank effects

The present dissertation focusses on bank effects. Bank effects can be defined as the hydrodynamic (quasi) stationary reactions on a vessel caused by a geometry parallel to a vessel's course.

The necessary elements for bank effects are:

- A vessel generating hydrodynamic forces; sailing and/or generating some flow with its propeller(s)
- A geometry interfering with the flow around the vessel; this geometry can be a sloped bank, quay wall, dredged channel among others.
- (quasi) stationary; the vessel and/or propeller must have a constant or almost constant (rotational) speed, the length of the geometry must be multiple the largest dimension of the vessel.

For the access channels to the Flemish harbours there are some specific areas where bank effects are seen as one of the major shallow water effects. Among many other locations these are for the access channel towards the Port of Antwerp in the Bend of

Bath (no. 2 in Figure 1.2), in the outer harbour of the Port of Zeebrugge along the Tern Peninsula (no. 1 in Figure 1.2) and in large parts of the Canal Ghent-Terneuzen (no. 3 in Figure 1.2).

At these three locations the geometry of the bank is very different. On the canal Ghent-Terneuzen there is a constant sloped bank of about 18° (1/3) at both sides over a long section of the canal. The sandy bottoms at the Bend of Bath and the outer harbour of Zeebrugge are less steep (7° (1/8) and 11° (1/5) respectively). The latter two are not constant sloped up to the free surface but end in a very gentle, almost flat, shallow water area. These three specific spots are all located in a very small geographic region but similar bank geometries can be found all over the world.

1.1.4 Merit

Ships must avoid colliding with each other or with static or dynamic obstructions. In Figure 1.3 the density of AIS transmitting ships all over the world is plotted. Europe is among the regions with the highest traffic densities.

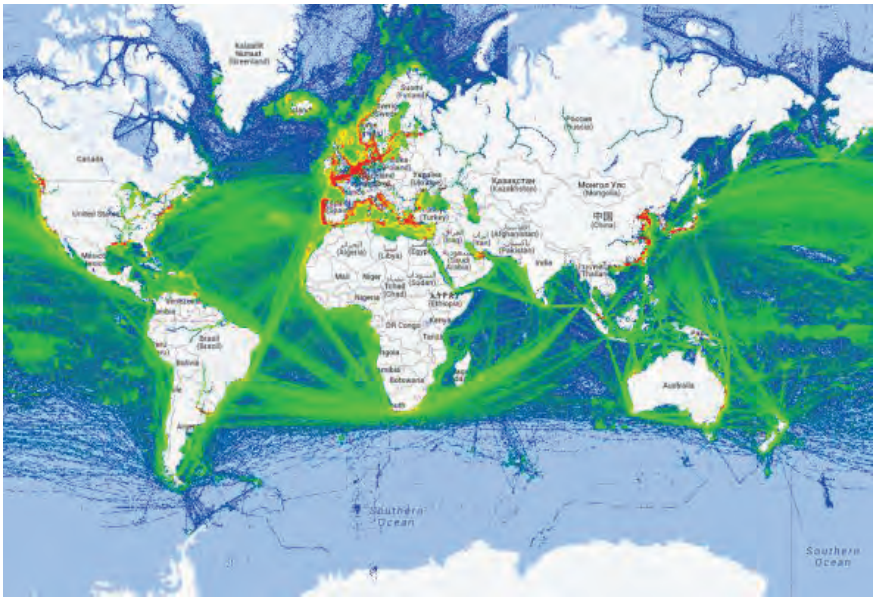

Figure 1.3 world density map of marine traffic (Anon 2014a)

In Figure 1.4 the density map of Dover Strait and the Belgian territorial waters is plotted. This region is among the most dense marine traffic regions of the world. In 2013 as much as 14 220 seagoing vessels called the Port of Antwerp (Anon 2014b). This is an average of about 80 seagoing ship motions (leaving or calling the harbour) every 24 hours (exclusive inland vessel traffic). In the same year some 800 tidal bound ships of which 198 +10 000 TEU container carriers called the same port.

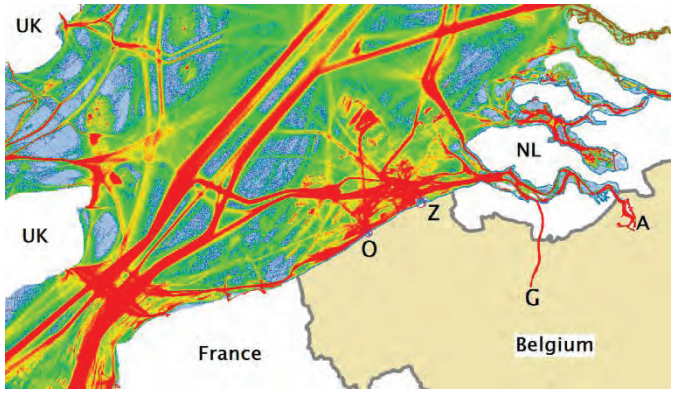

Figure 1.4 marine traffic density map of the Southern North Sea – English Channel area (Anon 2014a)

As a consequence of this dense traffic, an anomaly on the river Scheldt that jeopardizes the free passage of ships results in immediate and large economic consequences (estimates of losses exceeding 1 000 000 €/h are reported). Therefore, all ships must call or leave the harbour in a sufficiently safe manner.

For a waterway authority an important tool to increase or even guarantee this safety is by increasing the knowledge on shallow water hydrodynamics. This knowledge can then be incorporated in a simulator. These ship manoeuvring simulators are used to investigate and justify the admittance policy. The same simulators can also be used for training purposes of the pilots. Doing so the specific shallow water skills of pilots can be increased, furthermore pilots can be trained for future situations (new vessels and/or harbour layouts).

1.2 Objective

1.2.1 A mathematical model for bank effects

The main goal of present research is to create a mathematical model which outputs the ship – bank interaction forces. This mathematical model has to cope with the wide range of possible bank geometries and ship types. Finally this mathematical model can be implemented into ship manoeuvring simulators to create an accurate and reliable behaviour of ships sailing along different banks.

1.2.2 Procedure

Based upon an extensive literature study some insight is obtained in the hydrodynamics of bank effects. In literature there is also sought for available (raw) data which could be used as input for the regression models to define the coefficients of the mathematical model of bank effects sought for. Since there is only a very limited amount of data available (in open publications or through a confidential data exchange), the need for systematic test series in a towing tank dedicated to bank effects was necessary.

In the shallow water towing tank of FHR more than 12 000 model tests have been carried out with the focus on bank effects. These tests were carried out in the years 2008 and 2010 and are by far the most extensive set of model test data on bank effects. Different bank geometries were installed in the towing tank, three classes of bank types can be distinguished:

- Quay walls: vertical walls, most common for wharfs and other mooring locations
- Surface piercing banks: a constant sloped bank from the deepest part of the waterway up to the free surface, common in both manmade channels and natural rivers.
- Stepped or semi-submerged banks: a combination of a constant sloped section from the deepest part of the cross section up to a more shallow water depth and a

wider shallow area, common on a dredged channel in open water (e.g. at sea)

Figure 1.5 three classes of bank geometries: vertical quay wall, surface piercing and semi-submerged bank

Finally the mathematical model based upon all these model tests carried out in a towing tank can be implemented in a ship manoeuvring simulator which is used for training and research purposes.

1.2.3 Boundary conditions and basic assumptions

1.2.3.1 Limit to the modelled forces and moment

All forces acting on a three dimensional rigid body can be decomposed into three forces along and three moments around the three axes of a body fixed (right handed Cartesian) coordinate system. Therefore the bank effects can be split into a force in the longitudinal, lateral and vertical direction of the ship and a moment around the vertical axis and around the horizontal axes in the longitudinal and lateral directions. The major influences of the bank effects, however, are in the horizontal plane (parallel to the free surface). The present mathematical model is limited to the forces and moment acting in the horizontal plane:

- The longitudinal force X_{BANK}: oriented in the longitudinal direction of the ship
- The lateral force Y_{BANK}: oriented perpendicular to the longitudinal direction of the ship
- The moment N_{BANK} around the vertical axis of the ship

Although some observations of the sinkage are reported in present dissertation, it is out of the scope to focus on the influence of banks on the vertical sinkage of the ship (squat).

1.2.3.2 Steady state

In the present research only the steady state bank effects are modelled. Therefore the bank must have an (almost) unaltered geometry over a distance of multiple times the length of the ship. The mathematical model will be able to cope with minor changes in the bank geometry but it does not take into account the (time dependent) influence of short transition zones.

Furthermore the longitudinal dimension of the ship must be almost parallel to the bank at all times. Large drift angles and ship velocity vectors under a significant angle from the bank are out of the scope of current investigation.

1.2.3.3 Sailing ahead

The aim of the research is to accurately predict the bank effects when a ship sails in the restricted fairway towards or from the harbour of call, not during specific harbour manoeuvres such as swinging or the berthing procedure.

This means that the ship sails at a positive forward speed with a propeller rotating in a positive direction (engine order ahead which results in a rotation clockwise or counter clockwise depending whether the propeller is right or left handed).

1.2.3.4 User-friendly

The proposed mathematical model must be able to be implemented in a (FHR) ship manoeuvring simulator. This means that the mathematical model may not use a disproportional amount of computer power. The model must also be able of being implemented without outrageous changes in the structure of the mathematical model.

It is necessary that the mathematical model copes with all types of variable bank geometries both nearby the ship and further away.

1.2.3.5 Symbols

All symbols used are according to the International Towing Tank Conference (ITTC 2011) except the propeller thrust. According to ITTC both the draft of ship hull and the propeller thrust are symbolised by 'T' but to avoid confusion the draft of ship hull remains 'T' but the propeller thrust is from here on symbolised as 'T_P'.

If the parameter under consideration is not listed in the ITTC symbol list then a new symbol is attributed. The entire symbol list is added from page xxv on.

1.3 Chapter by chapter

In Chapter 2 a historic overview of relevant research is given based upon an extensive literature study. An overall view is given of bank effects based upon published research and a distinction is made between the different types of research (model scale, full scale, calculation methods).

The physics and hydrodynamic forces accountable for bank effects are explained in Chapter 3. In the same chapter the phenomenon of bank effects is explained and clarified with different examples. The direct consequences of bank effects on the manoeuvrability of a ship are shown.

All the relevant model tests which are carried out or acquired are extensively explained in Chapter 4. The facilities are described and the choices made for the test parameters and other input data clarified.

A generalised description of mathematical models and the base for the chosen type of mathematical model for bank effects can be found in Chapter 5. Some chosen or imposed boundary conditions are added in the same chapter.

The sixth chapter derives all details of the mathematical model of the lateral force at the aft perpendicular (Y_A). In the next Chapter 7 the mathematical model of the lateral force at the fore

perpendicular (Y_F) is clarified. Chapter 8 contains the explanation and derivation of the influence of the banks in the longitudinal direction X_{BANK}.

Chapter 9 contains the overall conclusions and some recommendations for future work.

Bank Effects

2 HISTORY OF BANK EFFECTS

2.1 Introduction

2.1.1 History of ship model testing

The first towing tank built in Torquay, England in 1871 by William Froude (Froude et al. 1955) marks the modern era of research on ship hydrodynamics. Before that time the shipbuilding industry relied more on tradition and experience than on systematic scientific research. The scientific research at those times was merely initiated out of scientific fascination.

Some illustrious researchers did execute some documented investigations with model scaled ships; Leonardo da Vinci (1452–1519) was one among them (Tursini 1953) (Figure 2.1 and Appendix 11.2). However, the focus in present work lies on the modern era of ship research.

Figure 2.1 extract from da Vinci's Viz. Folio 50/v codex G French Institute (Paris Manuscripts) with the three tested 'ships' on the top right corner of the left page (waterlines)

The mechanisation of ship propulsion in the 19th century triggered the need for systematic research on ship hydrodynamics. Initially the hydrodynamic research focuses mainly on the ship resistance and ship propulsion with the aim of increasing the forward speed (naval vessels) or decreasing the ship resistance (commercial vessels).

Next the focus of hydrodynamic research was extended to other ship hydrodynamic applications such as manoeuvring and course keeping in deep water. Finally the dramatic increase of the ship's main dimensions over the last decades (Figure 1.1) enhances the interest and significance of shallow water hydrodynamics.

Only the forces in the horizontal plane acting on the vessel induced by the presence of a geometry or bathymetry are considered. For a manoeuvring vessel the kinematics and dynamics in the horizontal plane are of main concern although the six degrees of freedom are not independent. This is also the main focus in this literature study of the past research in shallow water hydrodynamics in the modern era.

2.1.2 Classification of research

Since the 1950s research has been published on the influence of the bathymetry/geometry of the fairway on the behaviour of sailing vessels. Some publications summarize and analyse previously published works at the time (Raad voor Transportveiligheid 2004), (McArthur 2011).

A classification of research on bank effects can be based on the research methodology (Figure 2.2). A distinction will be made between:

- Model tests
- Full scale tests
- Mathematics

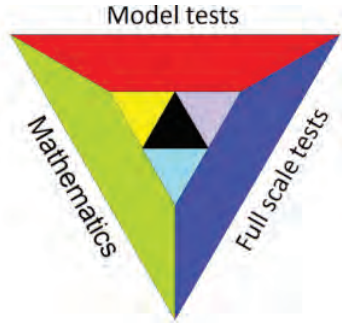

Figure 2.2 schematic overview of data type of historic research

All publications will be classified in these three classifications or in a combination of these classifications.

2.1.2.1 Model tests

Tests carried out with scaled down ship models can be captive or free sailing. During free sailing tests no forces can be measured, only the reaction (position in time) of the vessel on different influences (such as installed banks) can be registered.

During captive model tests the ship model can be towed through the towing tank on a straight line (with or without drift) or on a predefined curved path. These captive model tests can be carried out in a towing tank (most common facility for this type of tests), in a rotating arm facility or in a circulation water channel.

Different constructions can be installed in the facilities or the walls and/or bottom of the facility itself is used to induce bank effects on the ship model.

2.1.2.2 Full scale

Dedicated full scale trials on bank effects are very uncommon and expensive but researchers are sometimes tolerated on board as long as they do not interfere with the commercial activities of the vessel. Common full scale tests are carried out with accurate (D)GPS measurement devices to monitor the lateral and vertical motions of the vessel in the fairway. Full scale trials are always free sailing tests, no forces on the hull can be measured but the reaction of the ship on external influences can be monitored by

measuring the position of the vessel in time or by investigating the behaviour of (closed loop) control systems (rudder, propeller)

2.1.2.3 Mathematics

The final branch of data source for bank effects is more diverse and summarized as 'Mathematics'. Two types of models can be distinguished:

- mathematical models
- numerical models

Mathematical models are parameterized sets of equations based upon physical models, numerical models and/or full scale observations.

Numerical models are based on the combination of the discretization or simplification of the problem and fundamental equations. Examples of models based on discretization are numerical models based on potential flow or lifting line theory, computational fluid dynamics (CFD) and Reynolds Average Navier Stokes Equations (RANSE). If the ship geometry and by extension the entire problem is simplified, the slender body theories or other simple mathematical models such as potential flow or lifting line theory can be analytically solved. CFD and RANSE can solve complex, realistic geometries with the viscous effects being taken into account.

Over the last 60 years computing power has increased beyond imagination. At the time calculations could be carried out according to the potential flow or lifting line theory while for the last decades the importance and user-friendliness of CFD increase year after year together with its reliability. The more computer power the closer the solution to the full Navier-Stokes equation gets.

2.2 Model test based research

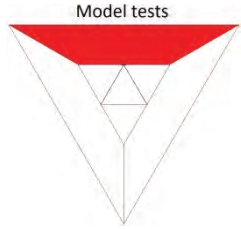

In the David Taylor Model Basin (Potomac, U.S.) model tests were carried out in 1946-1947 primarily to obtain knowledge to assist the Panama Canal Company (nowadays Panama Canal Authorities ACP) in the design of a new cross section for the canal across the isthmus of Panama. These tests were reanalysed in (Schoenherr 1960) to derive broadly applicable data for estimating the bank effects for full merchant ships (of that era). Remarkably the influence of the propeller on the bank effects (both sway force and yaw moment) is concluded to be of a minor influence. The lateral force is made dimensionless and analysed graphically.

Model tests dedicated to bank effects were carried out in the Seakeeping Laboratory of Tokyo University. The results obtained were analysed and published by (Fujino 1968). Linear equations of motion for the lateral force and yaw moment were formulated as a function of the distance from the centre line, (angular) velocity components of the ship and rudder angle. The coefficients were obtained for different conditions (water depth and lateral restriction due to banks) by performing PMM tests (Planar Motion Mechanism). The coefficients derived from these PMM tests were compared to investigate the influence of water depth and banks. The necessary conditions to have course stability in a canal were calculated for the tested water depths and forward speeds. In (Eda 1971) a similar research was carried out. Again equations based on captive motive model tests for the yaw moment and sway force were developed. The influence of the canal section was investigated and the relation with course stability checked. Based on the acquired knowledge a simulation of a ship navigating in a

channel was performed. Finally the acceptable main dimensions for both fairway and vessel for a safe passage were defined.

(Sturtzel et al. 1966) carried out model tests a few years before (Fujino 1968) with gauges registering the wave pattern at four discrete positions between the ship model and the rectangular wall of the tank. Drawings with isobars based upon the wave registrations are created to describe and understand the phenomenon of bank effects.

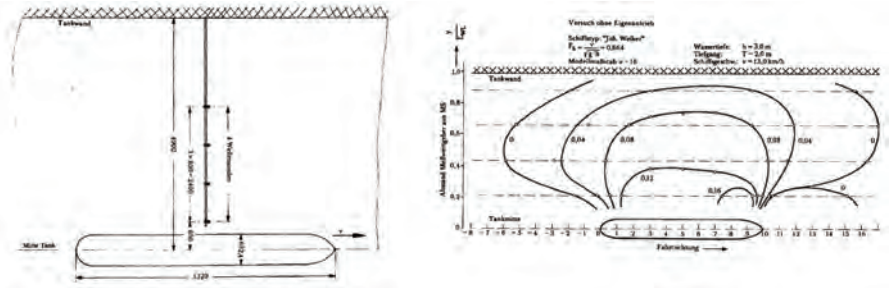

Figure 2.3 position of wave gauges (left) and isobars (right) from (Sturtzel et al. 1966)

Model tests carried out with a tanker model in a fairway with a rectangular cross section and along sloped banks as well as stepped banks at a range of lateral positions were discussed in (Fuehrer 1978). The lateral force at the bow and stern are qualitatively described. The influence on both lateral forces (at bow and at the stern) of the type of asymmetry, the geometry of the bank, the heading and the forward speed are described. It is noticed that at low forward speed there is always attraction towards the closest bank in combination with a bow away moment. Over the entire length of the vessel there is a depression between ship and bank. At higher speeds the bow is pushed away from the closest bank (high pressure between ship and bank at this relative longitudinal location) but the stern section is still attracted (depression) with an increased magnitude towards the bank resulting in a large bow away moment. In very shallow water an overall repulsion force is reported. The same model tests have

been analysed to obtain the required canal width for a safe navigation in (Römisch 1978). As a result a design guideline has been proposed for the minimal width of a canal. Both authors jointly published in (Fuehrer & Romisch 1983) and point out the relation between the external forces induced by bank effects and control forces of the rudder.

Dr. Nils H. Norrbin († 2011) performed important contributions to the topic of bank effects. One of his early publications (Norrbin 1974b) reports a set of captive and free sailing model tests with a tanker model in the proximity of surface piercing and semi-submerged vertical banks of variable length. He also reports that transient effects disappear for bank lengths of about six times the ship length. The superposition principle of the bank effects on port and starboard side is valid in a canal as well as sailing along only one bank. Even a small layer of water on a flooded (semi-submerged) bank decreases the magnitude of the bank effects substantially. In (Norrbin 1974a) the superposition principle is validated and pressure gauges show the physics of the transient bank effects caused by different types of (short) banks. Model tests along sloped banks are described in (Norrbin 1985). A mathematical model for yaw moment and sway force is suggested. The magnitude of this force and moment is inversely proportional to the distance to the bank and proportional to the square of the forward speed (in the considered range). The influence of the slope of the bank increases with decreasing water depth. In (Brix 1992) the mathematical model of (Norrbin 1974a) and (Norrbin 1985) is summarized and suggestions are made for optimization of the model.

An extensive model test program is reported in (Dand 1981) and (Dand 1982). In the test program ship models of two tankers, a general cargo ship, a container carrier and a passenger ship were involved. These ship models were towed along surface piercing banks as well as semi-submerged banks. The tests were carried out in a classic towing tank as well as a circulation water channel.

The results are discussed for the longitudinal force (resistance), lateral force, yaw moment and vertical sinkage and trim.

A limited set of model tests focussing on the differences between a vertical wall and a sloped bank (a slope angle of 45° or 1/1) are described in (Renilson & Munro 1989). The bank induced sway force and yaw moment were modelled and implemented in the ship manoeuvring simulator at the Australian Maritime College. The mathematical model was extended based upon new model tests along four different bank slopes, water depths, lateral positions, hull form, forward speed and propeller action in (Ch'ng & Renilson 1990; Ch'ng et al. 1993)

(Vantorre 1995) published a mathematical model based upon the model released by (Ch'ng et al. 1993) with regression coefficients based upon model tests. The tests were carried out with a partially laden 150 000 DWT bulk carrier and a Panamax bulk carrier. The latter was only tested at one water depth in a canal section with sloped banks on both sides while the first was towed in a captive way along a vertical bank at different water depths. One of the conclusions was the dependency on forward speed of the sway force and yaw moment even when both are made dimensionless by dividing by the square of the forward speed. Going from deeper water to (very) shallow water the overall attraction force appears to change in a repulsion force. The propeller action (first quadrant) results in an attraction force between the stern section and the closest bank and the direction associated with the rotation of the propeller (left or right) relative to the closest bank influences the sway force and yaw moment.

(Delefortrie & Hermans 2001) suggest a Taylor series expansion for a mathematical model for the sway force and the yaw moment. The coefficients of the Taylor series are based upon the model tests along a vertical quay wall carried out as reported in (Vantorre 1995). The model test database was extended with model tests carried out with a post Panamax container carrier (6 000 TEU) model towed along a vertical bank described in (Vantorre 2002;

Vantorre et al. 2003). In these publications the influence of the propeller action on sway force and yaw moment is introduced in the mathematical model by increasing the forward speed virtually with a forward speed depending on the thrust and diameter of the propeller. In the mathematical model the water depth is decreased with the average sinkage of the vessel due to squat. This is to cope with the higher influence in shallow water relative to deeper water.

Model tests with rather short ship models (Lpp $<$ 2m) are described and analysed in (Duffy et al. 2000; Duffy 2002). Two models from the MarAd systematic series and the S175 container carrier were towed at different distances and water depth along several semi-submerged sloped banks. The dependency of sway force and yaw moment on the tested parameters is shown and a rather analytical regression is carried out to obtain a mathematical model to implement in a ship-handling simulator.

At Statens Skepps Provnings Anstalt (SSPA) model tests to investigate the bank effects induced by sloped and semi-submerged banks have been carried out with ship models of a catamaran, ferry and tanker. These model tests are described and analysed in (Li et al. 2003). A mathematical model is proposed and copes with ship main characteristics, bank configuration, forward speed, propeller action and water depth (under keel clearance).

Model tests with inland waterway vessels towed under a drift angle along a bank are discussed in (Gronarz 2009). The author explains the cross terms between the bank effects and the drift angles. Although the deviation increases by splitting the phenomena into pure bank effects and pure drift effects some conclusions can be drawn on the influence of the drift angle on the bank effects. A mathematical regression model is proposed and fast time simulations are executed.

(Maimun et al. 2013) carried out model tests with a model of an LNG carrier. A rather unique relation between sway force and yaw

moment and the distance to the bank is found. The published tests are all characterised by a repulsion force away from the closest bank in both deep $\left(\frac{h}{T} > 3\right)$ and shallow water $\left(\frac{h}{T} = 1.2\right)$. The mathematical model is used to investigate the influence of the bank effects on the overall manoeuvrability of the LNG-carrier. In (Maimun et al. 2009) the same author reported a bow-in moment during model tests dedicated to bank effects.

In (Lataire et al. 2007), (Lataire & Vantorre 2008) and (Lataire, Vantorre & Eloot 2009) the "d2b" (distance to bank) and "equivalent blockage" concepts were introduced to account for arbitrary bank shapes and channel sections. The manufacturer of ship bridge simulator Kongsberg has implemented these concepts in its simulator software (Kongsberg 2012).

2.3 Mathematics based research

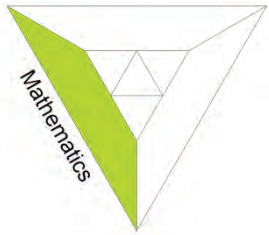

Comparisons between model tests and numerical calculations have been reported by many authors but calculating the bank effects only based on analytical methods is less common.

Potential flow calculations were described in (Newman 1965) with the focus on the pitch moment (around the y-axis) M and the vertical force Z. Based upon the Lagally's theorem the force and moment acting on the body can be found with the velocity potential in terms of a three dimensional source distribution within the body and its mirrored image to create a vertical wall. The influence of the wall and bottom are taken into account and investigated. A non-dimensional speed term is proposed based upon the water depth dependent Froude number.

(Yeung 1974; Ronald W Yeung & Tan 1980) published a time dependent calculation method based on the slender-body theory for the bank effects. A general theory for a single ship sailing in a non-uniform incident flow is clarified (for all 6 degrees of freedom). This theory is applied for the induction on the vessel of sway force and yaw moment because of the presence of an irregular coast line or fixed obstacles.

A different but similar calculation method (potential flow theory) as (Yeung 1974) is proposed in (Kijima & Qing 1987). The focus however is more on the design parameters of the harbour or canal than on the manoeuvrability of the vessel. Some calculated examples clearly show the influence of the sloped bank on the manoeuvrability of the vessel under consideration. It is concluded that the bank effects dramatically increase when the vessel's position is close to the corner of the wedge shaped bank wall (toe of the bank). Simulations predict the influence of a design on the capability of a vessel to overcome the influence of the bank on the manoeuvring behaviour.

With the potential flow theory (ideal fluid) and a numerical procedure for solving the integral equation as well as focussing on the Kutta condition (at the trailing edge of the vessel) (King & Tuck 1979) show the influence on the vessel of moving along a vertical wall or above a uniform beach. Both yaw moment and sway force are made dimensionless and compared for different water depths, slopes and lateral positions from the bank.

(Hsiung & Gui 1988) published also an extension of the numerical method published in (R W Yeung & Tan 1980). Different cases are calculated for a ship passing a range of constructions such as a circular pillar, sloped banks, vertical banks with a semi-circular mound (Figure 2.4) or a ship moving through a channel with hyperbolic plan view (Figure 2.4). Calculations are made for different more complex bank geometries in (Gui et al. 1990). Here, the Schwarz-Christoffel integral results in a set of non-linear equations which are solved through the Newton Raphson method.

All is based on the assumption of a non-viscous, irrotational and incompressible fluid. The main disadvantage of these assumptions are the total absence of any influence of the viscosity of the water (boundary layers).

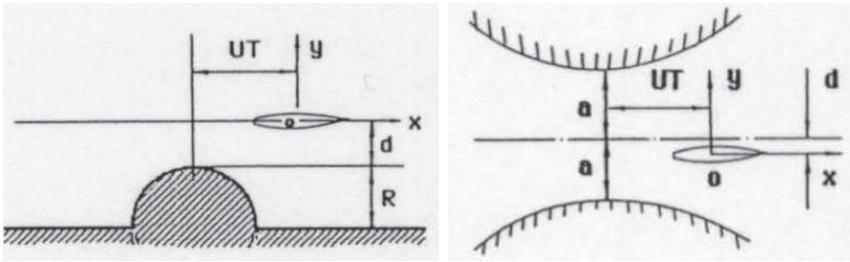

Figure 2.4 ship sailing along a semi-circular mound in the wall (left) and in a hyperbolic narrowing (and widening) canal (right). From (Hsiung & Gui 1988)

The time dependent transition from unrestricted sailing to sailing with a (sloped) bank at one side along the vessel is calculated with potential flow theory in (Lee & Lee 2008). When the bow reaches the bank a small bow- in moment towards the bank is observed. As the vessel sails for her entire length along the bank the previous observed attraction force and bow away moment are obtained again.

A very different type of numerical calculation is reported in (Lo, Su & Lin 2009; Lo, Su & Chen 2009). No potential flow theory based calculations but (CFD) calculations (Flow3D) are carried out (RANSE). Bank effects are calculated for a 3 600 TEU KRISO container carrier and commented. Unfortunately these calculations are not validated or compared with full scale nor model scale measurements.

2.4 Full Scale tests based bank effects research

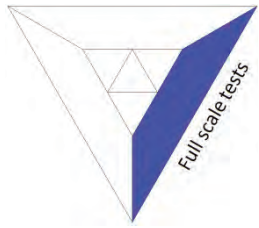

Full scale tests dedicated to bank effects are rare and research projects only based on full scale tests (without the comparison of model tests or mathematical computations) are even more scarce. At full scale only the effect and not the bank effect forces can be measured.

(Koslowski 2007) contains some explanation of the measurement system to monitor the primary and secondary wave system induced by a large container carrier on the river Elbe in a small yachting harbour. This type of research is interesting for the wave pattern generated on a bank by a vessel but is out of the scope of present research. In (De Roo & Troch 2013), among many others, a similar type of research is performed for the damage caused by an inland vessel on a natural protected bank.

2.5 Research based on model tests and mathematical models

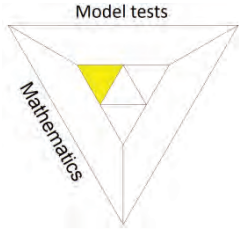

Together with model tests this is the most common type of research on bank effects. The outcome of a mathematical model or numerical calculations are compared to model test results for validation purposes.

In (Newman 1969) the potential flow calculation method as proposed in (Newman 1965) combined with Prandtl's lifting line theory is implemented for a body moving between two vertical walls. The calculations are compared to the model tests carried out by (Norrbin 1969).

For the 14th ITTC, (Norrbin 1975) summarizes the state of art (at that time) on shallow water hydrodynamics with a specific focus on bank effects. The physics as well as some mathematical models to predict force and moment are listed as well as model tests carried out in the scope of bank effects.

The importance of the under keel clearance on bank effects is pointed out in (Beck 1976; Beck 1977). The slender body potential flow theory is applied together with some assumptions on the vortex and blockage to be able to compare the forces and moments (side force, yaw moment, sinkage and trim) with model tests (Norrbin 1974b) on a vessel sailing at different lateral positions and water depths between two vertical walls.

The dimensions of existing navigation channels are assessed with the focus on the limitations because of increasing ship sizes in (Gates & Herbich 1977). The bank suction model proposed in (Schoenherr 1960) is used together with published models for squat, drift and rudder forces. The interesting concept of the Neutral Steering Line is defined as the position in the fairway where the lateral forces and yaw moments due to bank effects are counterbalanced. The measured and computed lateral force and yaw moment are compared to validate the models. This research is extended in (Gates & Herbich 1978) with the focus on the variation of the Neutral Steering Line caused by the asymmetry of the channel cross section and the required vessel drift and rudder angle to overcome the bank effects.

With the background from hydraulics in rivers and channels (Kolkman 1978) focusses on the current generated by the vessel in a confined waterway. Numerical calculations are executed with

different dimensions of the fairway and model tests are carried out to visualise the current on the free surface. The effects of propeller action and bottom friction (viscosity) are taken into account. Examples show the impact of different channel geometries on the vessel's response.

A theoretical study is carried out by Yasukawa to investigate the manoeuvrability of a vessel in an arbitrary shaped canal in (Yasukawa 1991). The theory is a hybrid model of the potential flow theory, slender body and panel method. The results are checked with model tests from Norrbin. A trajectory with fast varying width of the fairway is simulated and concluded that course keeping will be harsh. The open data on bank effects (Lataire, Vantorre & Eloot 2009) and some model tests on ship to ship interaction (Vantorre et al. 2001) are used to check the 3D-panel method by the same author in (Yasukawa et al. 2009).

A velocity potential is defined in (Miao et al. 2003) to calculate numerically the sway force and yaw moment induced by the proximity of a bank. The wave pattern at the free surface and the pressure distribution are calculated based upon the same theoretical method. A comparison is made with model tests carried out at the Australian Maritime College with a model with a length between perpendiculars of 1.77 m. The correlation in deep water was satisfying but in more shallow water it was not. The absence of the viscosity in the mathematical model in combination with the rather short ship model (with a larger influence of viscosity) is expected to be the reason of this difference. A similar conclusion can be drawn from (Xia & Miao 2004).

The influence of the tank walls during common resistance tests in a towing tank are quantified in (Kumar & Anantha Subramanian 2007). The flow around a model of an ocean going barge is numerically modelled with a volume of fluid (VOF) model. The influence of the tank width is investigated based upon the numerical calculation and based upon model tests with two models with a different scale of the same barge. It is concluded

that the influence of the tank walls during a resistance test is negligible if the tank width W exceeds 5 times the beam B of the vessel ($W/B>5$). It must be remarked that this is only checked for deep water ($h/T>7.5$) and therefore at rather low water depth dependent Froude numbers Fr_h.

CFD calculations with a commercially available Reynolds Averaged Navier Stokes Equitation (RANSE) model (Fluent) are reported in (Wang et al. 2010) . An SST $\kappa - \omega$ turbulence model is adopted to cope with the viscous flow field. Some of the calculations are compared with published results from model tests (Vantorre 2002) and a lot of variations on the position in the cross section and water depths are calculated.

In (Chetvertakov et al. 2011) first the problem is solved in a 2D calculation model. With the same commercial CFD-package as (Wang et al. 2010), Fluent, some calculations are made to be able to create a regression model for bank effects. This model takes the drift angle into account and is compared with model tests. The mathematical model is implemented in the ship manoeuvring simulator and tested.

The panel method (3D first order Rankine) is adopted to calculate the sway force and yaw induced by a vertical bank and a sloped (1/3) bank on an 8 000 TEU container carrier. These calculations are compared with the published open data on bank effects (Lataire, Vantorre & Eloot 2009).

(Zou et al. 2011; Zou & Larsson 2013) report an extensive comparison between CFD-calculations and model tests with a VLCC at different water depths and along different types of sloped banks. The focus lies mainly on the uncertainties of calculations and measurements. The RANS method could cope satisfactorily with trim and sinkage. This is much less the case for the (older) potential flow method which does not take into account viscosity since the fluid is idealized.

Overall it can be concluded that, although computer power has increased enormously over the last decades and numerical methods can cope and solve the Navier Stokes equation better, the numerical calculation of bank effects in shallow water remains challenging for both computer processors and their operators.

2.6 Research based on model tests and full scale measurements

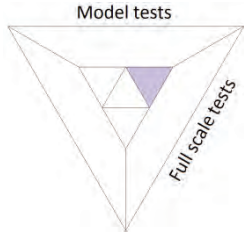

Model tests are used to develop a mathematical regression model for the sway force and yaw moment induced by the proximity of sloped and semi submerged banks in (Duffy et al. 2009). The important difference between a sloped bank and a semi-submerged bank is pointed out again together with an extensive description of the observed sway force and yaw moment for different types of bank geometry, water depths and ship-bank distance. The proposed mathematical model is implemented in the ship manoeuvring simulator and evaluated by experienced pilots from the port of Weipa (Australia).

2.7 Research based on model tests, full scale measurements and mathematical models

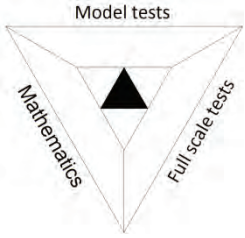

The combination of full scale tests, model tests and mathematical calculations (lifting line theory) was performed in (Brard 1951). The separation of the flow at high rudder angles in combination of a low Reynolds number on the rudder at model scale in the rotation arm facility, results in a scale effect of the influence of the rudder on the hull. The course stability is checked by extrapolating the results of dedicated captive model tests in the rotating arm facility without drift angle at different rotational speeds to a virtual straight line motion. Based upon model tests in the Paris model basin (towing tank), the non-dimensional longitudinal force, lateral force and yaw moment are compared in deep and shallow water with and without banks. The typical cross section of the Suez Canal was installed in the shallow water towing tank for the latter. The results are evaluated with the lifting line theory.

In (Fenical & Carter 2009) the in house developed numerical calculation method Vessel Hydrodynamics Longwave Unsteady is used to compare full scale measurements with model tests among others. The validation is done for berthed vessels by comparison with (Remery 1974), squat was compared with (Guliev 1971) and bank effects with (Lataire, Vantorre & Delefortrie 2009).

2.8 Summary

The literature study is split into three research methodologies (and all combinations of these three methodologies); model tests carried out in a towing tank (most are captive model tests), mathematics (potential flow theory, lifting line theory and the more up to date computational fluid dynamics CFD), and full scale observations.

Most of the research on bank effects was carried out in a towing tank. The test series seldom resulted in more than 100 different model tests. The knowledge obtained from the tests carried out in the towing tank results in mathematical models for specific combinations of ship and bank. Most tested bank geometries are a vertical quay wall (the wall of the towing tank could be used) and constant sloped banks.

Computational fluid dynamics still suffer from the complex boundary layer in shallow water and on the (non-symmetric) bathymetry. Although CFD becomes more and more user-friendly the application on bank effects remains challenging, with larger calculation times and complex meshing solutions compared to open water hydrodynamics.

Only a limited amount of tests are carried out at full scale, the vertical sinkage of the ship (squat) and not the forces in the horizontal plane induced by the banks nearby are investigated during these full scale measurements.

The only open data on bank effects, free to use and available in digital format, is published under the auspices of *the Knowledge Centre Manoeuvring in Shallow and Confined Water* although some more processed results based on model tests can be derived from other (older) publications.

Bank Effects

3 PHENOMENON: BANK EFFECTS

It is easier to rob by setting up a bank than by holding up a bank clerk.
Bertolt Brecht

Bank effects are known as the hydrodynamic influence of banks on the sailing vessel. This influence manifests on the vessel in various ways and can be split for, better understanding, into different sub-effects. Forces act on the vessel (lateral, longitudinal, vertical) as well as moments are induced resulting in a different trim, heading (yaw moment) and heel angle (roll moment).

In present chapter the phenomenon of bank effects is first explained with some basic physics and with an idealised fluid (potential flow theory). The importance and large influence of shallow water is made clear with the Kelvin wedge.

One model test carried out in a shallow water towing tank is used to show the hydrodynamics involved. A plot of the free surface is compared with the results from the previous simplifications done in the potential flow theory.

A track plot from a full mission bridge simulation on the river Scheldt is exemplified to show the impact of bank effects on this specific simulation run.

Finally, a real life calamity shows that bank effects played a role (among other factors) in the poor outcome of this specific passage on the river Scheldt.

3.1 Main principle

The fundamental principle of bank effects acts as follows: A moving displacement vessel displaces an amount of water (Archimedes' principle) and this amount of displaced water travels along the hull. For a vessel sailing forward this water runs from the bow towards the stern. On wide and open shipping routes (ocean) this water can travel almost without restrictions along and under the vessel. This water flow induces some hydrodynamic phenomena (squat among others) but no bank effects.

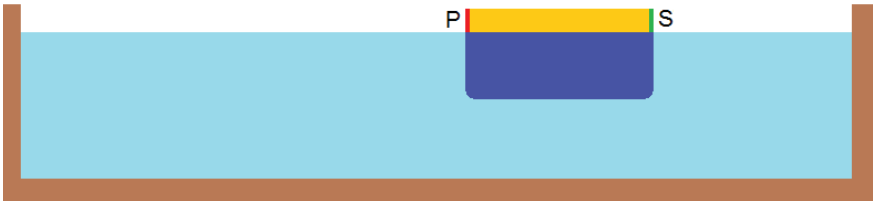

Figure 3.1 a simplified cross section of a vessel in a rectangular fairway (port side (P) to the left, starboard side (S) to the right).

In restricted waters the streamlines around the ship tighten. Now assume a vessel sailing on the starboard side in a fairway with a rectangular cross section (Figure 3.1). Similar as sailing on the ocean all the displaced water must travel along the vessel. (Actually this is only true as long as the vessel sails at a forward speed smaller than the critical speed so there is no presence of solitons and the conservation of mass over the cross section still stands.) In the situation as in Figure 3.1 there is a restriction for the water at the port and starboard sides due to the presence of the banks, and under the vessel between the keel of the ship and the bottom of the fairway.

Let us assume for reasons of explanation that 1/3 of the displaced water must travel under the vessel, 1/2 between the vertical wall and the vessel at port and finally 1/6 between the ship and the

closest wall at starboard. Three times more water at port than at starboard because of the smaller area at the starboard side than at the port side. At both sides the water is squeezed in (because of the presence of the ship) but relatively more at starboard than at port. To be able to evacuate the necessary amount of water the water velocity will be higher at the more confined side than the wider port side. The increase of water velocity will depend on the space available. The more space there is (in this example at port side), the lower the return speed will be (for the same forward speed of the vessel). Now there is a speed difference between port and starboard side of the vessel. In present example the return speed will be higher at the starboard side than at the port side.

The increased water flow between ship and wall will also create a pressure drop in the same area, the free surface level will drop in obedience to this pressure drop and because the pressure at the free surface must be the atmospheric pressure (as a consequence the hydrostatic pressure must drop). According to the Bernoulli principle, the speed difference (port and starboard) will introduce a pressure difference on the vessel hull. The higher the return speed, the lower the pressure. The pressure at the more restricted starboard side will be lower than at the port side. This pressure difference results in a force and moment acting on the vessel.

Not always but very common (as in previous example) the vessel will endure an attraction force directed towards the closest bank and a yaw moment pushing the bow away from the closest bank. Therefore *bank effects* are sometimes referred to as *bank suction*. However in some specific situations the vessel is pushed away from the closest bank and therefore the term bank effects is favoured in present dissertation. In the longitudinal direction the presence of banks will increase the longitudinal force acting as an added resistance.

3.2 Potential Flow

3.2.1 Rankine ovals

A simplified 3D potential flow is considered to verify the previous description of bank effects. The vessel is represented by a Rankine oval in a uniform flow of the same speed as the forward speed (over ground) of the vessel. The Rankine oval is a prolate spheroid with length Lpp (in the elongated direction) and a maximum width (or diameter) equal to the breadth of the vessel (Figure 3.2). The Rankine oval consists of a source – sink twosome with the same magnitude m (but with opposite signs).

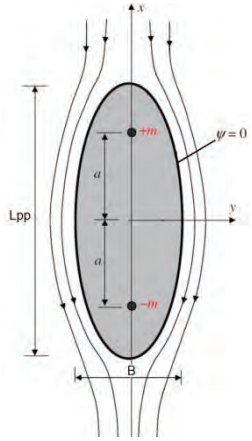

Figure 3.2 the streamlines around a Rankine oval in a uniform flow

Stream function of the 3D Rankine oval with coordinate system as in Figure 3.2:

$$\boldsymbol{\psi = Ux - \frac{m}{4\pi}\left(\frac{1}{\sqrt{(x+a)^2+y^2+z^2}} - \frac{1}{\sqrt{(x-a)^2+y^2+z^2}}\right)} \tag{3.1}$$

with *m* the magnitude of the source and sink and *a* half the distance between source and sink. The magnitude *m* and distance *a* must fulfil the following equations to obtain a Rankine oval of the required dimensions:

$$\frac{Lpp}{2a} = \sqrt{\frac{m}{\pi U a} + 1} \tag{3.2}$$

$$\frac{B}{2a} = \frac{m}{\pi U a}\left(\frac{\pi}{2} - \tan^{-1}\left(\frac{B}{2a}\right)\right) \tag{3.3}$$

3.2.2 Mirror planes

The bank or vertical quay wall is represented by introducing a second Rankine oval at twice the distance between the vessel's centreline and the wall. In this way a mirror is introduced, located at the same position as the vertical wall. There are no streamlines penetrating or leaving this mirror plane. There are only streamlines that are on and stay on that mirror plane. The potential flow is inviscid (no viscosity and thus no boundary layer) and irrotational (fluid elements have no angular velocity). The absence of the viscosity is a disadvantage of this potential flow method.

To implement the shallowness of the environment, two more Rankine bodies are added to create a second mirror plane to represent the bottom (Figure 3.3). Since the cross sections of the Rankine ovals are circles with a maximum diameter B, the draft of this oval is $\frac{B}{2}$. Therefore the pair of Rankine ovals (or better the source and sink) are positioned at a distance of $2\frac{h}{T}\frac{B}{2}$ or $\frac{hB}{T}$ from each other. This is to create the same water depth to draft ratio. Again no streamlines enter or leave this mirror plane but travel along that plane because of the absence of a boundary layer in an inviscid irrotational flow.

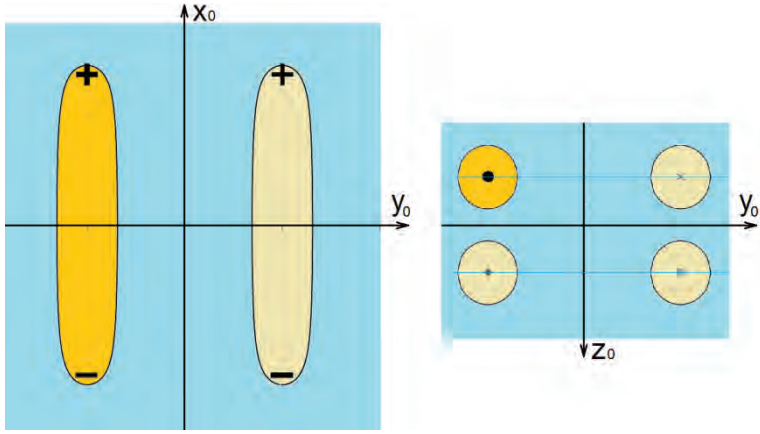

Figure 3.3 ideal fluid mirrors for introducing vertical bank and bottom (top side view, left) and two Rankine ovals to create a vertical bank (front view, right)

3.2.3 Pressure at the free surface

In the fluid as represented in Figure 3.3 only the Bernoulli wave system can be found because the free surface is imposed flat. The pressure at the 'free surface' is shown in Table 3.1. Since there is only one (ideal) fluid involved in the entire domain, there is no interface between two fluids (in case of a ship this is water and air) and as such no free surface. The pressure at the virtual free surface can be used to calculate a representing wave height.

x_0/Lpp	y_0/B 2.0	1.9	1.8	1.7	1.6	1.5	1.4	1.3	1.2	1.1	1.0	0.9	0.8	0.7	0.6	0.5	0.4	0.3	0.2	0.1	0.0
1.0	1	2	2	2	2	2	2	2	2	2	3	3	3	3	3	3	3	3	3	3	3
0.9	1	2	2	2	2	2	2	3	3	3	3	3	3	3	3	3	3	3	3	3	3
0.8	1	1	2	2	2	2	3	3	3	3	3	3	3	3	3	3	3	3	3	3	3
0.7	1	1	1	2	2	2	3	3	4	4	4	4	4	4	4	4	3	3	3	3	3
0.6	-1	0	0	0	1	2	3	4	5	5	6	6	5	4	3	3	2	2	1	1	1
bow 0.5	-3	-3	-3	-3	-3	-3	-3	-2	0				2	0	-1	-2	-2	-3	-3	-3	-3
0.4	-6	-6	-7	-8	-9	-10	-12	-15					-14	-12	-10	-9	-9	-8	-8	-8	
0.3	-8	-8	-9	-10	-11	-12	-13	-14					-14	-14	-13	-13	-12	-12	-12	-12	
0.2	-9	-9	-10	-10	-11	-11	-12	-13					-14	-14	-14	-13	-13	-13	-13	-13	
0.1	-9	-9	-10	-10	-11	-11	-12	-12					-13	-14	-14	-14	-14	-14	-14	-14	
0.0	-9	-9	-10	-10	-11	-11	-11	-12					-13	-13	-14	-14	-14	-14	-14	-14	
-0.1	-9	-9	-10	-10	-11	-11	-12	-12					-13	-14	-14	-14	-14	-14	-14	-14	
-0.2	-9	-9	-10	-10	-11	-11	-12	-13					-14	-14	-14	-13	-13	-13	-13	-13	
-0.3	-8	-8	-9	-10	-11	-12	-13	-14					-14	-14	-13	-13	-12	-12	-12	-12	
-0.4	-6	-6	-7	-8	-9	-10	-12	-15					-14	-12	-10	-9	-9	-8	-8	-8	
stern -0.5	-3	-3	-3	-3	-3	-3	-3	-2	0				2	0	-1	-2	-2	-3	-3	-3	-3
-0.6	-1	0	0	0	1	2	3	4	5	5	6	6	5	4	3	3	2	2	1	1	1
-0.7	1	1	1	2	2	2	3	3	4	4	4	4	4	4	4	4	3	3	3	3	3
-0.8	1	1	2	2	2	2	3	3	3	3	3	3	3	3	3	3	3	3	3	3	3
-0.9	1	2	2	2	2	2	2	3	3	3	3	3	3	3	3	3	3	3	3	3	3
-1.0	1	2	2	2	2	2	2	2	2	2	3	3	3	3	3	3	3	3	3	3	3

wall mirror plane

Table 3.1 pressure [10 N/m²] at 'free surface' in an ideal fluid and with 4 Rankine ovals to create a wall and shallow water, h/T 150%

High (green) and low (red) pressure regions (relative to the pressure at zero speed) can be distinguished in Table 3.1. The entire low pressure region at both sides of the vessel is responsible for the vertical sinkage (squat). The depression with a higher magnitude between ship and bank (starboard side) relative to the other side of the vessel (port) is responsible for the overall attraction force of the vessel towards the closest bank.

3.2.4 Idealised fluid

Some of the consequences of some drastic simplifications (idealised fluid) can be seen in Figure 3.4. In this figure the pressure at the 'free surface' for one lateral position (y_0=0.4 B from the vertical wall) is plotted. This plot is slightly similar as the

registration of a wave gauge at an earth fixed position. Remark the symmetry along the midship (position x_0=0). As a result of this symmetry the integrated pressure at the bow equals the pressure at the stern.

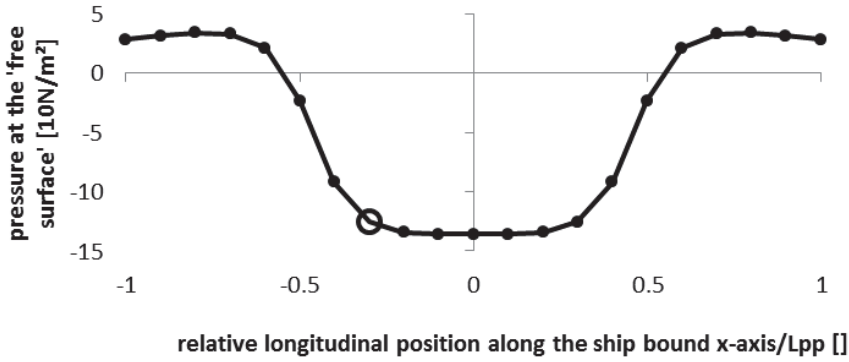

Figure 3.4 'free surface' pressure at one lateral position between ship and bank/mirror at y_0=0.4m

If the pressure over the entire domain is integrated the result will be zero. This is a consequence of D'Alembert's principle and means the vessel (represented by a Rankine oval) in an irrotational and non-viscid fluid does not have a resistance. The bow wave is compensated by the stern wave.

3.2.5 Attraction force

The lower pressure between the starboard side of the vessel and the vertical wall/mirror and the port side is shown in Figure 3.5. In this figure the pressure on the free surface, perpendicular to the vertical wall and at a position of 30% of Lpp behind the midship section is plotted. The pressure difference between both sides of the vessel is clearly seen. In between the vertical wall and the starboard side of the vessel the integrated pressure is lower than the integrated pressure at the port side. When integrated over the entire draft of the vessel/Rankine oval this pressure difference results in an overall force directed towards the bank (attraction of the vessel towards the bank).

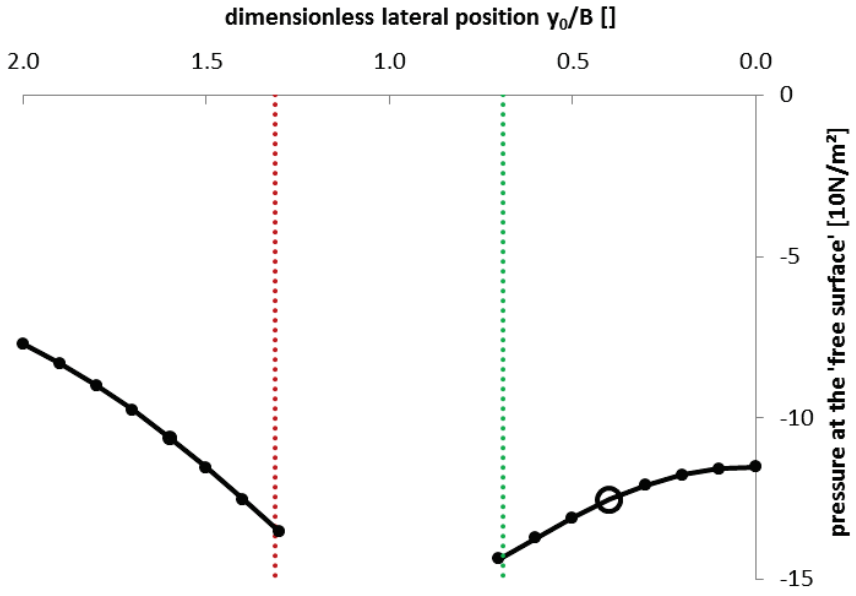

Figure 3.5 pressure at 'free surface' for one longitudinal position at both sides of the Rankine oval

3.3 Kelvin and Havelock

In Table 3.2 the pressure is shown at a very small water depth of only 110% of the draft of the vessel (again, in this Rankine case the draft always equals half the beam).

x_0/Lpp	y_0/B 2.0	1.9	1.8	1.7	1.6	1.5	1.4	1.3	1.2	1.1	1.0	0.9	0.8	0.7	0.6	0.5	0.4	0.3	0.2	0.1	0.0
1.0	2	2	2	2	2	2	2	2	3	3	3	3	3	3	3	3	3	3	3	3	3
0.9	2	2	2	2	2	2	3	3	3	3	3	3	3	3	3	3	3	3	3	3	3
0.8	1	2	2	2	2	3	3	3	3	4	4	4	4	4	4	4	4	4	4	4	4
0.7	1	1	2	2	2	3	3	4	4	4	5	5	5	4	4	4	4	4	3	3	3
0.6	-1	0	0	1	1	2	3	4	5	6	7	6	6	5	4	3	3	2	2	2	2
bow 0.5	-3	-3	-3	-3	-3	-3	-3	-2						0	-1	-2	-2	-2	-3	-3	-3
0.4	-6	-7	-7	-8	-9	-11	-13	-16						-15	-13	-11	-10	-9	-9	-8	-8
0.3	-8	-9	-10	-10	-11	-12	-14	-15						-16	-15	-14	-13	-13	-13	-12	-12
0.2	-9	-9	-10	-11	-11	-12	-13	-13						-15	-15	-14	-14	-14	-14	-14	-14
0.1	-9	-10	-10	-11	-11	-12	-12	-13						-14	-14	-14	-14	-14	-14	-14	-14
0.0	-9	-10	-10	-11	-11	-12	-12	-12						-14	-14	-14	-14	-14	-14	-14	-14
-0.1	-9	-10	-10	-11	-11	-12	-12	-13						-14	-14	-14	-14	-14	-14	-14	-14
-0.2	-9	-9	-10	-11	-11	-12	-13	-13						-15	-15	-14	-14	-14	-14	-14	-14
-0.3	-8	-9	-10	-10	-11	-12	-14	-15						-16	-15	-14	-13	-13	-13	-12	-12
-0.4	-6	-7	-7	-8	-9	-11	-13	-16						-15	-13	-11	-10	-9	-9	-8	-8
stern -0.5	-3	-3	-3	-3	-3	-3	-3	-2						0	-1	-2	-2	-2	-3	-3	-3
-0.6	-1	0	0	1	1	2	3	4	5	6	7	6	6	5	4	3	3	2	2	2	2
-0.7	1	1	2	2	2	3	3	4	4	4	5	5	5	4	4	4	4	4	3	3	3
-0.8	1	2	2	2	2	3	3	3	3	4	4	4	4	4	4	4	4	4	4	4	4
-0.9	2	2	2	2	2	2	3	3	3	3	3	3	3	3	3	3	3	3	3	3	3
-1.0	2	2	2	2	2	2	2	2	3	3	3	3	3	3	3	3	3	3	3	3	3

wall mirror plane

Table 3.2 pressure [10 N/m²] at 'free surface' in an ideal fluid and with 4 Rankine ovals to create a wall and shallow water, h/T 110%

Even at very low water depths (as in Table 3.2 with a h/T ratio of 1.10) there is no excessive high pressure region between the forward part of the vessel and the bank. This is because of two main simplifications; the potential flow is frictionless and the absence of an interface water – air.

3.3.1 Kelvin angle

The boundary condition on the free surface which imposes that all particles at the free surface always stay at the free surface, results in the dispersion relation. Because of the absence of a free surface there is no Kelvin wave system in present type of potential flow. Kelvin wave patterns can be modelled with potential flow but not without free surface as is the case in this assumption. Therefore the Kelvin angle is calculated according to (Havelock 1908). In this publication column "p" in Table III is incorrect, the correct values

are 10.00; 8.00; 6.00; 5.00; 4.00; 3.01; 2.07; 1.31; 1.08; 1.01; 1.00. This calculation error has no consequences.

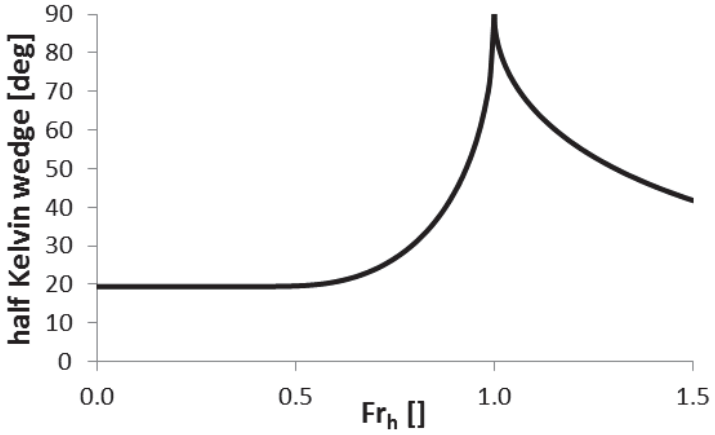

Figure 3.6 half the Kelvin wedge α in shallow but open water $(Fr_h = V/\sqrt{gh})$

$$\cos^2 \alpha = \begin{cases} \frac{8(1-2kh/\sinh 2kh)}{(3-2kh/\sinh 2kh)^2} & Fr_h < 1 \\ 1 - \frac{1}{Fr_h{}^2} & Fr_h \geq 1 \end{cases} \tag{3.4}$$

To obtain the shallow water wave number k_i (with i the i^{th} iteration) the iteration starts with the deep water wave number k_0:

$$k_0 = \frac{g}{(U \cos \alpha)^2} \tag{3.5}$$

And the iteration equals and stops when $k_i - k_{i-1} \approx 0$:

$$k_i = k_0 \tanh k_{i-1} h \tag{3.6}$$

Figure 3.6 shows the influence of the water depth dependent Froude number on half the Kelvin wedge α in the sub and super critical speed range. The Kelvin wedge remains 19°28'27" until Fr_h is about 0.5. From this speed on the angle increases rapidly up to the maximum of 90° at the critical speed. In confined water the critical speed will be smaller than Fr_h=1 (Schijf 1949) and as a consequence the Kelvin angle will increase at lower water depth dependent forward speeds.

3.3.2 Pressure shift

The increase of the Kelvin angle is a clear indication of shallow water effects (Soomere 2007) on the vessel. In shallow water the Kelvin angle α increases because of the influence of the bottom on the dispersion relation. This results in an increased pressure which creates a congestion in the gap between the first half of the vessel and the bank-bottom. The high pressure region according to the Bernoulli principle calculated with potential flow theory located more to the front of the vessel shifts into the fore region around the ship. This compensates and overcomes the Bernoulli depression (which is pushed backwards). Now there is a higher pressure region between vessel and bank along the first half of the vessel. This results in a repulsion force away from the closest bank at the fore part of the vessel.

The combination of the repulsion force at the forward part of the vessel and the attraction force at the aft results in a large bow-out moment. Sometimes the overall attraction force becomes even a repulsion away from the closest bank.

3.4 Model test example

More than 10 000 model tests especially dedicated to bank effects are carried out in the Towing Tank for Manoeuvres in Shallow Water (cooperation Flanders Hydraulics Research — Ghent University) in Antwerp, Belgium. These tests are extensively expounded in next Chapter 4.

Figure 3.7 model test with a tanker model in a rectangular cross section with width W=5B

3.4.1 Model test

Among all those tests some are carried out with a scale model of a Very Large Crude oil Carrier (VLCC) (Appendix 11.4.4) in a rectangular cross section. The width of this rectangle is five times the breadth of the vessel and the height is 1.5 times the draft (Figure 3.7). A mathematical model for the vertical sinkage and trim based upon these tests is published in (Lataire et al. 2012). The model is towed at a forward speed of 12 knots according to full scale (scale factor 75). During these model tests some wave gauges registered the free surface at different discrete positions (Figure 3.7 and Figure 3.8).

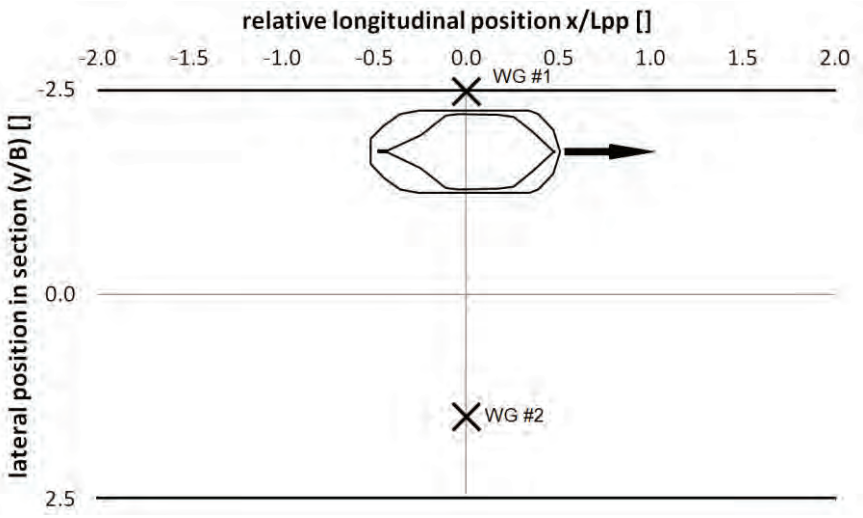

Figure 3.8 position of wave gauges × (WG#1 and WG#2) in the test section of the towing tank

One wave gauge (wave gauge #1) is positioned at the port side of the vessel and (very) close to the vertical wall (20 mm from the vertical wall, 180 mm from the flat of side of the vessel at port). The other gauge (wave gauge #2) is positioned at a lateral distance of 773 mm from the other wall (and at a lateral distance of 2120 mm from the starboard side of the ship model). Both at the fixed longitudinal position 19 m from the origin of the earth fixed coordinate system of the towing tank.

3.4.2 Registration of the free surface

The registrations of these gauges are analysed and ground the assumptions previously made on bank effects.

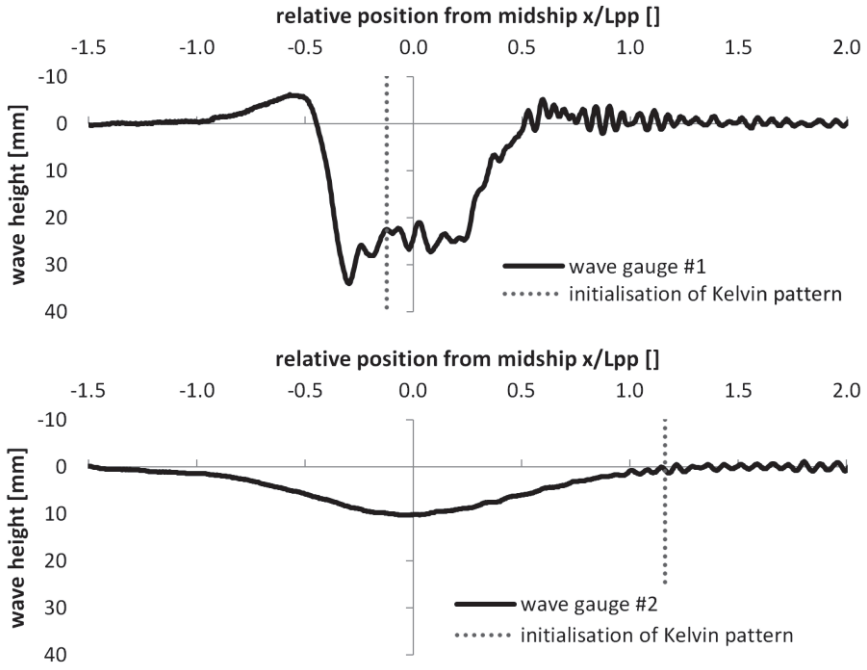

Figure 3.9 registration of wave gauges #1 & #2, dotted line is the expected initialisation of Kelvin pattern based upon (Havelock 1908)

In Figure 3.9 the two registrations of the wave gauges are plotted as a function of a dimensionless position of the vessel. A Fast Fourier Transformation (FFT) is executed for the registration of wave gauge #1 (Figure 3.10). For both registrations a high (about 2 Hz in FFT) and low order (about 0.2 Hz) frequency can be distinguished.

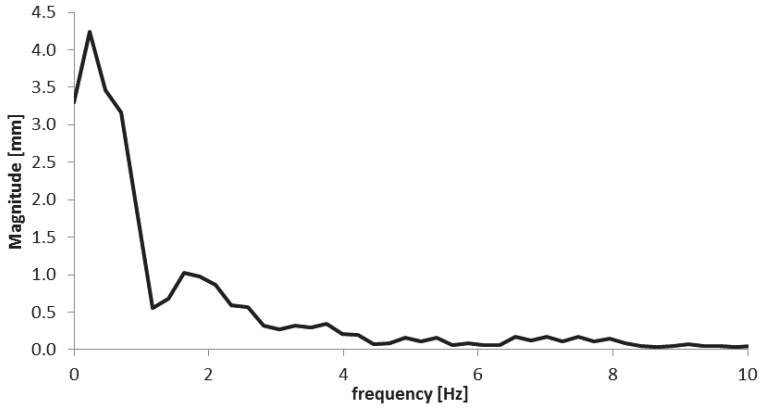

Figure 3.10 Fast Fourier Transformation of wave registration at wave gauge #1

3.4.3 Bernoulli wave system

The lower order frequency (with a wave length of about 1 ship length) is attributed to the Bernoulli system. The lower pressure region travels at the same speed but also at the same longitudinal position of the vessel over almost the entire width of the fairway. This lower order pressure distribution is in shape similar to the results obtained with the potential flow theory in section 0. The symmetry as mentioned in the potential flow between the fore and aft half of the vessel does not stand. The higher wave height at the bow than at the stern will result in (added) resistance. This also indicates a larger high pressure region at the fore than at the aft section. This, in combination with the asymmetry between port and starboard side, generates a yaw moment pushing the bow away from the closest bank.

This Bernoulli system with a broad area of water level drop around the vessel is also accountable for the vertical sinkage and trim of the vessel as well as the overall attraction force towards the vertical wall.

3.4.4 Kelvin wave pattern

The higher order frequency (in this example wave lengths of about 7% Lpp) is attributed to the Kelvin pattern. Remark the later initiation of this higher order frequency on wave gauge 2 compared to wave gauge 1. This is because of the position further away from the vessel. The exact initiation can be computed with basic goniometry and the Kelvin angle according to the correct water depth (Figure 3.9 and Figure 3.11).

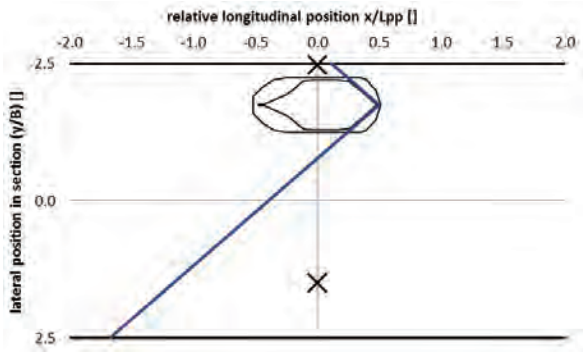

Figure 3.11 cusp locus according to Kelvin added (Fr_h=0.353)

The sooner initialisation of the Kelvin pattern is attributed to the full geometry of the vessel while the calculation is based upon a travelling point at the position at the forward perpendicular. If this point is shifted more towards the front of the vessel a better prediction is obtained (Appendix 11.3).

3.5 Simulation example

3.5.1 Trace

The full mission ship manoeuvring simulators at Flanders Hydraulics Research (in next chapter more details on these facilities are added) contain a mathematical model for bank effects as published in (Lataire & Vantorre 2008). The aim of present example is to show the need for an accurate and reliable model for the bank effects. In the specific example here two simulators are coupled and the meeting of two large container carriers (both with Lpp=381m) on the River Scheldt (close to the Europaterminal in the harbour of Antwerp, Belgium) is simulated. The vessel coming

from sea heading toward the Deurganck Dock (going north to south in the plot of Figure 3.12) is of most interest here.

3.5.2 Bow-away moment

Around green buoys 89A and 91 the vessel encounters an attraction force in combination with a bow-away moment (bow towards port) due to bank effects. The ship has a forward speed of about 12 knots at this moment which is a rather high speed sailing so close to the bank. The bow-away moment must be compensated with a rudder angle pointing the bow of the vessel again towards the green side of the natural river. The combination of the bow-away moment because of the bank effects and the moment induced with the rudder yawing the ship towards starboard results in a lateral shift directed to the other side of the fairway (although there is an attraction force directed to the green side by the bank). In this specific example this lateral shift is so drastic that the meeting of both ships was carried out green on green (non-conventional starboard-starboard) to be able to pass without harm.

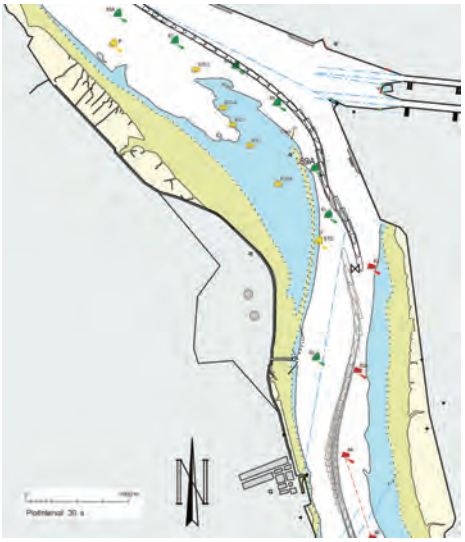

Figure 3.12 track plot of a simulation of a meeting of two large container carriers on the river Scheldt in the port of Antwerp with the ship going southwards suffering from bank effects at buoy 89A (from FHR m689/4 run 112)

The induced moment is by far the most dangerous consequence of bank effects. The vessel loses manoeuvrability because the moment must be compensated by the rudder while this rudder already must cover the track-keeping through the fairway itself. Because of the bow-away moment in combination with the (incomplete) compensation of this moment a lateral shift towards the centre of the fairway comes into existence and the vessel ends up at the wrong side of the river.

3.5.3 Propeller action

Sometimes the propeller action is decreased when a calamity is expected but this drop in (forward) propeller action decreases also the impact of the rudder on the manoeuvrability of the vessel. The ship already sails at a rather slow speed in confined waters compared to open and deep waters as well as the efficiency of the rudder without a jetstream generated by the propeller. Therefore it is recommended to keep the propeller rate at a minimal value when suffering from bank effects to keep the manoeuvrability of the vessel at a minimal level (Eloot et al. 2007).

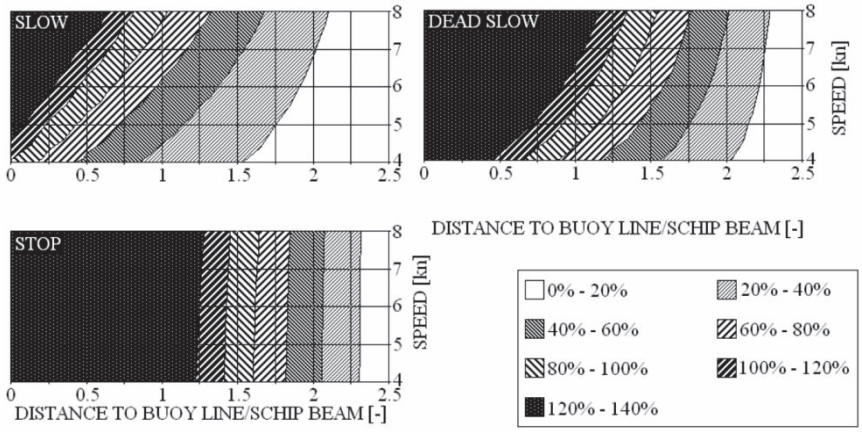

Figure 3.13 required rudder capacity to keep track in the Gaillard Cut (2007 situation) at different propeller rates when the ship is aligned before a meeting. From (Eloot et al. 2007)

In Figure 3.13 the required rudder capacity (maximum rudder deflection corresponds with 100%) to keep track is plotted for

three different propeller actions (stop, dead slow and slow), different forward speeds (4 up to 8 knots) and the ratio between the distance to the buoy line and the ship's beam. A larger magnitude of the rudder angle is required the closer the ship sails to the buoy line, the lower the propeller rate and the faster the ship sails.

3.6 Real life calamity

3.6.1 Pelican I and Maersk Bahrain

Sunday 20th April 2003 the container carrier Pelican I collided with the container carrier Maersk Bahrain in the Bend of Bath on the River Scheldt (Roemers & Pimentel 2005).

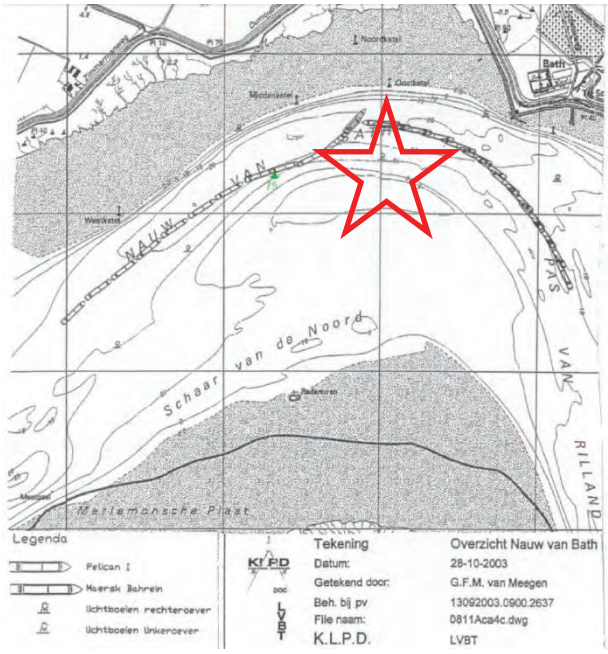

Figure 3.14 tracks of the vessels Pelican I (left) and Maersk Bahrain (right) before colliding from (Roemers & Pimentel 2005)

In Figure 3.14 the tracks of both vessels are plotted on the nautical map at the Nauw van Bath. The track of the Pelican coming from sea heading towards the harbour of Antwerp (easterly heading) is the vessel that suffered from bank effects. At

about buoy 75 the vessel is attracted towards the closest bank (Platen van Saeftinge), her bow is pushed away towards the centre of the fairway and heavy vibrations on the vessel are reported (Roemers & Pimentel 2005). These vibrations are known by pilots and occur when the waves coming from the vessel travel along the vessel at a higher speed than the critical speed. A breaking wave sailing along with the vessel can be observed (Figure 3.15).

Figure 3.15 standstill from video taken from the top deck of the Super Tanker looking down on three surfers in Summer 2006
www.youtube.com/watch?v=C5PsF7y1Jdk

Since the bow of the vessel is pushed away from the bank, the rate of turn to make the bend is not only diminished but the ship even turns into the wrong direction. The vessel starts turning to port while it must turn to starboard to make the curve in the fairway. This is why the Pelican ended at the wrong side of the river bumping into the container carrier Maersk Bahrain.

Figure 3.16 salvage of the Pelican I source:
www.cargolaw.com/images/disaster2003_pelican3.GIF

3.6.2 Simplification

Of course more elements than bank effects are involved preceding this calamity (such as propeller actions, rudder actions, miscommunication etc.) but for reasons of simplicity these are not taken into account here. It is out of the scope of present work to point out the responsible persons for this accident. This is done and published in (Roemers & Pimentel 2005). The sole aim of present example is to point out the importance of bank effects on a safe trip on a restricted and confined fairway.

Bank Effects

4 MODEL TESTS

There is only a very limited amount of test results dedicated to bank effects available in publications. In most published papers the data is incomplete or intentionally concealed. Furthermore most tests are carried out along a vertical wall which is only a very specific type of bank geometry. The types of bank geometries of interest for Flanders Hydraulics Research are not tested or published in a workable category of data.

Model tests in a towing tank cannot (and will not in the near future) be replaced by mathematical calculations such as Computational Fluid Dynamics (CFD) although the calculation power of computers keeps on increasing and CFD-programs become more user-friendly. It can be expected that both (CFD and model tests) will extend the knowledge of complex (shallow water) hydraulics with their specific merits. CFD-programs coping with the shallow water problem are rare and sometimes suffer from the main influence of all boundary layers (on the hull, appendages, bottom, banks). Furthermore the software and hardware do not become cheap (but open source CFD like OpenFOAM does exist). The calculation time to mathematically simulate only one steady state test carried out in a towing tank (less than one hour in between two runs) takes as much as 40 hours on 48 processors

(Capron & Barbieux 2012). On the other hand the running and investment cost of a towing tank must not be underestimated.

As bank effects are considered to be a decisive factor for the admittance policy for large, deep-drafted ships to ports making use of confined access channels, a research project on the topic was initiated by the administration of the Flemish Government. In 2006-2007 about 12.000 systematic model tests were carried out with two ship models and 8 different bank geometries in the Towing Tank for Manoeuvres in Shallow Water (cooperation Flanders Hydraulics Research — Ghent University) in Antwerp, Belgium. In 2010 this systematic series was extended with more than 2.000 model tests with 5 different ship models and 4 surface piercing bank geometries.

This data set is as far as known/published the most extensive and largest set of model tests dedicated to bank effects. This data set has been extended with some historic tests carried out at the same facilities in Antwerp (not specifically dedicated to bank effects but applicable) but also with some model tests which are obtained by a data exchange with a foreign research institute. This data exchange is carried out under a specific confidentiality agreement. Therefore these data are referred to from hereon as "*Data exchange 1*" or abbreviated to DE1.

4.1 Test Facilities

Different test facilities are used in present research. The main properties and particularities are explained.

4.1.1 Towing tank Flanders Hydraulics Research

4.1.1.1 Scope

Most of the tests have been carried out in the *shallow water towing tank of Flanders Hydraulics Research (cooperation Flanders Hydraulics – Ghent University)* or FHR towing tank. A technical overview of this towing tank can be found in (Van Kerkhove et al. 2009). Commissioned by the Flemish Government the towing tank was built in 1992 to provide more scientific insight into the shallow water issues encountered by the increasing vessel sizes calling the Belgian/Flemish harbours. Knowledge obtained in this towing tank provided the input to optimize the ship manoeuvring simulators at Flanders Hydraulics Research for shallow water navigation.

The reason of existence of the towing tank is thus slightly different from most tanks. There is no significant interest into resistance tests of new designs but merely on the shallow water manoeuvring behaviour of vessels calling the Belgian harbours. The equipment of the towing tank was designed for captive model testing but since 2009 the carriage has been adapted enabling free running manoeuvring tests.

4.1.1.2 Towing Tank

The FHR towing tank has a total length between the walls of 87.5m but because of the presence of wave damping devices, a wave generator and a harbour for model preparation the useful length for model tests is 68.0m. The width of the tank is equal to 7.0m over the entire useful length. In the early nineties these rather modest dimensions were thought to be sufficient for manoeuvring tests with ship models of about 4 m length between perpendiculars since the maximum forward speed during these tests is also modest (<1.5m/s).

The increasing ship sizes and according scale factor together with an increasing capacity created the need for a second, larger towing tank (Delefortrie et al. 2010). This new towing tank (main dimensions 150x20x1m³) is being designed and is planned to be built within the next years.

The present towing tank can contain only a water depth of 0.50m. Again this shallow water depth is consequent with the purpose of the tank. With this tank depth, water depths up to 250% of the draft of a typical ship model can be tested.

length over all	87.5	m
net length	68.0	m
width	7.0	m
max. water depth	0.5	m

Table 4.1 the main dimensions of the towing tank at FHR

Sometimes model tests are carried out in extremely shallow water. At rest there is only a very small absolute gap between the keel of the ship model and the bottom of the tank (about 15mm). For this reason it is of the utmost importance to have a very accurate bottom of the towing tank. After years of usage the bottom fell out of the required range and in 2008 the entire bottom was flattened again with a milling machine. After this operation an absolute accuracy of ±1mm over the entire surface of the tank is obtained (Appendix 11.4).

For the same reason the alignment and position of the rails running on both sides of the tank are checked regularly and adjusted if necessary.

4.1.1.3 Carriage

The base construction of the main carriage (Figure 4.1) is a combination of lateral and transversal girders running over the rails. The planar motion mechanism is the combination of a longitudinal carriage, lateral carriage and turning table, controlled independently, resulting in an arbitrary trajectory in the horizontal plane imposed on the ship model.

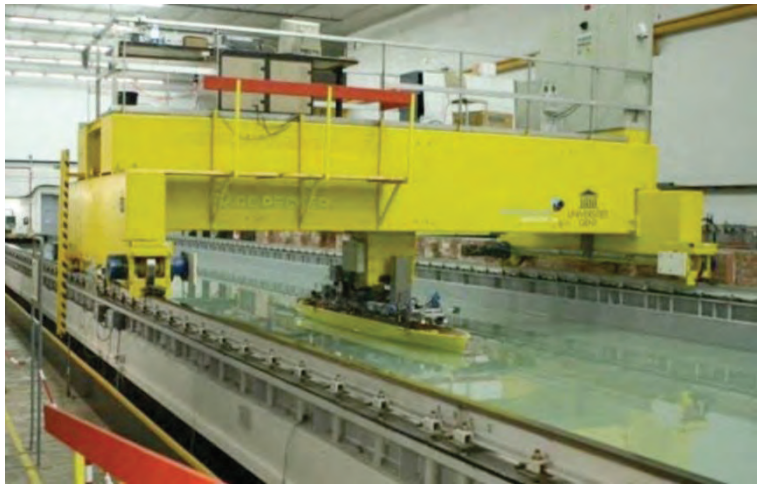

Figure 4.1 main carriage of FHR towing tank with a ship model in captive towing condition

A very unique feature of the carriage is the fully automated and unmanned manner of executing model tests. Experiments are executed in batch in a fully automatic way 24/7. Because of the time needed for the water to calm down in between two runs about 35 tests can be executed in 24 hours. The long term average is 25 model test runs a day because of the required build in time between projects, changing ship models, specific calibrations etc.

A predetermined trajectory is followed by the ship model during a captive manoeuvring test. Forces, positions, rate of turns, moments are measured of hull and appendages (Section 4.6.6) but also measurements of the wave system in the tank can be registered.

4.1.1.4 Interaction features

The tank is equipped with different devices to be able to investigate external influences or interactions with the ship model. A piston type wave generator is installed at the end of the towing tank (with a flap of the same width of the tank). Both regular and irregular wave patterns can be generated; typical results are the wave induced vertical ship model motions in shallow water.

The tank is also equipped with an auxiliary carriage for towing a second ship model independently from the ship model towed with the main carriage. This second carriage moves the ship model with a speed controlled belt, only at courses parallel to the longitudinal direction of the tank. With this device the overtaking, overtaken and meeting of two vessels can be simulated.

If the required speed in the longitudinal direction of the tank is the same for both vessels under consideration then a second beam can be attached to the main carriage. This has been done for tests on ship to ship interaction during lightering manoeuvres (Lataire et al. 2012) and ship – tug interactions (Geerts et al. 2011).

Volumes with a predefined shape are installed in the tank for the research on bank effects. Different types of concept to obtain these volumes can be distinguished. The more gently sloped banks consist of a protection layer on the bottom of the tank with pebbles on top of it and finished with a layer of screed (Figure 4.2). This type of banks can be used only once.

Figure 4.2 protection layer, pebbles and screed as finishing layer for gently sloped banks (under construction)

For steeper banks moulded modules are used which can be reused afterwards. Fibre reinforced concrete is poured into the mould and the blocks are aligned in the towing tank (Figure 4.3). Specific

attention is given to the toe of this bank which is sealed to the bottom to be water tight.

Figure 4.3 moulded block for a bank with slope 1/1

Less steep banks consisted out of a moulded toe, a support block and a water resistant plate (Figure 4.4) which is again sealed to the toe and the adjacent plates at all sides. This is very important to avoid water to leak through the bank (although both sides stand in the water).

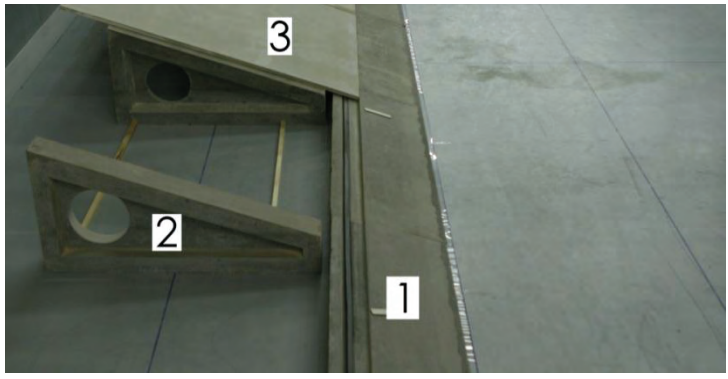

Figure 4.4 installed bank consisting of moulded toe (1), support (2) and water resistant plate (3)

Vertical banks are installed by carpentered constructions made of concrete plywood. These constructions are loaded with concrete tiles at the back to avoid floating and ensure a watertight sealing

between the installed bank and bottom of the towing tank. The gaps between separate blocks are also sealed (Figure 4.5).

Figure 4.5 vertically installed walls being sealed

4.1.2 Towing tank Data exchange 1

The model tests for data exchange 1 (DE1) are carried out in two different facilities. Some tests have been carried out in a deep water towing tank, others in the shallow water basin. This tank has a water depth of about 5 meters, a length of 50 times a standard length of the ship model and a width of 10 to 15 times the ship model's beam. The sloped banks were installed in the manoeuvring basin with a width of almost 50 times the ship's beam and a length of 20 times the length of the vessel. In this tank model tests can be carried out at very low water depths.

4.1.3 Ship Manoeuvring Simulator Flanders Hydraulics Research

4.1.3.1 Goals of a simulator

A better mathematical model to be implemented in the ship manoeuvring simulators of Flanders Hydraulics Research is one of the main reasons for the research on bank effects. Flanders Hydraulics Research owns three full mission bridge simulators, one of them is dedicated for inland vessels, the other for seagoing vessels or Voith Schneider propelled tug boats.

In general, ship manoeuvring simulators are used in two manners: The simulator can either be used for training purposes of pilots, captains or naval academy students or as a research tool for testing waterway designs in a virtual environment where human experience is of uttermost importance. The latter is the main but not the sole purpose of the FHR simulators, which are also used for training (river pilots, students, tug boat captains, etc.).

4.1.3.2 Elements of a simulator

The ship manoeuvring simulator consists of a mock-up of a ship's bridge with all necessary manoeuvring equipment. These can be hardware (tiller, telegraph, communications) or displayed on a LCD monitor (Electronic Chard Display Information System ECDIS, wind information, engine information, radar, alarms, CCTV,...). The outer image is projected on a standing tube (with the bridge in it) with the beamers projecting from the outside of the tube. The angle of projection defines the name of two simulators; SIM225 has an aerial view of 225° and SIM360+ has an all-round view with horizontal projection for lock approaches, berthing manoeuvres, passage of bridges, etc. (hence the "+" in the name). The inland navigation simulator (named Lara) uses seven 52 inch LCD-screens instead of projectors.

In a separate operator's room the complete boundary conditions can be set and changed in time. Among others these are; the area where the ship operates, wind force and direction, current, time (day/night), water level, season (date), other traffic, alarms (fire, engine...), operation of lock doors, tug assistance and so on.

4.1.3.3 Mathematical model

The force balance of the ship is determined (with a frequency of 10 Hz) based on the mathematical model of the ship and taking into account all external influences (banks, weather, current,...). The mathematical model resolves the force balance in the horizontal plane (longitudinal and lateral movement and yawing) and roll and vertical motions, the solutions are sent back to the bridge and visualisation devices (both on equipment and projection). The visuals are refreshed at 60 Hz (with linear

interpolation between two steps of the mathematical model) to obtain a smooth image.

The following influences can be taken into account in the present mathematical model (Figure 4.6). Some are very unique and based on very extensive in house research (e.g. mud layer (Delefortrie et al. 2005)) others are more straightforward (e.g. current, bank effects).

- recording forces, orders, position and speeds for subsequent analysis
- in case of a collision: registration of the collision (location, impact forces)
- the ship's track
- hydrodynamic forces: powers on hull, rudder, appendages
- shallow water effects (bottom level in function of location, water level in function of tides)
- propulsion (propeller, engine dynamics, bow thruster, stern thruster , malfunctions)
- restricted water effects (bank effects)
- aerodynamic forces (gusts of wind, wind direction and wind speed in function of location, shielding effect of large constructions or ships)
- wave drift (wave height and direction in function of the position)
- effects of non-uniform current (current speed and direction in function of position)
- contact forces (reaction and friction powers of fenders, pole and quays) with non-stationary hydrodynamic powers (current effects), in function of distance to quay-wall
- interaction with meeting and overtaking target ships.
- Manoeuvring in muddy navigation areas

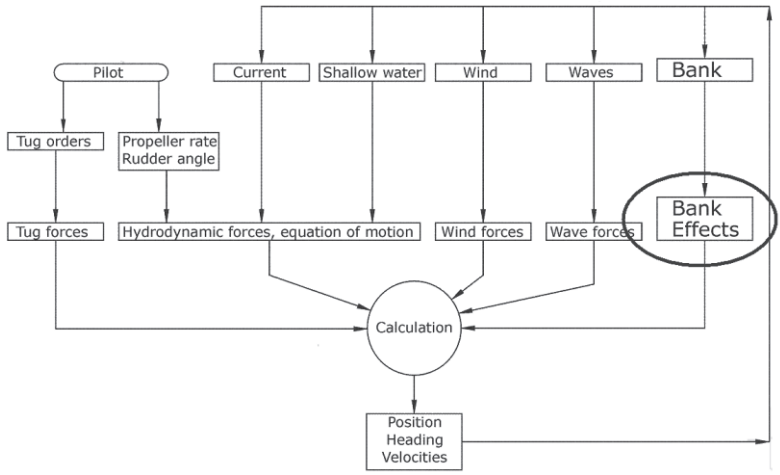

Figure 4.6 simplified mathematical model of the FHR simulators

4.2 Ship models

Only the ship models used during model tests on bank effects (sailing in a non-symmetric lateral position in the fairway) are taken into account. In Appendix 11.5 the linesplan and hydrostatic properties of all these ship models are listed.

4.2.1 Container carriers (2)

For the Belgian ports of Antwerp and Zeebrugge container carriers are responsible for the largest part of traffic (Figure 4.7). Therefore two ship models of container carriers have been used.

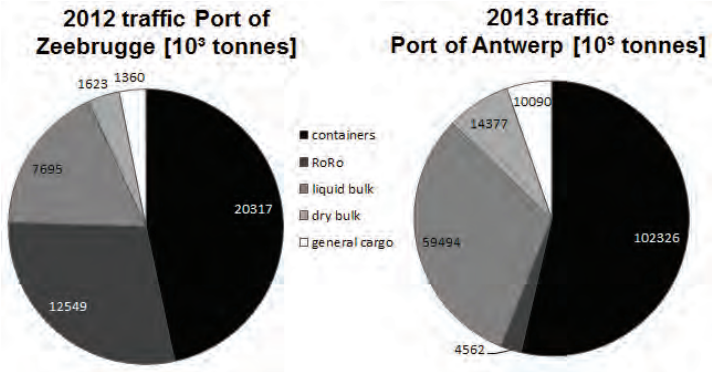

Figure 4.7 2012 traffic Port of Zeebrugge and 2013 traffic Port of Antwerp http://www.portofantwerp.com/nl/news/recordoverslag-haven-van-antwerpen-bevestigd and http://www.portofzeebrugge.be/en/node/495

4.2.1.1 8000 TEU container carrier C0U

Ship model C0U represents a single screw 8000 TEU container carrier on a scale 1/80.8. The ship model was commissioned in 2004 to replace the largest container carrier ship model (C0D, 6000 TEU) at FHR. The continuous increase in container ship sizes results that nowadays an 8000 TEU container carrier can contain not even half the amount of all containers that can be carried by the largest container carrier (Maersk Triple E class can carry 18000 TEU, www.worldslargestship.com).

The ship model C0U has been tested at three different drafts; two even keel and one with initial trim. The main hydrostatic properties and the linesplan are added in Appendix 11.5.1.

4.2.1.2 12000 TEU container carrier C0P

A second single screw container carrier ship model is used. C0P is a 12000 TEU container carrier with the maximum main dimensions that can call the to-be-finished Panama locks. This ship model has been built at a scale of 1/80 and only tested at the design draft of 15.20m full scale. Hydrostatics and the linesplan are added in Appendix 11.5.2.

4.2.2 Tankers (4)

4.2.2.1 LNG-tanker G0M

A dedicated terminal in the port of Zeebrugge serves as a gateway to supply Liquefied Natural Gas (LNG) dedicated for consumption in North West Europe and as a hub for the international natural gas market. LNG is delivered to the spot by LNG-tankers but also stored, traded and exported from the same location.

A ship model of the Belgian built 135 000 m³ LNG-tanker *Methania* has been tested along a wide range of bank geometries. The model has been tested at only the draft at full loaded sailing conditions since this is the more critical situation (smallest under keel clearance and relative dangerous cargo). Hydrostatic properties and the linesplan are available in Appendix 11.5.3.

4.2.2.2 VLCC T0Z

The ship model T0Z has the lines of the openly available KVLCC2 Moeri Tanker (Stern & Agdrup 2008) and is of high value for comparing towing tanks worldwide and for CFD-calculations in shallow water (Zou & Larsson 2013). Hydrostatics of this vessel have been published online and listed in Appendix 11.5.4. In the same Appendix 11.5.4 the lines plan is added. Although vessels with a draft of more than 20 m (as this vessel) can call none of the Belgian harbours, vessels with a high block coefficient and similar ratio between the main dimensions as T0Z do call the Flemish ports.

4.2.2.3 Tanker T0S

A limited amount of tests are carried out with a ship model of a smaller tanker (LxBxT 265.6x41.6x11.0). Other properties and linesplan are listed in Appendix 11.5.6.

4.2.2.4 British Bombardier T0H

This ship model of the tanker *British Bombardier* is only chosen because of its very modest main dimensions on model scale (Appendix 11.5.5). The draft during the model tests was unrealistically high because of the small displacement of the vessel compared to the relative high minimal weight of the device to connect this ship model with the carriage for PMM testing (Figure 4.8). In Appendix 11.5.5 the linesplan of this sixties design (built in 1962) is added.

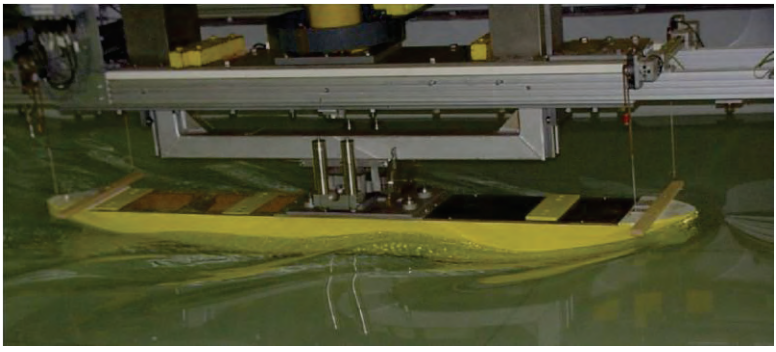

Figure 4.8 small freeboard on T0H during captive model tests

4.2.3 Ro-Ro vessels (3)

A lot of cars are transported out of (and into) Belgium through the harbours of Ghent, Antwerp (1.3 million cars in 2013) and Zeebrugge (1.7 million new cars in 2012) but also other RoRo-activities take place (flatbed trailers among other types).

4.2.3.1 Car carrier A01

This is a twin screw ship model of a car carrier and added to the program for its specific lines (Appendix 11.5.7) and twin screw propulsion system. For bank effects this means there is an active propeller relatively close to the bank compared to a single screw propulsion system.

4.2.3.2 RoRo ferry A0S

The model of this RoRo ferry is towed in the towing tank without a propeller attached to the model. This model is used only for a limited amount of tests. Properties can be found in Appendix 11.5.8.

4.2.3.3 Catamaran R0S

A very different geometry of the hull is added to the tests with this catamaran type of RoPax (Appendix 11.5.9). The twin hulls wave pattern will interfere and sailing along one bank the hull closer to the bank will endure much larger bank effects than the hull at the other side. Of course both hulls are rigidly connected and therefore the forces on the entire ship model and not on the separate hulls are measured.

4.2.4 Inland vessel B01

Model tests are carried out in the FHR shallow water towing tank with an inland vessel to provide the full bridge inland simulator Lara with dedicated mathematical models (in this specific case for bank effects). This model is based on the CEMT (Conférence Européenne des Ministres de Transport) class Va. Tests are carried out only at the design draft of the vessel. Hydrostatic properties and linesplan are added in Appendix 11.5.10.

4.2.5 Wigley hull W01

The final model used in present research on bank effects is a different type of model. It is not a scaled ship but a mathematically defined geometry with equation:

$$|y| = \begin{cases} B\frac{z}{T}\left(2-\frac{z}{T}\right)\frac{4x}{L}\left(1-\frac{x}{L}\right) & z < T \\ B\frac{4x}{L}\left(1-\frac{x}{L}\right) & z \geq T \end{cases} \tag{4.1}$$

Hydrostatic properties and the linesplan can be calculated analytically or with dedicated software (Appendix 11.5.11).

A Wigley hull is a popular and easy to mesh hull form for CFD-calculations. For comparison and calibration of these calculations the Wigley hull model is added to the database.

First letter	Ship type
C	Container carrier
G	Gas carrier
T	Tanker
A	Car carrier *(Autoboot)*
R	Catamaran (C occupied by Container carrier)
B	Inland vessel *(Binnenschip)*
W	Wigley hull

Table 4.2 name explanation for type of ship model (first letter)

4.3 Bank geometries

Different geometries of banks have been installed in the towing tanks to investigate the influence of the bank geometry on the forces and moments induced on the vessel. Only tests in a steady state regime condition are considered. Therefore the installed bank did not change in geometry for a significant amount of ship lengths (at least six ship lengths) before the ship model decelerates or another bank geometry starts. If more geometries are installed consecutively in the tank, the transition zone of one bank to another is constructed in such a way to create a smooth change in geometry. This is to avoid abrupt and long lasting transition effects.

Three types of installed banks can be distinguished in present (and other published) research:

- A vertical **quay** wall **QY**: A vertical wall is installed in the towing tank (or the walls of the tank itself are used). This quay runs from the bottom of the towing tank up to the free surface (and beyond).
- A **surface piercing** wall **SP**: A sloped bank runs at a constant slope from the bottom of the towing tank up to highest water level tested. This slope is expressed as the ratio between the rise and run with a normalised rise (Figure 4.9).

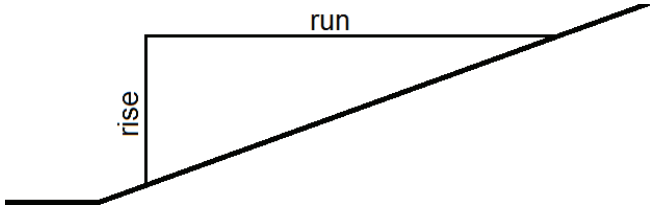

Figure 4.9 rise and run of a sloped bank

$$slope = \frac{rise}{run} \tag{4.2}$$

- A **semi submerged** bank **SS**: A sloped bank starts at the bottom of the towing tank but ends before the free surface is reached. After the slope there is a horizontal (submerged) plane until the wall of the towing tank or an installed vertical quay wall is reached (Figure 4.14).

4.3.1 Vertical quay walls QY

4.3.1.1 Occurrence

In the past, vertical quay walls were the most tested type of banks in a towing tank since the wall of the towing tank itself can be used. Doing so, no expensive geometries must be installed.

On natural rivers a vertical wall does (almost) not exist but in harbour environments it is frequently present. Ships berth at a vertical wall or a quay wall. So when a ship sails along a quay, it sails along a vertical wall. The steeper a bank the more expensive it is to construct and maintain. For this reason, vertical walls occur almost only at quays.

When a ship enters a lock, it is an extreme but common situation of a ship sailing along (two) vertical walls. A ship suffers from a wide range of other hydrodynamic influences entering or leaving a lock (Vantorre & Delefortrie 2013). These specific phenomena are however not in the scope of present research.

4.3.1.2 Quays

Without taking the water level into account, ten different cross sections with a vertical quay wall can be distinguished. Each vertical bank is named as follows: “QY_” (quay) + “0_” (1/slope)

+"W_h" (distance between toes of the banks in the cross section Figure 4.10) + the run of the opposite wall (for most banks a vertical wall or "0").

Figure 4.10 graphic interpretation of the distance W_h

Type	Run/rise	W_h	Opposite bank run/rise	Name
[]	[m/m]	[m]	[m/m]	[]
QY	0	0.812	0	QY_0_0.812_0
QY	0	0.966	0	QY_0_0.966_0
QY	0	1.314	0	QY_0_1.314_0
QY	0	1.933	0	QY_0_1.933_0
QY	0	3.865	0	QY_0_3.865_0
QY	0	4.400	4	QY_0_4.400_4
QY	0	6.330	0	QY_0_6.330_0
QY	0	7.00	0	QY_0_7.00_0
QY	0	10.00	0	QY_0_10.00_0
QY	0	33.00	0	QY_0_33.00_0

Table 4.3 name of the quay walls tested

The banks QY_0_0.812_0; QY_0_0.966_0; QY_0_1.314_0; QY_0_1.933_0; QY_0_3.865_0 have been used with only one ship model (T0Z) to investigate the influence of the blockage on the bank effects. The width W_h of these cross sections are equal to 1.05; 1.25; 1.70; 2.50 and 5.00 times the beam B of T0Z, respectively.

Bank QY_0_4.400_4 is the only vertical wall with a sloped bank at the other side (run equals 4 with rise 1). Because the lateral position of the carriage of the towing tank of FHR is limited, bank QY_0_6.330_0 was installed to be able to tow the ship model at a very close distance to the vertical wall.

QY_0_7.00_0 is the empty towing tank of FHR without any supplementary installed banks.

QY_0_10.00_0 is the empty deep water towing tank of DE1 while QY_0_33.00_0 is the shallow water towing tank from the same data exchange.

4.3.2 Surface piercing banks SP

Surface piercing banks with gentle slopes occur on natural rivers while steeper slopes are mostly present on manmade canal sections.

The most gently sloped surface piercing bank SP_8_4.030_0 has about the same slope (7°) as the (notorious) bend *Bocht van Bath* on the River Scheldt (no. 2 in Figure 1.2) in the Netherlands. This bend is seen as one of the more difficult obstacles (Eloot et al. 2007) for seagoing vessels calling or leaving the harbour of Antwerp (Belgium). These gentle slopes can also be interpreted as a "rising bottom" instead of a "sloped bank".

The slope of a sandy (dredged) bottom can be as steep as 1/5 (SP_5_4.030_0) and 1/4 (SP_4_4.400_0).

Slopes of 1/3 (SP_3_4.200_1) are more common on manmade canals such as Kanaal Gent-Terneuzen and canal docks in the inner harbour of Antwerp. Slopes of 1/1 are not significantly present in Belgium but appear worldwide, for example on the Panama Canal. Furthermore this is an interesting slope to have a wide range of slopes between the gentle slopes and a vertical quay wall (Figure 4.11).

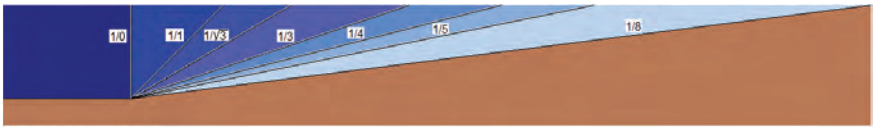

Figure 4.11 all surface piercing tested slopes sharing the same toe

The first and third slopes in Table 4.4 (SP_1_4.200_3; SP_3_4.200_1) are the opposite sides in the same cross section. Bank SP_4_4.400_0 is the sloped opposite side of QY_0_4.400_4.

Type	Run	W_h	Opposite bank run	Name
SP	1	4.200	3	SP_1_4.200_3
SP	$\sqrt{3}$	33.00	0	SP_$\sqrt{3}$_33.00_0
SP	3	4.200	1	SP_3_4.200_1
SP	3	5.730	0	SP_3_5.730_0
SP	4	4.400	0	SP_4_4.400_0
SP	5	4.030	0	SP_5_4.030_0
SP	8	4.030	0	SP_8_4.030_0

Table 4.4 names of the surface piercing banks

4.3.3 Semi-submerged banks SS

Sometimes channels are dredged in open water. Among many others this is the case for the approach channel (Scheur West, Pas van het Zand) towards the harbour of Zeebrugge in the North Sea (Figure 4.12). The water depth of the North Sea in that region is rather shallow (about 10 m under Lowest Astronomical Tide or even less) and a deepened channel is dredged. Doing so a cross section with a deeper part containing the fairway, a sloped bank (here a sandy bottom having a gentle slope) and flat section (the natural sea bottom). Such cross sections are installed in the towing tank and named semi-submerged banks.

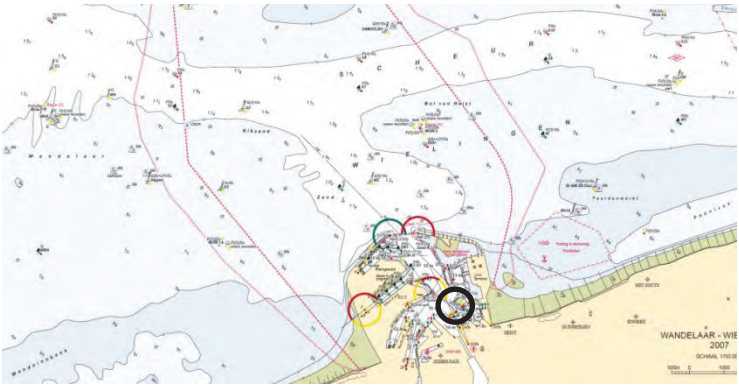

Figure 4.12 Zeebrugge and access channels *Pas van het Zand* and *Scheur*

In the outer harbour of Zeebrugge between the LNG-terminal and open sea there is the *Tern Peninsula* (Figure 4.13).

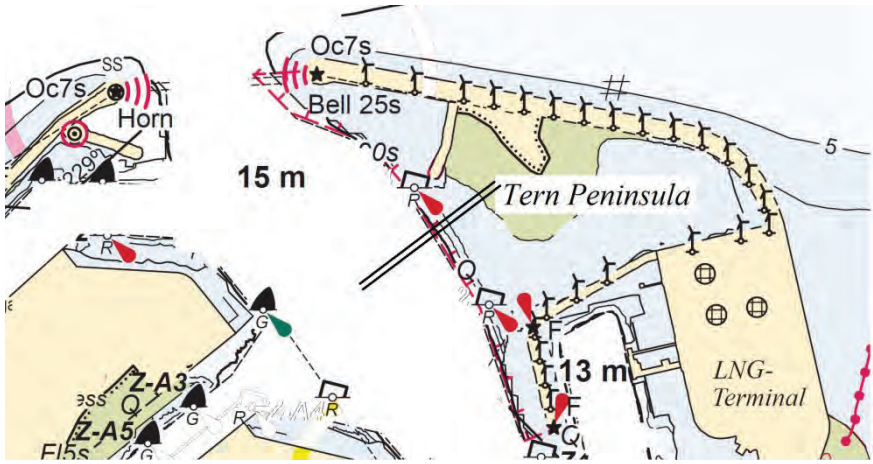

Figure 4.13 a semi-submerged bank section (parallel lines) in the Harbour of Zeebrugge, remark that a lot of navigation aids are removed for reasons of simplicity.

LNG-tankers calling or leaving this LNG-terminal will have to sail along this bank. The influence of the increased peninsula on these tankers was investigated and evaluated in (Lataire et al. 2008). The importance of the geometry of the submerged flat section was pointed out by (Norrbin 1974). Therefore the dimension (width and height) of the submerged flat section was also changed during the model tests (Table 4.5).

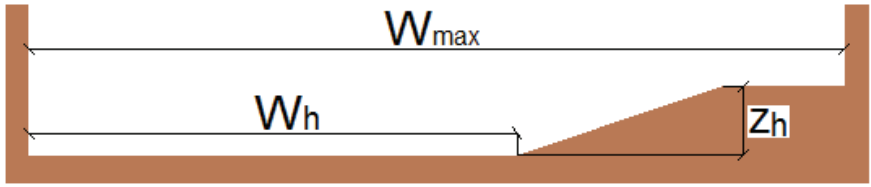

Figure 4.14 semi submerged bank properties W_{max}, W_h and z_h

If the water depth h is larger than z_h, then the geometry in Figure 4.14 is a semi submerged bank. The slope of the submerged bank is still expressed as the run referred to a normalised rise (=1m). The name of the bank under consideration is the combination of

the bank type, run of the submerged part, distance between toes of the banks W_h, total width of the section W_{max}. The run of the other bank is always a vertical wall (run equals 0) for all semi submerged banks. Therefore the 'opposite bank run' is not added in the semi submerged bank name.

type	run /rise	W_h	z_h	W_{max}	Opposite bank run/rise	Name
[]	[m/m]	[m]	[m]	[m]	[m/m]	[]
SS	0	33.00	0.245	33.45	0	SS_0_33.00_.245_33.45
SS	0	33.00	0.305	33.45	0	SS_0_33.00_.305_33.45
SS	0	33.00	0.305	39.00	0	SS_0_33.00_.305_39.00
SS	5	4.030	0.120	7.00	0	SS_5_4.030_.120_7.00
SS	5	4.030	0.150	5.335	0	SS_5_4.030_.150_5.335
SS	5	4.030	0.150	5.890	0	SS_5_4.030_.150_5.890
SS	5	4.030	0.150	7.00	0	SS_5_4.030_.150_7.00
SS	8	4.030	0.150	7.00	0	SS_8_4.030_.150_7.00

Table 4.5 geometric dimensions of the semi submerged banks

4.4 Test conditions

Four parameters varied during the model tests are summarized here: the water depth, the lateral position in the cross sections, the forward speed and propeller action.

4.4.1 Water depth

According to (PIANC Working group 20; 1992) the following classification can be made to indicate the shallowness of a fairway related to the vessels' draft:

- $3.0 < \frac{h}{T}$ deep
- $1.5 < \frac{h}{T} < 3.0$ medium deep
- $1.2 < \frac{h}{T} < 1.5$ shallow
- $1 < \frac{h}{T} < 1.2$ very shallow

In Figure 4.15 all water depth h to draft ratios are listed with the amount of model tests carried out for each ratio. The water depth

h is in this the deepest water depth in the cross section and does not change with the (lateral) position of the ship model in the cross section.

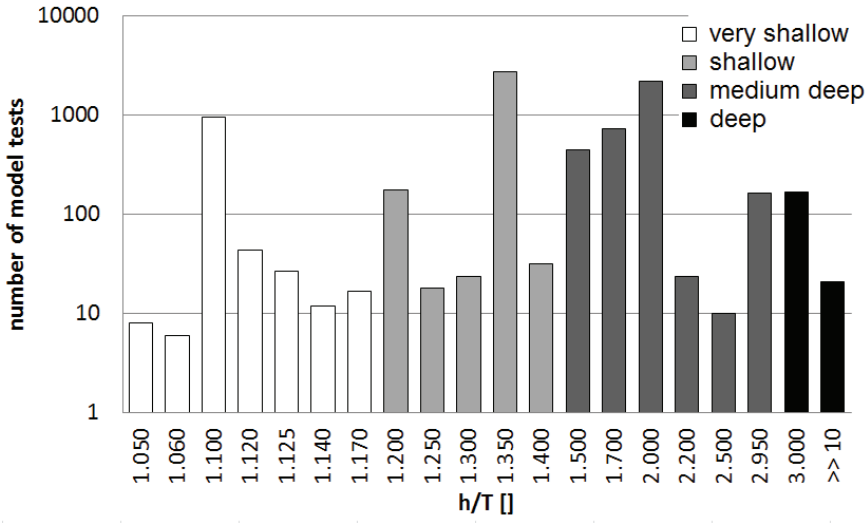

Figure 4.15 the number of model tests for each h/T ratio

Most of the ship models are tested in 2 to 4 different water depths. In this way, the range of water depths encountered by a seagoing deep drafted vessel approaching or leaving the Flemish harbours is covered. The LNG tanker, for example, is tested at 1.35 and 1.70 times the vessels draft which corresponds to the present practice at the harbour of Zeebrugge.

The tanker T0S is tested in 5 different water depths but the Ro-Ro ship A01 is tested in as much as 14 different water depths varying from 1.10 (very shallow) up to 2.20 (medium deep water) times the draft of the ship model.

4.4.2 Lateral position

The lateral position of a ship model in a towing tank with installed banks can be defined in different ways. The most straightforward but less physical is referring to the earth bound coordinate system of the towing tank itself. Doing so the installed banks have no influence on the lateral position.

For most model test series the following lateral positions have been tested whenever possible in the cross sections:

4.4.2.1 The Hydro-geometric centre

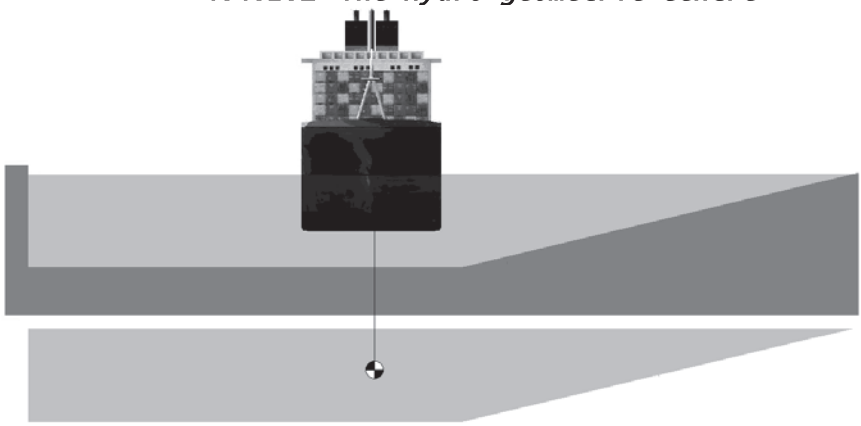

Figure 4.16 hydro-geometric centre and centre of gravity of the cross section

The hydro geometric centre is the lateral position in the cross section where the bank effect (yaw moment and sway force) of the port side bank is expected to compensate the sway force and yaw moment induced by the starboard sided bank.

This lateral position is approximated by the lateral position of the centre of gravity of the cross section. This position is calculated before the model tests are carried out.

4.4.2.2 The centre of the Towing Tank

This lateral position refers to towing along the centre line of the (empty) towing tank ($y_0=0$).

4.4.2.3 Ship's side above the toe of the bank

The side of the ship model closest to the bank is aligned with the start of the slope of the bank (the toe of the bank, Figure 4.17). This is the closest position to the bank with a constant water depth under the ship model.

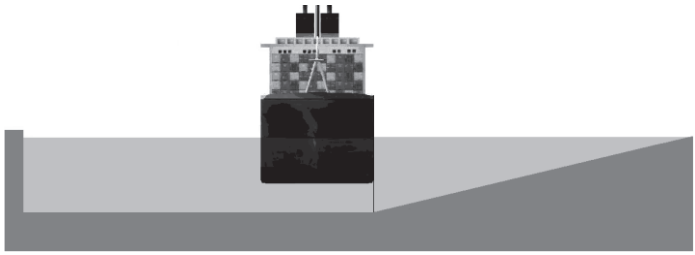

Figure 4.17 ship's side at toe of the sloped bank

4.4.2.4 Midship above toe of the slope

The ship model can be towed with its midship above the toe of the sloped bank as long as there is enough water under the keel and the slope of the bank is not too steep (Figure 4.18).

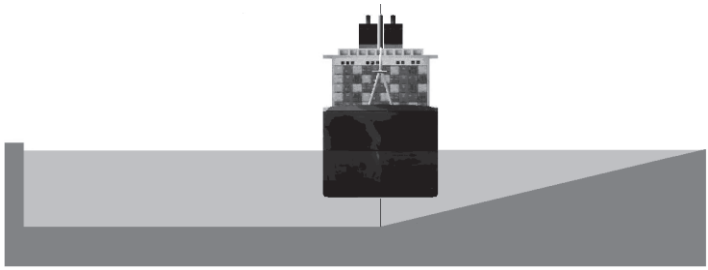

Figure 4.18 midship of the ship model above the toe of the sloped bank

In this position the water depth is not constant over the entire width of the ship model. As a consequence, the water depth for the ship model is not unambiguously defined.

4.4.2.5 Maximal lateral position

As close as physically possible without jeopardizing the ship model's safety. In practice there is at rest a minimal vertical gap of about 25mm between the ship model and the bank. This gap must be large enough to avoid the model to run aground because of the vertical sinkage and trim (squat) when towed. For reasons of safety the ship model's vertical motion is free but limited (in this position with 20mm).

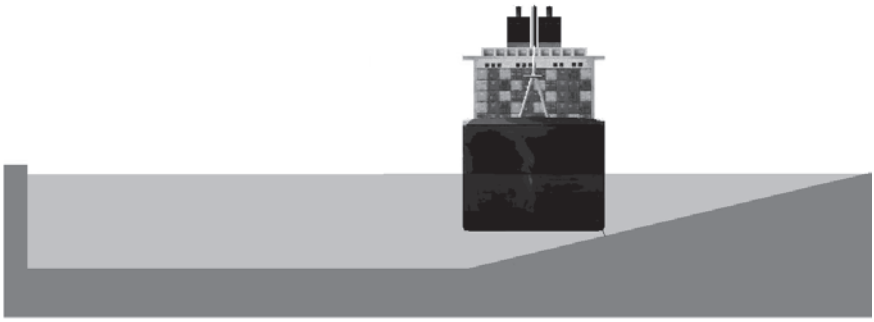

Figure 4.19 as close as possible, a minimal gap at all sides is realised

Again the water depth as experienced by the ship model is not defined straight forward.

4.4.2.6 Other lateral positions

The model tests are not limited to the lateral positions mentioned above. In a very wide cross section sometimes more lateral positions are added or less in a narrow section.

For example, systematic model tests have been carried out with ship model T0H in cross section QY_0_7.00_0. This small ship model is towed in this rectangular cross section at 9 different lateral positions to investigate the lateral influence zone of a bank (6.3.6).

4.4.3 Forward speed

Figure 4.20 shows the number of model tests carried out at each speed (rounded off to 0.1m/s). This is the forward speed of the ship model during the model test while it is towed by the PMM.

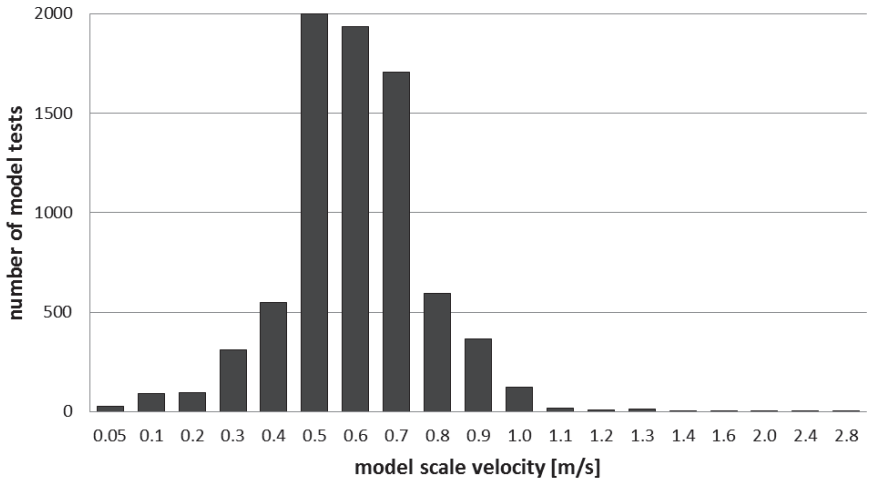

Figure 4.20 number of model tests carried out for each speed in m/s

Figure 4.21 shows the same number of speeds but now plotted to the representing full scale speed (in knots) based upon Froude's law.

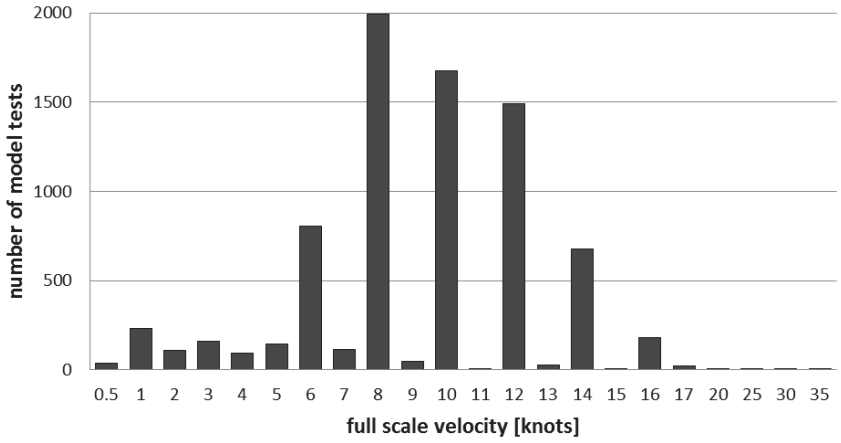

Figure 4.21 number of model tests for each speed scaled to full scale

In very shallow water most ship models are tested at 6, 8 and 10 knots full scale. In shallow water tests at 12 knots are added and 6 knots excluded. In medium and deep water, tests at 14 and 16 knots are also added to the program.

The tests carried out at speeds exceeding 20 knots and more are carried out with the high speed catamaran R0S.

Overall more velocities are tested depending on the specific cross section of the fairway. The number of velocities can be plotted to the dimensionless Froude Number based on the water depth Fr_h (Figure 4.22). The deepest water depth over the entire cross section is used for the calculation, the lateral position of the ship model (above) the bank will thus not change the corresponding Fr_h.

$$\boldsymbol{Fr_h} = \frac{\boldsymbol{V}}{\sqrt{\boldsymbol{gh}}} \tag{4.3}$$

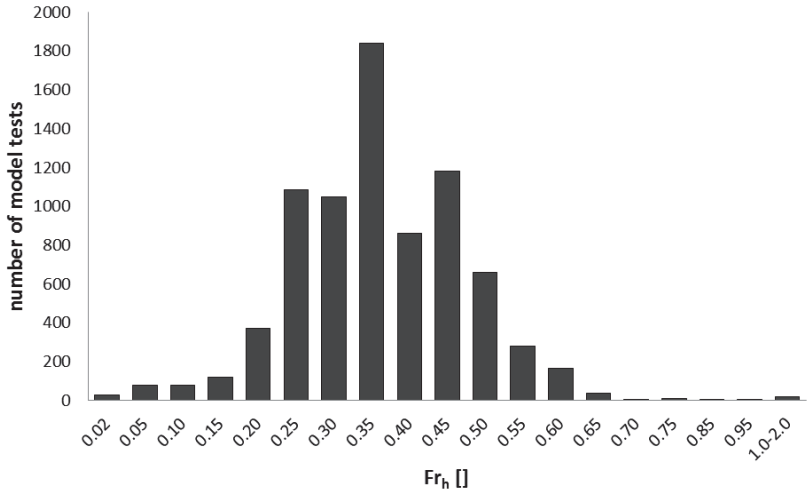

Figure 4.22 number of model tests for each water depth base Froude number Fr_h

In the very narrow cross sections (W_h<2B, Table 4.3) the model tests are carried out at very low speeds. The same is true for the tests with the Wigley hull W01 because of the scale factor of 1 for this specific 'ship' model. To be able to compare the speeds of all

ship models the velocity is made dimensionless by plotting the Froude number in Figure 4.23.

$$Fr = \frac{V}{\sqrt{gLpp}} \tag{4.4}$$

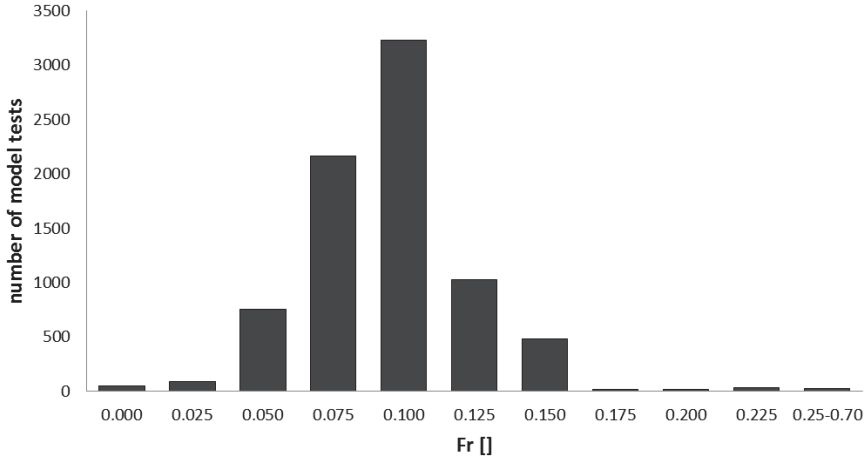

Figure 4.23 number of model tests for each Froude number

4.4.4 Propeller action

The ship models C0U, C0P, G0M, T0Z and B01 are equipped with one propeller and the ship model A01 with two propellers. The propeller rates are controlled with a dedicated system and a predefined rate of turn is imposed.

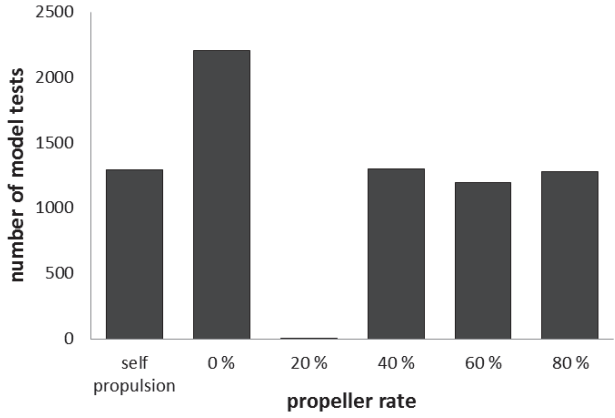

Figure 4.24 number of model tests for each propeller rate

Most ship models are towed at 0 rpm propeller rate (Figure 4.24). In this situation the propeller shaft is fixed at one position (no free wind milling of the propeller). The influence of the propeller is limited to an added drag (disturbing the stream lines at the stern section). A negative thrust is measured on the propeller shaft when towed (propeller acts like a parachute).

Other (positive) propeller rates are added to the program. These propeller rates can be fixed percentages of the propeller rate corresponding to telegraph position Full Ahead. For the ship models G0M and C0U the propeller rate is tested systematically from 0%, 40%, 60% up to 80% of the full ahead propeller rate (Figure 4.25).

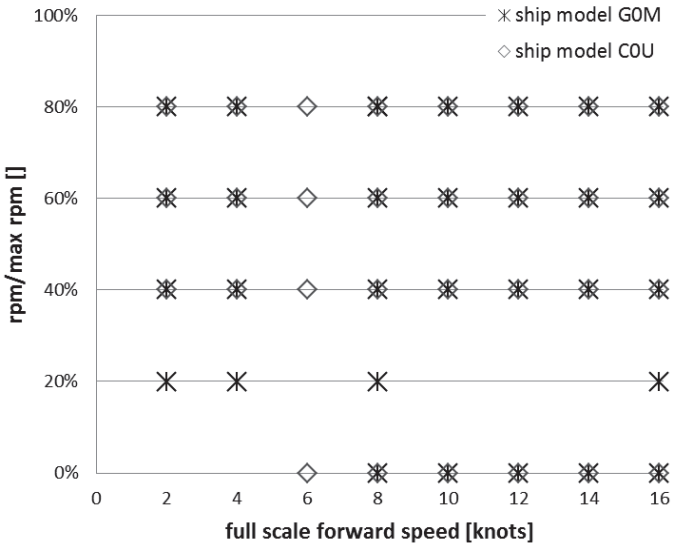

Figure 4.25 propeller rate relative to the propeller rate of full ahead plotted to the forward speed according to full scale in knots

For the ship models T0Z, C0P, A01 and B01 the propeller rate corresponding with self-propulsion in open water is added (Figure 4.26). In the confined cross sections with installed banks this is no longer at self-propulsion (no zero longitudinal force is measured)

because of the increased resistance induced by the bank effects (Chapter 8).

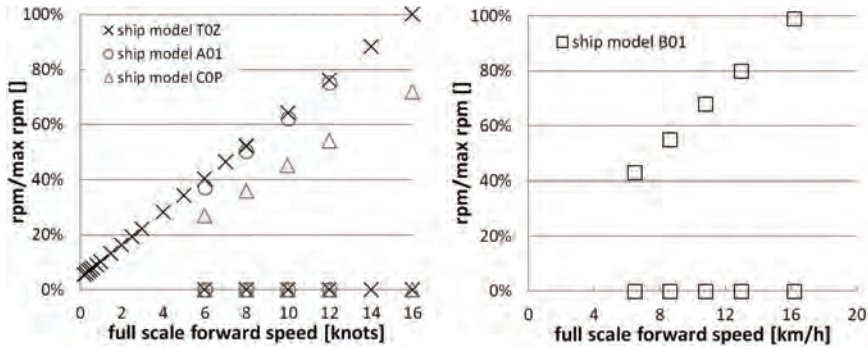

Figure 4.26 relative propeller rates plotted to the forward towing speed for the three seagoing vessels in knots (left) and the inland vessel in km/h (right).

4.5 Coordinate systems

4.5.1 Earth bound coordinate system, free surface

The earth fixed coordinate system is dedicated to each towing tank. For the FHR towing tank this is a rectangular, right handed earth bound coordinate system $O_0x_0y_0z_0$ (Figure 4.27). The $O_0x_0y_0$ plane is horizontal and coincides with the initial water plane at rest (free surface). The vertical $O_0x_0z_0$ plane is the longitudinal symmetry plane of the (empty) towing tank (at 3.5m from both longitudinal walls), with the vertical O_0z_0-axis directed downwards. The longitudinal position of the origin is located at the conventional home position of the towing carriage which is 4.0 m from the rear wall of the tank (harbour side).

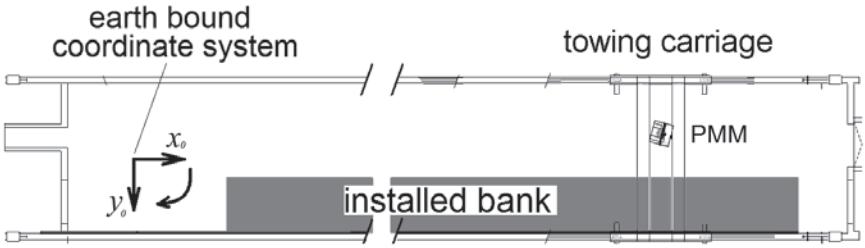

Figure 4.27 the earth bound coordinate system

4.5.2 Earth bound coordinate system, towing tank bottom

This is the same coordinate system as the previous but the origin is positioned on the bottom of the towing tank and not on the free surface. This coordinate system is of use to describe the installed banks, cross sections and other installations in the towing tank.

4.5.3 Ship bound coordinate system

During oblique towing the ship model is rigidly fixed to the carriage of the towing tank (but free to heave and trim). The ship fixed right handed, rectangular coordinate system *Oxyz* is positioned to the vertical axis of the yawing table of the planar motion mechanism. When the latter is at rest at its home position, *Oxyz* coincides with the earth bound system.

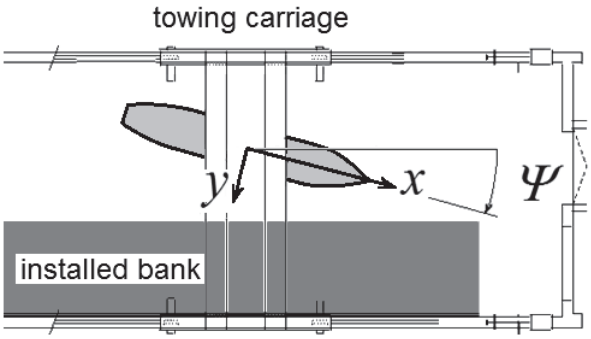

Figure 4.28 ship bound coordinate system

The ship model is mounted in such a way that the origin *O* is located at the midship section (½Lpp fore of the aft perpendicular), at the intersection of the longitudinal vertical symmetry plane and the waterline at rest. The longitudinal axis *Ox* is positive from stern to stem, the transversal axis *Oy* is positive towards starboard, and the vertical *Oz* axis is directed downwards. The yawing table imposes a heading angle ψ between the O_0x_0 axis and the *Ox* axis; a clockwise rotation is considered to be positive. The horizontal velocity vector $\vec{V}$ of the origin *O* is composed of the velocity components imposed by the longitudinal carriage (u_0) and the lateral carriage (v_0). $\vec{V}$ can be decomposed in components u and v according to the axes *Ox* and *Oy*, respectively.

4.6 Registrations

During captive manoeuvring tests, the ship model follows a predetermined trajectory applied by the towing carriage. The ship model is free to heave and pitch but is rigidly connected to the planar motion mechanism according to the other degrees of freedom.

During this trajectory the forces acting on the ship model (hull, rudder, propeller) are measured as well as positions of the hull (sinkage), propeller (rate of turn) and rudder (angle) (Figure 4.29). Other signals can be sampled as well, e.g. wave gauges mounted at a fixed location in the tank or attached to the towing carriage (fixed position relative to the ship model).

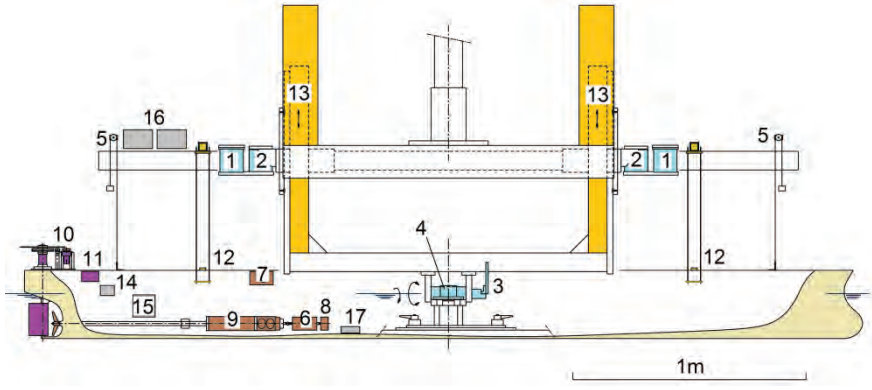

Figure 4.29 (1) longitudinal dynamometer (2x); (2) lateral dynamometer (2x); (3) roll moment measurement; (4) pitch and roll mechanism; (5) sinkage measurement (4x); (6) propeller motor; (7) propeller control; (8) propeller rate of turn meter; (9) thrust and torque gauge; (10) rudder mechanism; (11) rudder control; (12) limit vertical motion; (13) vertical guidance; (14) leakage pump; (15) battery; (16) amplifier; (17) leakage alarm

4.6.1 Hull

For the model tests carried out in the FHR towing tank the longitudinal and lateral components of the horizontal forces acting between the ship model and the planar motion mechanism in two measuring posts located aft and fore in the ship model are registered and converted to a longitudinal force X, a lateral force Y

and a yawing moment N, all expressed in the $Oxyz$ coordinate system. The roll moment K, preventing rotation around the Ox-axis, is measured separately for some ship models. The vertical motion of the ship model is measured at four positions (fore/aft, port/starboard) and converted into a running sinkage at the fore z_{VF} and aft perpendicular z_{VA}. This sinkage is considered to be positive in case of a downwards motion.

4.6.2 Propeller

If there is a propeller attached, the propeller rate is measured and controlled. On the propeller shaft the thrust T_P and torque Q_P are measured. The thrust T_P is a positive force when directed from stern to stem (as the propeller pushes the ship forward). When the vessel has a forward motion (sailing or towed) and the propeller rate is fixed at 0 rpm then the thrust T_P is negative.

The propeller rate n is positive turning clockwise for a right-handed propeller and counter clockwise for a left handed propeller (when looking forward). When the propeller generates a positive thrust having a positive propeller rate the torque Q_P on the propeller shaft is considered to be positive.

4.6.3 Rudder

The rudder angle can be controlled and measured (Figure 4.30). In present research the rudder angle is fixed at 0°. The forces and moment Q_R on the rudder stock are measured relative to the position of the rudder. The tangential force F_{TR} is positive directed from the trailing edge towards the leading edge of the rudder, the normal force F_{NR} is positive towards the starboard side. The rudder angle δ is positive and will result into a turning manoeuvre to port.

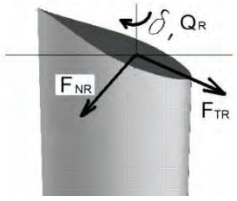

Figure 4.30 orientation of normal and tangential forces on rudder, rudder angle and torque

4.6.4 Free surface

For most of the tests the wave pattern between the ship model and the installed bank were registered by different wave gauges. The gauges are installed at different lateral but at the same longitudinal position in the towing tank. A descending water level generates an increasing value of the wave gauge signals (Figure 3.12).

4.6.5 Footage

Efforts are made to capture footage (video and pictures) during the entire project for example during the installation of banks (Figure 4.2) but also during the model tests itself (Figure 4.31). This is useful for backup and archive and for presentations.

Figure 4.31 a video still of the footage of model G0M sailing along SP_5_4.030_0

A selection of video footage can be seen at the website www.bankeffects.ugent.be.

4.6.6 Recapitulation

All forces, moments, positions derived during the tests carried out in the towing tank are listed here:

Hull:

- Running sinkage fore z_{VF} [mm]
- Running sinkage aft z_{VA} [mm]
- Longitudinal force X [N]
- Sway force Y [N]
- Yaw moment N [Nm]
- Roll moment K [Nm]

Propeller:

- Propeller thrust T_P [N]
- Propeller torque Q_P [Nmm]
- Propeller rate n [rpm]

Rudder:

- Rudder normal force F_{NR} [N]
- Rudder tangential force F_{TR} [N]
- Rudder torque Q_R [Nmm]
- Rudder angle δ [deg]

In appendix 11.6 the published open data is added.

4.7 Conclusion

An enormous amount of model tests were carried out. The input for these model tests are explained in this chapter. The test facilities (FHR towing tank, FHR simulators, data exchange towing tanks) are described. All the ship models used, are described (hydrostatics, lines plans) and reference is made to the relevant full scale counterpart.

All the details of the installed bank geometries are described and linked to real life locations. Three types of installed bank geometries can be distinguished: vertical quay walls, constant sloped banks and banks with the combination of a sloped part and a submerged flat part.

The water depths, lateral positions in the cross sections, forward speeds and propeller actions are listed and the chosen values clarified.

The relevant coordinate systems under consideration are explained and all the registered forces, moments and positions are made clear.

Finally the open data on bank effects is added.

Bank Effects

5 SCOPE OF THE MATHEMATICAL MODEL

The force balance of the ship in a simulator is determined based on the mathematical model of the ship (Section 4.2.3.3). This mathematical model itself is composed out of a wide set of sub-models that each cope with a specific phenomenon (such as bank effects) (Figure 4.7).

Three different types of mathematical models can be distinguished (Ankudinov et al. 1993):

- Pure mathematical modelling
- Physical based models
- Tabular models

5.1 Type and goal of the models

The goal is a reliable and robust mathematical model (based upon model tests) of the influence of all type of bank geometries on the behaviour of the vessel during a (manoeuvring) simulation. Simplicity is for practical implementations of importance and a physical background results in a wide range of the mathematical model.

5.1.1 Pure mathematical model

A force or moment is purely mathematically modelled by creating a polynomial expression as a function of the input parameters

(speed u, v; position y; propeller rate n;…) and the data set available.

$$\boldsymbol{Force/Moment} = \sum_{i,j,k,\ldots} \boldsymbol{u^i y^j n^k} \ldots \quad (5.1)$$

The main advantage of this type of mathematical model is the combination of high correlation between the experiments and the mathematical model, and a quick result.

The disadvantage of such a type of mathematical model is the absence of a physical interpretation of the formulation and the sometimes unexpected results of the mathematical model when interpolated or extrapolated out of the original data set. Furthermore the number of coefficients relative to the number of data points is rather high.

5.1.2 Physically based mathematical model

A physical background is used to build up the mathematical model. The measurements are interpreted and checked to different physical laws (Bernoulli's law, Newton's laws, conservation of mass).

A physically based mathematical model is more stable when interpolated or extrapolated out of the original range of the model tests. The mathematical model will also have a more limited amount of coefficients compared to pure mathematical modelling. The inaccuracy or deviation between the modelled values and measured values can be larger compared to the pure mathematical based models. However, relative to the number of coefficients the physically based mathematical model will be the more accurate out of the two.

5.1.3 Tabular mathematical models

A tabular mathematical model is a combination of a pure mathematical and physically based mathematical model. The formulation is based on physics but the set of coefficients changes for different ranges. This means that there exist different sets of coefficients for the same formula. Each set is valid within a predefined range which is based on the input parameters.

There is need for a large amount of coefficients and the physical meaning of the coefficients itself can be lost.

5.1.4 Chosen type of model

For reasons of simplicity the mathematical model for the bank effects will be a physically based model. The importance of a physical background on the formulation together with a small amount of coefficients is seen as a major advantage over the other type of mathematical models.

5.2 Modelled parameters

5.2.1 Degrees of freedom

All motions of a ship can be decomposed into six degrees of freedom; three translations and three rotations. The three translations in the ship bound coordinate axis (Section 4.6.3) are (Figure 5.1):

- Surge: translation along the x-axis
- Sway: translation along the y-axis
- Heave: translation along the z-axis

And the three rotations are:

- Roll: rotation around the x-axis
- Pitch: rotation around the y-axis
- Yaw: rotation around the z-axis

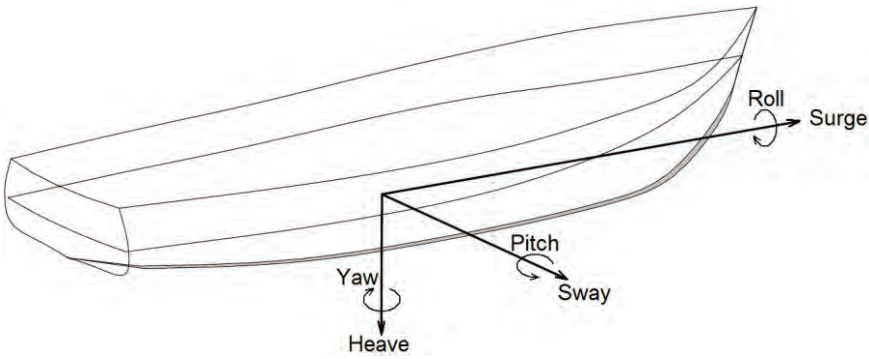

Figure 5.1 the six motions of a ship: three rotations and three translations in the ship bound coordinate system

The ship manoeuvring simulator solves the entire force package to calculate the required position of the next calculation step (0.1 seconds later). This position is calculated in the horizontal plane only in the FHR simulators. The integration of roll and vertical motions are planned in the near future. The major influences of bank effects on the vessel take also (but not only) place in this plane. The present mathematical model is therefore limited to the forces in the horizontal plane:

- Yaw moment N_{BANK}
- Longitudinal force X_{BANK}
- Lateral force Y_{BANK}

Vertical forces induced by bank effects which result in a new sinkage-trim combination of the vessel are not modelled. The same is true for the roll moment on the vessel.

When sailing (very) close to a bank the behaviour of appendages propeller and rudder will be influenced by the presence of the bank. These effects are also not taken into account in the present model.

5.2.2 Lateral force at the fore and aft perpendicular

The influence of the proximity of a bank on the forces parallel to the free surface can be interpreted in different ways. The most common interpretation is splitting into a lateral force Y_{BANK} (acting in the predefined origin of the ship bound coordinate system), a yaw moment N_{BANK} (around the vertical axis z of the same coordinate system) and a longitudinal force X_{BANK}.

The lateral force and yaw moment are interpreted differently in present dissertation:

- a lateral force acting at the forward perpendicular Y_F (This name is preferred over $Y_{F\ BANK}$ for reasons of simplicity)
- a lateral force acting on the aft perpendicular Y_A (Figure 5.2). (Again, Y_A is preferred over $Y_{A\ BANK}$ for its terseness)

The benefits of this itemization will be more comprehensible after the dedicated mathematical models for Y_A and Y_F are explained in Chapters 6 and 7 accordingly.

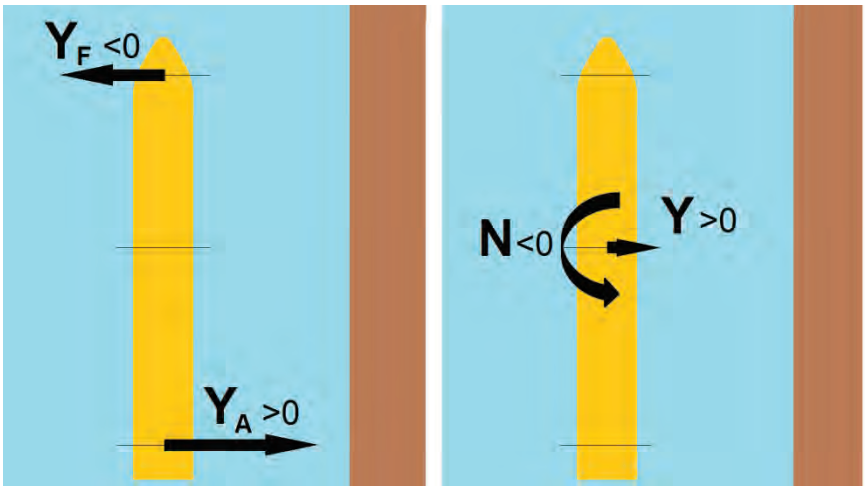

Figure 5.2 decomposition of yaw moment and sway force for common bank effects (attraction force Y in combination with a bow away moment)

It is obvious that for practical reasons such as the implementation of the mathematical model in an existing ship manoeuvring simulator, the lateral force Y and yaw moment N can be recomposed from the model of the lateral forces Y_F and Y_A.

$$\boldsymbol{Y = Y_F + Y_A} \tag{5.2}$$

$$\boldsymbol{N = \frac{Lpp}{2} Y_F - \frac{Lpp}{2} Y_A} \tag{5.3}$$

$$\boldsymbol{Y_A = \frac{Y}{2} - \frac{N}{Lpp}} \tag{5.4}$$

$$\boldsymbol{Y_F = \frac{Y}{2} + \frac{N}{Lpp}} \tag{5.5}$$

First the lateral force at the aft perpendicular will be analysed and a mathematical formulation proposed.

- The influence of an active propeller on the Y_A is more pronounced than working with the combination of overall lateral force and yaw moment.

- Sometimes the magnitude of the lateral force does not increase when sailing closer to the bank, under specific circumstances the sign even changes (attraction force becomes a repulsion force directed away from the closest bank). This phenomenon can better be explained (and modelled) based upon a lateral force at the aft and forward perpendicular.

5.2.3 Longitudinal force

A mathematical expression is proposed for the (sole) influence of the bank effects on the longitudinal force. This force is simply added to the other longitudinal forces. Cross terms between the bank effects and other devices such as hull, rudder and propeller generating longitudinal forces are not included.

5.3 Biased limits of the model

5.3.1 Quasi static

The mathematical model is based upon the measurements during the regime condition of model tests. The mathematical model will be valid for regime conditions. No transition or memory effects are taken into account.

Gentle changing slope geometries (relative to the length of the vessel under consideration) will not introduce overwhelming transition effects and will be coped with by the model . If a bank is relative short compared to the length of the ship then transition and memory effects will result in unreliable force predictions of the present model.

5.3.2 No drift and parallel to the bank

For the mathematical model the vessel is expected to sail without drift angle and parallel to the bank. During the captive model tests both conditions are easy to obtain but this is seldom the case during real time simulations or real life sailing conditions.

Most of the time the vessel manoeuvres on a fairway with small ($<5°$) drift angles and does not sail exactly parallel to the bank but also with minor angles between the bank and x-axis of the vessel.

To be able to cope with small drift angles and small angles between the bank and vessel the following parameters are used in the model to overcome this issue.

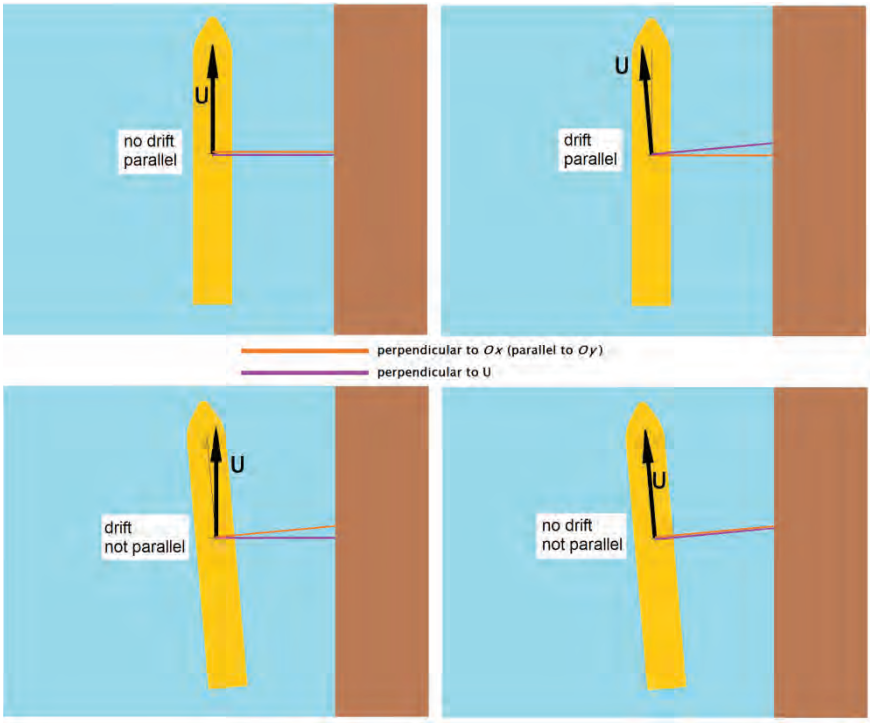

Figure 5.3 different combinations of drift of the vessel and parallelism to the bank

In Figure 5.3 all combinations of drift and parallelism to the bank are shown. The position from the bank can be based on the perpendicular to the heading of the vessel (orange line in Figure 5.3) or perpendicular to the velocity vector of the vessel (purple line in Figure 5.3).

For the application of the proposed mathematical model the velocity u (part of the velocity vector directed as the ship bound x-axis) will be used while the position of the vessel relative to the bank will be based on the perpendicular to the heading in the origin of the ship bound coordinate axis. With this convention the bank effects are absent when the ship is aligned parallel to the

bank and moves away from the bank with a pure sway without a forward speed (left in Figure 5.4). The bank effects are also absent when a ship sails away from the bank with a heading perpendicular to the bank (right in Figure 5.4).

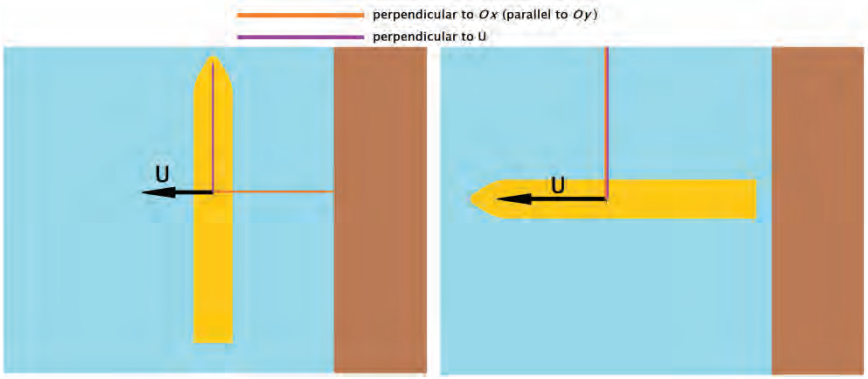

Figure 5.4 a ship sailing away from the bank without forward speed (on the left) or without lateral speed (on the right) generates no bank effects.

5.3.3 Advance speed and rotational speed

The mathematical model is limited for vessels sailing with a forward speed (positive advance speed V_A) in combination with a non-negative rotational speed of the propeller(s) n. This combination is known as the first quadrant for propellers (Carlton 2012). The model tests with a propeller rate of 0 rpm are according to the same author exactly on the boundary of the first and second quadrant.

$$\boldsymbol{u \geq 0} \qquad \boldsymbol{n \geq 0} \tag{5.6}$$

5.3.4 Forward speed limit

In (Lataire & Vantorre 2008) a mathematical model for the sinkage at the fore (z_{VF}) and aft (z_{VA}) perpendicular that takes into account an irregular bank geometry is suggested (equations 5.7 and 5.8). This equation contains the draft of the ship (T); the equivalent Froude number Fr_{eq} which takes into account the propeller action with V_{eq} (Section 6.1.3); the equivalent blockage m_{eq} (Section 8.3) and four coefficients ξ_{zi} determined with regression. Although the

model resulted in satisfying results for most of the tests, for some the deviation was unexpectedly large.

$$z_{VF} = T\,Fr_{eq}^2\left(m_{eq}\left(\xi_{zF1}Fr_{eq}^2 + \xi_{zF2}\right) + \xi_{zF3}Fr_{eq}^2 + \xi_{zF4}\right) \tag{5.7}$$

$$z_{VA} = T\,Fr_{eq}^2\left(m_{eq}\left(\xi_{zA1}Fr_{eq}^2 + \xi_{zA2}\right) + \xi_{zA3}Fr_{eq}^2 + \xi_{zA4}\right) \tag{5.8}$$

$$Fr_{eq} = \frac{V_{eq}}{\sqrt{g\,Lpp}} \tag{5.9}$$

For example the mathematical model was not satisfying for the container carrier C0U at 14 knots and $\frac{h}{T} = 1.35$. The tendency of the model was even wrong (the sinkage decreased while the mathematical model expected it to increase). Figure 5.5 shows the measured and modelled sinkage at the forward perpendicular along bank SS_5_4.030_.120_7.00.

Model tests with a wide range of forward speeds, propeller rates, distances to the bank are plotted in this Figure 5.5. As long as the modelled sinkage was smaller than 5.75mm the mathematical model was satisfying. Modelled sinkages between 5.75mm and 7.75mm correspond with measured sinkages between 4 and 6mm while modelled sinkages of 7.75mm and more correspond with measured sinkages of 3mm and less (negative running z_{VA} values mean the vessel at the forward perpendicular has a lower draft than in the initial zero speed condition, the bow rises).

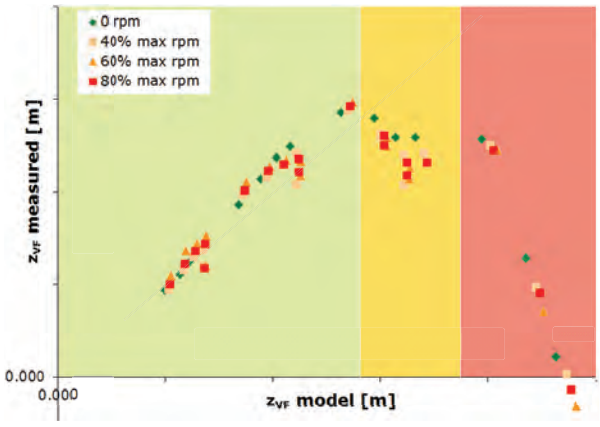

Figure 5.5 Different relations between the modelled running sinkage at the aft and the same sinkage as measured during EFDs*

** For reasons of confidentiality the actual values for forces and sinkages are intentionally left blank.*

Three regions can be distinguished in Figure 5.5: a region with satisfying results (green), unsatisfying results (red) and a transient region (yellow).

When all the tests with ship model C0U (=3617 validated model tests) are plotted on a graph with abscissa representing the ratio between speed and critical speed and ordinate the sinkage, Figure 5.6 is obtained. The critical speed is calculated as (Schijf 1949). In Schijf's formula the (classic) blockage *m* is used. This is the ratio between the midship area of the vessel A_M and area of the cross section of the waterway Ω.

$$\boldsymbol{m = \frac{A_M}{\Omega}} \tag{5.10}$$

$$\boldsymbol{Fr_{crit} = \left(2 \sin\left(\frac{Arcsin(1-m)}{3}\right)\right)^{\frac{3}{2}}} \tag{5.11}$$

In this figure all tests with a satisfying mathematical model are plotted green. The non-satisfying tests (yellow and red background in Figure 5.5) are plotted in red.

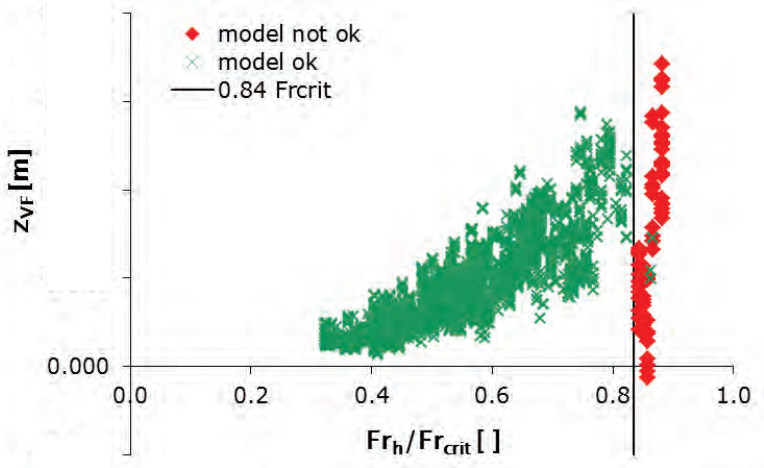

Figure 5.6 Running sinkage at the fore vs ratio to critical speed. Satisfying modelled sinkages are plotted green, unsatisfying red

The most plausible explanation for the non-satisfying tests is the relatively high speed referred to the critical speed. In a wide speed range the mean sinkage and trim increase with increasing speed.

At a certain speed the trim is increased so dramatically resulting in the bow to reposition to its original position. At this condition a significant mean sinkage is observed. These trim and sinkage values are caused by the increased height and significantly longer extension of the bow wave when the ship's speed is close to the critical speed. The large trim and mean sinkage combines into a decrease of the running sinkage fore.

A mathematical model coping with supercritical speeds is out of the scope of this research. There is a relation between the behaviour of the vessel and the ratio forward speed – critical speed. The proposed mathematical model is only valid when sailing slower than 84% of the critical speed (vertical black line in Figure 5.6).

$$Fr_h < 0.84 Fr_{crit} \tag{5.12}$$

This transition from sub-critical speed region to transcritical speed region is independently confirmed in (Hüsig et al. 2000).

5.4 Conclusion

Out of the different possible types of mathematical models for implementation into a ship manoeuvring simulator, the reason to choose for a physically based mathematical model is explained.

The bank effects acting in the horizontal plane on the ship's hull will be modelled. These forces are less conventionally split into a lateral force at the aft Y_A and at the forward perpendicular Y_F (instead of the more common overall lateral force Y_{BANK} and yaw moment N_{BANK}) and a longitudinal force X_{BANK}.

Some constraints and boundary conditions are explained such as the need for a quasi-static situation, no drift angle of the ship and only sailing parallel to the bank.

The mathematical model will cover ships sailing at a forward speed in combination with a non-negative propeller action. Furthermore the forward speed is limited to 84% of the critical speed.

Bank Effects

6 LATERAL FORCE AT THE AFT PERPENDICULAR

As mentioned in previous Chapter 5 the bank effects in the horizontal plane (parallel to the free surface) are split into one longitudinal force X_{BANK} and two lateral forces. The latter have their application point on the forward and aft perpendiculars, Y_F and Y_A.

First the mathematical model for the force at the aft perpendicular is explained in this dissertation. In the much simplified idea of bank effects the vessel acts as being attracted towards the bank but the point of application of this force is located at the second half of the vessel, closer to the aft perpendicular. This position of the point of application generates also a bow away moment.

Another reason to start with the lateral force at the aft perpendicular is the larger influence of the propeller on this force at the aft perpendicular than the lateral force at the forward perpendicular. Since the propeller is located very close to the aft perpendicular the influence of the propeller is much more significant at this position than on the lateral force at the forward perpendicular.

6.1 Velocity

6.1.1 Forward speed of the vessel

The lateral attraction force towards the bank is mainly generated by the pressure drop between ship and bank (Chapter 3). The pressure along the hull will decrease according to (Bernoulli 1713) with the square of the speed of the water particles flowing along that hull. The lateral force at the aft perpendicular is the integration of this pressure over the second half of the ship's hull. The magnitude of the lateral force at the aft perpendicular Y_A increases with the square of the combined speed of the speed of the vessel V augmented with the return flow δV.

$$\mathbf{Y_A} \propto (\mathbf{V} + \boldsymbol{\delta}\mathbf{V})^2 \tag{6.1}$$

The higher the forward speed, the higher the magnitude of the lateral force Y_A. The return flow (which is not constant at all positions) is difficult to determine and was measured in none of the model tests related to this research; the lateral force at the aft perpendicular Y_A is therefore plotted to the forward velocity of the vessel V. As could be expected the relation between both (Y_A and V) is from an order higher than quadratic because of the return flow δV not taken into account, in the example of (Figure 6.1) about 2.2. This higher order can be ascribed to the drop of the water surface around the ship (and thus the squat of the vessel) which further decreases the available space for the water.

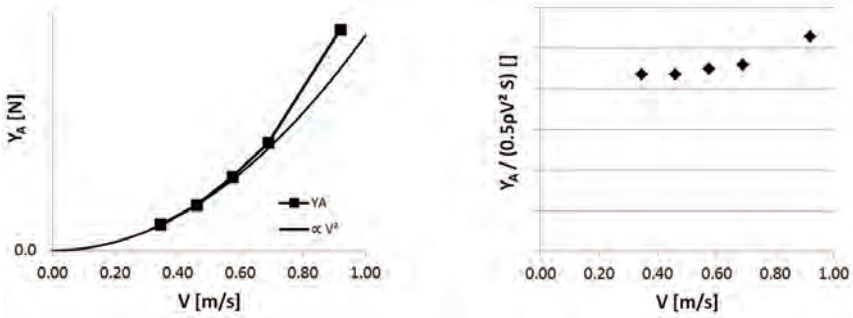

Figure 6.1 the lateral force at the aft perpendicular Y_A (left) and dimensionless $\frac{Y_A}{\frac{1}{2}\rho V^2 S}$ (right) plotted to the forward speed V for C0P, propeller rate 0 rpm, h=0.380m, position in SP_3_5.730_0 y_0=-2.193

The lateral force at the aft perpendicular is not modelled nor made dimensionless by dividing to $\frac{1}{2}\rho V^2 S$ because of the non-linearity between the force at the aft perpendicular and the square of the forward speed of the ship. A mathematical model that takes into account the influence of the return flow will be proposed.

6.1.2 Propeller action

The higher the velocity of the water between bank and vessel, the lower the pressure on the hull of the ship (Bernoulli's principle). A propeller generating (positive) thrust, at a positive rotational speed, accelerates the water flow passing the propeller disk and therefore increases the velocity of the water between bank and ship and thus decreases the pressure on that area of the hull. The influence of the propeller action on the lateral force at the aft perpendicular will be modelled as a partial increase of the forward speed of the vessel.

The thrust velocity V_T is calculated based upon the thrust T_P (as measured on the propeller shaft):

$$\frac{\mathbf{T_P}}{\frac{\mathbf{1}}{\mathbf{2}}\boldsymbol{\rho}\mathbf{A_0}\mathbf{V_T}^2} = \mathbf{1} \tag{6.2}$$

This velocity V_T is the velocity behind the propeller of a heavy loaded ship (when the generated thrust is large and/or the forward speed relative low) or a ship in bollard pull condition. *The* propeller induced velocity at a distance behind the propeller is:

$$\mathbf{U} = \mathbf{V_A}\left(-\mathbf{1} + \sqrt{\mathbf{1} + \frac{\mathbf{T_P}}{\frac{\mathbf{1}}{\mathbf{2}}\boldsymbol{\rho}\mathbf{A_0}\mathbf{V_A^2}}}\right) \tag{6.3}$$

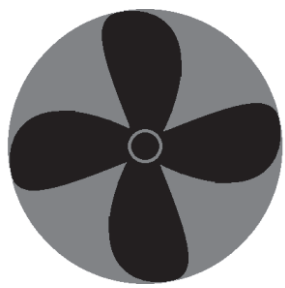

Figure 6.2 disc area A_0 (black+grey area) of a four bladed propeller

The disc area A_0 can be written as a function of the propeller diameter D:

$$\mathbf{A_0 = \pi \frac{D^2}{4}} \tag{6.4}$$

Or according to (Hartl 2011) with the radius r of the propeller:

$$\mathbf{A_0 = \frac{1}{2} \tau r^2} \tag{6.5}$$

When the ship model is towed in a towing tank with a forward speed and with propeller rate 0 rpm (Figure 4.25) the thrust as measured on the propeller shaft will be negative. To be able to calculate negative values for V_T the absolute value of T_P is used under the root and the root is multiplied by the sign of the thrust:

$$\mathbf{V_T = sign(T_P) \sqrt{\frac{|T_P|}{\frac{1}{2}\rho\pi\frac{D^2}{4}}}} \tag{6.6}$$

$$\mathbf{V_T = sign(T_P) \sqrt{\frac{8|T_P|}{\rho\pi D^2}}} \tag{6.7}$$

6.1.3 Equivalent velocity V_{eq}

In the mathematical model for Y_A the forward speed of the ship V will be augmented with a fraction $\xi_{VT,A}$ of the velocity V_T to incorporate the influence of the propeller action on the force Y_A.

$$\mathbf{V_{eq} = V + \xi_{VT,A} V_T} \tag{6.8}$$

The coefficient $\xi_{VT,A}$ is a positive number smaller than 1.

$$\mathbf{0 < \xi_{VT,A} < 1} \tag{6.9}$$

A ship sailing at a forward speed V will generate a return flow along the vessel. Between the (closest) bank and the vessel this return flow will increase even more when the propeller is activated. The propeller will generate a pressure drop along the aft body and the return flow will increase. This return flow is assumed to be the same return flow as the same vessel without propeller sailing at

the equivalent speed V_{eq}. There are no cross terms (propeller action in combination with the forward speed of the ship for example) in the formula for the equivalent velocity and the coefficient is constant for all (environmental) conditions. This is a simplification of reality for the mathematical model.

If the thrust on the propeller shaft is negative (e.g. the propeller is fixed or rpm set to 0) then this non-rotating (or slowly rotating) propeller is an obstruction for the return flow. The velocity V_T will in this case be negative and the return flow will be lower than can be expected according to the forward speed of the ship V without propeller influence. Again the magnitude of the lateral force Y_A will be related to the smaller speed V_{eq} because the velocity V_T is negative and V_{eq} will be smaller than V.

The magnitude of the lateral force at the aft perpendicular Y_A always increases for all combinations of position of the closest bank (port or starboard side) and direction of rotation of the propeller (left or right) when the propeller delivers a positive thrust (Li 2000).

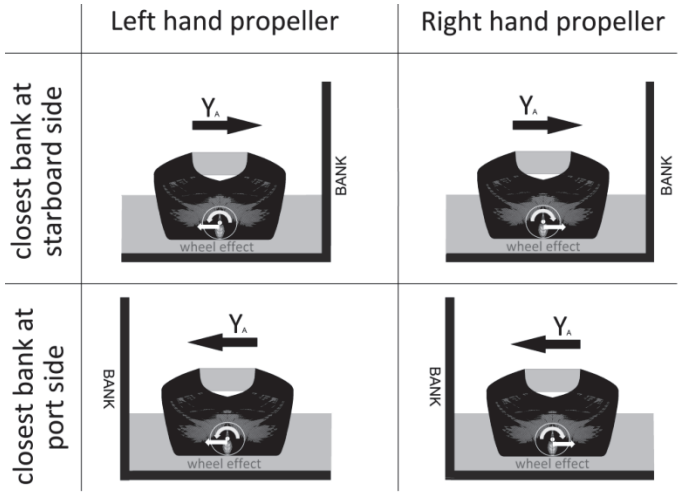

Figure 6.3 all combinations of position of closest bank and direction of rotation of the propeller (left and right handed) but always with the intention of a positive thrust

As shown in Figure 6.3 the wheel effect of the propeller sometimes increases the attraction force at the aft perpendicular (starboard bank & right handed propeller or portside bank & left handed propeller) and sometimes compensates the attraction force (starboard bank & left handed propeller or portside bank & right handed propeller). This asymmetric wheel effect is not taken into account in the present model for bank effects. In the FHR ship manoeuvring simulators the wheel effect is implemented independent of the bank effects. In this situation the banks are expected to have no influence on the wheel effect.

6.2 Lateral position in a rectangular cross section

The distance between a ship and a bank is unambiguously defined when sailing along a vertical bank at one side, while the navigation area is unlimited at the other side. A clear definition of the distance between the ship and any irregular bank geometry is not this straightforward. In the past the distance between ship and bank at half the draft (Ch'ng et al. 1993) or at other (averages of) discrete positions were chosen (e.g. mid height of bank slope in (Duffy 2002). The disadvantage of this method is the high sensitivity of the distance to bank on these arbitrary positions. Furthermore, the influence properties of the bank geometry might be excluded in the distance to the bank.

To check the impact of the lateral position on Y_A, first only model tests are considered with the model towed along a vertical quay wall. In Table 6.1 the test conditions and some ship properties are summarized.

Ship	B	T	C_M	W	W/B	h/T			
[ ]	[m]	[m]	[ ]	[m]	[ ]	[ ]			
B01	0.458	0.146	0.998	4.60	10.04	1.20	1.35	2.95	3.00
C0P	0.613	0.190	0.990	4.60	7.50	1.10	1.35	2.00	
C0U	0.530	0.149	0.979	6.33	11.94	1.10	1.35	2.00	
C0U	0.530	0.180	0.983	6.33	11.94	1.10	1.35	2.00	
G0M	0.594	0.157	0.984	6.33	10.66	1.35	1.70		
A01	0.620	0.148	0.947	4.60	7.42	1.10	1.35	2.00	

T0H	0.295	0.178	0.996	7.00	23.73	1.10	1.35	2.00	
T0Z	0.773	0.277	0.998	0.97	1.25	1.10	1.35	1.50	
T0Z	0.773	0.277	0.998	1.31	1.69	1.10	1.35	1.50	
T0Z	0.773	0.277	0.998	1.93	2.50	1.10	1.35	1.50	
T0Z	0.773	0.277	0.998	3.87	5.01	1.10	1.35	1.50	
T0Z	0.773	0.277	0.998	4.60	5.95	1.10	1.35	1.50	
T0Z	0.773	0.277	0.998	7.00	9.06	1.10	1.35	1.50	
T0S	0.930	0.292	0.996	33.0	35.48	1.06	1.12	1.20	1.40
T0S	0.930	0.292	0.996	10.0	10.75	17.13			
W01	0.400	0.250	0.662	4.60	11.50	1.10	1.35	1.50	

Table 6.1 main dimensions of the ship models and cross sections for model tests carried out along a vertical wall

The tanker T0Z is tested in a wide range of rectangular cross sections with a width as small as 105% of the ship's breadth up to the total width of the towing tank at Flanders Hydraulics Research (7.00m or more than 9 times the ship's beam). Based upon these model tests (about 1200 model tests, non-eccentric tests excluded) some first considerations can be made. These considerations are then extended to other vessels and bank geometries.

6.2.1 Function for the lateral position in a rectangular cross section

Overall the closer the distance between ship and bank the higher the magnitude of the lateral force Y_A. Sometimes the lateral position of the vessel in the fairway is expressed as the distance from the vertical wall y_{wall} (Figure 6.4), in other publications the distance from the centre line of the cross section y (Figure 6.4) is applied. In a rectangular cross section (composed of a flat bottom and two vertical walls separated with a distance W) the relation between y_{wall} and y can easily be written:

$$|y_{wall}| = \frac{W}{2} - \left(\frac{B}{2} + |y|\right) \tag{6.10}$$

Initially the inverse of these distances is used:

$$\frac{1}{|y_{wall}|} = \frac{1}{\frac{W}{2} - \left(\frac{B}{2} + |y|\right)} \tag{6.11}$$

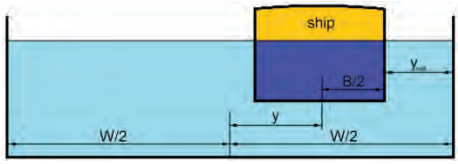

Figure 6.4 lateral positions y and y_{wall} in a rectangular fairway with width W

The magnitude for the lateral position y is zero when sailing at the centre line of the cross section (Figure 6.5). If the distance y_{wall} is larger than the influence distance from the nearest bank the value y will also be set to zero (as will be explained in section 6.2.5).

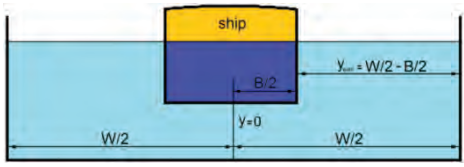

Figure 6.5 sailing on the centre line of a rectangular cross section (y=0)

If the ship is sliding with her side along the vertical wall (Figure 6.6):

$$|\mathbf{y}| = \frac{\mathbf{W}}{\mathbf{2}} - \frac{\mathbf{B}}{\mathbf{2}} = \frac{\mathbf{W-B}}{\mathbf{2}} \tag{6.12}$$

$$\mathbf{y_{wall}} = \mathbf{0} \tag{6.13}$$

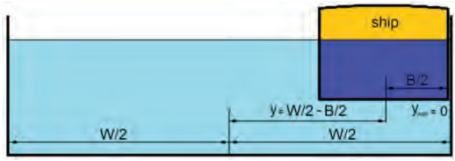

Figure 6.6 a ship laterally located as berthed along the vertical wall (y_{wall}=0)

The dimension of equation 6.11 is m^{-1} and can be made dimensionless by multiplying with $\frac{W-B}{2}$ [m] which is the distance for y_{wall} when sailing at the centre line of the fairway:

$$\frac{\frac{\mathbf{W-B}}{\mathbf{2}}}{|\mathbf{y_{wall}}|} = \frac{\frac{\mathbf{W-B}}{\mathbf{2}}}{\frac{\mathbf{W}}{\mathbf{2}} - \left(\frac{\mathbf{B}}{\mathbf{2}} + |\mathbf{y}|\right)} = \frac{\mathbf{1}}{\mathbf{1} - \frac{\mathbf{2|y|}}{\mathbf{W-B}}} \tag{6.14}$$

Equation 6.14 equals 1 when sailing on the centre line but shoots to infinity when the distance between the ship's side and vertical wall tends to zero.

$$\lim_{y_{wall}\to 0}\left(\frac{1}{1-\frac{2|y|}{W-B}}\right)=\infty \tag{6.15}$$

First the coefficient ξ_y is added to be able to control the slope of the function, the term $-\frac{1}{(1+\xi_y)}$ is also added to have a value equal to zero when sailing on the centre line:

$$\frac{1}{(1+\xi_y)-\left|\frac{2y}{W-B}\right|}-\frac{1}{(1+\xi_y)}=0 \tag{6.16}$$

Since it is feasible to limit the value of the relative lateral position of the vessel in the fairway to 1 (or -1 depending whether the closest wall is at the starboard (+1) or portside (-1)) the entire function is divided by the value which is obtained when there is no distance between the vessel's side and vertical wall (combining equation 6.14 and 6.16):

$$\frac{1}{(1+\xi_y)-1}-\frac{1}{(1+\xi_y)}=\frac{1}{\xi_y(1+\xi_y)} \tag{6.17}$$

The formulation for the effect of the lateral position of the vessel on the fairway $f(y)$ becomes:

$$f(y)=\frac{\frac{1}{(1+\xi_y)-\left|\frac{2y}{W-B}\right|}-\frac{1}{(1+\xi_y)}}{\frac{1}{\xi_y(1+\xi_y)}}=\frac{\xi_y\left|\frac{2y}{W-B}\right|}{(1+\xi_y)-\left|\frac{2y}{W-B}\right|} \tag{6.18}$$

When ξ_y is set to zero the equation 6.18 is zero for all lateral positions y and is therefore not usable. By definition the coefficient must satisfy:

$$0<\xi_y<\infty \tag{6.19}$$

To make a difference when sailing closer to a bank at port or at starboard, the sign of y $(sign(y)=y/|y| \text{ if } y\neq 0;\ \text{sign}(0)=0)$ is included:

$$f(y)=sign(y)\frac{\xi_y\left|\frac{2y}{W-B}\right|}{(1+\xi_y)-\left|\frac{2y}{W-B}\right|}=\frac{\xi_y y}{0.5(1+\xi_y)(W-B)-|y|} \tag{6.20}$$

In Figure 6.7 the relation between ξ_y, $\frac{2y}{W-B}$ and the result of the previous equation 6.20 is shown.

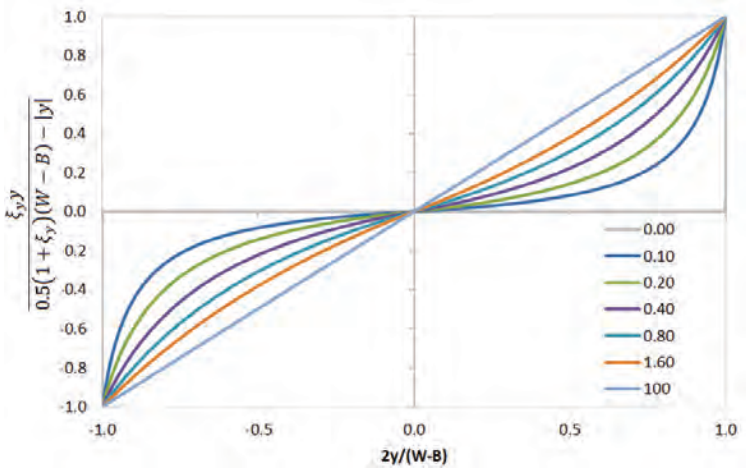

Figure 6.7 the influence of ξ_y on the lateral position parameter for all positions (from berthed at port side (-1) to berthed at starboard side (+1))

If the parameter $\xi_y = 0$ the function becomes a step function (equation 6.21).

$$\boldsymbol{lim}_{\xi_y \to 0} \frac{\xi_y y}{0.5(1+\xi_y)(W-B)-|y|} = \begin{cases} \mathbf{0}, & \left|\frac{\xi_y y}{0.5(1+\xi_y)(W-B)-|y|}\right| < \mathbf{1} \\ \boldsymbol{sign}(\boldsymbol{y}), & \left|\frac{\xi_y y}{0.5(1+\xi_y)(W-B)-|y|}\right| = \mathbf{1} \end{cases} \tag{6.21}$$

The function for the lateral position becomes a (constant sloped) straight line when the parameter ξ_y tends to infinity (equation 6.22)

$$\boldsymbol{lim}_{\xi_y \to \infty} \frac{\xi_y y}{0.5(1+\xi_y)(W-B)-|y|} = \frac{2y}{W-B} \tag{6.22}$$

For practical reasons during the regression the coefficient ξ_y is limited to:

$$\mathbf{10^{-4}} < \boldsymbol{\xi_y} < \mathbf{10^2} \tag{6.23}$$

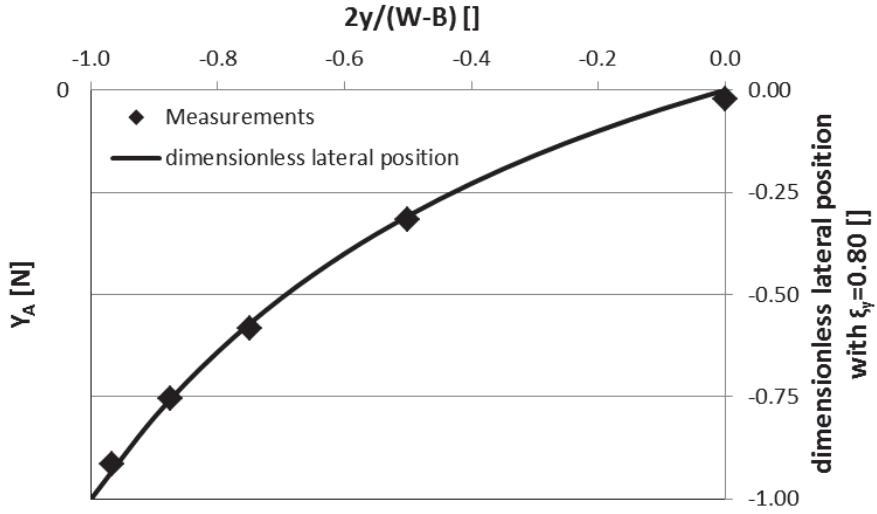

Figure 6.8 T0Z, QY_0_3.865_0, h=1.5T, 10kts

An example of equation 6.20 with the results of model tests are plotted in Figure 6.8. In this example the ship model T0Z is towed according to 10 knots full scale in a rectangular cross section with a water depth of 1.50 times the draft of the model and a section width W of 5 times the beam of the vessel. A close correlation between the lateral force at the aft perpendicular and equation 6.20 (with coefficient $\xi_y = 0.80$) is found.

6.2.2 Boundary layer

Overall, the closer a vessel sails to a bank, the higher the magnitude of the lateral force on the vessel is (if all other parameters such as the velocity, water depth remain the same). During some experiments, however, the magnitude of Y_A appeared not to increase with decreasing distance to the vertical wall. Among others, this was the case for the model tests with ship model T0Z tested in a water depth of 110% of the draft and at a towing speed of 0.357m/s (6 knots full scale) in a rectangular cross section with a width of five times the ship's beam. In these conditions six model tests were carried out at six different lateral positions.

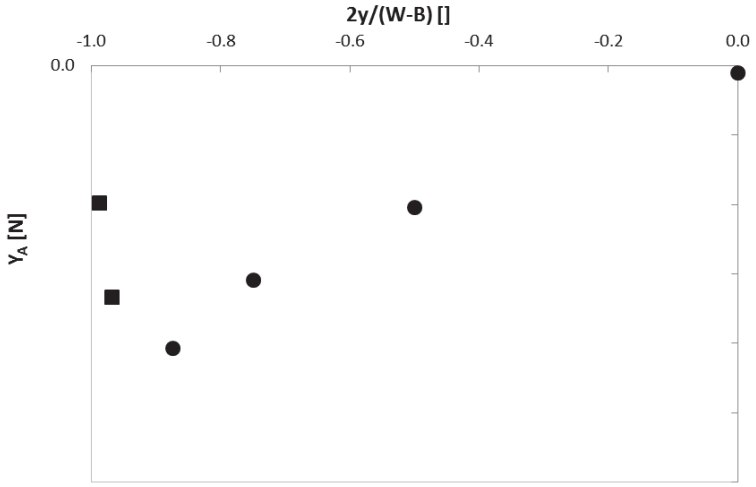

Figure 6.9 EFD for T0Z with h/T 1.10, 6kts full scale in cross section QY_0_3.865_0

Out of the six tested positions, the four Y_A values furthest away from the vertical wall (dots in Figure 6.9) are consistent with the previous tendency formulated above: the closer to the bank, the higher the magnitude of the lateral force Y_A. When sailing very close to the bank however the magnitude of the lateral force Y_A decreases with decreasing distance between ship and bank (the squares in Figure 6.9 are for model tests with a gap between ship and bank of 0.020 m or 2.6% B and 0.050 m or 6.5% B).

The lateral bank force Y_A comes into existence when sailing along a bank because of asymmetric streamlines between port and starboard side. The water displaced by the vessel must flow in the confined space between ship and bank at a higher rate than at the other (unrestricted or less restricted) side of the vessel. Again, the increased speed of the return flow will induce a lower pressure according to the Bernoulli principle.

All model tests are scaled according to the Froude's law, according to the ITTC Recommended Procedures and Guidelines (ITTC 2008). The boundary layer is not scaled properly according to this scale law. At model scale the boundary layer will always be (relatively)

thicker than the full scale boundary layer. The thickness of the boundary layer at the aft body of the vessel can be calculated according to (White 2003) and Prandtl & Von Karman's momentum law. The boundary layer thickness is defined as the locus of points where the velocity parallel to the plate reaches 99 per cent of the external velocity and is calculated with the skin friction law (a turbulent flow along the plate is assumed):

$$\boldsymbol{\delta = 0.16 \frac{Lpp}{\sqrt[7]{Re}}} \tag{6.24}$$

According to equation 6.24 the layer thickness is 0.091m for the example shown in Figure 6.9. The Reynolds number Re depends of the kinematic viscosity of the water ν. This viscosity changes with the temperature (Figure 6.10) but in this and next calculations the water temperature in the towing tank is assumed to be at 15°C at all times and the according kinematic viscosity ν is for all calculations 1.1386 10^{-6} m^2/s.

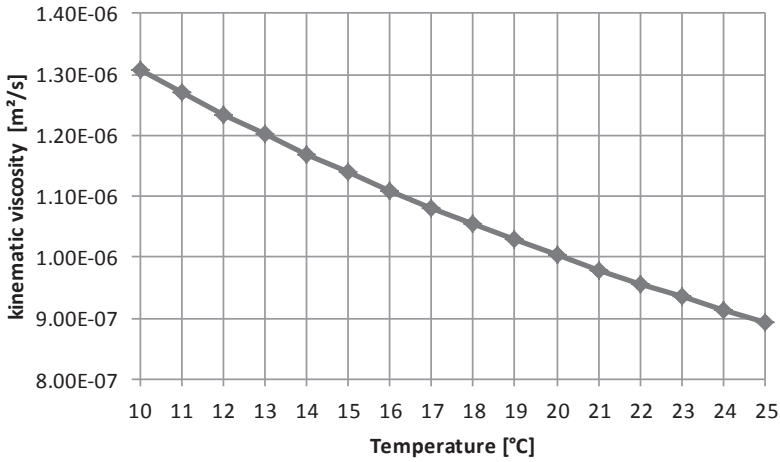

Figure 6.10 kinematic viscosity ν according to (ITTC 2011)

The velocity gradient between the ship model and the vertical wall is simplified in Figure 6.11. The velocity on the ship's hull is the same as the forward speed of the ship (earth bound coordinate system) while the velocity on the vertical wall is zero. Between ship

and vertical wall the return flow (opposite to the sailing direction of the ship) creates a pressure drop along the hull. When the distance between ship and vertical wall is sufficiently small (right hand side in the same figure), this return flow is diminished or vanishes because of the boundary layers. As a consequence the pressure drop between ship and wall decreases and sometimes even changes sign (resulting in a repulsion force away from the vertical wall instead of an attraction force towards the vertical wall).

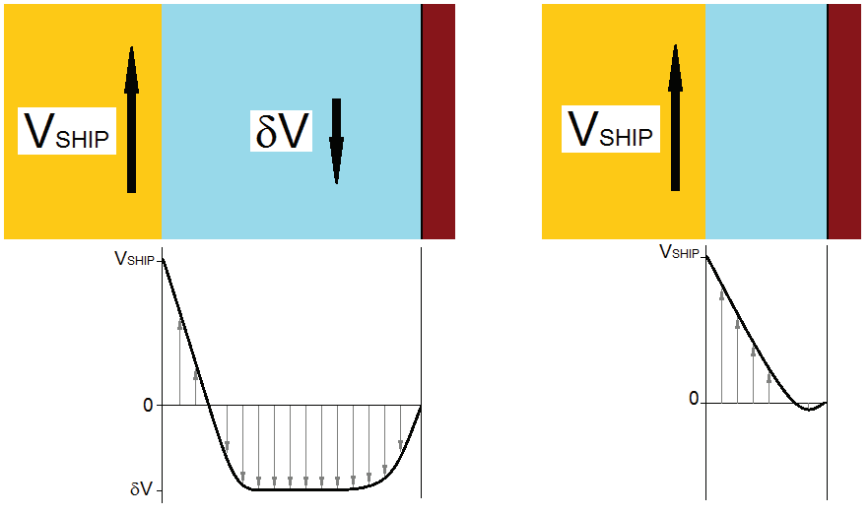

Figure 6.11 the velocity gradient (simplified to 2D) from the hull of the ship model to the surface of the vertical wall very close to the bank (right) and further away (left).

The two smallest distances between the ship's side and the vertical wall in Figure 6.9 are 0.020 m and 0.050 m (squares). The boundary layer is calculated (equation 6.24) to be 0.091m. As the boundary layer is thicker than the gap between ship and bank, it is expected that this boundary layer will limit the return flow. Again, if the return flow is sufficiently hindered, the pressure drop between ship and bank will be lower than expected. As a consequence the attraction force towards the bank will also be smaller. This is the physical interpretation of the previously

unexpected low magnitude of the lateral (attraction) force at very small distances between ship and bank.

In this paragraph, it will be investigated which ship-bank distance has to be maintained to avoid the influence of the boundary layer on the lateral force Y_A. This minimum distance is referred to as the the boundary layer influence thickness δ_{BLI}.

In this paragraph, it will be investigated which ship-bank distance has to be maintained to avoid the influence of the boundary layer on the lateral force Y_A. This minimum distance is referred to as the the boundary layer influence thickness δ_{BLI}.

6.2.2.1 Boundary layer influence thickness at the aft $\delta_{BLI,A}$

6.2.2.1.1 Water depth

The boundary layer influence thickness $\delta_{BLI,A}$ increases with decreasing water depths. In shallow waters more displaced water must be evacuated along the ship's sides than under the ship compared to sailing in deeper waters. As a consequence the return flow will be larger and the boundary layer will be felt sooner (or $\delta_{BLI,A}$ will increase). The Reynolds number Re used in equation 6.24 is based upon the forward speed of the vessel and will not change with an increasing or decreasing return flow.

$$\delta_{BLI,A} \propto \frac{T}{h} \tag{6.25}$$

6.2.2.1.2 Propeller action

Propeller action generating a positive thrust ($V_T>0$) will increase the influence thickness of the boundary layer. The active propeller must be supplied with water. The larger the propeller rate the larger the amount of water needed, and the higher the return flow must be. The influence of the propeller rate on $\delta_{BLI,A}$ is added by a non-dimensional speed ratio (equation 6.26). This ratio will only change if the ratio between the thrust velocity V_T and the velocity

of the vessel V changes and not if only the forward speed (and V_T accordingly) changes.

$$\boldsymbol{\delta_{BLI,A} \propto \frac{\xi_{BLI\,VT} V_T + V}{V}} \tag{6.26}$$

6.2.2.1.3 Equation

The boundary layer thickness is proportional to the multiplication of previous observations (equation 6.27)

$$\boldsymbol{\delta_{BLI,A} \propto \delta \left(\frac{T}{h}\right) \left(\frac{\xi_{BLI\,VT} V_T + V}{V}\right)} \tag{6.27}$$

A regression is made (with "R") by selecting the tipping points in the model tests. and thus the coefficient $\xi_{BLI\,VT}$ from equation 6.26 is derived. This coefficient $\xi_{BLI\,VT}$ equals ½ or only half of the thrust velocity V_T is taken into account. With equation 6.24 the following formulation for $\delta_{BLI,A}$ is found in equation 6.28:

$$\boldsymbol{\delta_{BLI,A} \propto \left(0.16 \frac{Lpp}{\sqrt[7]{Re}}\right) \left(\frac{T}{h}\right) \left(\frac{\frac{V_T}{2} + V}{V}\right) \propto \frac{Lpp}{\sqrt[7]{Re}} \frac{T}{h} \frac{(V_T + 2V)}{V}} \tag{6.28}$$

For a twin screw propelled ship the thrust measured on the propeller closest to the bank is taken into account to calculate V_T and thus $\delta_{BLI,A}$. Equation 6.28 still stands because V_T is the (theoretical) velocity in the propeller wake. Since the propeller diameter (relative to the main dimensions of the vessel) when there are two propellers instead of one will be smaller, the propeller area A_0 will also be smaller and only counts for half a ship. To explain this, the thrust measured on the port side propeller shaft T_{Pp} is assumed to be exactly the same as the thrust on the starboard shaft T_{Ps}. The average thrust velocity behind the vessel is:

$$\boldsymbol{V_{Tavg} = \frac{V_{Tp} + V_{Ts}}{2}} \tag{6.29}$$

Now δ_{BLI} can be calculated with this average thrust velocity:

$$\boldsymbol{\delta_{BLI,A} \propto \frac{\frac{V_{Tavg}}{2} + V}{V}} \tag{6.30}$$

If only the thrust on the shaft closer to the bank (e.g. at port side) is used, then:

$$\mathbf{V_{Tavg}} = \frac{\mathbf{V_{Tp}}+\mathbf{V_{Tp}}}{\mathbf{2}} = \mathbf{V_{Tp}} \tag{6.31}$$

$$\boldsymbol{\delta_{BLI,A}} \propto \frac{\frac{V_{Tp}}{2}+V}{V} \tag{6.32}$$

6.2.2.2 Scale effect of boundary layer influence thickness

Remark that the ratio between δ_{BLI} at model scale (subscript m for model) and at full scale (subscript s for ship) is not equal to the scale factor λ.

$$\frac{\delta_{BLIs}}{\delta_{BLIm}} \neq \lambda = \frac{Lpp_s}{Lpp_m} \tag{6.33}$$

The ratio between the full scale and model scale δ_{BLI} is calculated in equation 6.34:

$$\frac{\mathbf{\delta_{BLIs}}}{\mathbf{\delta_{BLIm}}} = \frac{\frac{\mathbf{Lpp_S}}{\sqrt[7]{\mathbf{Re_S}}}\frac{\mathbf{T_S}}{\mathbf{h_S}}\frac{(\mathbf{V_{TS}}+2\mathbf{V_S})}{\mathbf{V_S}}}{\frac{\mathbf{Lpp_m}}{\sqrt[7]{\mathbf{Re_m}}}\frac{\mathbf{T_m}}{\mathbf{h_m}}\frac{(\mathbf{V_{Tm}}+2\mathbf{V_m})}{\mathbf{V_m}}} \tag{6.34}$$

Equation 6.34 can first be simplified to $\left(\frac{\mathbf{T_s}}{\mathbf{h_s}} = \frac{\mathbf{T_m}}{\mathbf{h_m}}\right)$:

$$\frac{\mathbf{\delta_{BLIs}}}{\mathbf{\delta_{BLIm}}} = \frac{\frac{\mathbf{Lpp_S}}{\sqrt[7]{\mathbf{Re_S}}}\frac{(\mathbf{V_{TS}}+2\mathbf{V_S})}{\mathbf{V_S}}}{\frac{\mathbf{Lpp_m}}{\sqrt[7]{\mathbf{Re_m}}}\frac{(\mathbf{V_{Tm}}+2\mathbf{V_m})}{\mathbf{V_m}}} \tag{6.35}$$

If the ratio of the thrust T_P at full scale and model scale are λ^3 then:

$$\frac{\frac{V_{TS}+2V_S}{2V_S}}{\frac{V_{Tm}+2V_m}{2V_m}} \xrightarrow{T_{PS}=\lambda^3\ T_{Pm}} \mathbf{1} \tag{6.36}$$

Equation 6.35 can further be simplified to:

$$\frac{\mathbf{\delta_{BLIs}}}{\mathbf{\delta_{BLIm}}} = \frac{\frac{Lpp_s}{\sqrt[7]{Re_s}}}{\frac{Lpp_m}{\sqrt[7]{Re_m}}} = \frac{Lpp_s}{Lpp_m}\frac{\sqrt[7]{Re_m}}{\sqrt[7]{Re_s}} \tag{6.37}$$

If the model tests are carried out in the same fluid as the full scale fluid, the dynamic viscosity at model scale and at full scale will be the same, $\nu_m = \nu_s$. Standard model tests are carried out in fresh water (e.g. at 15°C: $\nu_m = 1.1386\mathrm{E}^{-6}\mathrm{m}^2/\mathrm{s}$) while most of the full scale

vessels sail in salty seawater (e.g. at 15°C: $\nu_s = 1.1892\mathrm{E}^{-6}\mathrm{m}^2/\mathrm{s}$). For reasons of simplicity for the explanation it is further assumed that both dynamic viscosities are equal. The ratio between the full scale boundary layer influence thickness and the thickness at model scale becomes:

$$\frac{\boldsymbol{\delta_{BLIs}}}{\boldsymbol{\delta_{BLIm}}} = \frac{\sqrt[7]{Re_m}}{\sqrt[7]{Re_s}}\lambda = \lambda\left(\sqrt[7]{\frac{V_m Lpp_m}{V_s Lpp_s}}\right) = \lambda\left(\frac{1}{\lambda\sqrt{\lambda}}\right)^{\frac{1}{7}} = \lambda^{\frac{11}{14}} \qquad (6.38)$$

In Figure 6.12 the ratio of equation 6.38 divided to the scale factor λ is plotted to that same scale factor. At a scale factor λ of 25 the boundary layer (influence thickness) will be about (relative) twice as thick on model scale as it is on full scale.

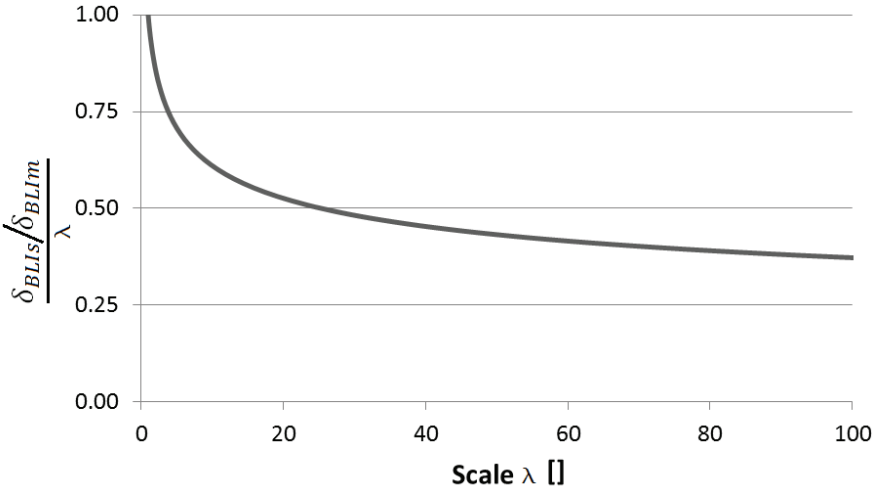

Figure 6.12 the influence of the scale factor λ on the boundary layer influence thickness

Figure 6.12 gives an indication of the $\delta_{BLI,A}$ for common dimensions on model scale and at full scale. The boundary layer influence thickness is at model scale about 0.04 to 0.06 m ($Re > 10^5$) and at full scale 1 to 3 m ($Re > 10^8$).

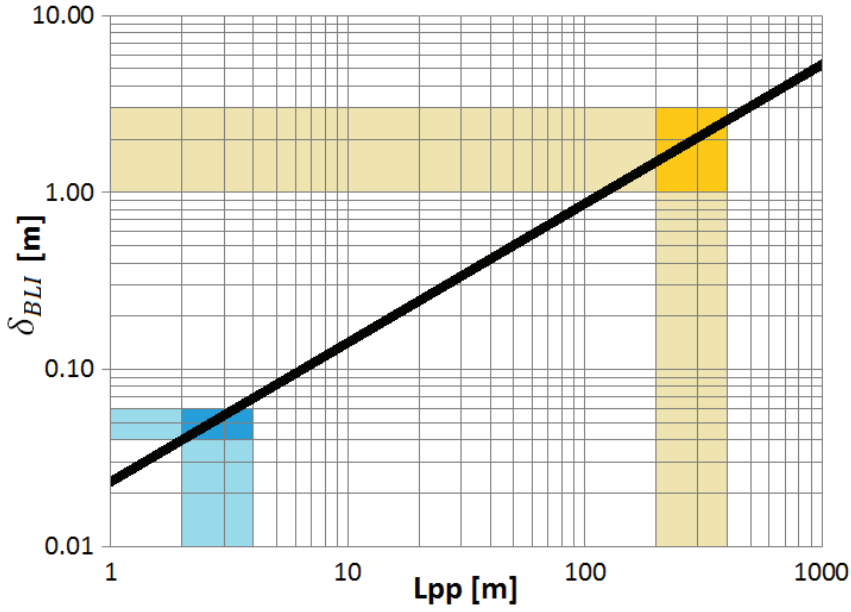

Figure 6.13 this is an indication of the thickness of δ_{BLI} at model scale (blue, 4-6cm) and full scale (yellow, 1-3m)

6.2.3 Function for the lateral position with boundary layer influence

Since the lateral force Y_A tends to go to zero when the gap y_{wall} between ship and bank disappears, the function for the lateral position f(y) is forced to be zero at $\frac{2y}{W-B} = 1$.

Now the distance to the wall is modelled as:

$$\mathbf{f(y)} = \begin{cases} \dfrac{\xi_y y}{0.5(1+\xi_y)(W-B)-|y|} & \mathbf{y_{wall} \geq \delta_{BLI,A}} \\ \dfrac{y_{wall}}{\delta_{BLI}} \dfrac{\xi_y y}{0.5(1+\xi_y)(W-B)-|y|} & \mathbf{y_{wall} < \delta_{BLI,A}} \end{cases} \tag{6.39}$$

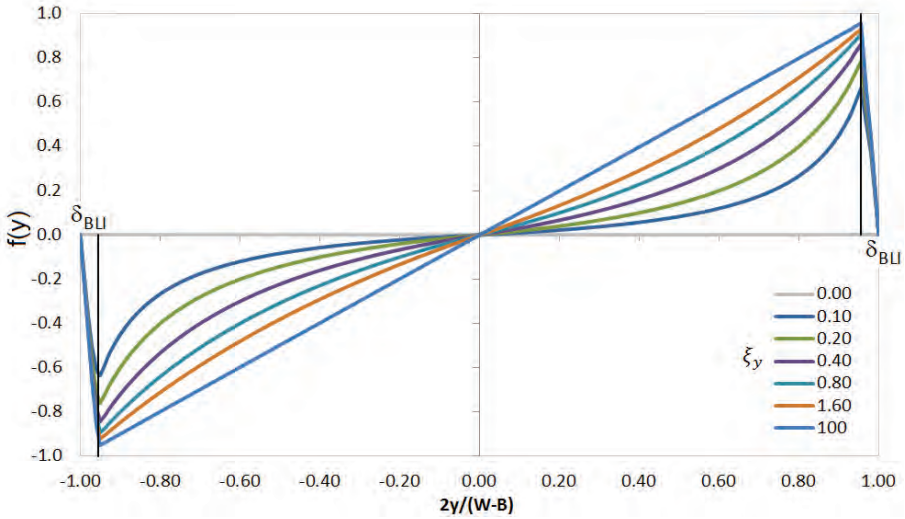

Figure 6.14 the function for the lateral position y taking into account δ_{BLI}

In Figure 6.14 the inverse of the equivalent wall distance parameter as modelled in a rectangular cross section is plotted for the entire range between -1 and 1. The decrease close to the bank is clearly visible. For one curve (here ξ_y=0.8) the region close to the starboard bank is plotted in Figure 6.15.

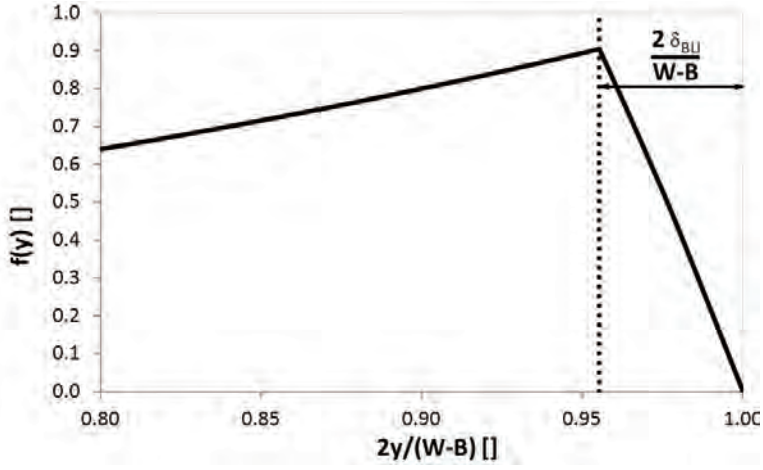

Figure 6.15 the function for the lateral position y taken into account δ_{BLI} closer to the starboard bank.

Now the distance to the wall (as modelled) is plotted in Figure 6.16 with the same tests as in Figure 6.9.

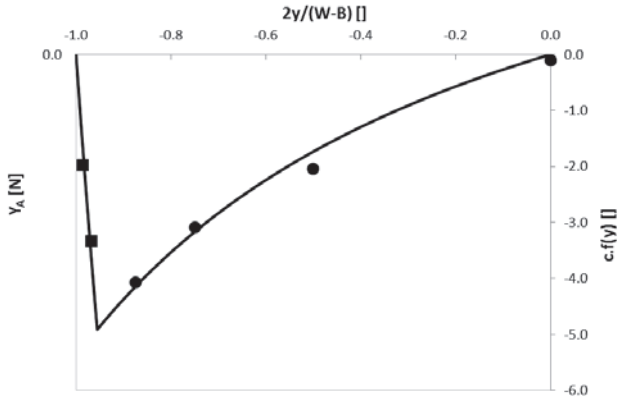

Figure 6.16 the function for the lateral position and model tests taken into account the boundary layer influence on model scale

The two previously unexpected low magnitudes for Y_A very close to the vertical wall (squares in Figure 6.9 and Figure 6.16) are in the influence zone of the boundary layer.

6.2.4 Midship coefficient C_M

The lateral distance y_{wall} between the Wigley hull and the vertical wall is for some tests smaller than $\delta_{BLI,A}$ but the magnitude of the lateral force at the aft perpendicular did not decrease as expected based upon the new insight.

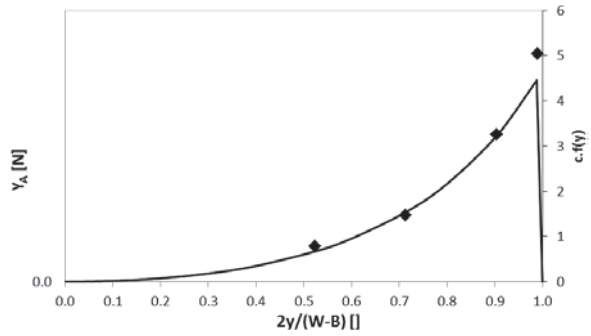

Figure 6.17 the Wigley hull towed at different lateral positions from a vertical wall W01, 0.73m/s, h/T=1.35

This behaviour is explained by the very different midship coefficient C_M of the Wigley hull (C_M =0.66) compared to the other ship models (>0.94) (Figure 6.18 and Table 6.1).

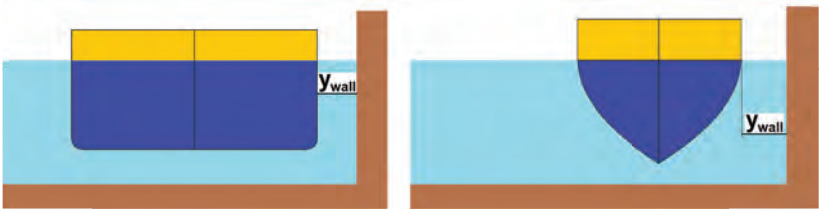

Figure 6.18 cross section for the ship models T0Z (left) and W01 (right)

The gap between ship and wall is much wider for the Wigley hull than the distance y_{wall} suggests because of this low C_M value. It is better to take the distance between ship and wall as the average distance over the entire draft of the vessel at the midship section.

$$y_{C_M} = \frac{W}{2} - \left(\frac{B}{2} + (1 - C_M)\frac{B}{2} + y_{wall}\right) = \frac{W}{2} - (2 - C_M)\frac{B}{2} - y_{wall} \qquad (6.40)$$

Equation 6.40 can also be written as a function of y:

$$y_{C_M} = y - (1 - C_M)\frac{B}{2} \qquad (6.41)$$

For the tanker T0Z with a C_M of 0.998 this does not change a lot but for the Wigley W01 with a C_M value equal to 0.662 the value y_{CM} is significantly different from y. Now the model tests as close as y_{wall}=0.020m are out of the influence of the boundary layer δ_{BLI} (Figure 6.19).

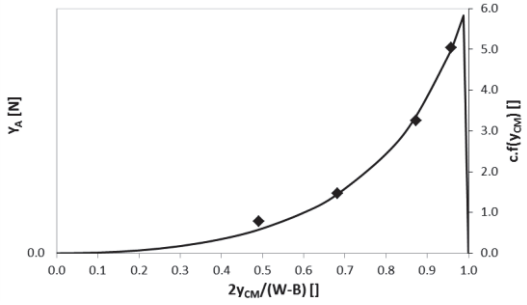

Figure 6.19 the lateral position taken the midship coefficient C_M into account

6.2.5 Influence width

6.2.5.1 Horizontal reach

A bank will only affect the pressure distribution on the hull and, therefore, the forces and moments on the ship if the distance between ship and bank is sufficiently small. As a result, for a particular ship a value for the ship-bank distance can be defined that - for practical application - can be considered as the boundary between open and confined water. If the ship-bank distance exceeds this value, no (significant) influence of the bank on her manoeuvrability will be observed. This horizontal reach has been investigated by Barrass (influence on squat) and Römisch in (Härting & Reinking 2004). Both proposed an expression only based on a main parameter of the ship (block coefficient C_B and length Lpp respectively).

A systematic series of tests has been carried out at Flanders Hydraulics Research (Lataire et al. 2007) to define a speed dependent expression of the horizontal reach (or influence width of the bank). For this specific purpose a (small) bare hull ship model of a tanker (T0H, Table 6.1) was towed in cross section QY_0_7.00_0 ("empty" towing tank) at 4 different forward speeds, 3 water depths and 11 lateral positions (Table 6.2).

h/T	U	2y/(W-B)	y_{wall}/B
[]	[m/s]	[]	[]
1.10	0.336	-0.164	-10.50
1.35	0.501	0.000	11.36
2.00	0.752	0.076	10.50
	1.003	0.164	9.50
		0.252	8.50
		0.340	7.50
		0.428	6.50
		0.516	5.50
		0.604	4.50
		0.692	3.50
		0.736	3.00

Table 6.2 properties of the model test environment to investigate the influence width

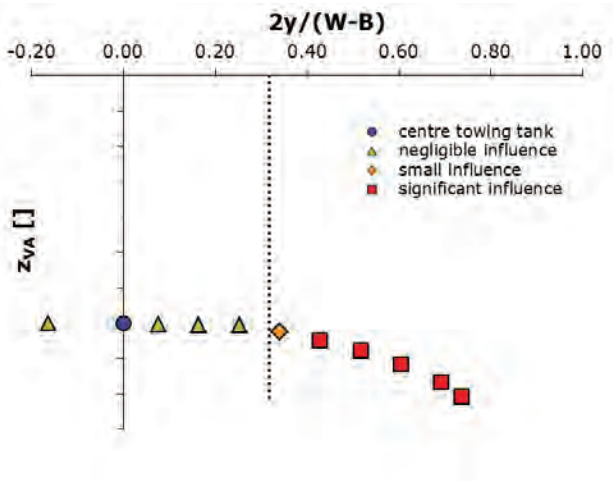

Figure 6.20 y_{infl} T0H, 1.003m/s, h=1.35T, running sinkage at the aft perpendicular

For all combinations of speed and water depth, the running sinkage at the aft perpendicular z_{VA} can be plotted as a function of the dimensionless lateral distance $\frac{2y}{W-B}$ (for reasons of simplicity C_M of ship model T0H 0.996 is rounded off to one). An example is given in Figure 6.20 for the model tests carried out in a water depth h=1.35 T and forward speed of 1.003m/s. The magnitude of the running sinkage at the stern z_{VA} increases once the vessel is in the influence zone of the bank. In this plot (Figure 6.20) three ranges can be distinguished (neglecting the model test on the centre line of the towing tank):

- If the distance to the bank is sufficiently large, the influence of the closest bank on the ship is negligible ▲;
- Close to the bank, a significant influence is generated ■;
- In between, the influence is measurable but not significant ◆.

Such a division in three ranges is carried out for all the model tests as listed in Table 6.2. The results of this classification are summarized in one graph (Figure 6.21) as a function of the non-dimensional lateral distance $\frac{2y}{W-B}$ and the water depth related Froude number Fr_h.

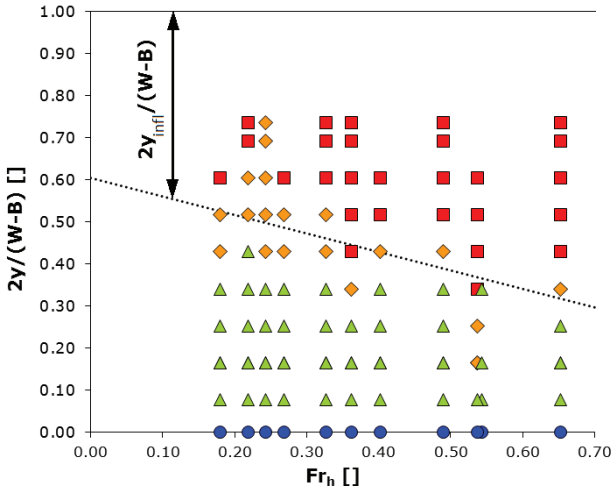

Figure 6.21 Fr_h and 2y/(W-B) for all EFD results with T0H in the empty towing tank QY_0_7.00_0 at different water depths and forward speeds

The dividing line (dotted line Figure 6.21) between combinations with significant influence and without significant influence shows dependency with the water depth dependent Froude number Fr_h. This division line is the influence distance sought for:

$$\mathbf{y_{infl}} = \mathbf{B(5Fr_h + 5)} \tag{6.42}$$

Equation 6.42 is based on the running sinkage at the aft because it is expected that this value is the most 'sensible' for the presence of a bank during model tests. The sinkage aft 'feels' the bank significantly faster than the forces. As comparison the same influence distance is calculated based upon the publication (Barrass 2004):

$$\mathbf{y_{infl}} = \mathbf{0.5\ B\left(\frac{7.04}{Cb^{0.85}}\right)} \tag{6.43}$$

and according to the publication (Römisch 2004) this is:

$$\mathbf{y_{infl}} = \mathbf{0.5\ \frac{Lpp}{0.3}} \tag{6.44}$$

From the point of view of ship manoeuvrability y_{infl} can be considered as the (half) width of the influence zone for bank effects. As a result, a ship sailing at a distance larger than this

distance from the closest bank undergoes no significant bank effects.

$$y_{wall} > y_{infl} - \frac{B}{2} \tag{6.45}$$

6.2.5.2 Ship's centre line further away from closest bank than y_{infl}

If the distance between the centre line of the ship and the closest bank is larger than the influence width y_{infl} then the value $f(y)$ must be zero (equation 6.46). The vessel sails as in a horizontal unrestricted (but shallow) fairway. There will be no influence of the bank on the vessel.

$$y_{wall} + \frac{B}{2} > y_{infl} \Rightarrow f(y) = 0 \tag{6.46}$$

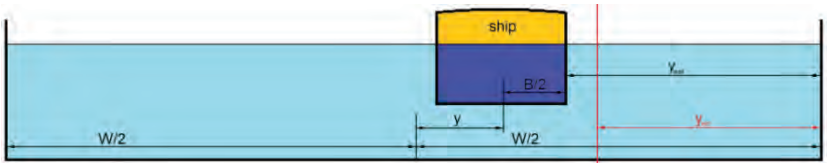

Figure 6.22 a vessel further away from the closest bank than y_{infl}; $y_{wall}+B/2>y_{infl}$

6.2.5.3 Width of the fairway wider than $2y_{infl}$

When sailing in a very wide fairway (Figure 6.23) not only the total width W of the fairway will be large but the function f(y) can also reach a high value. As a consequence the ratio $\frac{2y}{W-B}$ will tend to 1 (Equation 6.47) even when the gap between ship and bank y_{wall} is not (extremely) small.

$$\lim_{\substack{W\to\infty \\ y\to\infty/2}} \left(\frac{2y}{W-B}\right) = 1 \tag{6.47}$$

The sensitivity for the distance between ship and bank will be lost. Therefore W must be limited to the double of the influence width y_{infl} and the eccentricity y must be calculated accordingly.

$$\frac{W}{2} > y_{infl} \Rightarrow W = 2.y_{infl} \tag{6.48}$$

$$\frac{W}{2} > y_{infl} \Rightarrow y = y_{infl} - \left(\frac{B}{2} + y_{wall}\right) \tag{6.49}$$

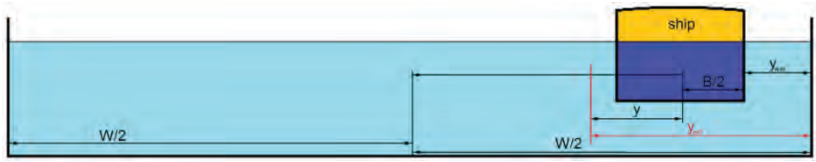

Figure 6.23 a vessel sailing in a cross section wider than 2 y_{infl}

6.2.6 Flow chart for f(y) in a rectangular cross section

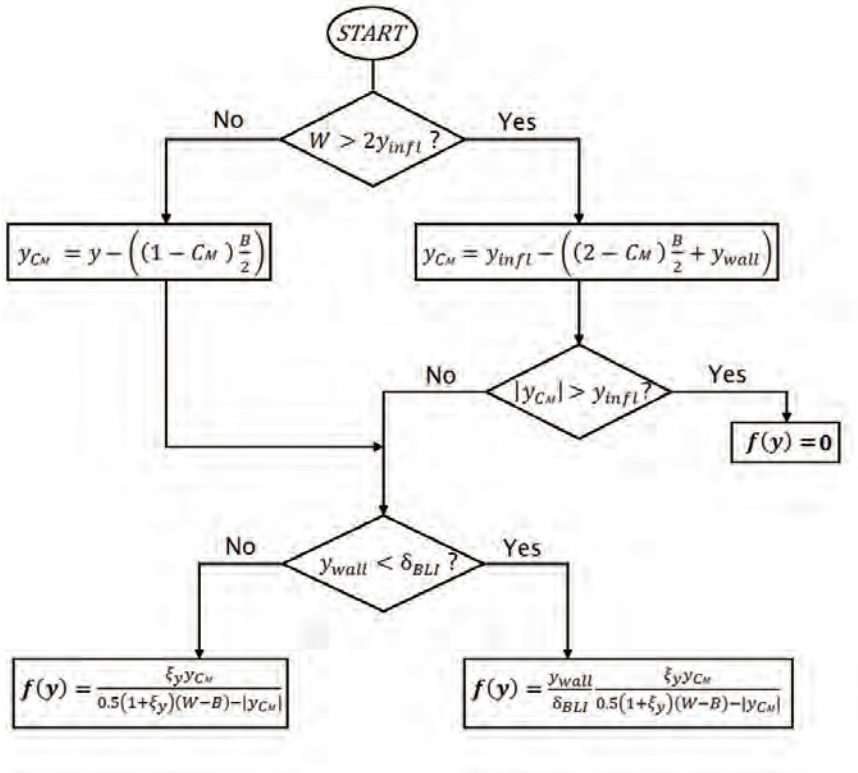

Figure 6.24 flow chart f(y) rectangular cross section

The flow chart to calculate f(y) takes the influence width y_{infl} and boundary layer influence thickness into account (Figure 6.24).

6.3 Lateral position in a random cross section

It is more seldom than common for a vessel to sail in a rectangular cross section. Sloped banks, dredged channels, natural river bottoms with a changeable bathymetry are much more common. As mentioned before, in these type of arbitrary cross sections the lateral position in the fairway is ambiguously defined. To overcome this problem first the surface piercing constant sloped banks are investigated, then the semi-submerged bank types and finally a solution for any random cross section will be given.

6.3.1 Surface piercing banks

Surface piercing banks are banks with a constant slope from the deepest part of the fairway up to the free surface. Ship model T0Z is tested along a wide range of different sloped banks. The combination and comparison between the model tests along a vertical wall and along the sloped banks are used to further extend the knowledge on the sloped banks.

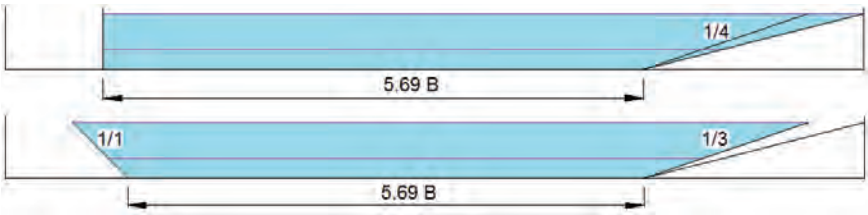

Figure 6.25 the test sections with surface piercing banks carried out in the FHR towing tank for ship model T0Z

The ship model T0Z has been tested at the same water depths and forward speeds along the vertical bank QY_0_4.400_4 as it was tested along the sloped banks SP_1_4.200_3, SP_3_4.200_1 and SP_4_4.400_0 (Figure 6.25). Along bank QY_0_4.400_4 the distance y_{wall} is straightforward to define. Because of the sloped opposite bank the distance y is calculated based upon the cross section area Ω:

$$y = \frac{1}{2}\frac{\Omega}{h} - \frac{B}{2} - y_{wall} \tag{6.50}$$

For all the water depth and forward speed combinations a set of the coefficients ξ_y and ξ_{YA} (equation 6.51) has been derived based upon the model tests with model T0Z along bank QY_0_4.400_4.

$$\mathbf{Y_A} = \xi_{\mathbf{Y_A}}\, \mathbf{f}(\xi_{\mathbf{y}}, \boldsymbol{y}) \tag{6.51}$$

Based upon these two coefficients ξ_y and ξ_{YA} the equivalent distance y_{eq} has been calculated with the same model (equation 6.51) and coefficients (according to the same water depth and forward speed) and Y_A along banks SP_1_4.200_3, SP_3_4.200_1 and SP_4_4.400_0.

Now the position of a vertical wall which generates the same Y_A as the sloped and surface piercing wall under consideration is determined. This distance y_{eq} shows the position of a vertical wall that results in the same force at the aft perpendicular in the same conditions (water depth, forward speed and blockage).

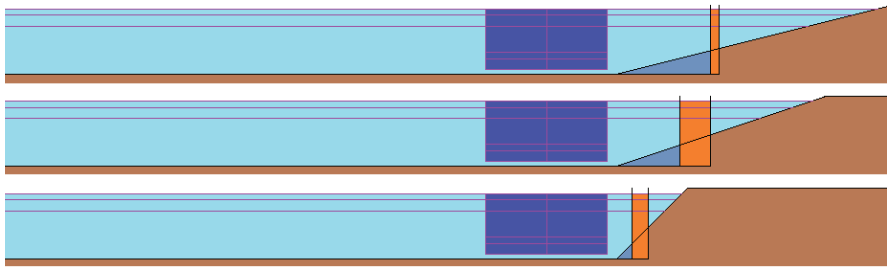

Figure 6.26 the position of the vertical wall equivalent to a sloped wall that results in the same Y_A

For the three sloped banks from Figure 6.25 the distance y_{eq} is plotted in Figure 6.26 as a wall with a thickness. This thickness originates from the different y_{eq} for each water depth and forward speed. The wall thickness is generated based upon the minimal and maximal values for y_{eq}.

A new expression to include the influence of the lateral position in the mathematical model must cope with all the influences of a sloped bank:

- The further from the vessel the smaller the influence of the geometry. There is no or almost no influence at a distance larger than the influence width y_{infl} from the vessel.
- No or almost no influence of the bathymetry should be observed at a depth much deeper than multiple times the draft.
- All types of geometries must be covered. (sloped banks, semi-submerged banks, changing slope angles, random bank geometries such as natural riverbeds, dredged channels, dredged fairway at sea…)

6.3.2 Semi-submerged banks

All model tests carried out with model T0Z are tests along a surface piercing bank. To check the influence of semi-submerged banks, the model tests carried out with the model C0U are used. To be valid for the model, all distances y between centre ship and bank must be larger than $B/2 + \delta_{BLI,A}$.

$$\frac{B}{2} + \delta_{BLI,A} < y < y_{infl} \tag{6.52}$$

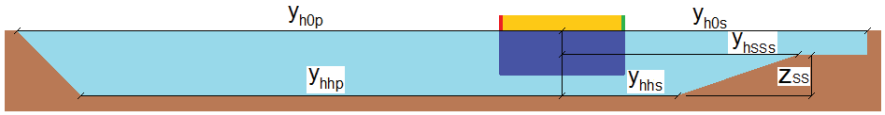

Figure 6.27 definition of discrete lateral positions of importance in a semi submerged bank configuration

6.3.3 Weight factor w

The weight factor *w* (not to be confused with the vertical velocity component) is a value between 0 and 1 which indicates the influence of a water particle on the bank effects on a ship. A water particle closer to the hull will have a value closer to 1. The weight factor will tend to zero once the water particle is out of the horizontal reach (y_{infl}). The closer the water particle located to the free surface, the larger the weight factor *w* of that water particle.

The 'value' of a water particle decreases with the distance from the vessel and the closer to the bottom. By definition at the cross section of the centre line of the ship and the free surface (at rest) the weight factor is 1. The weight factor is graphically shown in Figure 6.28.

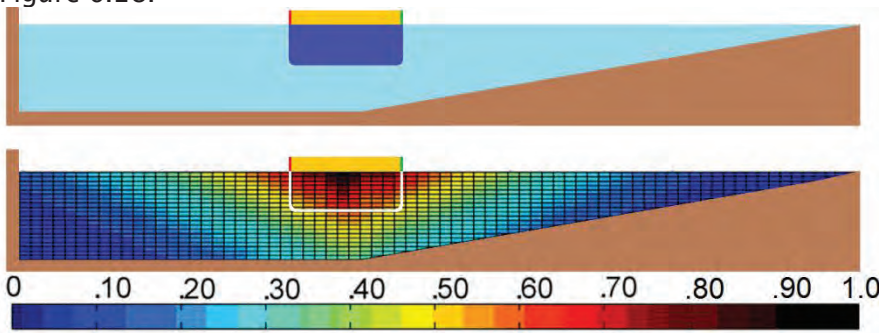

Figure 6.28 the ship in a cross section and a graphical representation of the weight distribution in the same cross section

The weight factor w is a decreasing exponential function, analogous to Norrbin's factor (Norrbin 1974). The expression of the weight distribution w in the ship bound coordinate system is:

$$\mathbf{w} = \mathbf{e}^{-\left(\xi_y \frac{|y|}{y_{infl}} + \xi_z \frac{|z|}{T}\right)} \tag{6.53}$$

6.3.3.1 χ Rectangle

The 'weight' χ of any arbitrary area A is defined as:

$$\chi = \oiint_A \; w \, dA \tag{6.54}$$

Figure 6.29 weight distribution of a rectangular section

For a rectangle with coordinates (y_1,z_1); (y_2,z_1); (y_1,z_2); (y_2,z_2) (Figure 6.29) the double integral of equation 6.54 can be solved analytically:

$$\chi_{rect} = \int_{z_1}^{z_2} \int_{y_1}^{y_2} e^{-\left(\xi_y \frac{|y|}{y_{infl}} + \xi_z \frac{|z|}{T}\right)} dy \, dz \tag{6.55}$$

$$\chi_{rect} = -\frac{y_{infl} T}{\xi_y \xi_z} \left(e^{-\xi_y \frac{y_1}{y_{infl}} - \xi_z \frac{z_1}{T}} - e^{-\xi_y \frac{y_2}{y_{infl}} - \xi_z \frac{z_1}{T}} - e^{-\xi_y \frac{y_1}{y_{infl}} - \xi_z \frac{z_2}{T}} + e^{-\xi_y \frac{y_2}{y_{infl}} - \xi_z \frac{z_2}{T}} \right) \tag{6.56}$$

6.3.3.2 χ ship

The 'weight' χ_{ship} covered by a rectangle B T at the position of the ship is:

$$\chi_{ship} = \int_0^T \int_{-\frac{B}{2}}^{\frac{B}{2}} e^{-\left(\xi_y \frac{|y|}{y_{infl}} + \xi_z \frac{|z|}{T}\right)} dy\, dz \tag{6.57}$$

$$\chi_{ship} = 2\frac{y_{infl}\, T}{\xi_y \xi_z}\left(1 - e^{-\frac{\xi_y B}{2y_{infl}}}\right)\left(1 - e^{-\xi_z}\right) \tag{6.58}$$

6.3.3.3 χ ocean

The integral 6.54 has a non-infinite solution for an infinite area. The weight of an infinitely wide and deep ocean is calculated:

$$\chi_{ocean} = 2\int_0^\infty \int_0^\infty e^{-\left(\xi_y \frac{|y|}{y_{infl}} + \xi_z \frac{|z|}{T}\right)} dy\, dz \tag{6.59}$$

$$\chi_{ocean} = 2\frac{y_{infl}\, T}{\xi_y \xi_z} \tag{6.60}$$

6.3.3.4 Distance to bank d2b

The weight at both sides of the vessel can be calculated with equations 6.61 and 6.62. All 'water particles' are taken into account, also the particles at a distance further away from the vessel than y_{infl} because the weight value w for these particles will be insignificantly small.

$$\chi_s = \int_0^h \int_0^{y_s} e^{-\left(\xi_y \frac{|y|}{y_{infl}} + \xi_z \frac{|z|}{T}\right)} dy\, dz \tag{6.61}$$

$$\chi_p = \int_0^h \int_0^{y_p} e^{-\left(\xi_y \frac{|y|}{y_{infl}} + \xi_z \frac{|z|}{T}\right)} dy\, dz \tag{6.62}$$

A graphical interpretation of χ_p and χ_s is shown in Figure 6.30. The value χ for a trapezoidal cross section is analytically derived in Appendix 11.7.

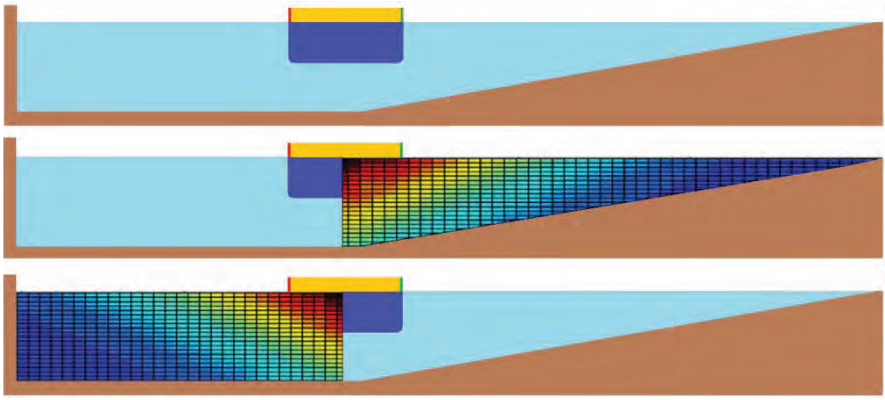

Figure 6.30 graphical interpretation of χ_P (the integrated and weighted area at port) and χ_S (the integrated area at starboard)

The dimensionless distance to bank parameter d2b is by definition:

$$\frac{1}{d2b} = \boldsymbol{d2b^{-1}} = \frac{\frac{\chi_{ship}}{2}}{\chi_s} - \frac{\frac{\chi_{ship}}{2}}{\chi_p} = \frac{\chi_{ship}}{2\chi_s} - \frac{\chi_{ship}}{2\chi_p} \tag{6.63}$$

$$\boldsymbol{d2b} = \frac{2}{\chi_{ship}} \frac{\chi_p \chi_s}{\chi_p - \chi_s} \tag{6.64}$$

It is the purpose of $d2b^{-1}$ to be proportional to the force Y_A (equation 6.65). This is obtained through the coefficients ξ_y and ξ_z. These coefficients are calculated with the regression program "R" (Venables et al. 2002) and the outcome from the model tests.

$$\mathbf{Y_A} \propto \boldsymbol{d2b^{-1}} \tag{6.65}$$

When sailing on the centre line of a symmetric cross section then χ_s will be equal to χ_p and thus $d2b^{-1}$ will be zero. When sailing in unrestricted waters the values χ_s and χ_p again will be equal and as a consequence $d2b^{-1}=0$.

6.3.3.5 Relation $d2b^{-1}$ and Y_A

The lateral force at the aft perpendicular Y_A of ship model T0Z is plotted in Figure 6.31. This plot contains results from model tests carried out at a forward speed according to 10 knots full scale, a water depth of 150% of the draft and a propeller rate 554rpm (model scale). Six different bank geometries are included; three vertical banks and three surface piercing banks, with four different lateral positions y for each bank.

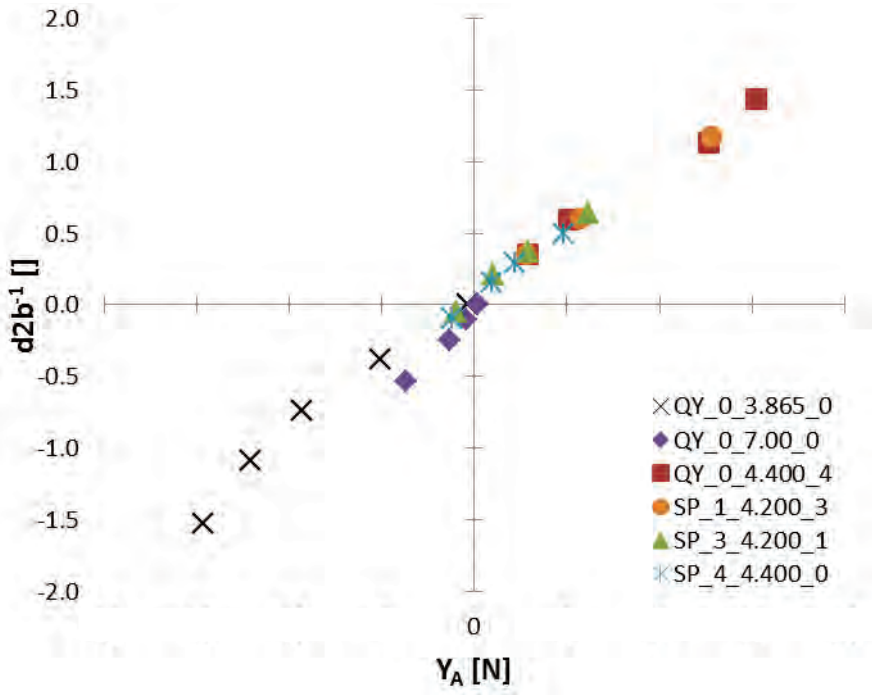

Figure 6.31 $d2b^{-1}$vs Y_A for T0Z, 10kts, 554rpm, h=1.50T

The positive propeller action will generate a positive non-zero thrust and as a consequence a thrust velocity V_T. The influence of this thrust is not taken into account in Figure 6.31. The difference in bank geometry between a vertical bank and, for example, a slope of 1/4 (SP_4_4.400_0) is almost eliminated.

6.4 Water depth

The water depth is very straightforward when a ship sails over a perfectly flat and horizontal bottom. If the bathymetry is more irregular the water depth is not that easy to define. Furthermore the water depth of importance can be different depending of the field of application.

6.4.1 Definitions of the different water depths in an irregular cross section

6.4.1.1 Towing tank water depth h

Figure 6.32 water depth h, the deepest water depth in the cross section or 'towing tank water depth'

All the model tests were carried out in a towing tank with a flat bottom with banks installed. For the model tests under consideration the banks were installed directly on the bottom of the towing tank, no false bottoms as in (Sano et al. 2012) are installed. The water depth h is defined as the deepest water depth in the towing tank, measured as the distance between the original bottom of the towing tank and the free surface at rest (Figure 6.33). This water depth h is independent of the installed banks, and of the position of the ship model in the towing tank. This water depth is more practical in nature than physically based. This is the water depth of importance for the technical personnel of the towing tank who carries out the model tests (or create the input files in case of the FHR towing tank).

6.4.1.2 Average water depth of the cross section h_{avg}

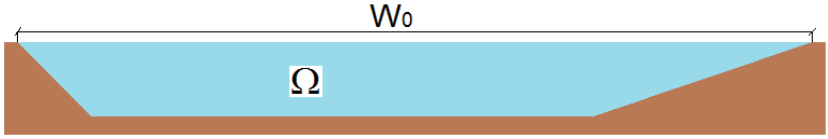

Figure 6.33 the cross section area Ω and width at the free surface W_0

The width at the free surface is W_0 [m] and the area of the cross section of the fairway is Ω [m²]. The ratio between both is the average water depth of the cross section h_{avg}.(equation 6.66, Figure 6.33).

$$h_{avg} = \frac{\Omega}{W_0} \tag{6.66}$$

This is again independent of the ship but only dependent of the geometry of the cross section. This water depth is important to calculate the critical speed of the cross section (Section 6.5).

6.4.1.3 Water depth for the ship h_{ship}

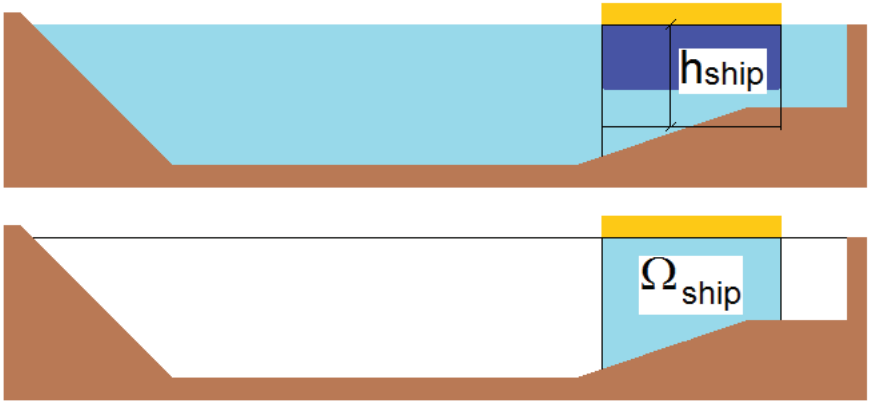

Figure 6.34 average water depth at the position of the vessel h_{ship}

$$h_{ship} = \frac{\Omega_{ship}}{B} \tag{6.67}$$

The water depth the ship 'feels' depends on the bathymetry but also on the position of the vessel in this bathymetry. The water depth h_{ship} is defined as the average of the local water depth under the vessel (equation 6.67 and Figure 6.34). The value for Ω_{ship} is the area at the midship section of the vessel from starboard to port, from the bottom up to the free surface. The water depth h_{ship} is of importance to calculate the water depth dependent Froude Number Fr_h.

$$Fr_h = \frac{V}{\sqrt{g\, h_{ship}}} \tag{6.68}$$

6.4.2 Influence of the water depth

6.4.2.1 Unexpected observation

The lateral attraction force at the aft perpendicular is expected to increase as the water depth decreases. Assume a vessel sailing in a rectangular cross section at a constant forward speed and a distance y_{wall} ($>\delta_{BLI}$) from the closest bank. When this ship sails in this cross section in deep water, a part of the displaced water can rather easily travel in the (wide) gap between the ship's keel and bottom. Now the same ship sails under exactly the same conditions but the water depth is decreased to shallow water. The same amount of water displaced by the vessel cannot travel as easily between keel and bottom because this gap is much reduced in shallow water. Therefore, more water will travel along both sides of the ship's hull. This will result in a higher pressure drop between ship and bank and thus a higher magnitude of the attraction force.

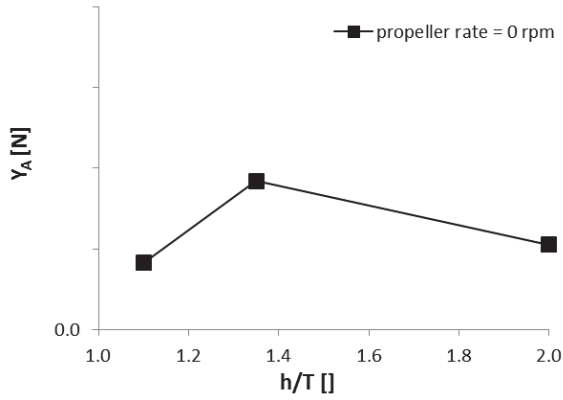

Figure 6.35 Y_A for C0U at 10 knots full scale, bank QY_0_6.330_0 and y_{wall}=1.130m

If the forces measured during the model tests with ship model C0U (with fixed propeller = 0 rpm) are compared under exactly the same circumstances but only the water depth varies, then the lateral force Y_A did not increase with decreasing water depth (Figure 6.35). This unexpected relation was not unique but

systematic for almost all tests carried out without a positive thrust T (or with fixed propeller).

Sailing from medium deep $\frac{h}{T} = 2.0$ to shallow water $\frac{h}{T} = 1.35$ the magnitude of the attraction force Y_A increases. Sailing from shallow water $\frac{h}{T} = 1.35$ to very shallow water $\frac{h}{T} = 1.1$ the force Y_A does not increase but decreases. The explanation for this behaviour is found in the boundary layer thickness, similar as in section 6.2.2.2.

6.4.2.2 Extra model tests with a wide range of water depths

First the water depth is sought for when the force Y_A no longer increases with decreasing water depth. The influence of two parameters must be distinguished and separated: first the influence of the water depth on the magnitude of the lateral force at the aft Y_A, second the influence of the (active) propeller on the same force (Figure 6.36).

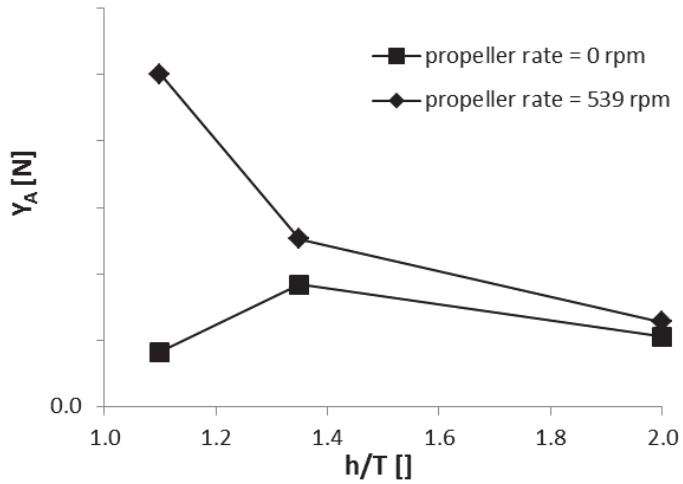

Figure 6.36 Y_A for C0U at 10 knots full scale, bank QY_0_6.330_0 and y_{wall}=1.130m with and without active propeller action

As mentioned before the smaller the under keel clearance the larger the velocity of the return flow. The larger the return flow, the lower the pressure at the stern of the vessel and the larger the

magnitude of the attraction force at the aft perpendicular Y_A. This assumption seems to be valid for the model tests as shown in Figure 6.36 with a propeller rate of 539 rpm (80% of max rpm). As mentioned in 6.4.2.1, the model tests with a fixed propeller (0 rpm) do not act as expected. The magnitude of the attraction force is at the shallowest water depth, the lowest. This observation still stand for all model tests carried out in 2008 (Lataire et al. 2009) and 2010 (Lataire et al. 2012b). All these model tests were carried out at three water depths for each ship model.

h	h/T	u	n	2y/(W-B)	Y
[m]	[]	[m/s]	[rpm]	[]	[m]
0.163	1.10	0.437	0.000	0.000	0.000
0.166	1.12	0.582	0.000	0.646	2.060
0.169	1.14	0.728	0.000	0.784	2.500
0.173	1.17	0.873	0.000		
0.178	1.20	0.437	269		
0.185	1.25	0.582	364		
0.192	1.30	0.728	452		
0.200	1.35	0.873	546		
0.207	1.40				
0.222	1.50				
0.326	2.20				

Table 6.3 model test program (#207) in search for the unexpected water depth influence

In 2013 model tests were carried out in the towing tank of FHR (without installed banks; QY_0_7.00_0). The chosen ship model was A01 (twin screw ship model of a car carrier). For a combination of forward speeds, propeller rates (port and starboard propeller always at the same rate) and lateral positions the tests are repeated for 11 different water depths h (Table 6.3, Figure 6.37). First only the model tests with a fixed propeller (=0 rpm) are considered.

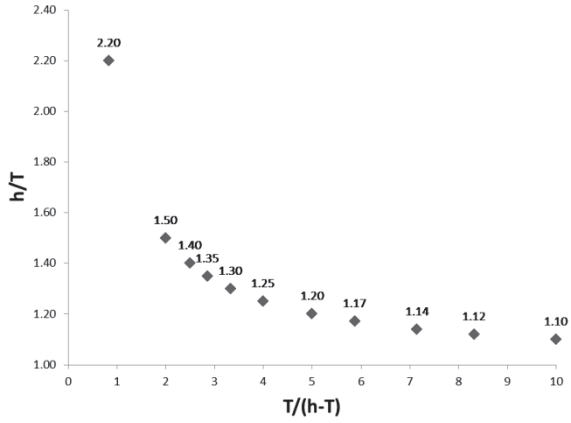

Figure 6.37 the wide range of tested water depths with ship model A01 in cross section QY_0_7.00_0

The water depth h in Figure 6.37 is expressed as T/(h-T) or h/T with h the original water depth in the towing tank without taking into account the drop of water level due to the moving ship model.

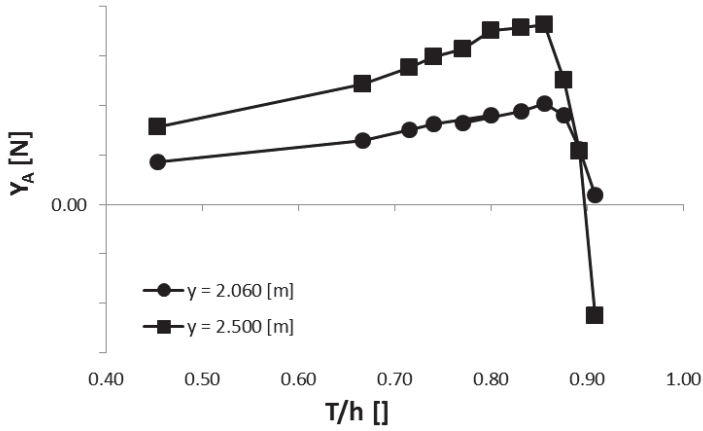

Figure 6.38 the lateral force at the aft perpendicular Y_A plotted to the draft to water depth ratio (ship model A01, 0 rpm)

In Figure 6.38 the lateral force at the aft perpendicular (positive is attraction towards the bank) is shown for 11 draft to water depth ratios. The forward speed of the model was 0.582m/s (at λ = 50 this is 8 knots full scale) and the propeller attached but fixed at 0 rpm. The lateral position of the model in the towing tank y was

2.060m eccentric and 2.500m. For both lateral positions the attraction force increases with decreasing water depth until a critical value is reached (somewhere between T/h 0.80 and 0.90). Since the displaced water will have a higher velocity when a larger volume is forced to flow along the vessel and not under the vessel (which is the case at lower water depths) the pressure drop between wall and vessel will decrease and the attraction force will increase.

At very shallow water, however, the magnitude of the attraction force decreases with decreasing water depth. In very shallow water this force even changed into a repulsion force directed away from the closest wall for some tests. It is assumed that this unexpected effect is caused by the boundary layer between keel and bottom, analogue as for the boundary layer thickness influence $\delta_{BLI,A}$ between the ship and wall (section 6.2.2.1).

At model scale the distance $\delta_{BLI,A}$ is the minimal thickness between the ship's side and bank to be able to measure the lateral force Y_A without having significant influence of the boundary layer. If this minimal distance is smaller than $\delta_{BLI,A}$, then there is an influence of the boundary layer on Y_A and as a consequence this force Y_A can no longer be scaled according to Froude's law.

$$\mathbf{h_{min} = T + \delta_{BLI,A}} \tag{6.69}$$

Based upon the same formula for $\delta_{BLI,A}$ (equation 6.28) for the minimal distance between ship's side and bank, the minimal water depth h_{min} can be calculated (equation 6.69, Figure 6.39).

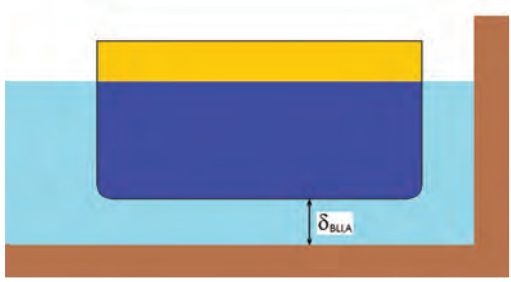

Figure 6.39 the minimal under keel clearance and $\delta_{BLI,A}$ at the aft

In Figure 6.38 the value h_{min} according to equation 6.69 is 1.19 T (or T/h = 0.84). This means that at a water depth smaller than 1.19 T the (viscous) influence of the boundary layer comes into play. The boundary layer makes the water to get stuck and this results in a higher pressure between ship and environment. This causes the decrease in attraction force (or in extreme conditions even a repulsion force) in (very) shallow water. This transition point will come into existence at model scale (relative) faster than at full scale.

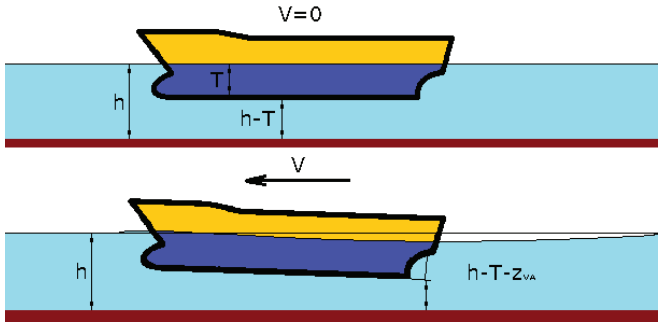

Figure 6.40 influence of running sinkage at the aft z_{VA} on the under keel clearance

The effective under keel clearance at the aft perpendicular will decrease because of the squat (Lataire et al. 2012a). The squat at the aft perpendicular results in an increased running sinkage z_{VA}. Now the running under keel clearance at the aft perpendicular $\left(\frac{T}{h_{min}-T-z_{VA}}\right)$ will be plotted to Y_A as to take into account this phenomenon (Figure 6.40).

$$\mathbf{h_{min} - T - z_{VA} = \delta_{BLI,A}} \tag{6.70}$$

In Figure 6.41 a vertical line is added with an abscissa equal to $\left(\frac{T}{\delta_{BLI,A}}\right)$. The value $\delta_{BLI,A}$ is a function of the measured thrust T_P and will therefore change (slightly) for all tests in Figure 6.41. The average value is used. The forces plotted on the right hand side of this vertical line are influenced by the boundary layer, the forces on the left are not.

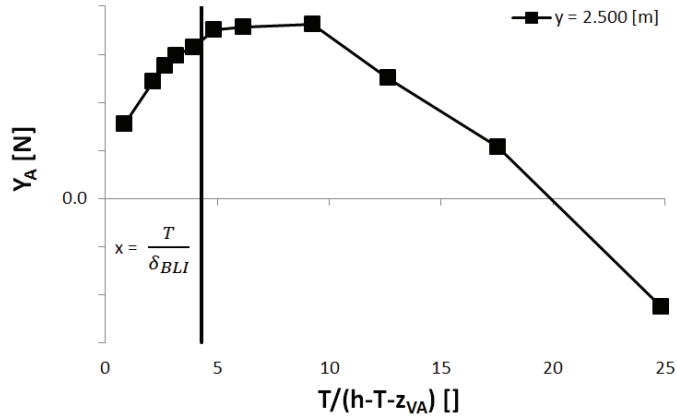

Figure 6.41 Y_A plotted to the net under keel clearance and with the indication of the influence zone of the boundary layer for zero propeller speed on model scale

For the other velocities the same distinction between the presence and absence of the boundary layer influence seems valid. Note that the formulation for $\delta_{BLI,A}$ is only based upon the lateral gap between ship and (vertical) bank and applied to the gap between bottom and keel.

6.4.2.3 Including the positive propeller action

Based upon the model tests with ship model C0U (with an example as shown in Figure 6.36) the behaviour in very shallow water seems very different with and without a propeller that generates a positive thrust. To be able to exclude the possibility that this behaviour is ascribed to the influence of the proximity of the bank on the active propeller (and the wake it produces) instead of the bank effects on the hull, the measured force (T_P) and torque (Q_P) on the propeller stock are plotted for a selection of tests in Figure 6.42.

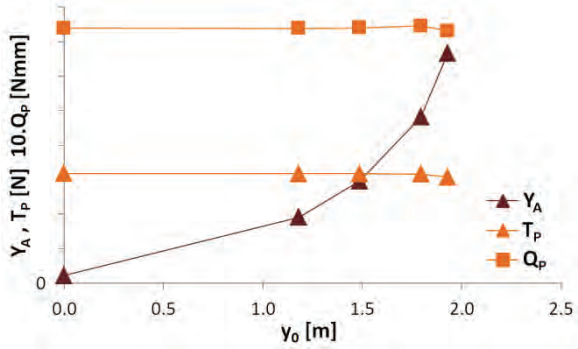

Figure 6.42 Ship model C0P in cross section SP_3_4.200_1 according to 10 knots full scale at a propeller rate 402rpm, h/T=1.35

This figure shows that both the propeller generated thrust T_P and torque Q_P hardly change at the different lateral positions in cross section SP_3_4.200_1. Since this force and torque are about constant, the advance speed of the propeller V_A can be expected to be constant. This means that the supply of water towards the propeller is not (or only to a minor extent) influenced by the proximity of the banks.

The systematic model tests with ship model A01 in a wide range of water depths are also carried out with a propeller rate according to self-propulsion in open and deep water for each velocity (Table 6.3).

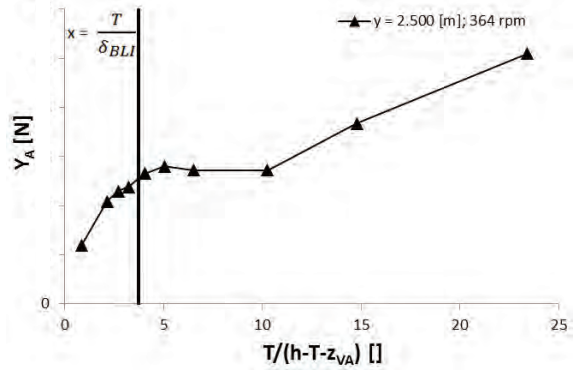

Figure 6.43 Y_A plotted to the under keel clearance and with the indication of the influence zone of the boundary layer for an active propeller generating positive thrust

Due to the propeller action the attraction force at the aft perpendicular increases dramatically at the extreme shallow water depths. The previous assumption, however, still stands. What is seen in Figure 6.43 is a combination of different influences. At water depths deeper than h_{min} the attraction force increases with decreasing water depth. At water depths close to h_{min} the attraction force Y_A does not change much with decreasing water depth. At extreme shallow water the magnitude of the lateral force at the aft perpendicular increases rapidly with decreasing water depth.

In Figure 6.44 the water depth and propeller action on the lateral force Y_A is conceptually separated. The dashed line is the force Y_A plotted to the water depth as if there is a fixed propeller (propeller rate = 0 rpm) and forced through the origin. This curve is similar as the line in Figure 6.41. The dotted line in Figure 6.44 is the influence of the active propeller on the force Y_A for a wide range of water depths. The full line in Figure 6.44 is the superposition of the dashed and dotted line. This line is the simplification of the results shown in Figure 6.43.

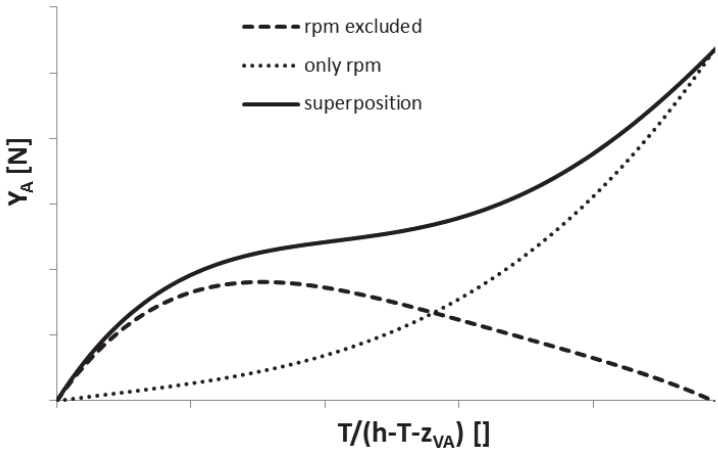

Figure 6.44 concept of the superposition of the lateral force and propeller action

The influence of the boundary layer which acts as an obstruction for the return flow is partly overcome by the rotating propeller. The propeller action will increase the velocity between ship and wall. The active attraction of water by the propeller results in a pressure drop and amplifies attraction towards the bank at the aft perpendicular.

The problem with scale effects at water depths smaller than h_{min} still stands. It is only the influence of the propeller that masks the influence of the boundary layer. This is even more true when only a limited number of water depths are tested (as was the case in Figure 6.36).

6.4.3 Mathematical model water depth influence

6.4.3.1 Midship coefficient

To take into account the midship coefficient of the vessel (as done in section 6.2.4) the following ratio is used instead of $\frac{T}{h_{ship}-T-z_{VA}}$:

$$\frac{T}{h_{ship}-T-z_{VA}} \rightarrow \frac{C_M T}{h_{ship}-C_M T-z_{VA}} \tag{6.71}$$

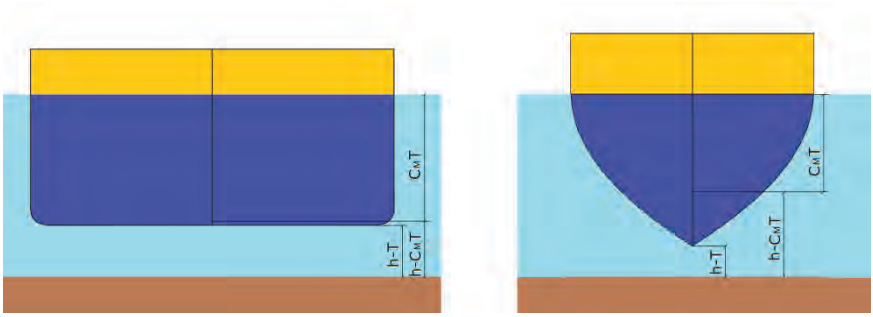

Figure 6.45 graphical interpretation of the different influence of C_M on the relative water depth for a common seagoing vessel (left) and the rather unique shaped W01 (right)

This equation 6.71 will only differ to a minor extent at moderate and deep water if the midship coefficient is not taken into account (or $C_M = 1$). In shallow and very shallow waters this ratio will increase slightly for most vessel types (Figure 6.46). For the ship

model W01 (Wigley hull) this is more significant because of the extremely low C_M value (Table 6.1) as graphically shown in Figure 6.45 (the running sinkage at the aft perpendicular z_{VA} is not accounted for).

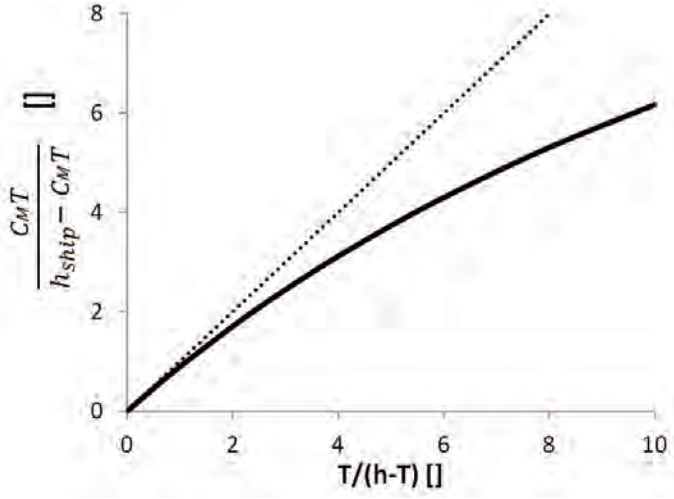

Figure 6.46 relation between relative water depth with and without the midship coefficient taken into account, here for ship model A01

6.4.3.2 Boundary layer influence on Y_A

The proposed mathematical model for the lateral force at the aft perpendicular Y_A will be split into two parts; a branch when the water depth h_{ship} is deeper than h_{min} and a second branch for water depths more shallow than h_{min}. The latter will result in the mathematical model for deeper water ($h_{ship} > h_{min}$) multiplied by the ratio of the effective under keel clearance ($h_{ship}-C_M T-z_{VA}$) and $\delta_{BLI,A}$. The model tests carried out in a water depth lower than h_{min} are not taken into account for defining the coefficients of the regression of the model.

$$Y_A \propto \begin{cases} d2b^{-1} f(V_{eq}) & h_{ship} - C_M T - z_{VA} \geq \delta_{BLI,A} \\ \frac{h_{ship} - C_M T - z_{VA}}{\delta_{BLI,A}} d2b^{-1} f(V_{eq}) & h_{ship} - C_M T - z_{VA} < \delta_{BLI,A} \end{cases} \quad (6.72)$$

6.5 Forward speed, water depth and propeller action

A method to implement the influence of the forward speed of the vessel, the water depth and characteristics of the propeller action in the mathematical model for the lateral force at the aft perpendicular Y_A is sought for. A mathematical model based on physics with only a limited amount of coefficients is the objective.

6.5.1 Tuck number Tu

In (Tuck 1966) the dimensionless Tuck number Tu was introduced (Figure 6.47). This dimensionless number increases rapidly when a vessel sails at a velocity V closer to the critical speed in open water $(Fr_h = 1)$. The forward velocity of the ship V is made dimensionless by dividing through the critical velocity in open water $\sqrt{gh_{ship}}$. This ratio is the water depth dependent Froude number Fr_h.

$$\boldsymbol{Fr_h} = \frac{\boldsymbol{V}}{\sqrt{\boldsymbol{gh_{ship}}}} \tag{6.73}$$

$$\boldsymbol{Tu(V)} = \frac{\boldsymbol{Fr_h}^2}{\sqrt{|\boldsymbol{1-Fr_h}^2|}} \tag{6.74}$$

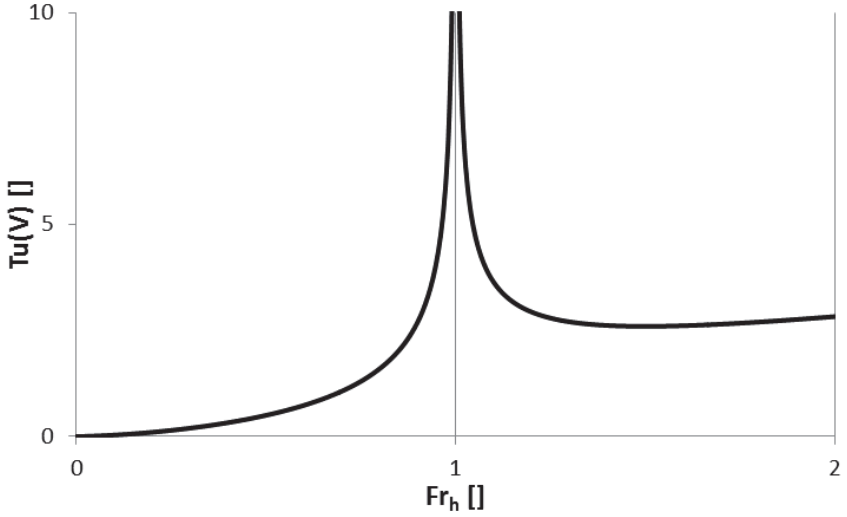

Figure 6.47 the Tuck number Tu(V) in the sub (Fr_h<1) and super critical (Fr_h>1) speed region

The Tuck number Tu(V) does not take into account the (lateral) restriction of the fairway. However, this restriction will decrease the critical speed. Furthermore present research is limited to velocities smaller than 84% of the critical speed (Section 5.3.4)

6.5.2 Blockage m

The critical velocity decreases in confined waters and will be smaller than $\sqrt{gh}$. In (Schijf 1949) the critical velocity V_{crit} is calculated taking into account the blockage m. The blockage is known as the ratio between the midship area A_M and the cross section Ω (as in section 5.3.4).

If a vessel sails close to one bank in a very wide cross section the area Ω must be limited. The bathymetry at a lateral distance y_{infl} and beyond located from the vessel is therefore not taken into account:

$$\boldsymbol{\Omega_{lim}} = \int_0^h \int_{-y_{infl}}^{y_{infl}} \boldsymbol{d\Omega} \tag{6.75}$$

Now the blockage is:

$$\boldsymbol{m_{lim}} = \frac{\boldsymbol{A_M}}{\boldsymbol{\Omega_{lim}}} = \frac{\boldsymbol{C_M.BT}}{\boldsymbol{\Omega_{lim}}} \tag{6.76}$$

A disadvantage of limiting the cross section to the influence width is that the minimal value for the blockage in shallow unrestricted waters is no longer zero but will have a minor value (Equation 6.77).

$$\boldsymbol{m_{min}} = \frac{\boldsymbol{A_M}}{\boldsymbol{2y_{infl}h}} = \frac{\boldsymbol{T}}{\boldsymbol{10h}} \frac{\boldsymbol{C_M}}{\boldsymbol{Fr_h+1}} < \frac{\mathbf{1}}{\mathbf{10}} \frac{\mathbf{1}}{\mathbf{1}} = \mathbf{0.1} \tag{6.77}$$

The dimensionless critical speed Fr_{crit} according to (Schijf 1949) is shown in Equation 5.10. When the critical speed in this equation is calculated with the cross section within the influence width Ω_{lim} then the critical speed $Fr_{crit,lim}$ is obtained.

$$\boldsymbol{Fr_{crit,lim}} = \left(\mathbf{2}\, \boldsymbol{sin}\left(\frac{\boldsymbol{Arcsin(1-m_{lim})}}{\mathbf{3}}\right)\right)^{\frac{3}{2}} \tag{6.78}$$

This dimensionless speed can be made with dimension by multiplying by $\sqrt{gh_{avg}}$. This water depth h_{avg} is the ratio between

the (limited) cross section area Ω (equation 6.75) and the width on the free surface W_0. The latter is the summation of the width on the free surface at port y_{h0p} and starboard y_{h0s} side of the vessel (measured from the centre line of the vessel). Again both distances are limited to y_{infl} (if $y_{h0} > y_{infl}$ than $y_{h0} = y_{infl}$).

$$\boldsymbol{W_0 = y_{h0p} + y_{h0s}} \tag{6.79}$$

$$\boldsymbol{h_{avg} = \frac{\Omega}{W_0}} \tag{6.80}$$

Remark that the water depth h_{avg} in a canal section does not take the water depth under the vessel into account but the average over the entire cross section (within the limits defined by y_{infl}). Now the critical speed is:

$$\boldsymbol{V_{crit} = \sqrt{g h_{avg}}\, Fr_{crit,lim} = \sqrt{g h_{avg}}\left(2\,sin\left(\frac{Arcsin(1-m_{lim})}{3}\right)\right)^{\frac{3}{2}}} \tag{6.81}$$

6.5.3 Tuck number including critical speed

The Tuck number is now adapted to Tu_m so the vertical asymptote (Figure 6.47) is located at the critical speed (which takes into account the limited blockage as in equation 6.79 and Figure 6.48):

$$\boldsymbol{Tu_m(V) = \frac{\left(\frac{Fr_h}{Fr_{crit,lim}}\right)^2}{\sqrt{1-\left(\frac{Fr_h}{Fr_{crit,lim}}\right)^2}} = \frac{\frac{h_{avg}}{h_{ship}}\frac{V^2}{V_{crit,lim}^2}}{\sqrt{1-\frac{h_{avg}}{h_{ship}}\frac{V^2}{V_{crit,lim}^2}}}} \tag{6.82}$$

The numerator of equation 6.82 can be written as (this is derived in Appendix 11.8):

$$\boldsymbol{\frac{h_{avg}}{h_{ship}}\frac{V^2}{V_{crit,lim}^2} = \frac{V^2}{g h_{ship}\left(2\,sin\left(\frac{Arcsin(1-m_{lim})}{3}\right)\right)^3}} \tag{6.83}$$

And as such the Tuck number equals:

$$\boldsymbol{Tu_m(V) = \frac{\frac{V^2}{g h_{ship}\left(2\,sin\left(\frac{Arcsin(1-m_{lim})}{3}\right)\right)^3}}{\sqrt{1-\frac{V^2}{g h_{ship}\left(2\,sin\left(\frac{Arcsin(1-m_{lim})}{3}\right)\right)^3}}}} \tag{6.84}$$

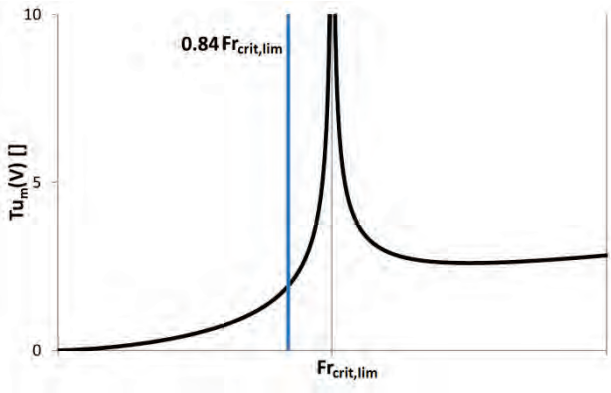

Figure 6.48 Tuck number including blockage ratio m and the limiting forward speed for the mathematical model

In Figure 5.5 the ratio between the critical Froude number based upon the blockage m and the water depth dependent Froude number was shown to indicate the limits of the model. In Figure 6.49 the same data is plotted but the critical speed $Fr_{crit,lim}$ is calculated with the limited blockage m_{lim}. Only minor differences between Figure 5.5 and Figure 6.49 can be observed (although more than 50% of these tests shifted closer to the critical speed). The same conclusion still stands for the behaviour of the ship when the critical speed is calculated within the influence width:

$$Fr_h < 0.84 Fr_{crit,lim} \tag{6.85}$$

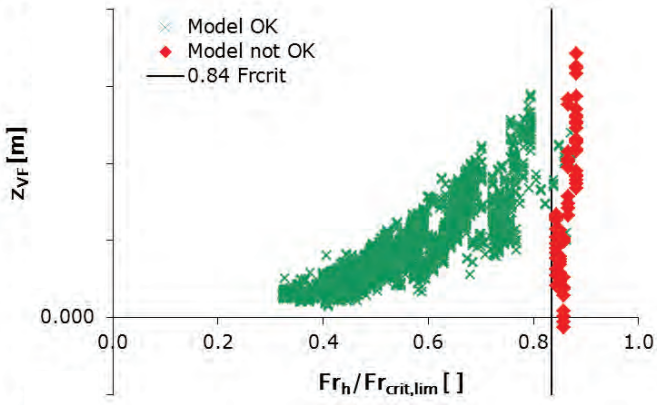

Figure 6.49 running sinkage at the fore to the ratio to the critical limited speed

6.5.4 Propeller

The influence of the propeller action is implemented by increasing (or decreasing) the forward velocity of the vessel V with a fraction ξ_{VT} of the derived velocity V_T (section 6.1.3). V_T is based upon the thrust delivered by the propeller on the propeller shaft T_P. In the case of a fixed propeller (propeller rate = 0 rpm), the propeller acts as a source of increased resistance. The thrust is negative and the equivalent speed V_{eq} will be smaller than the forward speed of the vessel V. If the propeller delivers a positive thrust, an extra component is added to the forward speed of the vessel and V_{eq} is larger than the forward speed of the vessel.

Only the thrust delivered by the propeller closest to the closest bank is taken into account in case of a twin screw vessel.

$$\boldsymbol{Tu_m(V + \xi_{VTA} V_T) = Tu_m(V_{eq}) = \frac{\frac{h_{avg}\ \ V_{eq}^2}{h_{ship} V_{crit,lim}^2}}{\sqrt{1-\frac{h_{avg}\ \ V_{eq}^2}{h_{ship} V_{crit,lim}^2}}}} \qquad (6.86)$$

6.5.5 Validation of the Tuck number $Tu_m(V_{eq})$

The Tuck number $Tu_m(V_{eq})$ from equation 6.87 takes into account:

- V; the forward speed through the water of the vessel
- V_T; the propeller action
- m_{lim}:; the dimensions of the fairway (Ω_{lim}) and the midship area (A_M)

$$\mathbf{Tu_m(V_{eq}) = Tu_m(V + \xi_{VTA} V_T) = \frac{\frac{(V+\xi_{VTA}V_T)^2}{gh_{ship}\left(2\sin\left(\frac{\mathrm{Arcsin}(1-m_{lim})}{3}\right)\right)^3}}{\sqrt{1-\frac{(V+\xi_{VTA}V_T)^2}{gh_{ship}\left(2\sin\left(\frac{\mathrm{Arcsin}(1-m_{lim})}{3}\right)\right)^3}}}} \qquad (6.87)$$

In Figure 6.50 and Figure 6.51 the lateral force at the aft perpendicular (with dimension N) is plotted to the dimensionless $Tu_m(V_{eq})$. In both plots all the tests without boundary layer

influence are plotted. A wide range of water depths, ship speeds and propeller actions are included.

$$\mathbf{Y_A} \propto \boldsymbol{Tu_m}\left(\boldsymbol{V_{eq}}\right) \tag{6.88}$$

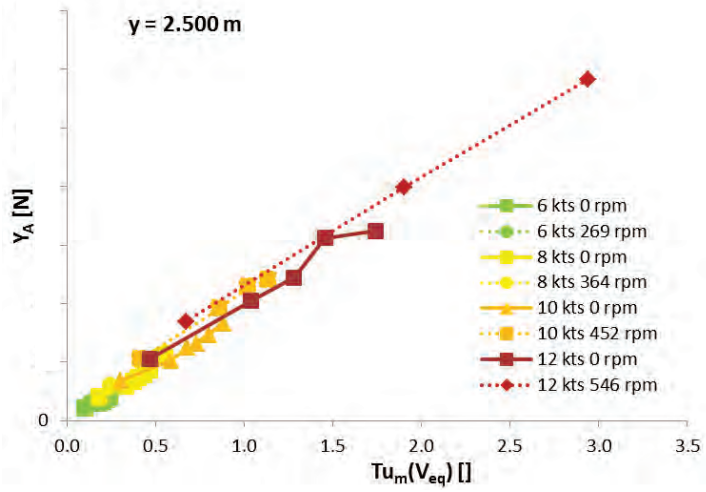

Figure 6.50 Y_A plotted to $Tu_m(V_{eq})$ for all the model tests with A01 without influence of the boundary layer in cross section QY_0_7.00_0 at a lateral position y = 2.500m

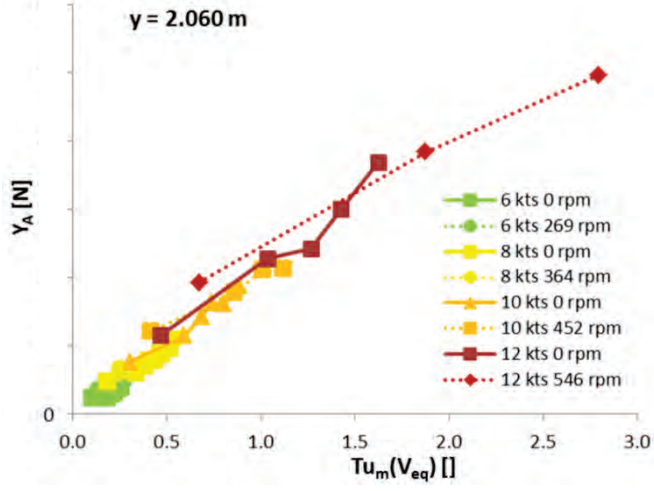

Figure 6.51 Y_A plotted to $Tu_m(V_{eq})$ for all the model tests with A01 without influence of the boundary layer in cross section QY_0_7.00_0 at a lateral position y = 2.060m

6.6 Correlation with running sinkage

Although the squat or running sinkages are out of the scope of this work, it cannot be neglected that there is a connection between the running sinkages and the forces induced due to bank effects. Therefore the running sinkage at the fore and aft relation are plotted for a selection of model test results with the force Y_A (Figure 6.52).

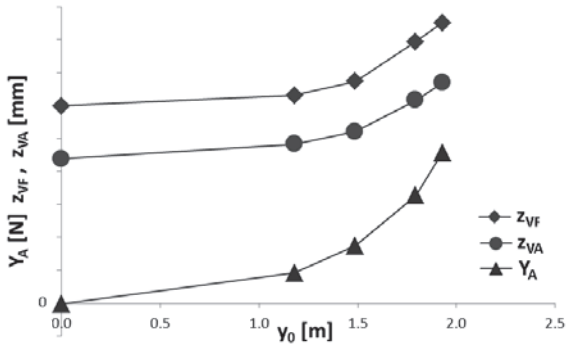

Figure 6.52 running sinkages (z_{VF} and z_{VA}) and lateral force at the aft for ship model C0P in cross section SP_3_4.200_1 according to 10 knots full scale at propeller rate 402 rpm and relative water depth h/T=1.35

As is the case for the force Y_A, the closer the ship sails to the bank, the larger the magnitude of the running sinkage. This is true for both running sinkages (at the fore and at the aft). The trim of this ships does not change significantly.

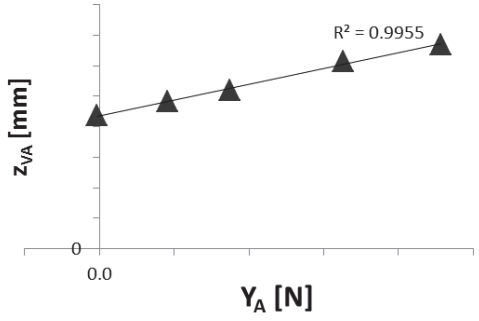

Figure 6.53 running sinkage at the aft plotted as a function of the lateral force at the aft for the same conditions as in Figure 6.52

Figure 6.53 shows the high correlation between the running sinkage at the aft z_{VA} and the lateral force at the aft perpendicular Y_A. Remark that bank effects will increase the running sinkage when sailing on the centreline of a symmetric cross section (when the lateral force Y_A will be zero under the same conditions).

6.7 Mathematical model for Y_A

6.7.1 The mathematical model for Y_A

The combination of equation 6.65 and equation 6.88 results in:

$$\mathbf{Y_A} \propto \mathbf{d2b^{-1}}\ \boldsymbol{Tu_m(V_{eq})} \tag{6.89}$$

The right hand side (which is dimensionless) is multiplied by the displacement force Δ [N] of the ship under consideration:

$$\boldsymbol{\Delta = \rho g \nabla} \tag{6.90}$$

To get an equation instead of a proportion the constant ξ_ρ is added:

$$\mathbf{Y_A} = \begin{cases} \boldsymbol{\xi_\rho\ \Delta\ d2b^{-1}\ Tu_m(V_{eq}),\ (h_{ship} - C_M T - z_{VA}) \geq \delta_{BLI,A}} \\ \boldsymbol{\frac{h_{ship}-C_M T-z_{VA}}{\delta_{BLI,A}}\ \xi_\rho\ \Delta\ d2b^{-1}\ Tu_m(V_{eq}),\ (h_{ship} - C_M T - z_{VA}) < \delta_{BLI,A}} \end{cases} \tag{6.91}$$

6.7.2 Recapitulation of all the coefficients of the model Y_A

Only four coefficients are used in the mathematical model for Y_A. This set of four coefficients is only valid for one displacement condition of one ship and within the boundaries of the mathematical model.

- ξ_ρ [0,+∞] copes with the overall proportionality of the model and the force Y_A
- ξ_{VTA} [0,1] part of the thrust velocity V_T to be added to the forward speed V to create the equivalent velocity V_{eq}.

- ξ_y $[0, +\infty]$ the lateral decrease of the weight factor w for the water particles away from the ship
- ξ_z $[0, +\infty]$ the vertical decrease of the weight factor w towards the bottom

A set of these four coefficients is calculated for each ship model at each draft tested with the software "R" and the results from the model tests (all water depths, banks, velocities and lateral positions). For reasons of confidentiality these coefficients are not included in the present dissertation.

Because of the high mathematical stability of the mathematical model a set of these four coefficients can be created based on all the sets of coefficients available and the main hydrostatic properties of the (unknown) ship under consideration.

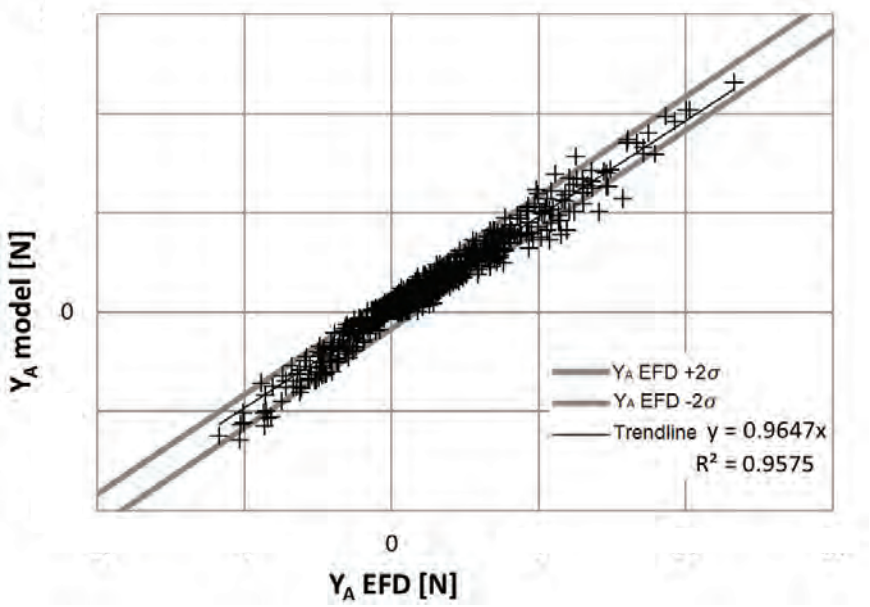

Figure 6.54 C0U T1454.4 model vs EFD, all tests out of δ_{BLI}

In Figure 6.54 the lateral force at the aft perpendicular Y_A for ship model C0U (at a draft of 0.180m) based upon 1154 model tests is plotted to the result from the mathematical model. Overall the results are satisfying and within the boundaries defined by 2σ.

6.8 Conclusions

The lateral position of a ship in a rectangular cross section is unambiguously determined and the closer the ship sails to the vertical wall, the larger the magnitude of the lateral force at the aft perpendicular. A function of the lateral position in a rectangular cross section (equation 6.92) proportional to the magnitude of the lateral force is proposed.

$$f(y) = \frac{\xi_y y}{0.5(1+\xi_y)(W-B)-|y|} \tag{6.92}$$

There is a minimal gap between ship and bottom/wall to overcome the influence of the boundary layer on the force Y_A. This minimal distance is defined as δ_{BLI} and can be calculated (equation 6.93). This gap is assumed to have the same stretch between the side of the ship and the vertical wall as between the ship's keel (taking into account the running sinkage at the aft) and the bottom of the cross section. The deeper the ship sails in the boundary layer influence, the smaller the magnitude of the force Y_A.

$$\delta_{BLI,A} \propto \frac{Lpp}{\sqrt[7]{Re}} \frac{T}{h} \frac{(V_T+2V)}{V} \tag{6.93}$$

There is a limit to the distance between a ship and bank to induce bank effects. This distance is the influence width y_{infl}:

$$y_{infl} = B(5Fr_h + 5) \tag{6.94}$$

The weight factor w is introduced to take into account all the finesses of a random geometry of a cross section. This 'weighted' surface is then integrated to χ and with this value the distance to bank d2b can be calculated. The magnitude for Y_A is proportional to $d2b^{-1}$.

$$w = e^{-\left(\xi_y \frac{|y|}{y_{infl}} + \xi_z \frac{|z|}{T}\right)} \tag{6.95}$$

$$\chi = \oiint_A w \, dA \tag{6.96}$$

$$d2b = \frac{2}{\chi_{ship}} \frac{\chi_p \chi_s}{\chi_p - \chi_s} \tag{6.97}$$

An equivalent forward speed V_{eq} is introduced to take into account the forward speed of the ship and the actions of the propeller. This equivalent speed is then incorporated in the adapted Tuck number which takes into account the blockage ratio of the cross section.

$$\mathbf{V_T} = \mathbf{sign(T_P)}\sqrt{\frac{8|\mathbf{T_P}|}{\rho\pi\mathbf{D^2}}} \tag{6.98}$$

$$\mathbf{V_{eq}} = \mathbf{V} + \boldsymbol{\xi}_{\mathbf{VTA}}\mathbf{V_T} \tag{6.99}$$

$$\boldsymbol{Tu_m(V)} = \frac{\left(\frac{Fr_h}{Fr_{crit,lim}}\right)^2}{\sqrt{1-\left(\frac{Fr_h}{Fr_{crit,lim}}\right)^2}} \tag{6.100}$$

If a ship does not sail in the influence of the boundary layer then the lateral force is always directed towards the closest bank (attraction force) and the formulation for the lateral force at the aft perpendicular of the bank effects Y_A is as simple as:

$$\mathbf{Y_A} = \boldsymbol{\xi}_{\boldsymbol{\rho}}\,\boldsymbol{\Delta}\,\mathbf{d2b^{-1}}\;\mathbf{Tu_m(V_{eq})} \tag{6.101}$$

This formulation contains only four coefficients to be determined for each ship at each draft.

Bank Effects

7 LATERAL FORCE AT THE FORWARD PERPENDICULAR

The lateral force at the forward perpendicular Y_F in some conditions behaves very similar to the lateral force at the aft perpendicular Y_A, sometimes it does not. The force Y_F behaves different than Y_A on the influence of the water depth and propeller action.

The influence of the propeller action is much less present than it is for the lateral force at the aft perpendicular because of the relative position between the propeller(s) and the forward perpendicular.

The water depth (or under keel clearance) has a more prominent influence. In deep water the lateral force at the forward perpendicular acts very similar to the lateral force at the aft perpendicular. In these conditions the attraction force is directed towards the closest bank with a magnitude smaller than the attraction force at the aft perpendicular. The combination of these two forces results in an overall attraction force and bow-away moment. In very shallow water the lateral force at the forward perpendicular becomes a repulsion force away from the closest bank. The magnitude of this repulsion can become larger than the magnitude of the attraction force at the aft perpendicular. As a result the vessel is pushed away from the closest bank with a large bow away moment.

The mathematical model for the lateral force at the forward perpendicular Y_F will be formulated by checking the different influences such as forward speed, propeller action, bathymetry.

7.1 Velocity

7.1.1 Forward speed

If the physical phenomenon of bank effects is simplified and seen as a pure Bernoulli effect, then the higher the forward speed the larger the bank effects and in casu the larger the magnitude of the lateral force at the forward perpendicular Y_F. If the vessel sails at a higher speed along a bank then the return flow between ship and bank increases with increasing vessel speed and the pressure drop between ship and bank results in a larger attraction force towards the closest bank.

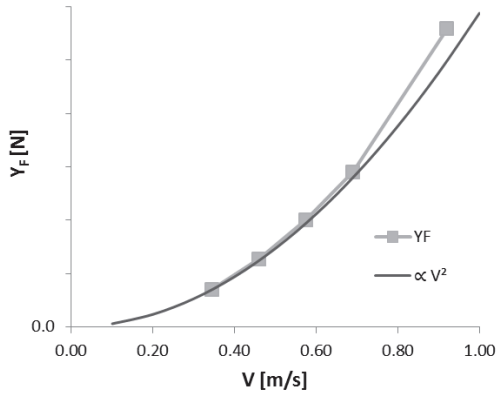

Figure 7.1 the lateral force Y_F plotted to the forward speed. Ship model C0P, rpm=0, water depth h=2.0T, at a distance from the wall y_{wall}=0.860 m in QY_0_4.400_4

In Figure 7.1 the lateral force at the forward perpendicular during model tests carried out with C0P towed along the vertical bank QY_0_4.400_4 at a distance y_{wall} = 0.860 m and fixed propeller shaft (0 rpm) is plotted for different forward speed. These forward speeds correspond to 6, 8, 10, 12 and 16 knots full scale (at a scale 1/80). The forward speed is the only variable in the entire test setup of the plotted values in this figure. In the same Figure

7.1 a quadratic function $f(V) \propto V^2$ (through the data point at 6 knots) is also plotted. This function indicates the higher than quadratic order for the magnitude of the lateral force for these specific model tests since the lateral forces are systematically larger than this function. In Figure 7.2 the same results as in Figure 7.1 are plotted but the values Y_F are divided by $\frac{1}{2}\rho V^2$. Again in this figure the higher than quadratic order of the forward speed to the lateral force at the forward perpendicular Y_F is shown. The same is true for all tested ship models in deep water $\left(\frac{h}{T} \geq 2\right)$.

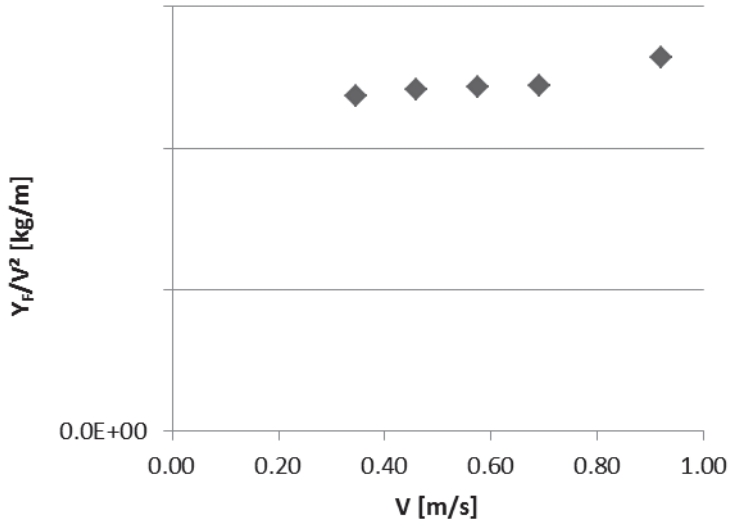

Figure 7.2 the lateral force Y_F divided to the square of the forward speed V^2 for Ship model C0P, rpm=0, water depth h=2.0T, at a distance from the wall y_{wall}=0.860 m in QY_0_4.400_4 C0P

The higher than quadratic relation between the lateral force and the forward speed is explained by (Tuck 1966) (among others) because of the larger return flow because of the narrowness between the ship and bank and/or the ship and bottom.

The influence of the under keel clearance $\left(\frac{h}{T}\right)$ will be elaborately explained in Section 7.3. In very shallow water $\left(\frac{h}{T} \approx 1.10\right)$ the lateral force at the forward perpendicular Y_F will always be a

repulsion force and thus changes sign from deep (attraction) to shallow water (repulsion).

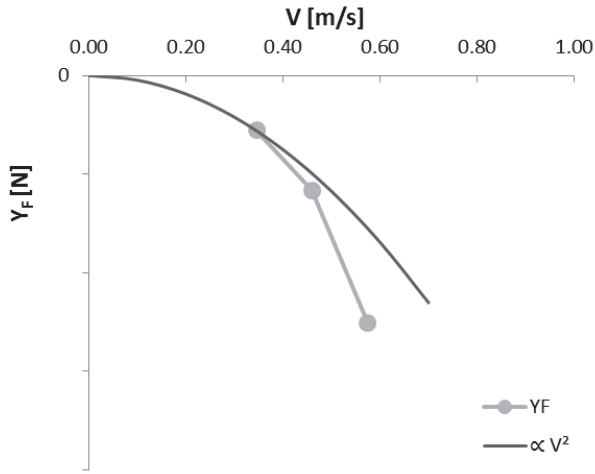

Figure 7.3 the lateral force Y_F plotted to the square of the forward speed V^2 for ship model C0P, rpm=0, water depth h=1.10T, at a distance from the wall y_{wall} = 0.860 m in QY_0_4.400_4 C0P

Similar as for the attraction force Y_F in deep water, the magnitude of the repulsion force Y_F in very shallow water (h/T=1.10) increases more than quadratic with the forward speed as is shown for a limited amount of tests in Figure 7.3. The same observation remains true for the other tested ship models.

7.1.2 Propeller influence

7.1.2.1 Relative distance between forward perpendicular and the propeller

All propellers under consideration are located at the aft section of the vessel and (when working) accelerate water to create thrust. This acceleration of the surrounding water creates a higher velocity of the water particles surrounding the ship's hull. This effect is much more present at the region around the aft perpendicular than at the forward perpendicular obviously because of the relative position of the propeller from these perpendiculars.

The ratio between the length between perpendiculars and the propeller diameter $\frac{Lpp}{D}$ indicates how far the forward perpendicular is relatively located from the propeller. For a long and narrow ship (compared to beam and draft) with relative small propeller (e.g. ship model B01) this ratio will be large (or the propeller is relatively far away from the forward perpendicular), while for a shorter ship (again relative to beam and draft) with larger propeller (T0Z) this ratio will be lower.

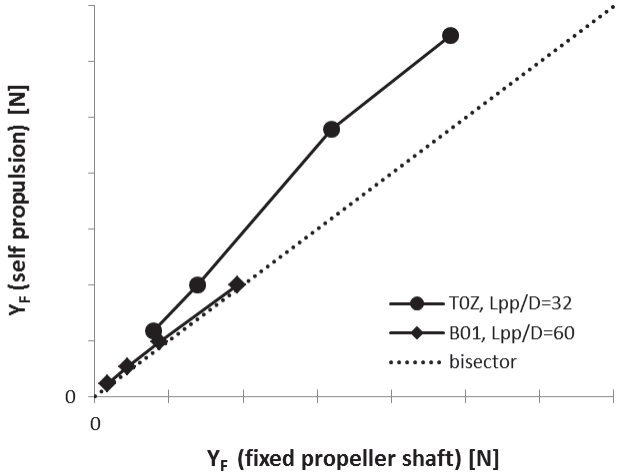

Figure 7.4 the lateral force at the forward perpendicular without an active propeller action (0 rpm) plotted for the same test with active propeller action (according to self-propulsion in open water)

For a limited amount of tests the lateral force at the forward perpendicular Y_F (Figure 7.4) with a propeller rate according to open water self-propulsion is plotted to the same test conditions but with a fixed propeller set to zero rpm.

The ratio between both plotted lateral forces Y_F in Figure 7.4 indicates the influence of the propeller actions on Y_F. If this ratio is close to 1 (or the data points located close to the bisector) then the influence of the propeller on Y_F is very small or non-existent. For ship model B01 (with a $\frac{Lpp}{D} = 60$) there seems to be no difference at all between the results for Y_F obtained with and without active propeller action.

Ship model T0Z (with $\frac{Lpp}{D} = 32$) has its propeller relatively close to the forward perpendicular. This is also seen in the significant increase of the lateral force Y_F when the propeller runs compared to the same lateral force Y_F with a fixed propeller (0 rpm).

7.1.2.2 Equivalent velocity

For reasons of consistency the proposed mathematical model will always take into account the influence of the propeller action on the lateral force at the forward perpendicular Y_F. Similar as for the lateral force at the aft perpendicular Y_A this influence will be implemented by partially increasing the forward speed of the vessel with the velocity V_T (Section 6.1.3).

$$\boldsymbol{V_T = sign(T)\sqrt{\frac{|T|}{\frac{1}{2}\rho\pi\frac{D^2}{4}}}} \tag{7.1}$$

$$\boldsymbol{V_{eq} = V + \xi_{VTF} V_T} \tag{7.2}$$

The coefficient ξ_{VTF} for the model Y_F will always be smaller than ξ_{VTA} in the model for Y_A of the same ship. This is because the much lower influence of the propeller actions on the lateral force at the forward perpendicular Y_F compared to the same influence on the lateral force at the aft perpendicular Y_A.

For ship model B01 the coefficient ξ_{VTF} will be zero (or very close to zero) as the absence of propeller influence is shown in Figure 7.4.

7.2 Lateral position

7.2.1 Distance to bank d2b

The distance between the ship and bank will change the magnitude of the lateral force at the forward perpendicular. Overall the closer the ship sails to a bank, the larger the magnitude of the force Y_F will be. This is very similar as for the lateral force at the aft perpendicular Y_A. In previous Chapter 6 the non-dimensional ship-bank distance *d2b* is proposed. Different from other authors this ship-bank distance *d2b* takes into account all properties of the entire bank geometry. The magnitude of the attraction force at the aft perpendicular was found to be proportional to the inverse of this *d2b*.

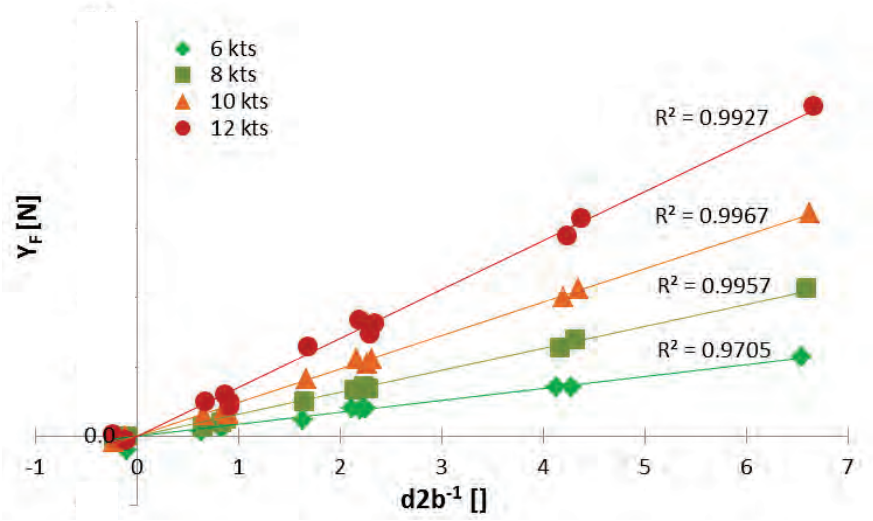

Figure 7.5 the force YF for ship model C0P at all lateral positions and banks tested with a water depth h=2.0 T

First the relation between the same non-dimensional distance to bank d2b and the lateral force at the fore perpendicular Y_F is checked. In Figure 7.5 the force Y_F is plotted to $d2b^{-1}$ for ship model C0P at four different forward speeds with fixed propeller shaft (0 rpm) and at all different lateral positions sailing along all the banks tested with this ship model (QY_0_4.400_4, SP_1_4.200_3, SP_3_4.200_1 and SP_4_4.400_0) in a water depth

of twice the ship models' draft at rest. A very good correlation is found.

$$\boldsymbol{Y_F \propto d2b^{-1}} \tag{7.3}$$

Remark that the d2b in Figure 7.5 is calculated with the two coefficients ξ_y and ξ_z, both coefficients having been calculated based upon a regression with the lateral force at the aft perpendicular. This rather surprisingly good correlation with these coefficients gives the opportunity for a mathematical model with the same coefficients ξ_y and ξ_z for each ship's loading condition (and as a consequence the same value for d2b) for both the lateral force at the fore and at the aft perpendicular.

Thus, a set of coefficients ξ_y and ξ_z can be calculated for the lateral force at the aft and forward perpendicular separately based upon each force or only one set for ξ_y and ξ_z for both lateral forces which is based upon both lateral forces.

7.2.2 Boundary layer

When sailing very close to a vertical wall the magnitude of the lateral force at the aft perpendicular appears not to increase any longer when sailing closer to the wall. This was ascribed to the influence of the (viscous) boundary layer on the ship. This same behaviour was not or almost not observed at the forward perpendicular.

The boundary layer develops from the bow towards the stern section (for a forward sailing ship). This boundary layer becomes thicker (the more) towards the aft part of the ship. At the first half of the ship (model) the boundary layer is much less developed and thinner than at the aft part of the ship. As a consequence the boundary layer thickness influence will also be much thinner at the forward half of the ship than at the aft part of the ship. This is the reason why the influence of the boundary layer on the behaviour of the lateral force at the forward perpendicular Y_F is absent or only very minor.

$$\frac{\delta}{x} = \frac{0.16}{\sqrt[7]{Re}} \tag{7.4}$$

$$\frac{\delta}{x} = \frac{5.0}{\sqrt{Re}} \tag{7.5}$$

Equations 7.4 and 7.5 give the ratio between the boundary layer thickness δ and x, the distance from the most forward part of the submerged hull. Equation 7.4 is for a turbulent flow ($Re > 10^6$) and equation 7.5 the relative thickness for a laminar flow. A laminar flow can be expected at the initial first section of the ship model, this flow will become turbulent further towards the stern of the model. For all the tests carried out at FHR under consideration none of the models was equipped with turbulence stimulation strips or other device to stimulate the flow to be turbulent.

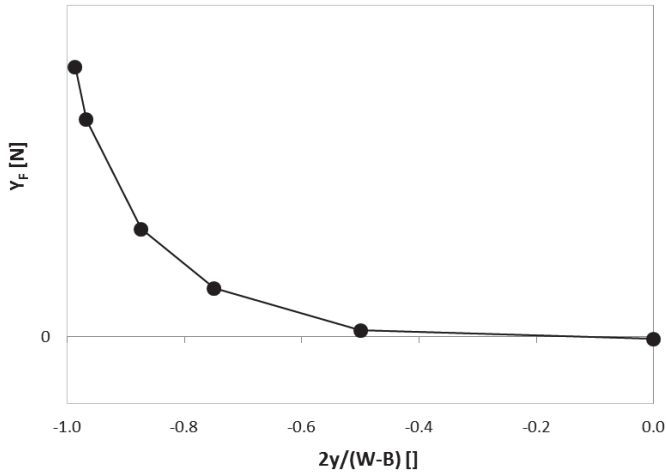

Figure 7.6 EFD for T0Z with h/T = 1.10, 8 knots full scale in cross section QY_0_3.865_0

The lateral force at the forward perpendicular Y_F measured during six model tests in a rectangular cross section are depicted in Figure 7.6. Different from the lateral force at the aft perpendicular, the magnitude for Y_F keeps on increasing the closer the ship model is towed along the vertical bank.

7.3 Water depth

In Figure 7.7 the lateral force at the forward perpendicular is plotted for three different water depths. These tests are carried out with ship model C0U at 8 knots full scale (scale 80.8), propeller rate 360 rpm along bank SS_5_4.030_.120_7.00 with the ship's side at the toe of the sloped part of the semi submerged bank. The attraction force Y_F increases, as expected, from deeper water $\left(\frac{h}{T} = 2.0\right)$ to shallow water $\left(\frac{h}{T} = 1.35\right)$ but from this shallow water to very shallow water $\left(\frac{h}{T} = 1.10\right)$ the attraction force Y_F changes sign and becomes a repulsion force. The magnitude of the repulsion force is about ten times the magnitude of the attraction force at $\frac{h}{T} = 1.35$

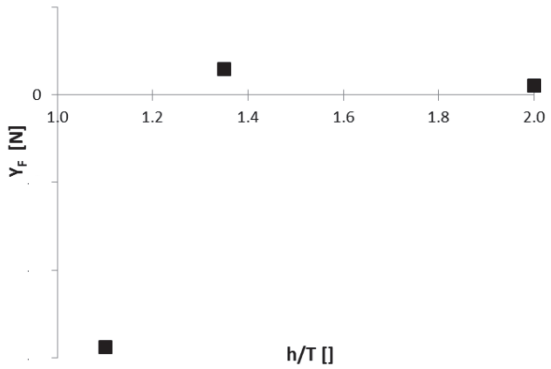

Figure 7.7 Y_F for three water depths C0U at 8 knots, propeller rate 360 rpm, bank SS_5_4.030_.120_7.00; <0 is a repulsion force; >0 attraction towards the bank

Based upon all the model tests, the lateral force at the forward perpendicular changes sign when all except the water depth remains the same. In deeper water $\frac{h}{T} > 1.5$ there is always attraction or the lateral force Y_F is directed towards the closest bank.

7.3.1 Relation to Y_A

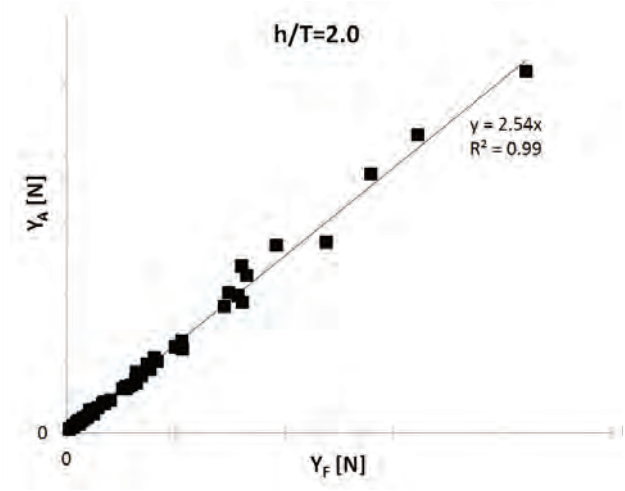

Figure 7.8 the force Y_F plotted to the force Y_A for C0P, n=0 rpm, h/T =2.0

In even deeper water $\frac{h}{T} \geq 2$ the ratio between the attraction force at the forward perpendicular Y_F and the attraction force at the aft perpendicular Y_A is about constant (Figure 7.8). This indicates that the same formula 6.87 as suggested for Y_A can be used with different values for the coefficients. (Actually there is a minimal need for different values for the coefficient ξ_ρ).

$$\boldsymbol{Y_{F_{(h>2T)}} = \xi_\rho \, \Delta \, d2b^{-1} \; Tu_m(V_{eq})} \tag{7.6}$$

In more shallow water ($\frac{h}{T} = 1.35$) the relation between the lateral force at the fore and at the aft perpendicular becomes a lot more messy (Figure 7.9). Attraction forces $Y_F > 0$ and (bigger) repulsion forces $Y_F < 0$ at the forward perpendicular are observed at this water depth.

The close relation with the attraction force at the aft perpendicular is lost. Therefore the same formulation for Y_F as for Y_A can no longer be used. The model will be extended to be able to cope with the changing sign of the lateral force at the forward perpendicular.

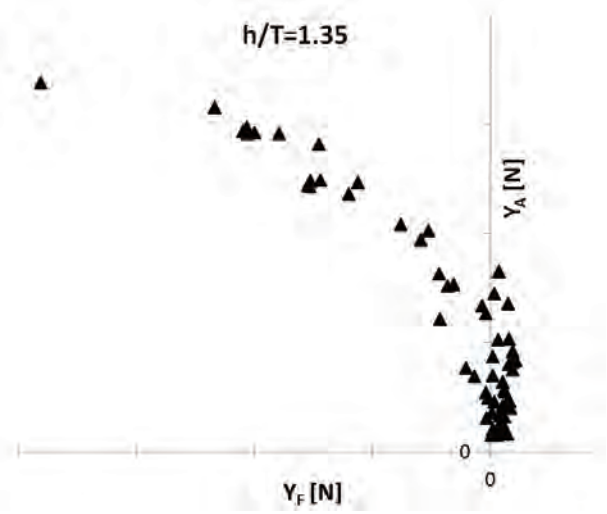

Figure 7.9 the force Y_F plotted to the force Y_A for C0P, n=0 rpm, h/T = 1.35

In even more shallow water the force at the forward perpendicular Y_F flipped sign compared to the deep water case and (almost) always is a repulsion force (Figure 7.10). The correlation with the force at the aft perpendicular seems to be entirely lost.

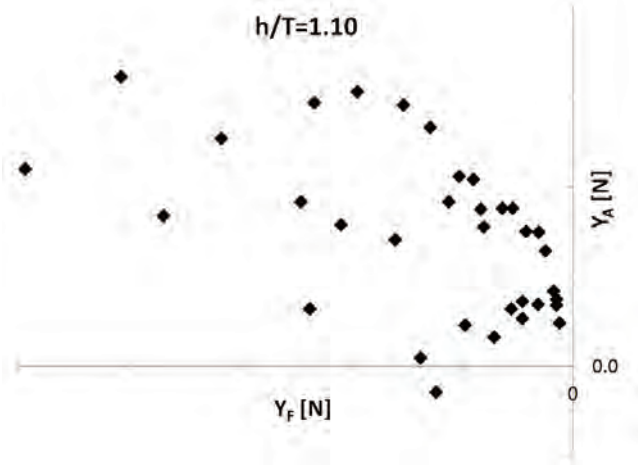

Figure 7.10 the force Y_F plotted to the force Y_A for C0P, n=0 rpm, h/T = 1.10

The overall behaviour of the sign of the lateral force at the forward perpendicular Y_F is summarized in Figure 7.11.

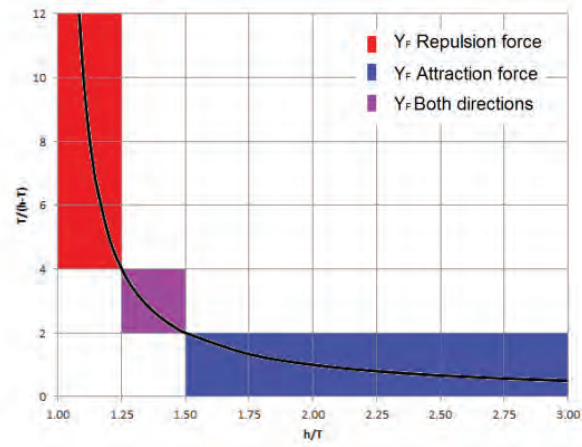

Figure 7.11 three regions of behaviour of the lateral force at the forward perpendicular induced by the proximity of a bank.

7.3.2 Under keel clearance

Systematic model tests in the FHR towing tank (without additional banks) have been carried out with ship model A01 for a wide range of water depths. In Figure 7.12 the lateral force at the forward perpendicular Y_F is plotted to the ratio $\frac{T}{h-T}$ (deep to shallow water is directed from left to right).

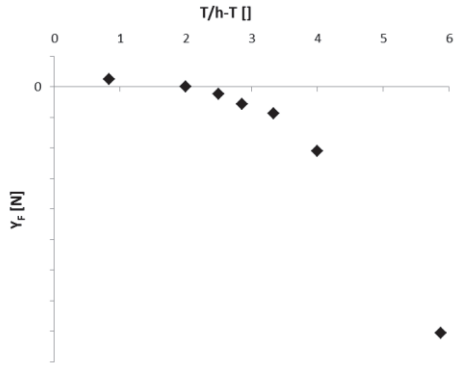

Figure 7.12 lateral force at the forward perpendicular for a wide range of water depths (here expressed as the ratio $\frac{T}{h-T}$) for ship model A01, in the FHR towing tank at lateral position y = 2.5m, according to 10 knots full scale, fixed propeller shaft 0 rpm

In this Figure 7.12 a positive Y_F value indicates an attraction force towards the closest bank ($\frac{h}{T} > 1.5$ or $\frac{T}{h-T} < 2$). For more shallow water ($\frac{h}{T} < 1.5$ or $\frac{T}{h-T} > 2$) the lateral force at the forward perpendicular Y_F is directed away from the closest bank (or a repulsion force). The more shallow the water, the larger the magnitude of the repulsion force Y_F. The magnitude of the repulsion force in very shallow water is a multiple of the attraction force in deep water.

In Figure 7.13 the forward speeds according to 6, 8 and 12 knots full scale are added to the 10 knots of Figure 7.12 but plotted to the ratio $\frac{h}{T}$. The increase in magnitude of the repulsion forces at higher speeds and more shallow water is clearly visible.

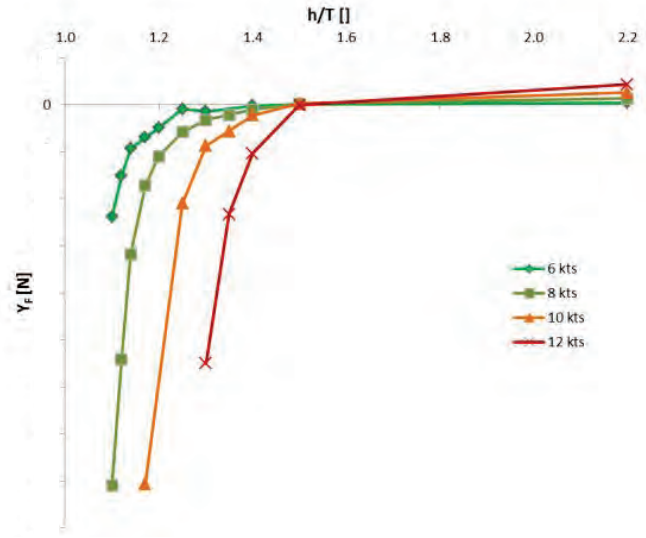

Figure 7.13 ship model A01, n=0 rpm; forces at the forward perpendicular for a wide range of water depths. The positive attraction force in deeper water can be modelled with the model as presented for Y_A.

In Figure 7.8 the correlation with the attraction force at the aft perpendicular and the forward perpendicular in deep water is shown. Therefore the proposed mathematical model for the lateral force at the aft perpendicular can be used (with different values for

the coefficients) for the attraction force at the forward perpendicular in deep water $Y_{F\,(h>2T)}$ (equation 7.6).

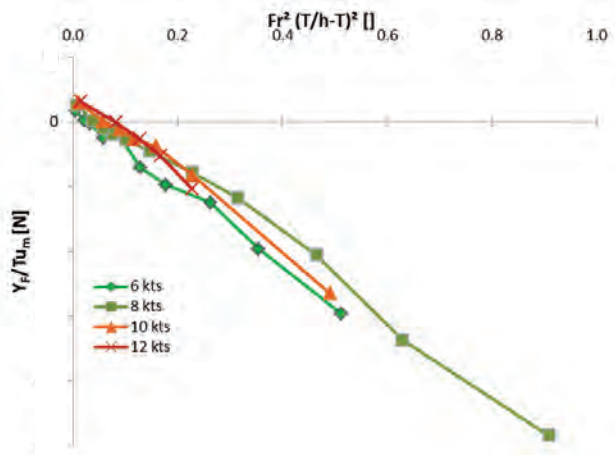

Figure 7.14 $\frac{Y_F}{\Delta T u_m(V)}$ for the model tests with A01 along bank QY_0_7.00_0 at a lateral position y=2.500m with a fixed propeller shaft plotted to $Fr^2\left(\frac{T}{h-T}\right)^2$

The lateral force at the forward perpendicular Y_F is divided by the dimensionless Tuck number Tu_m (that takes into account the blockage of the fairway under consideration) and plotted on the ordinate of Figure 7.14. The abscissa of the same figure contains the square of the product of the Froude number $\left(Fr = \frac{V}{\sqrt{g.Lpp}}\right)$ and the draft to keel clearance ratio $\frac{T}{h-T}$. The ratio of the lateral force at the forward perpendicular and the Tuck number Tu_m is about proportional (with a constant shift) to (Equation 7.7):

$$\frac{Y_F}{Tu_m} \propto Fr^2\left(\frac{T}{h-T}\right)^2 \tag{7.7}$$

This abscissa is a type of cross term between the forward speed of the vessel and the relative water depth.

Because of the much larger magnitude of the repulsion force in very shallow water compared to the attraction force in deep water, Figure 7.14 hides the conclusion that the force Y_F acts proportional to Y_A in deep water.

7.4 Mathematical model for Y_F

7.4.1 In deep water h>2T

In deep water (h>2T) the lateral force at the forward perpendicular can be modelled according to the formula which has the same composition as the lateral force at the aft perpendicular Y_A (out of the influence of the boundary layer):

$$\boldsymbol{Y_{F_{(h>2T)}} = \xi_\rho \, \Delta \, d2b^{-1} \; Tu_m(V_{eq})} \tag{7.8}$$

The same coefficients ξ_y and ξ_z as for Y_A could be used but new coefficients ξ_ρ and ξ_{VTF} must be derived from dedicated EFD.

7.4.2 In (very) shallow water h<1.25T

In (very) shallow water $(h < 1.25T)$ the (shifted) linearity with $Fr^2 \left(\frac{T}{h-T}\right)^2$ must be implemented:

$$\frac{Y_{F(h<1.25T)}}{Tu_m(V_{eq})} \propto \xi_{shift} + Fr^2 \left(\frac{T}{h-T}\right)^2 \tag{7.9}$$

The ratio $\frac{T}{h-T}$ goes to infinity when the water depth h is as low as the draft:

$$\boldsymbol{lim_{h \to T} \left(\frac{T}{h-T}\right) = \infty} \tag{7.10}$$

This is both physically and practically not desired. This would result in enormous lateral forces in very shallow water in the ship manoeuvring simulator. The magnitude of the lateral force at the forward perpendicular will not be infinitely large in extreme shallow water. Similar as for the lateral force at the aft perpendicular the boundary layer on both ship and bottom will temper this steep increase in magnitude.

At the forward half of the ship the boundary layer will be (much) thinner than on the aft half of the ship's surface because of the lower local Reynolds number (Figure 7.15).

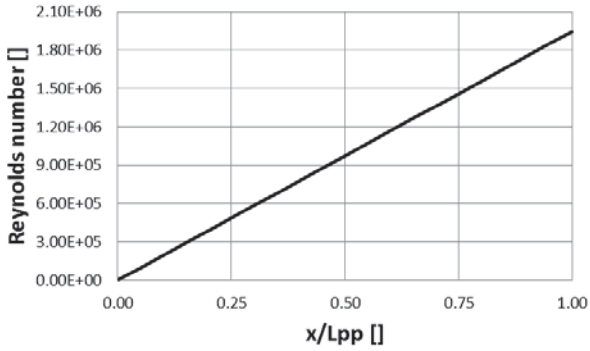

Figure 7.15 Reynolds number along the hull for ship model A01 at model scale according to 8 knots full scale

This thinner boundary layer will also result in a thinner boundary layer influence thickness compared to the lateral force at the aft perpendicular. The same formula as equation 6.28 is used but the distance between the perpendiculars is replaced by half the distance between the perpendiculars in both the calculation for the Reynolds number and $\delta_{BLI,F}$. The influence of the propeller on the boundary layer at the forward half of the ship is also neglected. This results in a new Equation 7.11

$$\boldsymbol{\delta_{BLI,F}} \propto \frac{Lpp}{2}\frac{1}{\sqrt[7]{\frac{Re}{2}}}\frac{T}{h}\frac{2V}{V} \approx \mathbf{0.9}\frac{Lpp}{\sqrt[7]{Re}}\frac{T}{h} \tag{7.11}$$

Similar as at the aft perpendicular the influence of the boundary layer on the mathematical model is taken into account by decreasing the magnitude with the ratio of the penetration into the boundary layer influence $\left(h_{ship} - T - z_{VF}\right)$ and the thickness of the boundary layer influence $\delta_{BLI,F}$.

7.4.3 Transition from deep to (very) shallow water

An analytical formulation is sought for, and found, to cope with the different mathematical model for Y_F in deep water ($h>2T$), shallow water ($h<1.25T$) and all water depths in between ($1.25\ T<h<2\ T$). Therefore a simplified solution for a hyperbolic function (derived in Appendix 11.6) is shown and equation 7.12.

Actually this (half) of a hyperbolic function is simplified to two half lines with a common initial point.

$$\boldsymbol{f(x) = 1 - \frac{|x-x1|+(x-x1)}{2\ slope}} \tag{7.12}$$

If the abscissa x in equation 7.12 is changed into $\boldsymbol{Fr^2\left(\frac{T}{h-T}\right)^2}$ and the constants ξ_h and ξ_{hT} added then equation 7.13 is obtained:

$$\boldsymbol{f\left(Fr^2\left(\frac{T}{h-T}\right)^2\right) = 1 - Fr^2\ \frac{\frac{T^2}{(h-T)^2} - \xi_{hT}{}^2 + \left|\frac{T^2}{(h-T)^2} - \xi_{hT}{}^2\right|}{2\,\xi_h{}^2}} \tag{7.13}$$

The coefficients ξ_h and ξ_{hT} are always positive $(\xi_h, \xi_{hT} > 0)$. The coefficient ξ_h controls the slope of the decreasing part of the two half lines. The larger this coefficient the steeper the slope will be for the same Froude number Fr. The coefficient ξ_{hT} marks the boundary of the water depth when the model for Y_F is similar to the lateral force at the aft perpendicular Y_A and without added influence of the water depth (Figure 7.16).

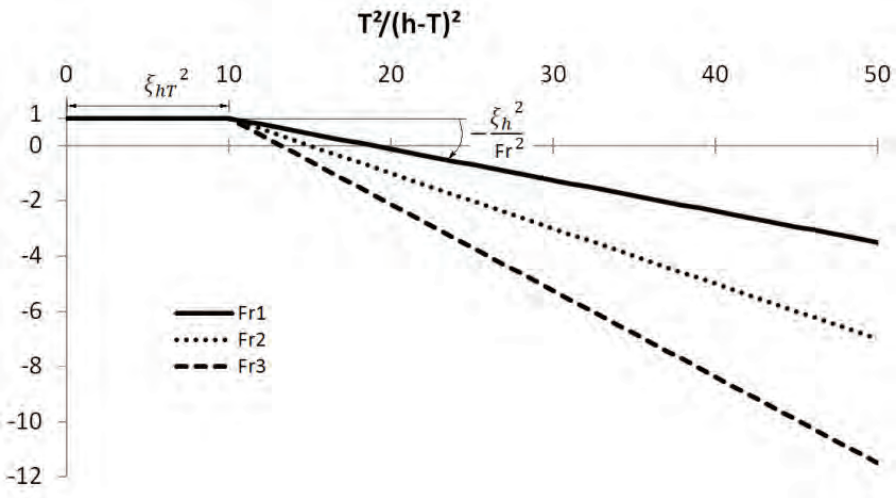

Figure 7.16 water depth and forward speed change between attraction and repulsion at the forward perpendicular with three Froude numbers Fr1 < Fr2 < Fr3

Remark that there is no influence of the propeller action on the sloped section ($\frac{T}{h-T} > \xi_{hT}$) plotted in Figure 7.16

7.4.4 Unlimited water depth range

Now the mathematical model for Y_F over the entire water depth range is:

$$Y_F = \begin{cases} \xi_\rho \, \Delta \, d2b^{-1} \; Tu_m(V_{eq}) \left(1 - Fr^2 \frac{\frac{T^2}{(h-T)^2} - \xi_{hT}{}^2 + \left|\frac{T^2}{(h-T)^2} - \xi_{hT}{}^2\right|}{2\xi_h{}^2}\right) & h_{ship} - C_M T - z_{VF} \geq \delta_{BLI,F} \\ \frac{h_{ship} - C_M T - z_{VF}}{\delta_{BLI,F}} \xi_\rho \, \Delta \, d2b^{-1} \; Tu_m(V_{eq}) \left(1 - Fr^2 \frac{\frac{T^2}{(h-T)^2} - \xi_{hT}{}^2 + \left|\frac{T^2}{(h-T)^2} - \xi_{hT}{}^2\right|}{2\xi_h{}^2}\right) & h_{ship} - C_M T - z_{VF} < \delta_{BLI,F} \end{cases} \quad (7.14)$$

If $\frac{T}{h-T} < \xi_{hT}$ (mainly deeper water) then the lateral force at the forward perpendicular is proportional to Y_A. While in more shallow water the attraction force first decreases, changes sign and finally becomes a repulsion force away from the closest bank (out of the boundary layer influence thickness):

$$Y_F = \begin{cases} \frac{T}{h-T} \leq \xi_{hT} & \xi_\rho \Delta \, d2b^{-1} \; Tu_m(V_{eq}) \\ \frac{T}{h-T} > \xi_{hT} & \xi_\rho \Delta \, d2b^{-1} \; Tu_m(V_{eq}) \left(1 - \frac{Fr^2}{\xi_h{}^2}\left(\frac{T^2}{(h-T)^2} - \xi_{hT}{}^2\right)\right) \end{cases} \quad (7.15)$$

The sign of the force changes (or an attraction force at the forward perpendicular becomes a repulsion force) when $Fr^2 \frac{\left(\frac{T}{h-T}\right)^2 - \xi_{hT}{}^2}{\xi_h{}^2} = 1$, actually the lateral force at the forward perpendicular Y_F is zero or absent in this specific condition. Equation 7.16 shows the draft to under keel clearance ratio when Y_F of the mathematical model always equals zero (Appendix 11.7):

$$\frac{T}{h-T} = \sqrt{\frac{\xi_h{}^2}{Fr^2} + \xi_{hT}{}^2} \quad (7.16)$$

When Y_F equals zero there will still be a lateral force at the aft perpendicular Y_A directed towards the closest bank (attraction). The absence of Y_F and the attraction force Y_A will act on the vessel as the combination of an overall attraction force in combination with a bow-away moment. In very shallow water the magnitude of the lateral repulsion force at the forward perpendicular will be larger than the attraction force at the aft perpendicular. In this situation the overall lateral force will result in a repulsion away from the closest bank and this will be combined with a (larger) bow away moment.

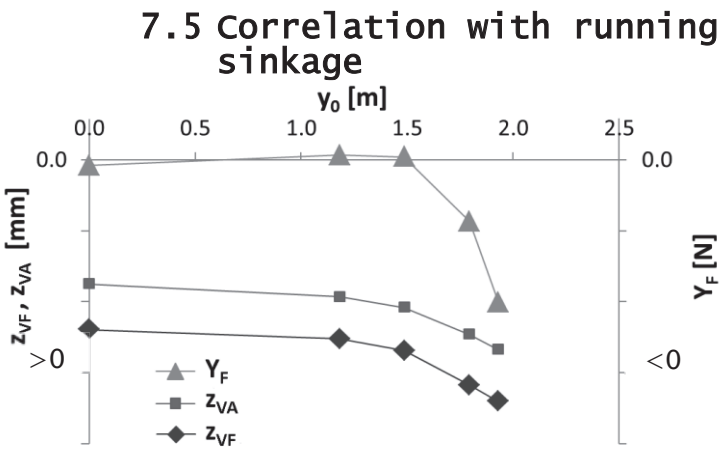

Figure 7.17 running sinkages and lateral force at the fore for ship model C0P in cross section SP_3_4.200_1 according to 10 knots full scale at propeller rate 402 rpm and relative water depth h/T=1.35

As in Figure 6.52 the running sinkages at the fore and aft are plotted with the lateral force, here Y_F. Around the water depth of 1.35T (as in Figure 7.17) the sign of the lateral force at the fore changes. Because of this changing sign, the correlation between the running sinkage at the fore (with a magnitude systematically increasing with a decreasing distance between ship and bank) and the lateral force at the fore Y_F are not as high as is the case for Y_A and z_{VA} (Figure 6.53).

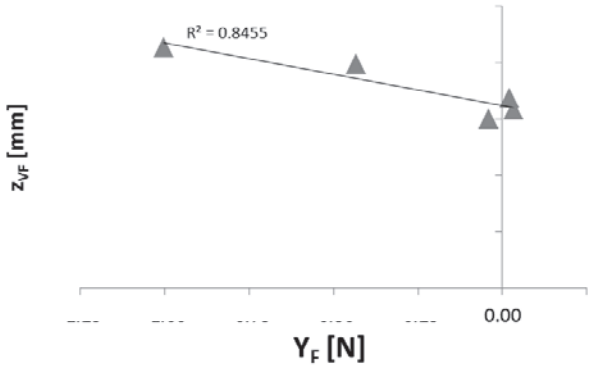

Figure 7.18 running sinkage at the fore plotted to the lateral force at the fore for the same conditions as in Figure 7.17

7.6 Conclusions

In the present chapter, it is justified that the magnitude of the lateral force at the forward perpendicular is considered/formulated as proportional to the inverse of the distance to bank $d2b^{-1}$ (as explained in Chapter 6 for the lateral force at the aft perpendicular).

Again an equivalent velocity is proposed to cope with both the forward speed and the propeller action.

$$\boldsymbol{V_{eq} = V + \xi_{VT,F} V_T} \tag{7.17}$$

The influence of the propeller action on the lateral force at the forward perpendicular Y_F is much less compared to the influence on the force Y_A. For some narrow and long ship types this influence is even absent. For reasons of consistency the formulation for the equivalent speed remains the same but for some ship types the coefficient $\xi_{VT,F}$ tends to zero.

There is no or almost no influence on the lateral force at the fore perpendicular Y_F of the boundary layer. This is because the boundary layer is not or only partially developed at the first half of the ship and this boundary layer is significantly thinner than at the second half, hence the important influence on Y_A (and much less or not on Y_F).

The water depth has a major impact on the force Y_F. In very deep water there is always attraction towards the closest bank while in very shallow water a repulsion force away from the closest bank is consistent. In between, the force can have both directions and therefore a relative water depth and Froude number dependent half line combination is introduced $f\left(Fr^2\left(\frac{T}{h-T}\right)^2\right)$. A positive value indicates an attraction force, a negative value a repulsion away from the closest bank.

$$\boldsymbol{f\left(Fr^2\left(\frac{T}{h-T}\right)^2\right) = 1 - Fr^2 \frac{\frac{T^2}{(h-T)^2} - \xi_{hT}{}^2 + \left|\frac{T^2}{(h-T)^2} - \xi_{hT}{}^2\right|}{2\xi_h{}^2}} \tag{7.18}$$

The lateral force at the forward perpendicular induced by bank effects can be mathematically modelled as:

$$Y_F = \begin{cases} \xi_\rho \, \Delta \, d2b^{-1} \; Tu_m(V_{eq}) \left(1 - Fr^2 \frac{\frac{T^2}{(h-T)^2} - \xi_{hT}{}^2 + \left|\frac{T^2}{(h-T)^2} - \xi_{hT}{}^2\right|}{2\xi_h{}^2}\right) & h_{ship} - C_M T - z_{VF} \geq \delta_{BLI,F} \\ \frac{h_{ship} - C_M T - z_{VF}}{\delta_{BLI}} \xi_\rho \, \Delta \, d2b^{-1} \; Tu_m(V_{eq}) \left(1 - Fr^2 \frac{\frac{T^2}{(h-T)^2} - \xi_{hT}{}^2 + \left|\frac{T^2}{(h-T)^2} - \xi_{hT}{}^2\right|}{2\xi_h{}^2}\right) & h_{ship} - C_M T - z_{VF} < \delta_{BLI,F} \end{cases} \tag{7.19}$$

This formulation consists of six independent coefficients $(\xi_\rho \; \xi_y \; \xi_z \; \xi_{VT,F} \; \xi_{hT} \; \xi_h)$ of which two $(\xi_y \; \xi_z)$ can be taken identical with the mathematical model for Y_A for the same ship at the same initial draft.

In Figure 7.19 the lateral force at the fore Y_F derived from EFD is plotted to its corresponding result from Equation 7.19. A decent but modest correlation coefficient (R^2=0.87) is found. This rather modest correlation is ascribed to the sensibility of the lateral force at the fore perpendicular to the water depths. The transition zone from a repulsion force to an attraction force (between h/T 1.25 and 1.50, Figure 7.11) results in some uncertainty to the model.

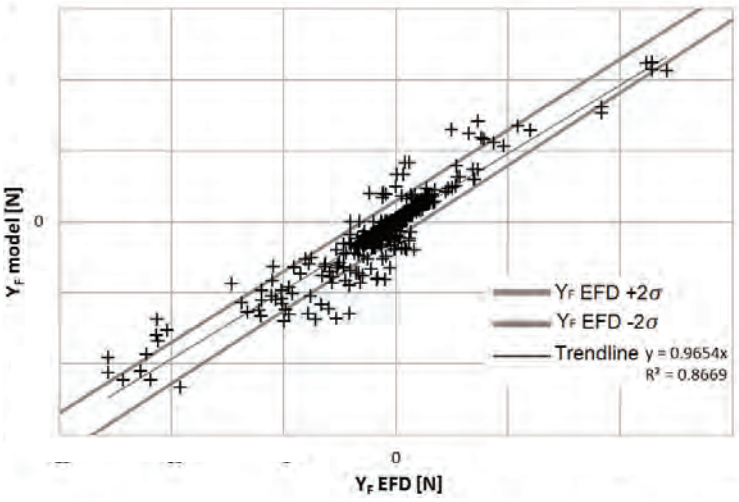

Figure 7.19 the lateral force Y_F for ship model C0U (at a draft of 0.180m) plotted to the result from the mathematical model (all speeds, propeller rates, banks, lateral positions)

In Figure 7.20 only the deep water ($h/T>1.8$) tests are plotted. A much larger correlation ($R^2=0.95$) is observed since the lateral force at the fore is in this deeper water always an attraction force.

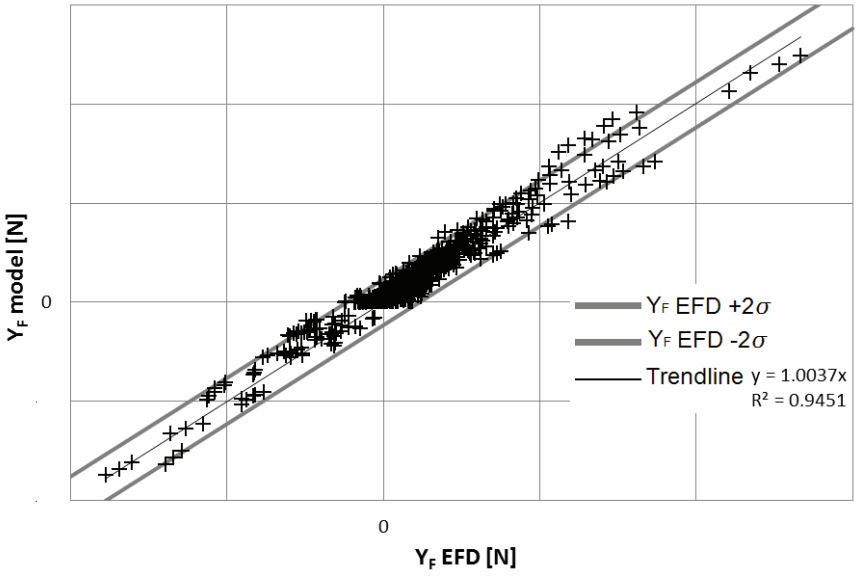

Figure 7.20 the lateral force Y_F for ship model C0U plotted to the result from the mathematical model (only deep water, #643 model tests)

Bank Effects

8 LONGITUDINAL BANK FORCE

The longitudinal bank force X_{BANK} is formulated based upon the superposition principle which is used in the mathematical models of the ship manoeuvring simulators at FHR. This means that the overall longitudinal force X can be split into a set of components based upon different influence factors separately. For each component (or influence factor) a mathematical model is formulated without interference of the other influences (no cross terms). Three types of influences (each composed of different influences) can be distinguished;

- ship
- environment
- moving targets

The overall longitudinal force is the summation of all the separate, independent influences:

$$\boldsymbol{X = X_{SHIP} + X_{ENVIRONMENT} + X_{MOVING}} \tag{8.1}$$

Ship:

These are the longitudinal forces based on properties of the ship:

$$\boldsymbol{X_{SHIP} = X_H + X_P + X_R + X_{ANCH} + X_{MOOR}} \tag{8.2}$$

- X_H Hull (resistance) at a specific water depth

- X_P Propeller (including the thrust T_P of main propeller(s), bow and stern thrusters as well as the thrust deduction factor t)
- X_R Rudder (main rudder(s), bow rudder)
- X_{ANCH} Anchor (when deployed the longitudinal part of the anchor force)
- X_{MOOR} Mooring lines (when applicable the longitudinal forces of all the mooring equipment)

Environment:

The influence of the sailing area and environmental circumstances on the longitudinal force X:

$$\boldsymbol{X_{ENVIRONMENT} = X_{BANK} + X_{WIND} + X_{COL} + X_{WAVE} + X_{RET} + X_{CUR}} \quad (8.3)$$

- X_{BANK} Bank effects
- X_{WIND} Wind effects
- X_{COL} Collision force (physical contact with an obstruction such as bottom, quay wall, lock,…)
- X_{WAVE} Wave (added resistance because of the sea state)
- X_{RET} Retardation (time dependent forces when entering or leaving a lock or other watery cul-de-sac)
- X_{CUR} Current

Moving targets:

The ship under consideration also interacts with moving targets such as other vessels nearby or the tug boats attached to the vessel.

$$\boldsymbol{X_{MOVING} = X_{STS} + X_{TUG}} \quad (8.4)$$

- X_{STS} Interaction with other vessels
- X_{TUG} Tug

Now not the entire longitudinal force X (with all its components) is modelled but only the influence of the banks on the force directed along the longitudinal axis of the vessel: X_{BANK}. The superposition principle for the overall longitudinal force X is accepted (and as a consequence the presence of cross terms neglected).

8.1 Limits to the model tests

8.1.1 Extracting X_{BANK}

Three different types of longitudinal forces are measured during the model tests (see also Chapter 4):

- the overall longitudinal force X (measured between ship model and carriage)
- the thrust T_P delivered by the propeller(s), measured on the propeller shaft(s).
- the force X_R on the rudder directed in the longitudinal direction of the vessel. If the rudder angle δ is set to zero then:

$$\boldsymbol{X_R(\delta = 0) = F_{TR}} \tag{8.5}$$

As a consequence the longitudinal force X_{BANK} must be derived from these three measured longitudinal forces X, X_R and T_P. In equation 8.6 these three longitudinal forces are combined in one equation (with t the thrust deduction):

$$\boldsymbol{X = X_H + (1 - t)T_P + X_R + X_{BANK}} \tag{8.6}$$

The open water resistance R_{OW} (< 0) of the vessel is the summation of the longitudinal force of the hull and the longitudinal forces on the appendages (in the present case the longitudinal force of the rudder):

$$\boldsymbol{R_{OW} = X_H + F_{TR}} \tag{8.7}$$

$$\boldsymbol{X = R_{OW} + (1 - t)T_P + X_{BANK}} \tag{8.8}$$

Or the component of the bank effects directed in the longitudinal direction can be decomposed as:

$$\boldsymbol{X_{BANK} = X - (R_{OW} + (1 - t)T_P)} \tag{8.9}$$

Equation 8.9 is a simplification of reality since the presence of a bank very close to the rudder and propeller will have an influence on both F_{TR} as well as T_P. Furthermore, the propeller-hull interaction through the thrust deduction factor t can also be

expected to be influenced by the surrounding bathymetry. For reasons of simplicity all these influences are neglected and only the overall longitudinally directed bank effects are modelled.

Most ship models are tested in open water to define the self-propulsion point (equilibrium between propeller rate and forward speed). At self-propulsion in open water (absence of bank effects, presence of shallow water) the overall longitudinal force X is zero by definition:

$$\boldsymbol{X_{self-prop} = 0 = R_{OW} + (1 - t)T_P} \tag{8.10}$$

The longitudinal hull force X_H and thrust deduction t are derived from dedicated model tests (ITTC 2002) carried out in the towing tank at different water depths without banks installed. The propeller rate for self-propulsion is sought for during these tests. As such, for each forward speed a propeller rate is defined so the delivered thrust on the propeller shaft T_P results in the absence of a longitudinal force (X=0) between the ship model and the carriage of the towing tank.

Model tests are carried out at different forward speeds with the same ship model along installed banks in the towing tank. These tests are (among others) carried out at propeller rates that match to the corresponding open water self-propulsion point (same forward speed). When sailing in the confined cross sections at these forward speed and propeller rate combination, the measured longitudinal force X is no longer absent but a negative force or added resistance is measured. This longitudinal force is based upon previous simplifications assumed to be the longitudinal bank effect X_{BANK} sought for:

$$\boldsymbol{X_{BANK} = X - (R_{OW} + (1 - t)T_P) = X} \tag{8.11}$$

8.1.2 Scaling

The longitudinal force is scaled from model scale to full scale according to (ITTC 2008). This includes a part of the longitudinal force to be scaled according to Froude's law and a part scaled according to the Reynolds's law. The bank effects are mainly generated by inertial and gravitational forces and therefore the force X_{BANK} will be scaled (entirely) to full scale according to Froude's law.

If a vessel would sail as close to the wall or bottom so the influence of the boundary layer comes into existence then the longitudinal bank effect X_{BANK} will be influenced by the viscosity of the fluid. As a consequence of this is, the scaling to full scale must be partly done according to Reynolds's law (the viscosity influence) and partly by Froude's law (the inertial and gravitational influence). With the results from model tests available, this split cannot be made and therefore only model tests out of the influence of the boundary layer will be taken into account in the regression for X_{BANK}.

8.2 Velocity and water depth

8.2.1 Forward speed

The longitudinal force X measured during model tests with T0Z is plotted to its corresponding full scale speed in Figure 8.1. The propeller rate corresponds to self-propulsion in open water for each speed. The tests are carried out in cross section QY_0_3.865_0 with water depth h=1.5 T and at a lateral position from the centre line y=B.

A more than linear increase of the magnitude for X with increasing forward speed is observed in Figure 8.1. As could be expected the faster the forward speed, the larger the increase of resistance because of the presence of banks.

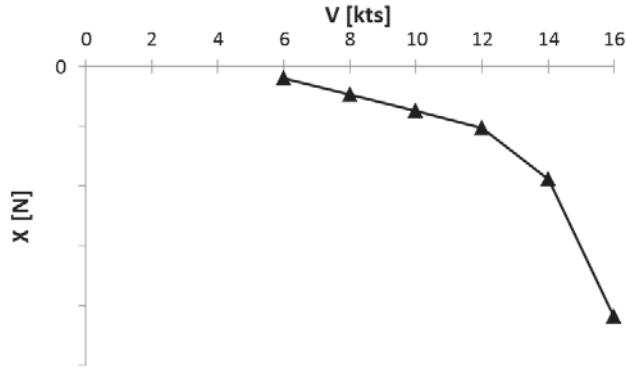

Figure 8.1 the magnitude of the force X increases with increasing forward speed

8.2.2 Water depth

The same model tests as in Figure 8.1 are plotted together with similar model test conditions with a water depth to draft ratio of 1.35 in Figure 8.2. The decreasing water depth results in an increasing resistance of the longitudinal force X (or if the previous assumption still stands X_{BANK}). This increase in magnitude of the force X is more prominent the higher the forward speed.

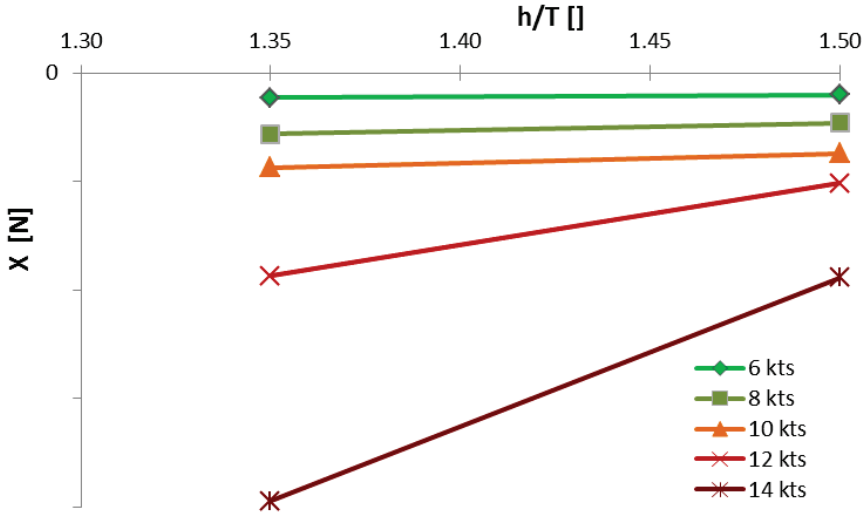

Figure 8.2 water depth to draft ratio plotted to the longitudinal force X

8.2.3 Adapted Tuck $Tu_m(V_{eq})$

Similar as for the lateral forces at the fore and aft perpendiculars the longitudinal bank effect force X_{BANK} appears to be proportional to the Tuck number $Tu_m(V_{eq})$.

$$\boldsymbol{X_{BANK} \propto Tu_m(V_{eq})} \tag{8.12}$$

This relation (8.12) cannot be visualised because the influence of the blockage m_{eq} (next section) cannot be entirely extracted from the plot. The blockage m_{eq} is not constant for the ten tests plotted in Figure 8.2 thus cannot be excluded in Figure 8.3 to support relation 8.12. In Figure 8.3 the correlation between the adapted Tuck number Tu_m and the longitudinal force X_{BANK} is visualised and the value m_{eq} is added as a label to the data points.

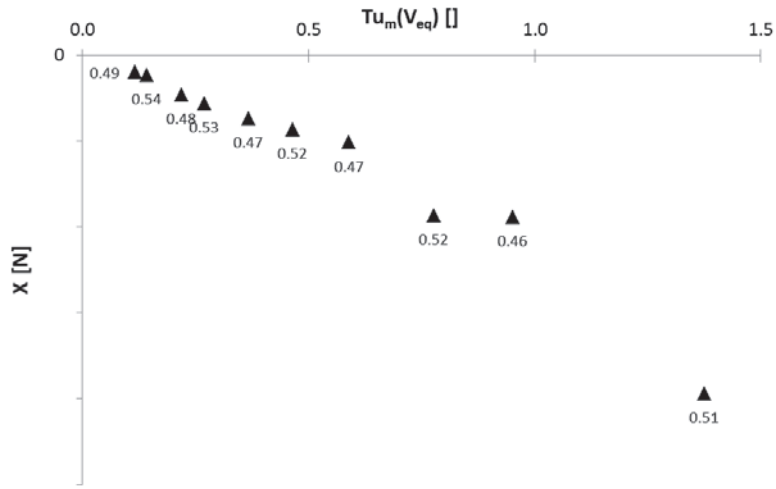

Figure 8.3 relation between adapted Tuck number Tu_m and the longitudinal force for the same tests as in Figure 8.2 but with a variation of m_{eq} from 0.46 up to 0.54 (added as label to the data points)

This Tuck number $Tu_m(V_{eq})$ is calculated with the equivalent velocity as defined and derived in Chapter 6 with the lateral force at the aft perpendicular. The coefficient ξ_{VTA} is incorporated from the regression based on the lateral force at the aft perpendicular Y_A.

8.3 Lateral position and equivalent blockage m_{eq}

8.3.1 Lateral position

The behaviour of the force X_{BANK} on the lateral position in a cross section is different from the lateral forces Y_A and Y_F. Sailing on the centre line of a symmetric cross section the forces Y_A and Y_F will be zero but the longitudinal force X_{BANK} will not. At this symmetric position there will be influence of both banks on the longitudinal force of the vessel. Different from the lateral forces both banks will not counteract each other. Therefore the factor d2b is inadequate to take the lateral position of the vessel into account for X_{BANK}. A new type of blockage ratio will be suggested.

Figure 8.4 shows the influence of the lateral position on the longitudinal force X_{BANK}. In this example the ship model T0Z is towed according to a velocity of 8 knots full scale in the rectangular cross section QY_0_3.865_0 with a water depth of 1.50 T. The closer the ship sails to the bank the larger the magnitude of the negative force X with a non-zero value at y = 0. These tests are carried out at a propeller rate of 452 rpm which is according to self-propulsion in open water at this forward speed. The measured force X in Figure 8.4 is adopted as the longitudinal force of the bank effect X_{BANK}. The negative sign of this force indicates an increase of resistance.

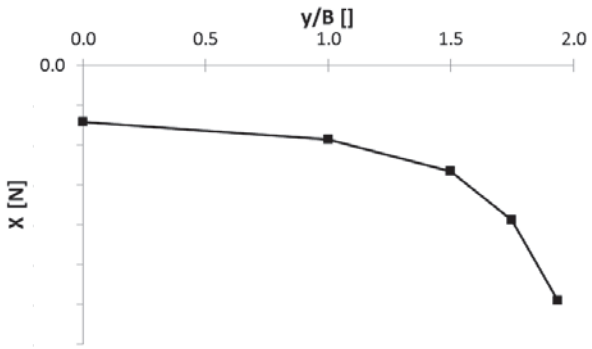

Figure 8.4 influence of the lateral position on the longitudinal bank effect X_{BANK} in the rectangular cross section QY_0_3.865_0

8.3.2 The equivalent blockage

The (classic) blockage m indicates the amount of space a vessel utilizes in the entire cross section of a fairway. If a ship sails in unrestricted waters ($\Omega = \infty$) then the blockage m will be zero. If a ship is squeezed in a cradle with the form of the mould of the midship then m will have the theoretical peak value of 1. The blockage m (equation 5.10) does not change if the same vessel is located at a different position in the same cross section. To overcome this constraint, the equivalent blockage m_{eq} is introduced. Some conditions with this new equivalent blockage must be fulfilled beforehand;

- The equivalent blockage must take into account the area of the cross section Ω but also be sensible for the relative position of the ship in the cross section.
- Furthermore the equivalent blockage must be zero when sailing in unrestricted areas (similar to the 'classic' blockage m which will be zero in this situation) and have one as maximal value (in theory).

The equivalent blockage m_{eq} takes into account the weight distribution w (and the integration χ) as expressed in Section 6.3.3. The equivalent blockage is defined as (for all values $\chi > 0$):

$$\boldsymbol{m_{eq}} = \frac{\chi_{ship}}{\chi_s + \chi_p} - \frac{\chi_{ship}}{\chi_{ocean}} \tag{8.13}$$

The ratio $\frac{\chi_{ship}}{\chi_{ocean}}$ is subtracted from the ratio $\frac{\chi_{ship}}{\chi_s+\chi_p}$ to have a zero m_{eq} when sailing in open and deep water. Both χ_{ship} and χ_{ocean} can be calculated analytically and do not depend on the geometry or position in the cross section.

$$\boldsymbol{\chi_{ship}} = \mathbf{2}\frac{y_{infl}\,T}{\xi_y \xi_z}\left(\mathbf{1} - \boldsymbol{e}^{-\frac{\xi_y B}{2y_{infl}}}\right)\left(\mathbf{1} - \boldsymbol{e}^{-\xi_z}\right) \tag{8.14}$$

$$\boldsymbol{\chi_{ocean}} = \mathbf{2}\frac{y_{infl}\,T}{\xi_y \xi_z} \tag{8.15}$$

In deep and open water the equivalent blockage m_{eq} is zero. This is chosen as such to be consistent with the 'classic blockage m'

which also is zero in infinitely open waters. There are physical reasons to contradict this choice. In infinitely deep and wide water there will also be a return flow around the forward sailing vessel, this return flow will generate also an augmented resistance but it is important to be aware of the point of reference for the resistance. If the unrestricted water is the point of reference then the equivalent blockage must be zero. If the resistance with the return flow excluded is the point of reference, then the equivalent blockage does not tend to zero in unrestricted deep waters. It is chosen to force the equivalent blockage to zero in unrestricted deep waters since it is much more obvious to take the unrestricted water condition with return flow as a reference.

The same equivalent blockage tends to 1 when the vessel is squeezed in the theoretical smallest section BT. These extreme are similar to the extreme of the 'classic blockage'.

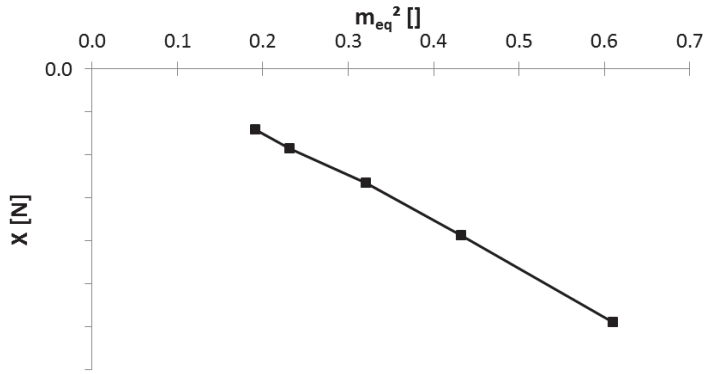

Figure 8.5 relation between X_{BANK} and the square of m_{eq} for the same tests as plotted in Figure 8.4

Figure 8.5 shows the relation between the longitudinal force X and the square of m_{eq} for the same model tests as plotted in Figure 8.4. If the (almost) linear relation between m_{eq}^2 and X is extrapolated to a $m_{eq}=0$ then a minor value for X is obtained. This shift is dedicated to errors induced in the assumption that $X = X_{BANK}$ and will be neglected during the regression to calculate the relevant coefficients.

8.4 Correlation with running sinkage

For the running sinkage it is also hard to distinguish the impact of the banks from all other influences. Different from the lateral force and similar to the longitudinal force the influence of the banks on the sinkage will be non-zero when sailing on the centre line of a symmetric cross section. The overall tendency and behaviour of the longitudinal force and running sinkage are similar (Figure 8.6)

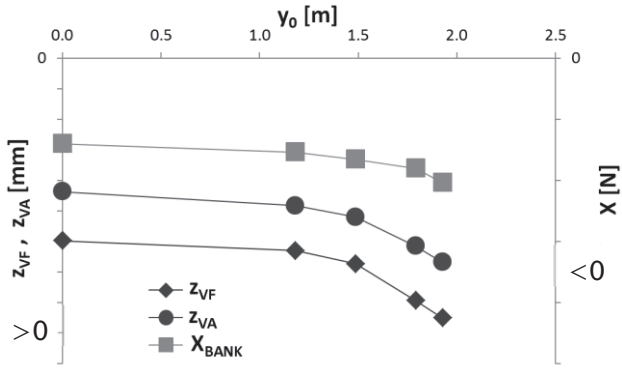

Figure 8.6 running sinkages and longitudinal force X for ship model C0P in cross section SP_3_4.200_1 according to 10 knots full scale (propeller rate 0 rpm) and relative water depth h/T=1.35

In Figure 8.7 the longitudinal force X is plotted to the three running sinkages for the same model tests as in Figure 8.6.

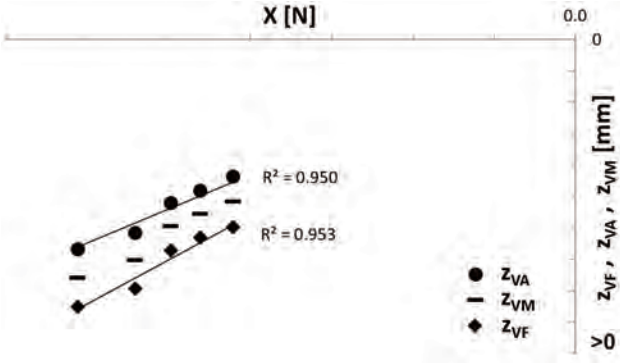

Figure 8.7 running sinkages (z_{VF}, z_{VM}, z_{VA}) and longitudinal force X for ship model C0P in cross section SP_3_4.200_1 according to 10 knots full scale (propeller rate 0 rpm) and relative water depth h/T=1.35

8.5 Mathematical model for X_{BANK} and conclusions

The product of the square of the equivalent blockage m_{eq} and the adapted Tuck number Tu_m are proportional to the longitudinal bank force:

$$\boldsymbol{X_{BANK} \propto m_{eq}^2\, Tu_m(V_{eq})} \tag{8.16}$$

The right hand side of equation 8.16 is multiplied with the displacement force Δ to introduce the dimension Newton and with ξ_ρ to cope with the proportionality:

$$\boldsymbol{X_{BANK} = \xi_\rho \Delta\, m_{eq}^2\, Tu_m(V_{eq})} \tag{8.17}$$

The longitudinal force X (assumed to be equal to X_{BANK}) for all model tests with T0Z at a propeller rate according to self-propulsion in open water and without influence of the boundary layer are plotted in Figure 8.8 (171 model tests). The relation between the modelled force and force derived from model tests is satisfying although some deviation is observed. Some reasons for this deviation are ascribed to the error introduced in defining the force X_{BANK}. Since the mathematical model for X_{BANK} runs on only one dedicated coefficient ξ_ρ because the coefficient ξ_{VTA} is annexed from the lateral force Y_A. This model is therefore seen as a very robust mathematical model.

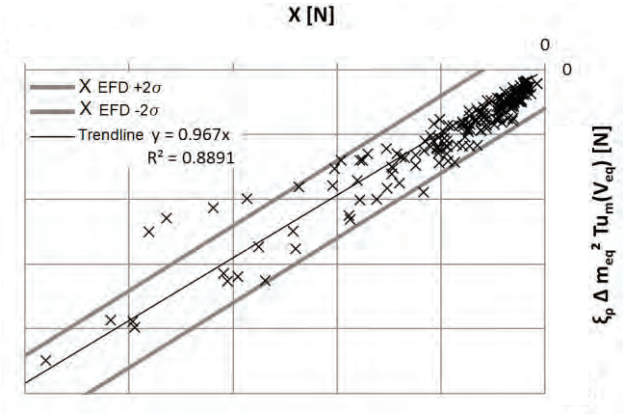

Figure 8.8 the model for X_{BANK} plotted to the force X_{BANK} derived from model tests with ship model T0Z

For reasons of consistency with Figures 6.55 and 7.20 the results for the mathematical model and from EFD are plotted for ship model C0U in Figure 8.9.

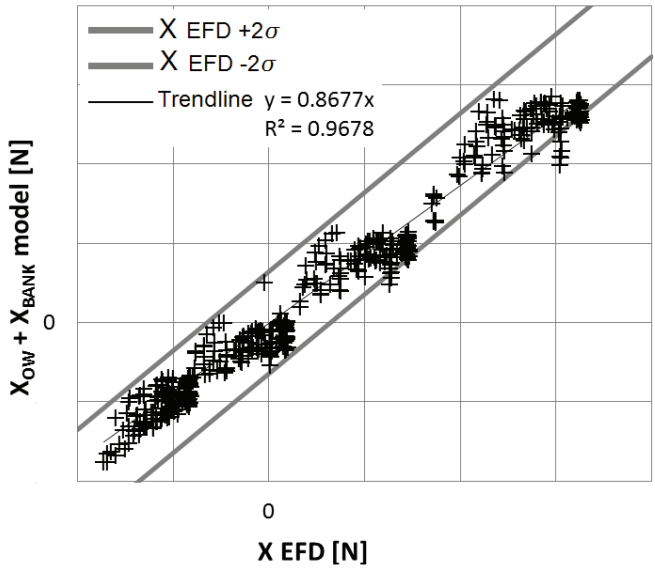

Figure 8.9 the longitudinal force X for ship model C0U (at a forward speed according to 8 knots full scale) plotted to the result from the mathematical model (all propeller rates, banks, lateral positions, #513 model tests)

Bank Effects

9 CONCLUSIONS AND RECOMMENDATIONS

The extensive research into publications on bank effects resulted in a broad insight in the phenomenon but also made the need for new model tests clear. Tests on bank effects were carried out and reported in the past but sometimes the ship models are outdated or the tests were not carried out along the bank geometries of interest for the Flemish harbours.

Flanders Hydraulics Research carried out an enormous amount (+12 000) of model tests dedicated to bank effects in their shallow water towing tank. This data set was even extended with data acquired from a friendly institute. Together, these are the model tests for the foundation of the present mathematical model for bank effects.

9.1 Bank effects acting in the horizontal plane

Only the forces acting in the horizontal plane (parallel to the free surface) are considered for the mathematical model for bank effects. These forces are commonly split in two forces, longitudinal X_{BANK} and lateral directed Y_{BANK}, and a moment N_{BANK} around the vertical axis. The present mathematical model, however, splits the bank effects of the horizontal plane in three forces:

- The longitudinal force X_{BANK}
- The lateral force at the forward perpendicular Y_F
- The lateral force at the aft perpendicular Y_A

It was decided to make use of this unconventional decomposition of the horizontal forces and moment because of the different behaviour in shallow water of the fore part compared to the aft part of the ship. With basic statics the yaw moment N_{BANK} and overall lateral force Y_{BANK} can easily be derived from these two forces Y_F and Y_A.

9.1.1 The longitudinal force X_{BANK}

The longitudinal force X_{BANK} induced by the proximity of a bank or banks on a ship acts always on that ship as an additional resistance. The magnitude of this added resistance increases with an increasing forward speed of the ship. A propeller generating a positive thrust will increase the magnitude of the bank effects in the longitudinal ship direction (x).

The interaction between the sailing area and the ship has the following impact on this resistance force: the more shallow and/or the more narrow the fairway, the larger this resistance. A more eccentric position of the ship in the cross section will also result in a larger magnitude of the longitudinal force X_{BANK}.

9.1.2 The lateral force at the forward perpendicular Y_F

The lateral force at the forward perpendicular Y_F in very deep water is always an attraction force pointed towards the closest bank. In very shallow water this force is directed away from the closest bank or a repulsion force. The lateral force in the sign changing region between deep and shallow water is dependent of the forward speed of the ship.

The magnitude of the lateral force at the forward perpendicular Y_F, either an attraction or a repulsion force, will increase with the forward speed of the ship, or when the ship sails closer to the bank, or in a more confined cross section (with a larger blockage ratio). The propeller actions (located close to the aft perpendicular) have only a minor influence on this lateral force at the forward perpendicular.

9.1.3 The lateral force at the aft perpendicular Y_A

At the aft perpendicular the lateral force Y_A is for all water depths an attraction force directed towards the closest bank. The attraction force at the aft perpendicular Y_A is always larger than the attraction force at the forward perpendicular Y_F (in deeper water). The combination of these two forces results in an overall attraction towards the closest bank in combination with a bow out moment away from the closest bank. In very shallow water the magnitude of the repulsion force at the forward perpendicular is sometimes larger than the attraction force at the aft perpendicular. Both forces will then result in an overall repulsion force away from the closest bank in combination with a (large) bow away moment.

The faster the ship sails, the larger the attraction force at the aft perpendicular will be. This attraction force will also increase when the propeller is loaded more.

A more narrow distance between ship and bank or keel and bottom will also result in a larger attraction Y_A. The same is true for a larger blockage ratio (more confined waters).

9.2 Mathematical model

The previously described influences of the proximity of banks on a sailing ship are implemented in a mathematical model. This mathematical model consists out of different parameters which cope with specific environmental factors or ship properties.

9.2.1 Parameters

9.2.1.1 Propeller loading, speed, blockage ratio and water depth

The loading of the propeller (thrust T_P) is first transformed into a velocity V_T (equation 9.1) and then this velocity is partially ($\xi_{VT,A}$, $\xi_{VT,F}$) added to the forward velocity of the ship V to result in the equivalent velocity V_{eq} (equation 9.2).

$$\boldsymbol{V_T = \frac{T_P}{|T_P|}\sqrt{\frac{8|T_P|}{\rho\pi D^2}}} \tag{9.1}$$

$$\boldsymbol{V_{eq} = V + \xi_{VT} V_T} \tag{9.2}$$

The equivalent velocity is used as input to calculate the Tuck number. Through the limited blockage ratio (m_{lim}) this Tuck number Tu_m takes into account the decreased critical speed ($Fr_{crit,lim}$) in more confined waters.

$$\boldsymbol{m_{lim} = \frac{A_M}{\Omega_{lim}}} \tag{9.3}$$

$$\boldsymbol{Fr_{crit,lim} = \left(2\,sin\left(\frac{Arcsin(1-m_{lim})}{3}\right)\right)^{\frac{3}{2}}} \tag{9.4}$$

$$\boldsymbol{Tu_m(V_{eq}) = \frac{\left(\frac{Fr_h}{Fr_{crit,lim}}\right)^2}{\sqrt{1-\left(\frac{Fr_h}{Fr_{crit,lim}}\right)^2}}} \tag{9.5}$$

The longitudinal force X_{BANK} and both lateral forces Y_F and Y_A are proportional to the Tuck number calculated with equivalent forward speed $Tu_m(V_{eq})$.

9.2.1.2 Lateral position

The closer a ship sails to a bank, the larger the bank effects will be. A value indicating the distance between a ship and any random bank geometry which takes into account all the nuances of that geometry is needed. Therefore the weight distribution is introduced. The weight factor (w) is a value between 0 and 1 (equation 9.6) to indicate the impact of the relative position on the bank effect. The largest value for w (= 1) is located at the intersection of the (undisturbed) free surface and the X-Z plane in the ship bound coordinate system. The weight factor is a value exponentially decreasing the further the point of consideration is away from the location of that peak point (Figure 9.1).

$$w = e^{-\left(\xi_y \frac{|y|}{y_{infl}} + \xi_z \frac{|z|}{T}\right)} \tag{9.6}$$

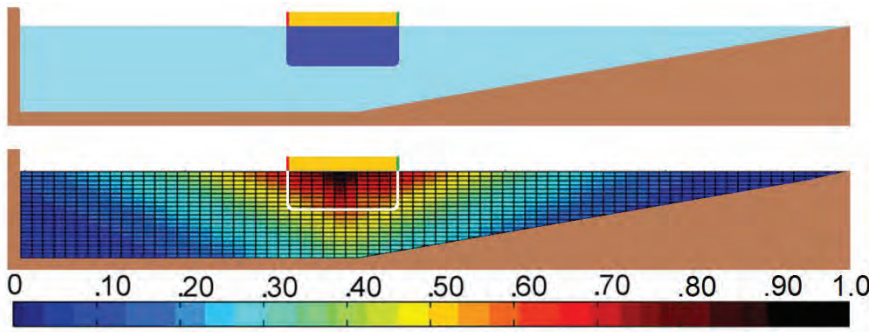

Figure 9.1 weight distribution w in a cross section with vertical wall and surface piercing bank

The 'weight' χ is the integral over the area under consideration. This area (A) can be the ship ($_{ship}$), the port ($_{p}$) or starboard side ($_{s}$) of the cross section or even an infinite large area at borders at infinity ($_{ocean}$). The 'weight' is always a positive value.

$$\chi = \oiint_A w \, dA \tag{9.7}$$

The distance between ship and bank is mathematically modelled with the parameter d2b. The inverse of this value ($d2b^{-1}$) is zero when sailing on the centre line of a symmetric cross section and

its magnitude can become very large when sailing very close to a bank.

$$d2b = \frac{2}{\chi_{ship}} \frac{\chi_p \chi_s}{\chi_p - \chi_s} \tag{9.8}$$

An equivalent blockage m_{eq} is introduced to take into account the bank geometry on the longitudinal force X_{BANK}. The distance to bank d2b cannot be used since the inverse of this value is zero on the centre line of the cross section when the longitudinal bank effects are not.

$$m_{eq} = \frac{\chi_{ship}}{\chi_s + \chi_p} - \frac{\chi_{ship}}{\chi_{ocean}} \tag{9.9}$$

Unlike the 'classic' blockage ratio (m), the equivalent blockage (m_{eq}) is influenced by the relative position of the ship in the fairway, and is zero when sailing in deep and open water.

9.2.1.3 Stretches of the model

At a sufficient distance between ship and bank, bank effects do not occur. This distance is the influence width (y_{infl}) and is larger/greater in shallow water or if the ship sails faster.

$$y_{infl} = B(5Fr_h + 5) \tag{9.10}$$

The area of the cross section of the fairway (Ω) is virtually restricted by this influence width. Now the (classic) blockage ratio (m) will no longer be zero when sailing in a cross section open at one side.

All bodies travelling through a (viscous) fluid will have a boundary layer attached to its wetted surface. Thus, this boundary layer will be present on both full scale ship as well as model scaled ship but the boundary layer will be relatively thicker at model scale than at full scale. This boundary layer will have a large influence on the (behaviour of the) bank effects when a ship sails at an extremely close distance to the boundaries of the cross section. Because of the return flow along the hull there will also be a boundary layer attached to the bank and/or the bottom.

The influence of the boundary layer observed on model scale cannot be scaled up to real life in the same manner as other forces are scaled up. Therefore the boundary layer thickness influence δ_{BLI} is introduced. This thickness calculates the minimal distance between hull and environment (bank or bottom) to avoid the influence of the boundary layer on bank effects.

$$\boldsymbol{\delta_{BLI}} \propto \frac{\boldsymbol{Lpp}}{\sqrt[7]{\boldsymbol{Re}}} \frac{\boldsymbol{T}}{\boldsymbol{h}} \frac{(\boldsymbol{V_T}+2\boldsymbol{V})}{\boldsymbol{V}} \tag{9.11}$$

This thickness δ_{BLI} is relatively thicker on model scale than at full scale because of the different Reynolds number (present model tests are scaled according to Froude's law). The regression software to determine the coefficients of the mathematical model did not take into account model tests with the ship model in the boundary layer thickness influence but the influence itself is implemented in the mathematical model. The boundary layer develops from the leading edge of the body (the bow of a forward sailing ship) towards the trailing edge (the stern section of a forward sailing ship). The boundary layer is thicker at the aft half of the hull than at the forward half and therefore the influence of the boundary layer is mainly observed on the lateral force at the aft perpendicular Y_A. The lateral attraction force at the aft perpendicular Y_A will decrease once the vessel gets more and more into the boundary layer thickness influence (δ_{BLI}). This value becomes zero when the gap between ship and bathymetry (bank or bottom) disappears.

9.2.2 Formulae

The formulae given for the three forces in the horizontal plane induced by bank effects are valid for all water depths and bank geometries with sufficient length compared to the main dimensions of the ship (steady state condition). One set of coefficients (Table 9.1) is needed for each loading condition of each ship (type).

9.2.2.1 X_{BANK}

The mathematical model of the longitudinal (added resistance) force induced by the presence of banks is modelled as follows:

$$\boldsymbol{X_{BANK} = \xi_\rho \Delta\, m_{eq}^2\, Tu_m(V_{eq})} \tag{9.12}$$

The coefficients ξ_y and ξ_z to calculate the value m_{eq} (through χ) are identical for all three forces (X_{BANK}, Y_F and Y_A). The coefficient ξ_{VT} for the calculation of the equivalent velocity V_{eq} is the same for this longitudinal force X_{BANK} as it is for the lateral force at the aft perpendicular Y_A. The only unique coefficient left is ξ_ρ.

9.2.2.2 Y_F

The lateral force at the forward perpendicular is proportional to the Tuck number ($Tu_m(V_{eq})$), the inverse of the distance to bank ($d2b^{-1}$) and displacement force (Δ). The drastic influence of the relative water depth is implemented with a dimensional speed (Froude number Fr) and relative water depth (T/(h-T)) dependent function.

$$\boldsymbol{Y_F}\begin{cases} \boldsymbol{\xi_\rho\, \Delta\, d2b^{-1}\, Tu_m(V_{eq})\left(1 - Fr^2\, \frac{\frac{T^2}{(h-T)^2} - \xi_{hT}{}^2 + \left|\frac{T^2}{(h-T)^2} - \xi_{hT}{}^2\right|}{2\xi_h{}^2}\right)} & \boldsymbol{h_{ship} - C_M T - z_{VF} \geq \delta_{BLI,F}} \\ \boldsymbol{\frac{h_{ship} - C_M T - z_{VF}}{\delta_{BLI,F}}\, \xi_\rho\, \Delta\, d2b^{-1}\, Tu_m(V_{eq})\left(1 - Fr^2\, \frac{\frac{T^2}{(h-T)^2} - \xi_{hT}{}^2 + \left|\frac{T^2}{(h-T)^2} - \xi_{hT}{}^2\right|}{2\xi_h{}^2}\right)} & \boldsymbol{h_{ship} - C_M T - z_{VF} < \delta_{BLI,F}} \end{cases} \tag{9.13}$$

In deep water the function $\left(1 - Fr^2\, \frac{\frac{T^2}{(h-T)^2} - \xi_{hT}{}^2 + \left|\frac{T^2}{(h-T)^2} - \xi_{hT}{}^2\right|}{2\xi_h{}^2}\right)$ equals 1, in very shallow water this function can have very low negative values and as a consequence the lateral force at the forward perpendicular will be a powerful repulsion force away from the closest bank.

9.2.2.3 Y_A

The lateral force at the aft perpendicular will have a different behaviour when the distance between ship and bank or bottom is closer than the boundary layer influence thickness or not. At full scale this boundary layer thickness between ship and bank will only occur along vertical banks and even then only in very specific situations such as the sliding along an approach wall before a lock (Panama, Dunkerque). In the proposed mathematical model this is not incorporated. When the wall is not vertical then the boundary layer thickness can almost not be penetrated.

$$\boldsymbol{Y_A} = \begin{cases} \boldsymbol{\xi_\rho\, \Delta\, d2b^{-1}\; Tu_m(V_{eq}),\;\; (h_{ship} - C_M T - z_{VA}) \geq \delta_{BLI,A}} \\ \boldsymbol{\frac{h_{ship}-C_M T-z_{VA}}{\delta_{BLI,A}}\, \xi_\rho\, \Delta\, d2b^{-1}\; Tu_m(V_{eq}),\;\; (h_{ship} - C_M T - z_{VA}) < \delta_{BLI,A}} \end{cases} \quad (9.14)$$

The distance between the deepest drafted section of the ship (running sinkage taken into account) and the bottom is not exceptionally smaller at full scale than the boundary layer thickness influence. Therefore the mathematical for Y_A is split in two parts whether the running under keel clearance ($h_{ship}-T-z_{VA}$) is larger than δ_{BLI} or not.

9.3 Practical implementation

The proposed mathematical model for the (horizontal) bank effects (X_{BANK}, Y_F and Y_A) runs on a set of nine unique coefficients (Table 9.1). These coefficients are identified with regression software provided with the results from model tests carried out in a towing tank. The overall longitudinal force X_{BANK}, lateral force Y_{BANK} and yaw moment N_{BANK} is requested by the ship manoeuvring simulator the following derivation can be made:

$$\boldsymbol{Y_{BANK} = Y_F + Y_A} \quad (9.15)$$

$$\boldsymbol{N_{BANK} = \frac{Lpp}{2} Y_F - \frac{Lpp}{2} Y_A} \quad (9.16)$$

For the calculation of the bank effects the largest impact and computer time for a ship manoeuvring simulator is the running calculation for the weight distributions χ_p and χ_s. Both are the results of a (discretised) integration of a major section of the cross

section. The bathymetry up to the free surface will also be necessary or a simplification (extrapolation) to the free surface will be necessary to be able to calculate both weight distributions correctly.

	ξ_ρ	ξ_y	ξ_z	ξ_{VT}	ξ_h	ξ_{hT}
Y_F	✓			✓/0	✓	✓
Y_A	✓	✓	✓	✓	-	-
X_{BANK}	✓				-	-

Table 9.1 overview of the set of coefficients for one ship at one loading condition

9.4 Future work

No research is complete without some recommendation and suggestions for extra work.

A dedicated set of model tests to be able to define all the coefficients of the model can be sought for. However, if the bank effects for one ship and bathymetry combination is requested then it will always be more accurate to test this specific situation in the towing tank and define the coefficients based upon these tests compared to using a kind of overall generic test program.

The influence of the relative angle between the ship and bank can be investigated. The angle between both can originate from sailing at a drift angle with a heading parallel to the bank, with the ship hull parallel to the bank with the heading non-parallel or a combination of both.

Time series and time dependencies of changing bank geometries (both rapid and gentle) are to be checked.

The concept of the weight factor (and corresponding weight distribution χ) could be checked for the running sinkage (fore and aft). As such, the influence of the banks on the vertical sinkage and trim (or squat) could be incorporated (or updated) in the ship manoeuvring simulator.

When sailing very close to the bottom or bank the influence on appendices such as propeller(s) and rudder(s) are in present research neglected. In the extreme situation (moments before bank or bottom impact) the behaviour of rudder and propeller can be of importance. Therefore this can be investigated more closely.

The impact of the boundary layer influence on shallow water hydrodynamics must be investigated more closely. It can be expected that this boundary layer influence in very shallow water is not restricted to bank effects but also acts on other elements of the manoeuvrability of a ship.

The scaling from model scale to full scale of model tests carried out at very small distances between the ship model and other constructions (bottom, bank, specific installations) should be checked. This can be done by using computational fluid dynamics (CFD) or with geosim model tests. The latter is repeating the same model test but with ship models at a different scale of the same full scale ship. The ship models and environment (water depth, section width, bank geometry) are geometrical identical (but have different dimensions because of the different scales involved). As such, the influence of the boundary layer can be investigated more closely by comparing the results since the Froude number will be the same at all scales but the Reynolds number will not when carrying out model tests at a different scale.

Bank Effects

10 BIBLIOGRAPHY

Ankudinov, V., Kaplan, P. & Jacobsen, B., 1993. *Assessment and Principal Structure of the Modular Mathematical Model for Ship Maneuverability Prediction and Real-Time Maneuvering Simulations.* MARSIM '93, pp.71 - 77.

Anon, 2014a. *Marine Traffic*, www.marinetraffic.com.

Anon, 2014b. Port of Antwerp, http://www.portofantwerp.com/nl/news/recordoverslag-haven-van-antwerpen-bevestigd.

Barrass, C.B., 2004. *The Phenomena of Interaction of Ships in Confined Waters.* In Ship Design and Performance for Masters and Mates. Elsevier, pp. 180-190.

Beck, R.F., 1976. *Forces and Moments on a Ship Moving in a Canal*, Report, (179), pp.1-49.

Beck, R.F., 1977. *Forces and Moments on a Ship Moving in a Shallow Channel.* Journal of Ship Research, 21(2), pp.107-119.

Bernoulli, J., 1713. *Ars conjectandi: Opus posthumum: accedit tractatus de seriebus infinitis, et Epistola Gallicè Scripta de ludo pilae reticularis.*

Brard, R., 1951. *Maneuvering of Ships In Deep Water , in Shallovv Water , and in Canals.* In Summer meeting of the Society of Naval Architects and Marine Engineers. Washington D.C., USA, pp. 229–257.

Brix, J., 1992. *Manoeuvring Technical Manual.* Schiff und Hafen, 5, pp.71–78.

Capron, A. & Barbieux, V., 2012. Intermediate report Partial contract 3 *Numerical calculation of scenarios at variance with those tested in the towing tank.* Report

Carlton, J., 2012. *Marine Propellers and Propulsion.* Book

Ch'ng, P.W. & Renilson, M.R., 1990. *The Effect of Bank Slope and water Depth on the Forces on a Ship in Restricted Water.* In Third Australian Port and Harbour Engineering Conference. pp. 1–5.

Ch'ng, P.W., Doctors, L.J. & Renilson, M.R., 1993. *A Method of Calculating the Ship-Bank Interaction Forces and Moments in Restricted Water.* International Shipbuilding Progress, 40(421), pp.7–23.

Chetvertakov, A.M., Lebedeva, M.P., Nikushchenko, D. V & Maritime, K., 2011. Numerical Investigation of Bank Influence on a Ship Motion. In 2nd International Conference on Ship Manoeuvring in Shallow and Confined Water: Ship to Ship Interaction, May 18 – 20, 2011, Trondheim, Norway. pp. 83–88.

Crane, C., 1979. *Maneuvering Trials of 278,000 DWT Tanker in Shallow and Deep Waters.* SNAME Transactions, 87, pp.251–283.

Dand, I.W., 1981. *Some Measurements of Interaction Induced by Surface – Piercing and Flooded Banks* , Report 110(August), pp.1–92.

Dand, I.W., 1982. *On Ship–Bank Interaction*. In Transactions of the Royal Institution of Naval Architects. London, UK, pp. 25–40.

De Roo, S. & Troch, P., 2013. *Field Monitoring of Ship Wave Action on Environmentally Friendly Bank Protection in a Confined Waterway.* Journal of Waterway, Port, Coastal, and Ocean Engineering, 139(6), pp.527–534.

Delefortrie, G. & Hermans, P., 2001. *Wiskundige formulering van oevereffecten voor scheepsmanoeuvreersimulatie* , pp.1–302. Master Thesis

Delefortrie, G., Lataire, E. & Mostaert, F., 2010. *Haalbaarheidsstudie tweede sleeptank*: deelrapport 1. Overzicht activiteiten 09/2009 – 08/2010 , 457_11. Report

Delefortrie, G., Vantorre, M. & Eloot, K., 2004. *Linear Manoeuvring Derivatives in Muddy Navigation Areas.* The Transactions of the Royal Institution of Naval Architects: International Journal of Maritime Engineering, 146(Part A4), pp.1–13.

Delefortrie, G., Vantorre, M. & Eloot, K., 2005. *Modelling Navigation in Muddy Areas through Captive Model Tests.* Journal of Marine Science and Technology, 10(4), pp.188–202.

Duffy, J., Renilson, M. & Thomas, G., 2009. *Simulation of Ship Manoeuvring in Laterally Restricted Water.* In International Conference on Ship Manoeuvering in Shallow and Confined Water: Bank Effects 2009. pp. 85-94.

Duffy, J.T., 2002. *The Effect of Channel Geometry on Ship Operation in a Port.* In 30th PIANC-AIPCN Congress, 22-26 September 2002, Sydney, Australia. Sydney, Australia, pp. 1-12.

Duffy, J.T., Renilson, M. & Smith, I., 1998. *The Effect of Bank Geometry on the Simulation of Ship Manoeuvring in Restricted Water*. In Proceedings of the International Conference on Safe Navigation beyond 2000. Gdynia, Poland, pp. 1-17.

Eda, H., 1971. *Directional Stability and Control*. In Annual meeting of the Society of Naval Architects and Marine Engineers. New York, USA, pp. 72-116.

Eloot, K., Vantorre, M. & Delefortrie, G., 2006. *Prediction of Ship Manoeuvrability of an 8000 TEU Containership in Deep and Shallow Water: Mathematical Modelling and Captive Model Testing.* Marine Simulation and Ship Manoeuvrability: Proceedings of the International Conference MARSIM 2006, Terschelling, The Netherlands.

Eloot, K., Verwilligen, J. & Vantorre, M., 2007. *A Methodology for Evaluating the Controllability of a Ship Navigating in a Restricted Channel.* In Archives of Civil and mechanical engineering: quarterly. Oficyna Wydawnicza Politechniki Wroclawskiej, pp. 91-104.

Fenical, S.W. & Carter, J.D., 2009. *Comprehensive Hydrodynamics Model for Prediction of Sinkage, Mooring Forces, Bank Hydrodynamic Effects and Coastal Impacts*. In K. Eloot & M.

Vantorre, eds. International Conference on Ship Manoeuvering in Shallow and Confined Water: Bank Effects 2009. Antwerp, Belgium: R.I.N.A., pp. 23–29.

Froude, W., Abell, W.S., Gawn, R.W.L. & Duckworth, A.D., 1955. *The Papers of William Froude, 1810–1879*: With a Memoir by Sir Westcott Abell and an Evaluation of William Froude's Work by R.W.L. Gawn: Collected Into One Volume.

Fuehrer, M. & Römisch, K., 1983. *The Effects of Hydrodynamic Forces on Ships Navigating through Canals – A Contribution to an Estimation of the Manoeuvrability of Ships in a Restricted Channel*. Bulletin of the Permanent International Association of Navigation Congresses, 57(43), pp.10–20.

Fuehrer, M., 1978. *The Results of Systematic Investigations into Lateral Forces for Determining the Effects of Hydraulic Asymmetry and Eccentricity on the Navigation of Seagoing Ships in Canals.* In Symposium on Aspects of Navigability. pp. 1–18.

Fujino, M., 1968. *Experimental Studies on Ship Manoeuvrability in Restricted Waters Part I*. International Shipbuilding Progress, 15(168), pp.279–301.

Gates, E.T. & Herbich, J.B., 1977. *Mathematical Models for the Design, Operation and Economic Analysis of Deep-Draft Navigation Channels*. In International Navigation Congress. pp. 175–182.

Gates, E.T. & Herbich, J.B., 1978. A Mathematical Model for the Review or Design of Deep-Draft Navigation Channels with Respect to Vessel Drift and Rudder Angles. In Proceedings Symposium "Aspects of Navigability." International Association for Hydraulic Research, pp. 1–14.

Geerts, S., Vantorre, M., Eloot, K., Huijsmans, R. & Fierens, N., 2011. *Interaction Forces in Tug Operations*. In B. Pettersen, T. E. Berg, K. Eloot, & M. Vantorre, eds. Second International Conference on Ship Manoeuvring in Shallow and Confined Water: Ship to Ship Interaction. Trondheim, Norway: R.I.N.A, pp. 153-163.

Gronarz, A., 2009. *Investigation of the Influence of a Vertical Wall on a Ship Moving with Drift Angle*. International Conference on Ship Manoeuvring in Shallow and Confined Water: Bank Effects, pp.77-83.

Gui, Q.Y., Chuang, J.M. & Hsiung, C.C., 1990. *Computation of Ship Interaction Forces and Moments in Restricted Waterways Using the Numerical Conformal Mapping Method.* International Shipbuilding Progress, 37(412), pp.401-419.

Guliev, U.M., 1971. *Calculs relatifs au déjaugeage de navires qui naviguent dans des eaux profondes et dans des chenaux*. PIANC Bulletin, I(7), pp.21-26.

Härting, A. & Reinking, J., 2004. *Aspects of Underkeel Clearance in Analysis and Application*. In Squat Workshop 2004. Elsfleth/Oldenburg, Germany, pp. 1-231.

Hartl, M., 2011. The Tau Manifesto. www.TauDay. com

Havelock, T., 1908. *The Propagation of Groups of Waves in Dispersive Media, with Application to Waves on Water* Produced by a Travelling Disturbance. Proceedings of the Royal Society of London, pp.398-430.

Hsiung, C.C. & Gui, Q., 1988. *Computing Interaction Forces and Moments on a Ship in Restricted Waterways.* International Shipbuilding Progress, 35(403), pp.219-254.

Hüsig, A., Linke, T. & Zimmermann, C., 2000. *Effects from Supercritical Ship Operation on Inland Canals.* Journal of Waterway, Port, Coastal, and Ocean Engineering, (126), pp.130–135.

ITTC, 2002. *The Manoeuvring Committee – Final Report and Recommendations to the 23rd ITTC*. In Proceedings of the 23rd ITTC. Venice, Italy, pp. 159–222.

ITTC, 2008. *ITTC Recommended Procedures and Guidelines* – Testing and Extrapolation Methods Manoeuvrability Captive Model Test Procedures, p.21.

ITTC, 2011. *Fresh Water and Seawater Properties*, p.45.

ITTC, 2011. *ITTC symbols and terminology list*. US Naval Academy, (September), p.170.

Kijima, K. & Qing, H., 1987. *Manoeuvring Motion of a Ship in the Proximity of Bank Wall*. Journal of the Society of Naval Architects of Japan, 1987(162), pp.125–132.

King, G.W. & Tuck, E., 1979. *Lateral Forces on Ships in Steady Motion Parallel to Banks or Beaches.* Applied Ocean Research, 1(2), pp.89–98.

Kolkman, P.A., 1978. *Ships Meeting and Generating Currents.* IAHR–Symposium on Aspects of Navigability of Constraint Waterways, Including Harbour Entrances, Delft, The, pp.1–26.

Kongsberg, 2012. *Kongsberg Release Notes* – SBS Polaris 7.1.1.

Koslowski, J., 2007. *Ship–induced Riverbank and Harbour Damage*. Hydro International, (September), pp.2–4.

Kumar, M. & Anantha Subramanian, V., 2007. *A Numerical and Experimental Study on Tank Wall Influences in Drag Estimation.* Ocean Engineering, 34(1), pp.192-205.

Lataire, E. & Vantorre, M., 2008. *Ship-Bank Interaction Induced by Irregular Bank Geometries*. In 27th Symposium on Naval Hydrodynamics. Seoul, Korea, pp. 5-10.

Lataire, E., Vantorre, M., Laforce, E., Eloot, K. & Delefortrie, G., 2007. *Navigation in Confined Waters: Influence of Bank Characteristics on Ship-Bank Interaction*. In Proceedings of the 2nd International Conference On Marine Research And Transportation, Ischia, Naples, Italy, 28-30 june 2007. [S.n.].

Lataire, E., Vantorre, M. & Delefortrie, G., 2009. *Captive Model Testing for Ship-to-Ship Operations*. In MARSIM '09 Conference, Proceedings. Panama City, Panama: [S.n.], pp. M-14-1/10.

Lataire, E., Vantorre, M. & Delefortrie, G., 2012(a). *A Prediction Method for Squat in Restricted and Unrestricted Rectangular Fairways*. Ocean Engineering, 55, pp.71-80.

Lataire, E., Vantorre, M. & Delefortrie, G., 2012b. *Squat in Open and Confined Canals: Comparison between Empirical Methods and Towing Tank Measurements*. In MARSIM 2012. pp. FP2-2/1-15.

Lataire, E., Vantorre, M. & Eloot, K., 2009. *Systematic Model Tests on Ship-Bank Interaction Effects*. International Conference on Ship Manoeuvring in Shallow and Confined Water: Bank Effects, pp.9-22.

Lataire, E., Vantorre, M., Delefortrie, G. & Candries, M., 2012. *Mathematical Modelling of Forces Acting on Ships During Lightering Operations*. Ocean Engineering, 55, pp.101-115.

Lataire, E., Vantorre, M., Laforce, E. & Mostaert, F., 2008. *Invloed van een ophoging van het sternenschiereiland op oevereffecten*, 741/3, p.11. Report

Lee, C.-K. & Lee, S.-G., 2008. *Investigation of Ship Maneuvering with Hydrodynamic Effects between Ship and Bank*. Journal of Mechanical Science and Technology, 22(6), pp.1230–1236.

Li, D., 2000. Experiments on Bank Effects under Extreme Conditions, (Report 113). Report

Li, D., Ottosson, P. & Tragardh, P., 2003. *Prediction of Bank Effects by Model Tests and Mathematical Models*. In MARSIM 2003. pp. 1–12.

Lo, D.C., Su, D.-T. & Chen, J.-M., 2009. *Application of Computational Fluid Dynamics Simulations to the Analysis of Bank Effects in Restricted Waters*. The Journal of Navigation, 62(03), pp.477–491.

Lo, D.C., Su, D.-T. & Lin, I., 2009. *Applying Computational Fluid Dynamics to Simulate Bank Effects*. In Proceedings of 19th International Offshore and Polar Engineering Conference. Osaka, Japan, pp. 466–471.

Maimun, A., Priyanto, A., Rahimuddin., Baidowi, A. & Nurcholis, 2009. *Ship Manoeuvring in Shallow Water with Ship–Bank Interaction Effects*. In International Conference on Ship Manoeuvering in Shallow and Confined Water: Bank Effects 2009. pp. 1–6.

Maimun, A., Priyanto, A., Rahimuddin, Sian, A. Y., Awal, Z. I., Celement, C. S., Nurcholis & Waqiyuddin, M., 2013. *A Mathematical Model on Manoeuvrability of a LNG Tanker in Vicinity of Bank in Restricted Water*. Safety Science, 53, pp.34–44.

McArthur, P.J.J., 2011. *New thinking in Ship Generated Hydrodynamic Fields: Introducing Concepts for Predicting Bank Suction and Rejection*. In Second International Conference on Ship Manoeuvring in Shallow and Confined Water: Ship to Ship Interaction. R.I.N.A., pp. 239–252.

Miao, Q., Xia, J., Chwang, A. & Duffy, J., 2003. *Numerical Study of Bank Effects on a Ship Travelling in a Channel*. In 8th International conference on numerical ship hydrodynamics. pp. 1–8.

Newman, J.N., 1965. *The Force and Moment on a Slender Body of Revolution Moving Near a Wall*, (December 1965), pp.1–17.

Newman, J.N., 1969. *Lateral Motion of a Slender Body Between Two Parallel Walls*. Journal of Fluid Mechanics, 39(01), pp.97–115.

Norrbin, N.H., 1969. *Analytical Modelling and Experimental Results for Confined Water Tanker Manoeuvring*, (113). Report

Norrbin, N.H., 1974 (a). *A Method for the Prediction of the Manoeuvring Lane of a Ship in a Channel of Varying Width*. In Symposium on Aspects of Navigability. pp. 1–18.

Norrbin, N.H., 1974 (b). *Bank Effects on a Ship Moving through a Short Dredged Channel*. In R. D. Cooper & S. W. Doroff, eds. 10th ONR. Office of Naval Research, pp. 71–88.

Norrbin, N.H., 1975. *Manoeuvring in Confined Waters: Interaction Phenomena Due to Side Banks or Other Ships*. In Proceedings of the 14th I.T.T.C. Ottawa, Canada, p. Appendix VIII: 450–486.

Norrbin, N.H., 1985. *Bank Clearance and Optimal Section Shape for Ship Canals*. In 26th International Navigation Congress. PIANC, pp. 167–178.

PIANC Working group 20, 1992*. Capability of Ship Manoeuvring Simulation Models for Approach Channels and Fairways in Harbours*. Report

Promotie Binnenvaart Vlaanderen, 2013. *Promotie Binnenvaart Vlaanderen Jaarverslag 2013*.

Raad voor Transportveiligheid, 2004. *Themastudie naar roeruitval op binnenschepen*, pp.1–115. Report

Remery, G.F.M., 1974. *Mooring Forces Induced by Passing Ships.* In 6th Offshore Technology Conference. Houston, USA, pp. 349–363 (Paper OTC 2066).

Renilson, M.R. & Munro, A., 1989. *The Effect of Shape and Angle on Bank Interaction*. The Naval Architect, (March 1989), pp.1–2.

Robbins, A. & Thomas, G., 2013. *When is Water Shallow?* The Transactions of the Royal Institution of Naval Architects: International Journal of Maritime Engineering, 155(Part A3).

Roemers, D. & Pimentel, D.J., 2005. *Uitspraak van de Raad voor de Scheepvaart inzake de aanvaring van het Maltezer containerschip "Pelican I" op de Westerschelde, met het onder de vlag van de Bahama's varende containerschip "Maersk Bahrain"* , 86(86), pp.1–32. Juridisch verslag

Römisch, K., 1978. *Contribution to a Determination of the Required Canal Width*. In Symposium on Aspects of Navigability. pp. 1–13.

Römisch, K., 2004. *Squat-Berechnung unter Beachtung Hydromechanischer Randbedingungen* (Computation of Ship Squat under Hydro-mechanical Criteria). Squat Workshop.

Sano, M., Yasukawa, H. & Hata, H., 2012. *Experimental Study on Ship Operation in Close Proximity to Bank Channel*. In MARSIM 2012. pp. FP8-3/1-10.

Schijf, J.B., 1949. *Protection of Embankments and Bed in Inland and Maritime Waters, and in Overflow or Weirs*. In XVII International Navigation Congress, Lisbon, Section I. pp. 61-78.

Schoenherr, K.E., 1960. *Data for Estimating Bank Suction Effects in Restricted Water and on Merchant Ship Hulls*. In 1st Symposium on ship maneuverability. SNAME, pp. 199-210.

Soomere, T., 2007. *Nonlinear Components of Ship Wake Waves.* Applied Mechanics Reviews, 60(3), pp.120-138.

Stern, F. & Agdrup, K., 2008. *SIMMAN 2008 Workshop on Verification and Validation of Ship Maneuvering Simulation Methods*. In Workshop Proceedings. p. 2008.

Sturtzel, W., Graff, W. & Müller, E., 1966. *Untersuchung der verformung der wasseroberfläche durch die verdrängungsströmung bei der Fahrt eines schiffes auf seitlich beschränktem, flachem Fahrwasser*. Forschungsberichte des Landes Nordrhein-Westfalen, (1725), pp.1-71.

Tuck, E.O., 1966. *Shallow-Water Flows Past Slender Bodies*. Journal of Fluid Mechanics, 26, pp.81-95.

Tursini, L., 1953. *Leonardo da Vinci and the Problems of Navigation and Naval Design*. Quarterly Transactions of the Institution of Naval Architects, 95(2), pp.97-102.

Van Kerkhove, G., Vantorre, M. & Delefortrie, G., 2009. *Advanced Model Testing Techniques for Ship Behaviour in Shallow and Confined Water*. Proceedings of The First International Conference on Advanced Model Measurement Technology for the EU Maritime Industry, p.29.

Vantorre, M. & Delefortrie, G., 2013. *Behaviour of Ships Approaching and Leaving Locks: Open Model Test Data for Validation Purposes*. In 3rd International Conference on Ship Manoeuvring in Shallow and Confined Water: with non-exclusive focus on Ship Behaviour in Locks. R.I.N.A., pp. 337-352.

Vantorre, M., 1995. *Experimental Study of Bank Effects on Full form Ship Models*. In Proceedings of Mini Symposium on Ship Manoeuvrability. Fukuoka, Japan: West-Japan Society of Naval Architects, pp. 85-101.

Vantorre, M., 2002. *Modelling of Ship-Bank Interaction Forces*. In IST, The Ship Interaction with the Waterway,, 13-15 June. pp. 1-17.

Vantorre, M., Candries, M. & Verwilligen, J., 2014. *Optimisation of Tidal Windows for Deep-Drafted Vessels by Means of a Probabilistic Approach Policy*. In PIANC World Congress San Francisco pp. 1-18.

Vantorre, M., Delefortrie, G., Eloot, K. & Laforce, E., 2003. *Experimental Investigation of Ship-Bank Interaction Forces*. In MARSIM 2003. pp. 1-10.

Vantorre, M., Laforce, E. & Verzhbitskaya, E., 2001. *Model Test Based Formulations of Ship-Ship Interaction Forces for Simulation Purposes*. In IMSF - 28th annual general meeting, Genoa, Italy.

Venables, W., Smith, D. & Team, R.D.C., 2002. An Introduction to R, Manual

Wang, H., Zou, Z., Xie, Y. & Kong, W., 2010. *Numerical Study of Viscous Hydrodynamic Forces on a Ship Navigating near Bank in Shallow Water*. In Proceedings of the Twentieth International Offshore and Polar Engineering Conference. ISOPE, pp. 523-528.

White, F.M., 2003. *Fluid Mechanics*. p.736. Book

Xia, J. & Miao, Q., 2004. *Effects of Unsymmetric Flow on a Ship Traveling in a Channel*. Journal of Ship Mechanics, 8(3), pp.1-12.

Yasukawa, H., 1991. *Bank Effect on Ship Maneuverability in a Channel with Varying Width*. Transactions of the West-Japan Society of Naval Architects, 81, pp.85-101.

Yasukawa, H., Kawamura, S., Tanaka, S. & Sano, M., 2009. *Evaluation of Ship-Bank and Ship-Ship Interaction Forces Using a 3D Panel Method.* In K. Eloot & M. Vantorre, eds. International Conference on Ship Manoeuvring in Shallow and Confined Water: Bank Effects. International Conference on Ship Manoeuvering in Shallow and Confined Water: Bank Effects 2009. Antwerp, Belgium: R.I.N.A, pp. 127-133.

Yeung, R.W. & Tan, W.T., 1980. *Hydrodynamic Interactions of Ships with Fixed Obstacles*. Journal of Ship Research, 24(1), pp.50-59.

Yeung, R.W., 1974. *Applications of Slender-body Theory to Ships Moving in Restricted Shallow Water*. In Symposium on aspects of navigability. pp. 1-17.

Zou, L. & Larsson, L., 2013. *Computational Fluid Dynamics (CFD) Prediction of Bank Effects Including Verification and*

Validation. Journal of Marine Science and Technology, 18, pp.310–323.

Zou, L., Larsson, L., Delefortrie, G. & Lataire, E., 2011. *CFD Prediction and validation of Ship–Bank Interaction in a Canal*. In B. Pettersen, T. E. Berg, K. Eloot, & M. Vantorre, eds. Second International Conference on Ship Manoeuvring in Shallow and Confined Water: Ship to Ship Interaction. pp. 413–422.

Bank Effects

11 Appendices

11.1 Map of the Port of Antwerp

11.2 Leonardo da Vinci's Viz. Folio 50/v 51/r codex G French Institute (Paris Manuscripts)

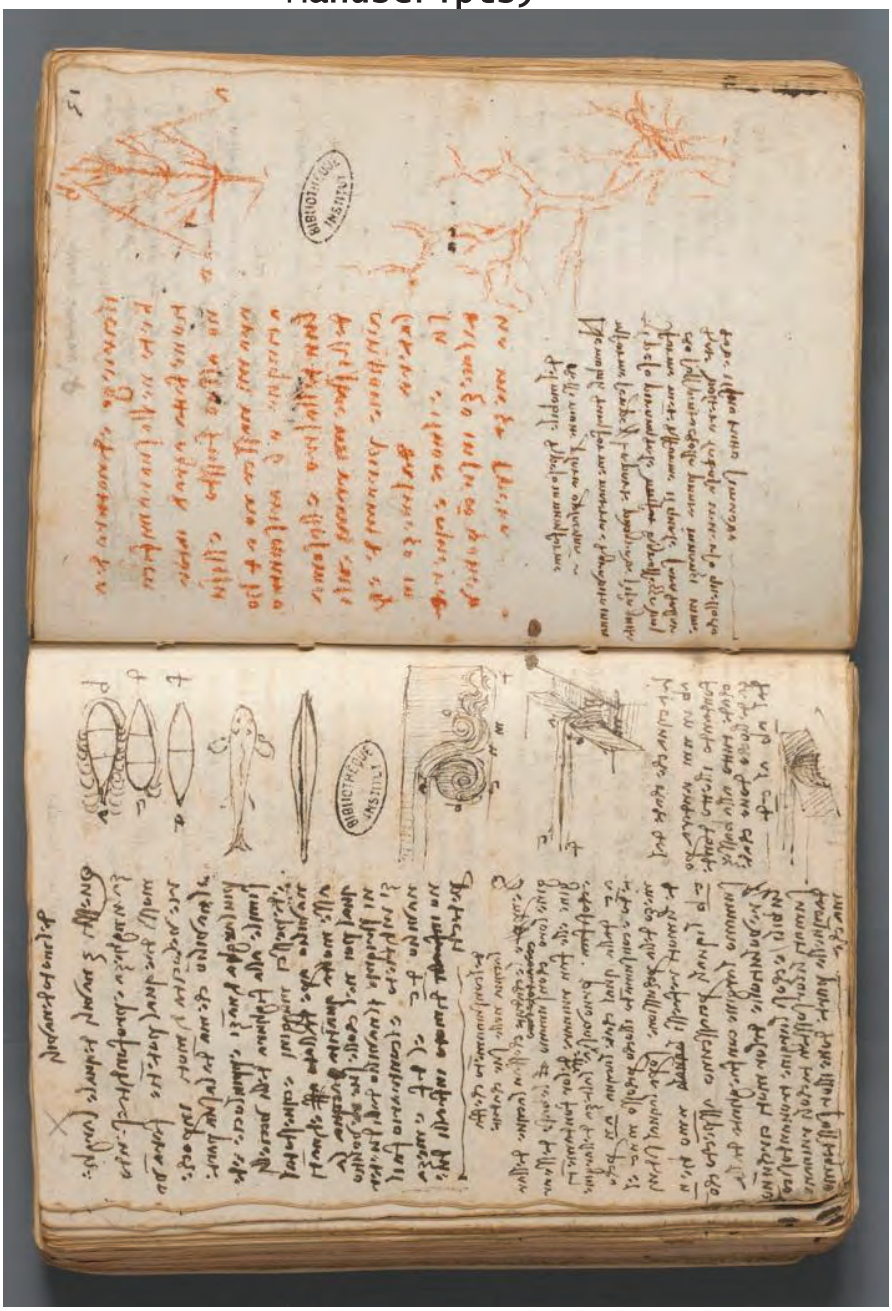

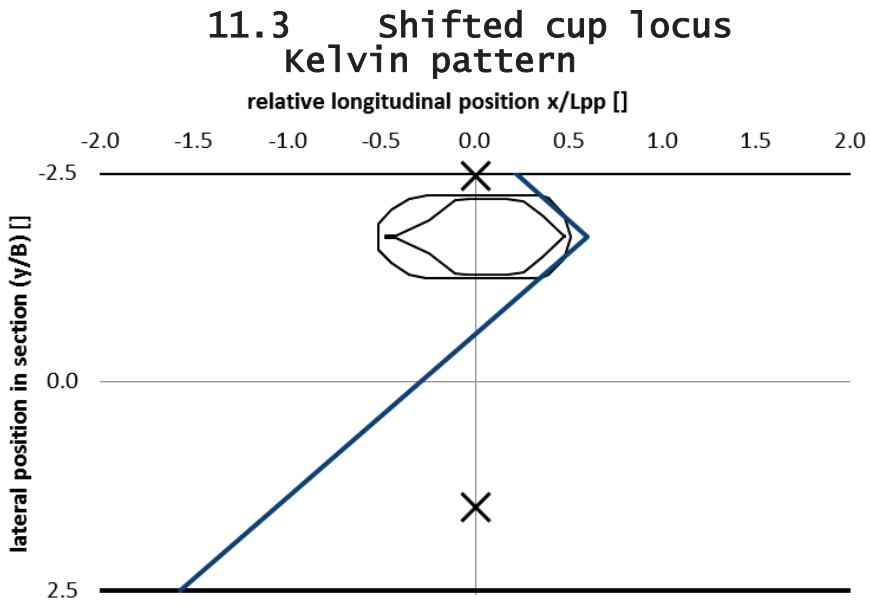

Figure 11.1 top side view of shifted forward cup locus Kelvin pattern

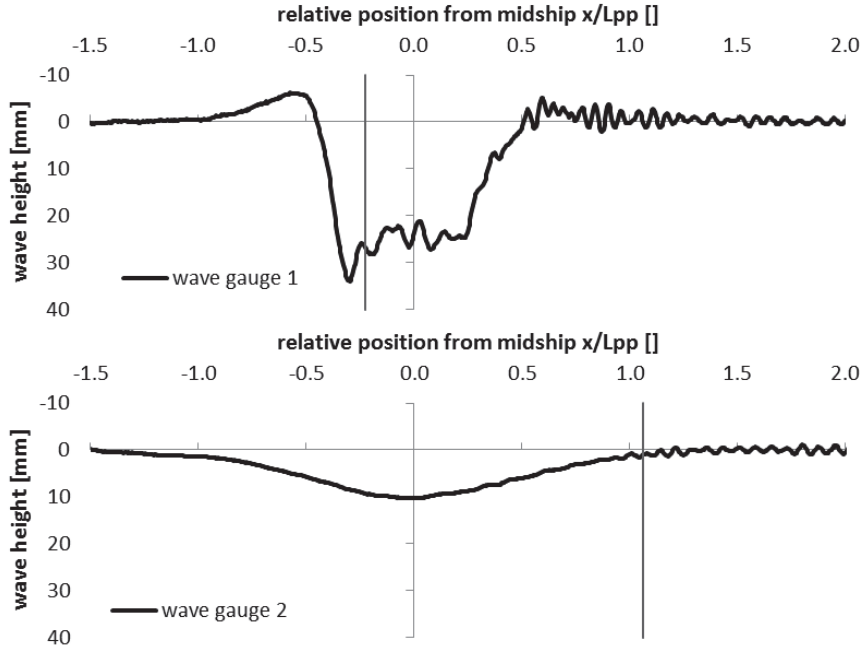

Figure 11.2 indication of the initiation of the shifted forward Kelvin pattern (vertical line) added to the wave registration at two lateral positions

11.4 Main dimensions towing tank FHR and bathymetry of the bottom after milling

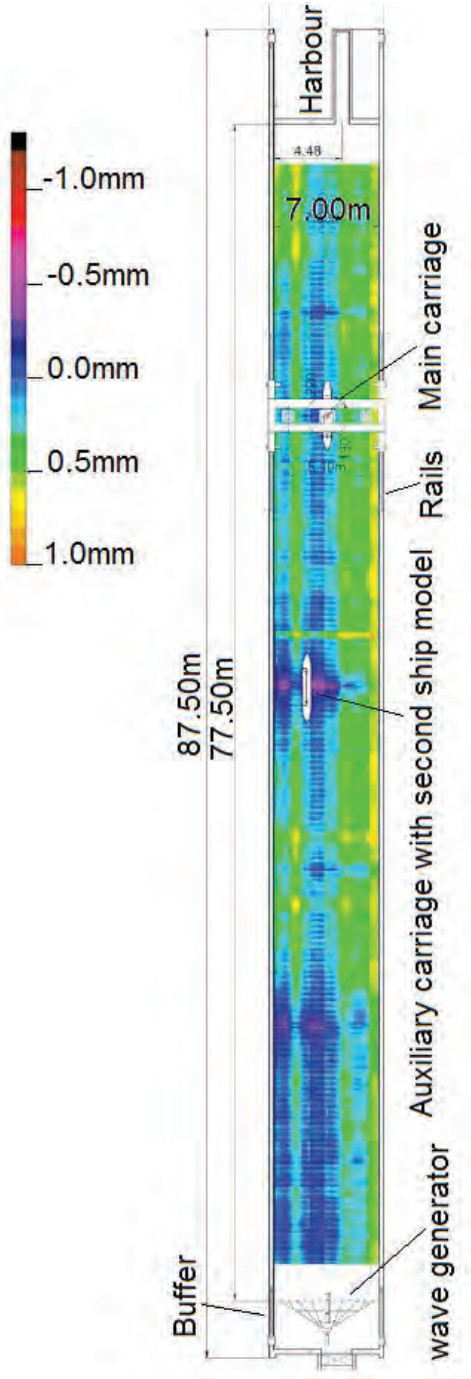

11.5 Lines plans and hydrostatics of the ship models

11.5.1 Ship model C0U

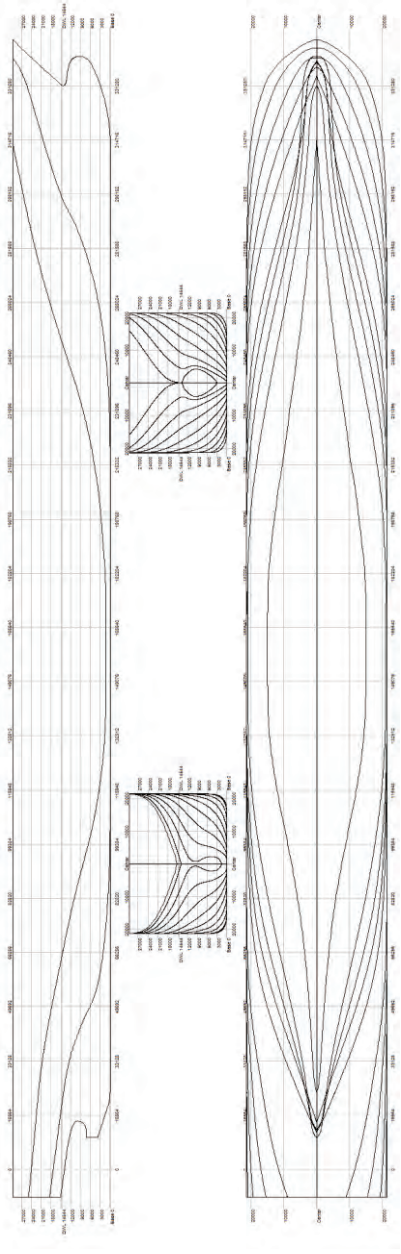

Figure 11.3 container carrier (8 000 TEU) C0U linesplan, full scale

		C0U T1200		C0U T1454		C0U Ttrim	
λ	[]	*1*	80.8	*1*	80.8	*1*	80.8
Lpp	[m]	*331.28*	4.100	*331.28*	4.100	*331.28*	4.100
L_{OA}	[m]	*353.90*	4.380	*353.90*	4.380	*353.89*	4.380
B	[m]	*42.82*	0.530	*42.82*	0.530	*42.82*	0.530
T_F	[m]	*12.00*	0.1485	*14.54*	0.180	*13.00*	0.161
T_A	[m]	*12.00*	0.1485	*14.54*	0.180	*14.50*	0.180
T_M	[m]	*12.00*	0.1485	*14.54*	0.180	*13.75*	0.170
∇	[m^3]	*108838*	0.206	*136718*	0.259	*128080*	0.243
C_B	[ ]	*0.64*	0.64	*0.66*	0.66	*0.62*	0.62
C_{PR}	[ ]	*0.65*	0.65	*0.67*	0.67	*0.67*	0.67
S	[m^2]	*15708*	2.406	*17812*	2.728	*17211*	2.636
L_{CB}	%	*0.167*	0.167	*-0.042*	-0.042	*-0.679*	-0.679
V_{CB}	[m]	*6.475*	0.080	*7.863*	0.097	*8.184*	0.101
A_W	[m^2]	*10655*	1.632	*11350*	1.738	*11229*	1.720
C_W	[ ]	*0.751*	0.751	*0.800*	0.800	*0.792*	0.792
L_{CF}	[m]	*165.9*	2.053	*159.8*	1.978	*159.5*	1.974
C_M	[ ]	*0.979*	0.979	*0.983*	0.983	*0.931*	0.931
KM	[m]	*18.74*	0.232	*18.53*	0.229	*19.33*	0.239
KM_L	[m]	*577.0*	7.141	*539.9*	6.682	*565.2*	6.995

Table 11.1 main hydrostatic properties at the three tested loading conditions for ship model C0U at model and full scale

11.5.2 Ship model C0P

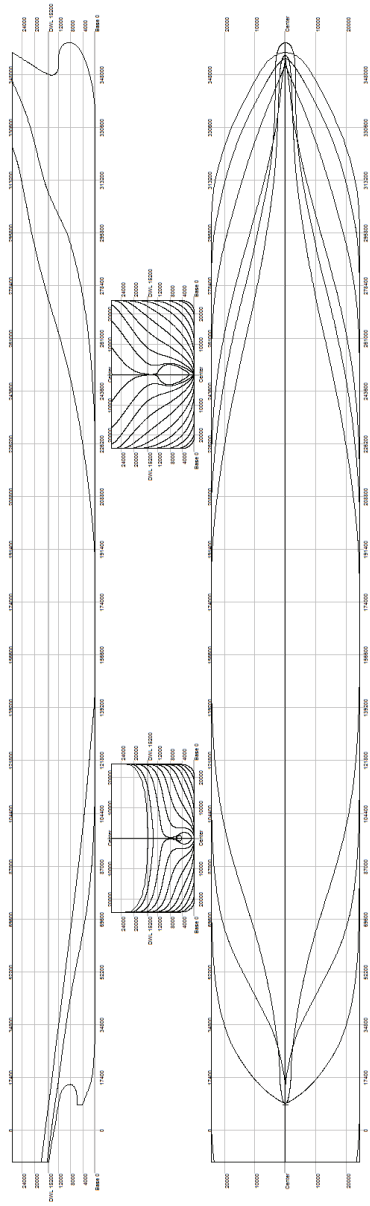

Figure 11.4 linesplan 12 000 TEU container carrier C0P at full scale

		C0P T1520	
λ	[]	*1*	80
Lpp	[m]	*348.00*	4.350
L_{OA}	[m]	*369.17*	4.615
B	[m]	*48.80*	0.610
T_F	[m]	*15.20*	0.1900
T_A	[m]	*15.20*	0.1900
T_M	[m]	*15.20*	0.1900
∇	[m^3]	*167817*	0.328
C_B	[ ]	*0.65*	0.65
C_{PR}	[ ]	*0.66*	0.66
S	[m^2]	*21460*	3.353
L_{CB}	%	*-2.402*	-2.402
V_{CB}	[m]	*8.501*	0.106
A_W	[m^2]	*14649*	2.289
C_W	[ ]	*0.863*	0.863
L_{CF}	[m]	*151.1*	1.889
C_M	[ ]	*0.990*	0.990
KM	[m]	*23.91*	0.299
KM_L	[m]	*700.5*	8.756

Table 11.2 main hydrostatic properties for ship model C0P at model and full scale

11.5.3 Ship model G0M

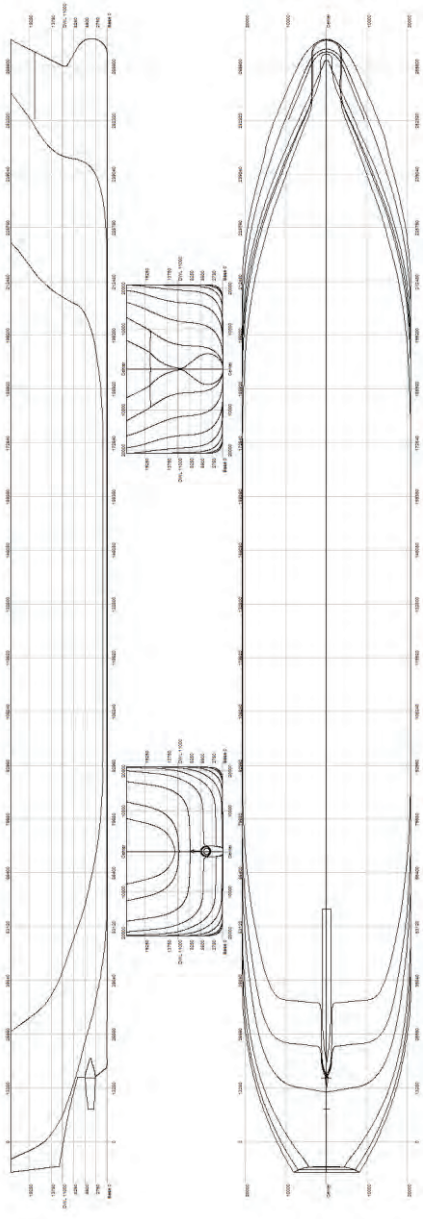

Figure 11.5 linesplan LNG-tanker G0M at full scale

		G0M T1100	
λ	[]	*1*	*70*
Lpp	[m]	*265.60*	3.809
L_{OA}	[m]	*280.03*	4.000
B	[m]	*41.60*	0.594
T_F	[m]	11.00	0.1571
T_A	[m]	11.00	0.1571
T_M	[m]	*11.00*	0.1571
∇	[m^3]	*93641*	0.273
C_B	[ ]	*0.77*	0.77
C_{PR}	[ ]	*0.78*	0.78
S	[m^2]	*14133*	2.884
L_{CB}	%	*0.472*	0.472
V_{CB}	[m]	*5.802*	0.083
A_W	[m^2]	*9530.5*	1.945
C_W	[ ]	*0.859*	0.859
L_{CF}	[m]	*126.21*	1.803
C_M	[ ]	*0.984*	0.984
KM	[m]	*18.84*	0.269
KM_L	[m]	*472.3*	6.747

Table 11.3 main hydrostatic properties for ship model G0M at model and full scale

11.5.4 Ship model T0Z

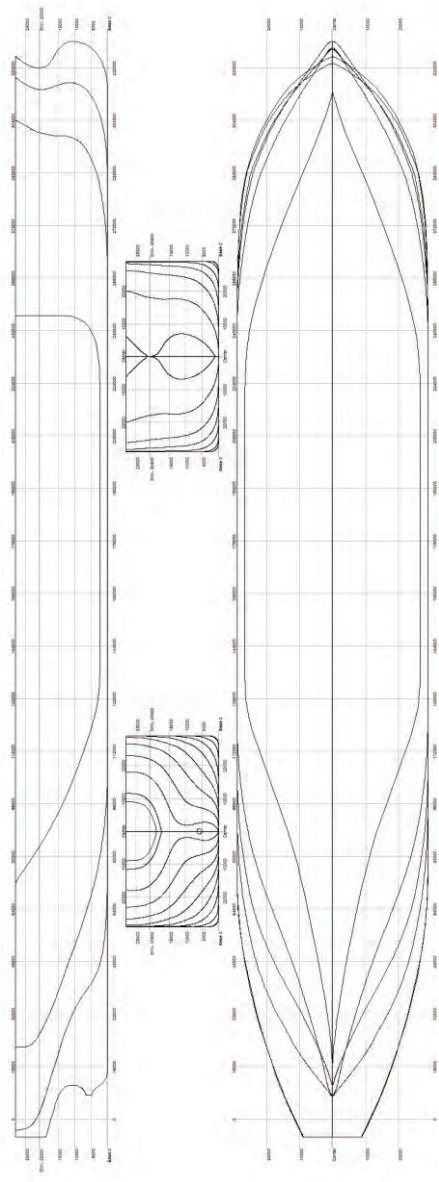

Figure 11.6 linesplan of the Very Large Crude Carrier T0Z (KVLCC2) at full scale

		FS T0Z T208	
λ	[]	*1*	*75*
Lpp	[m]	*320.00*	4.267
L_{OA}	[m]	*333.58*	4.448
B	[m]	*58.00*	0.773
T_F	[m]	20.80	0.277
T_A	[m]	20.80	0.277
T_M	[m]	*20.80*	0.277
∇	[m^3]	*311378*	0.738
C_B	[ ]	*0.81*	0.81
C_{PR}	[ ]	*0.81*	0.81
S	[m^2]	*27599*	4.906
L_{CB}	%	*3.426*	3.426
V_{CB}	[m]	*10.877*	0.145
A_W	[m^2]	*16673*	2.964
C_W	[ ]	*0.898*	0.898
L_{CF}	[m]	*160.22*	2.136
C_M	[ ]	*0.998*	0.998
KM	[m]	*24.23*	0.323
KM_L	[m]	*396.9*	5.292

Table 11.4 main hydrostatic properties for ship model T0Z at model and full scale

11.5.5 Ship model T0H

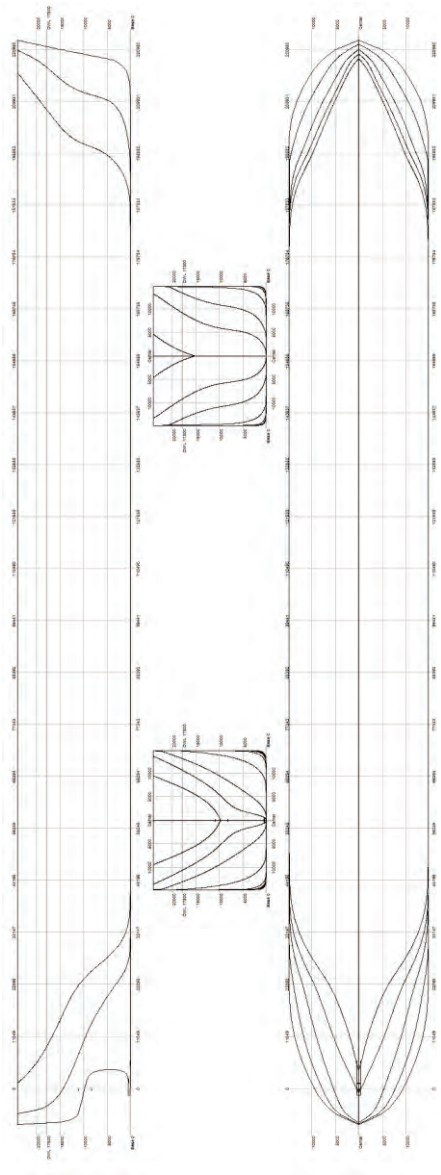

Figure 11.7 linesplan of the British Bombardier tanker T0H at model scale

		T0H T1780	
λ	[]	*1*	*75*
Lpp	[m]	*165.74*	2.210
L_{OA}	[m]	*173.71*	2.316
B	[m]	*22.17*	0.296
T_F	[m]	13.35	0.178
T_A	[m]	13.35	0.178
T_M	[m]	*13.35*	0.178
∇	[m^3]	*41625*	0.099
C_B	[ ]	*0.85*	0.85
C_{PR}	[ ]	*0.85*	0.85
S	[m^2]	*7338*	1.305
L_{CB}	%	*0.351*	0.351
V_{CB}	[m]	*6.917*	0.092
A_W	[m^2]	*3437.156*	0.611
C_W	[ ]	*0.936*	0.936
L_{CF}	[m]	*81.02*	1.080
C_M	[ ]	*0.997*	0.997
KM	[m]	*10.01*	0.134
KM_L	[m]	*176.8*	2.357

Table 11.5 main hydrostatic properties for ship model T0H at model and full scale

11.5.6 Ship model T0S

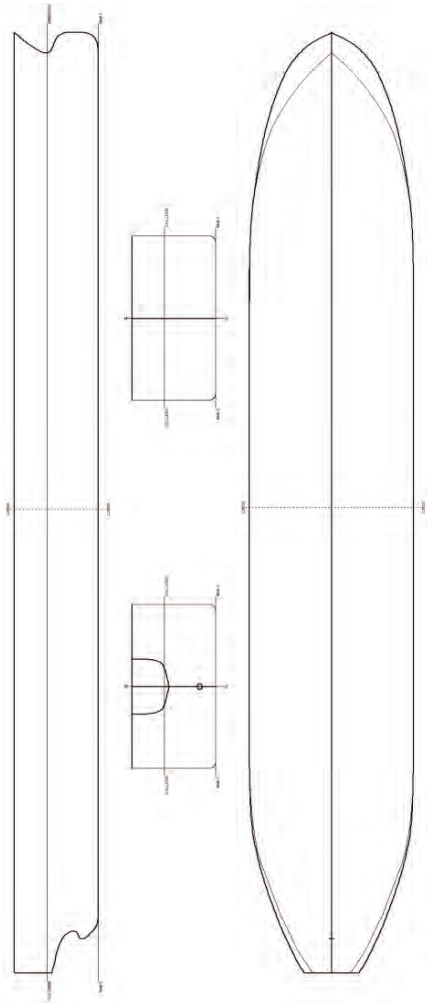

Figure 11.8 main views of the oil tanker T0S at full scale

		FS T0S Tanker T1350	
λ	[]	*1*	46.25
Lpp	[m]	*238.00*	5.146
L_{OA}	[m]	*246.69*	5.334
B	[m]	*43.00*	0.930
T_F	[m]	13.50	0.292
T_A	[m]	13.50	0.292
T_M	[m]	*13.50*	0.292
∇	[m³]	*112377*	1.136
C_B	[ ]	*0.81*	0.81
C_{PR}	[ ]	*0.82*	0.82
S	[m²]	*14520*	6.788
L_{CB}	%	*2.781*	2.781
V_{CB}	[m]	*7.052*	0.152
A_W	[m²]	*9179.3*	4.291
C_W	[ ]	*0.897*	0.897
L_{CF}	[m]	*116.72*	2.524
C_M	[ ]	*0.996*	0.996
KM	[m]	*18.33*	0.396
KM_L	[m]	*329.9*	7.132

Table 11.6 main hydrostatic properties for ship model T0S at model and full scale

11.5.7 Ship model A01

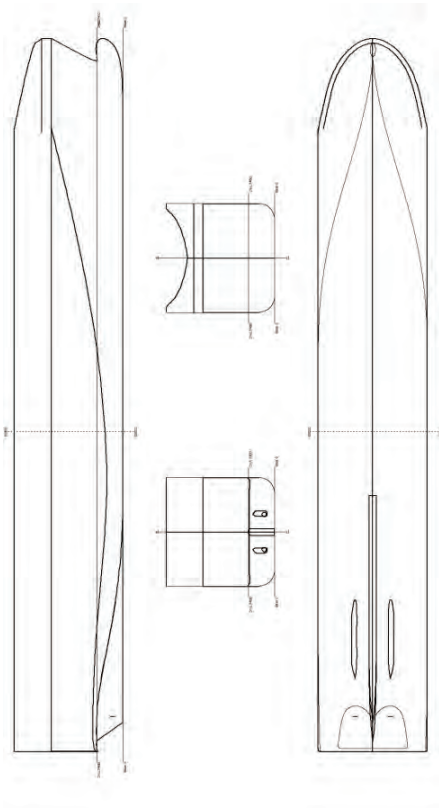

Figure 11.9 main views of the car carrier A01 at full scale with a simplified section above water

		FS A01 T740	
λ	[]	*1*	50
Lpp	[m]	*190.00*	3.800
L_{OA}	[m]	*203.00*	4.060
B	[m]	*31.00*	0.620
T_F	[m]	7.40	0.1480
T_A	[m]	7.40	0.1480
T_M	[m]	*7.40*	0.1480
∇	[m^3]	*27185*	0.217
C_B	[ ]	*0.62*	0.62
C_{PR}	[ ]	*0.66*	0.66
S	[m^2]	*7185*	2.874
L_{CB}	%	*-2.528*	-2.528
V_{CB}	[m]	*4.135*	0.083
A_W	[m^2]	*4816.6*	1.927
C_W	[ ]	*0.818*	0.818
L_{CF}	[m]	*79.48*	1.590
C_M	[ ]	*0.947*	0.947
KM	[m]	*17.16*	0.343
KM_L	[m]	*394.7*	7.894

Table 11.7 main hydrostatic properties for twin screw auto carrier A01 at model and full scale

11.5.8 Ship model A0S

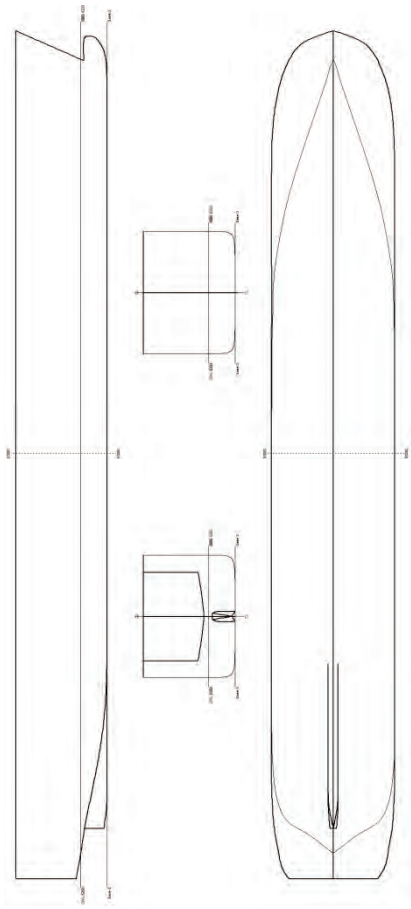

Figure 11.10 main views of the RoRo car carrier A0S at full scale

		FS A0S T620	
λ	[]	*1*	*37.5*
Lpp	[m]	*186.17*	4.965
L_{OA}	[m]	*200.19*	5.338
B	[m]	*29.00*	0.773
T_F	[m]	*6.20*	0.1653
T_A	[m]	*6.20*	0.1653
T_M	[m]	*6.20*	0.1653
∇	[m^3]	*22865*	0.434
C_B	[ ]	*0.68*	0.68
C_{PR}	[ ]	*0.70*	0.70
S	[m^2]	*6042*	4.297
L_{CB}	%	*-2.949*	-2.949
V_{CB}	[m]	*3.411*	0.091
A_W	[m^2]	*4579.856*	3.257
C_W	[ ]	*0.848*	0.848
L_{CF}	[m]	*84.48*	2.253
C_M	[ ]	*0.971*	0.971
KM	[m]	*15.88*	0.424
KM_L	[m]	*445.1*	11.869

Table 11.8 main hydrostatic properties for ship model A0S at model and full scale

11.5.9 Ship model R0S

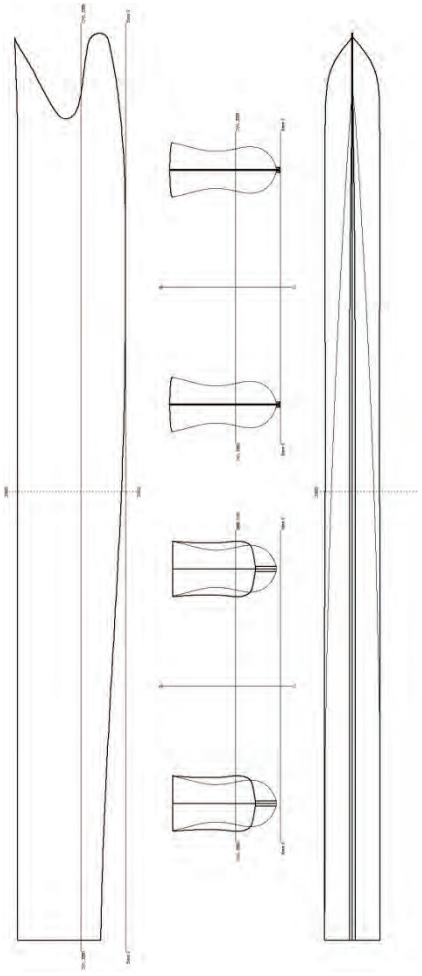

Figure 11.11 linesplan of the fast RoPax Catamaran R0S at full scale

		FS R0S T335	
λ	[]	*1*	*40*
Lpp	[m]	*68.90*	1.723
L_{OA}	[m]	*69.75*	1.744
B	[m]	*4.20*	0.105
B_S	[m]	*17.60*	0.440
T_F	[m]	*3.35*	0.0838
T_A	[m]	*3.35*	0.0838
T_M	[m]	*3.35*	0.0838
∇	[m^3]	*905*	0.014
C_B	[ ]	*0.18*	0.18
C_{PR}	[ ]	*0.73*	0.73
S	[m^2]	*997*	0.623
L_{CB}	%	*-3.427*	-3.427
V_{CB}	[m]	*2.158*	0.054
A_W	[m^2]	*380*	0.238
C_W	[ ]	*1.314*	1.314
L_{CF}	[m]	*25.15*	0.629
C_M	[ ]	*0.245*	0.245
KM	[m]	*35.11*	0.878
KM_L	[m]	*112.0*	2.800

Table 11.9 main hydrostatic properties for catamaran R0S at model and full scale

11.5.10 Ship model B01

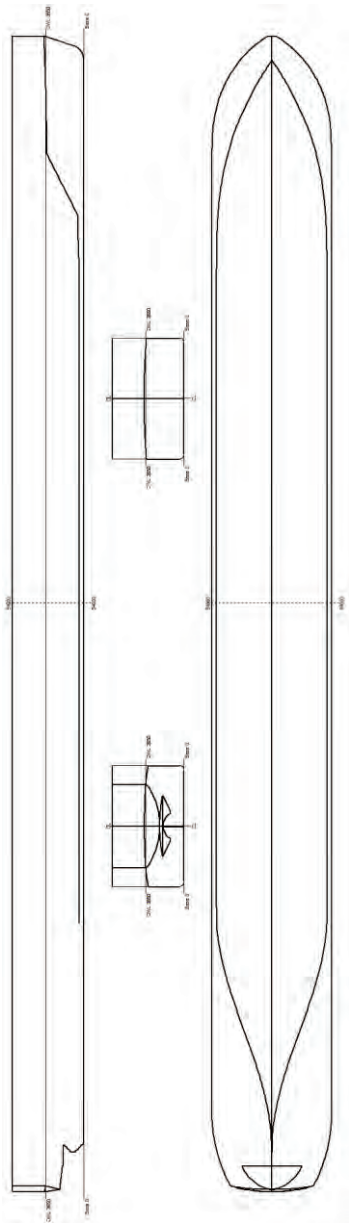

Figure 11.12 main views of the inland vessel of Class Va at full scale

		FS B01 T365	
λ	[]	*1*	25
Lpp	[m]	*108.00*	4.320
L_{OA}	[m]	*109.95*	4.398
B	[m]	*11.45*	0.458
T_F	[m]	3.65	0.1460
T_A	[m]	3.65	0.1460
T_M	[m]	*3.65*	0.1460
∇	[m³]	*4096*	0.262
C_B	[ ]	*0.91*	0.91
C_{PR}	[ ]	*0.91*	0.91
S	[m²]	*1909*	3.055
L_{CB}	%	*1.967*	1.967
V_{CB}	[m]	*1.894*	0.076
A_W	[m²]	*1215.4*	1.945
C_W	[ ]	*0.983*	0.983
L_{CF}	[m]	*54.13*	2.165
C_M	[ ]	*0.998*	0.998
KM	[m]	*5.03*	0.201
KM_L	[m]	*281.9*	11.277

Table 11.10 main hydrostatic properties for the inland vessel B01 at model and full scale

11.5.11 Model W01

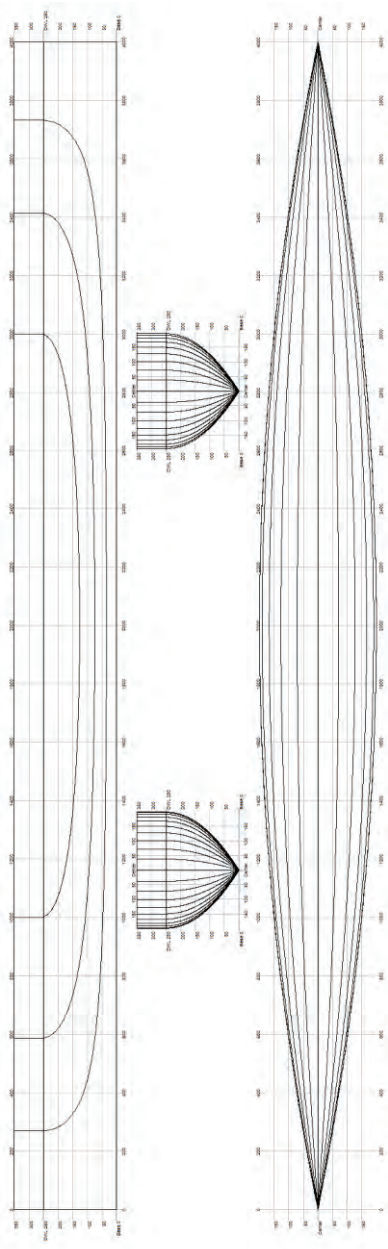

Figure 11.13 linesplan of the four meter long Wigley hull

		W01 T25
λ	[]	-
Lpp	[m]	*4.000*
L_{OA}	[m]	*4.000*
B	[m]	*0.400*
T_F	[m]	0.25
T_A	[m]	0.25
T_M	[m]	*0.250*
∇	[m^3]	*0.177*
C_B	[ ]	*0.44*
C_{PR}	[ ]	*0.67*
S	[m^2]	*2.377*
L_{CB}	%	*0.004*
V_{CB}	[m]	*0.156*
A_W	[m^2]	*1.066*
C_W	[ ]	*0.667*
L_{CF}	[m]	*2.00*
C_M	[ ]	*0.662*
KM	[m]	*0.212*
KM_L	[m]	*5.0*

Table 11.11 main hydrostatic properties for the Wigley hull

11.6 Open data

A set of measured data, free to use, is released in (Lataire et al. 2009). The data set consists (out) of two different subsets, the first subset contains measured running sinkages (z_{VF} and z_{VA}) of the container carrier C0U sailing along bank SP_8_4.030_0 at four different speeds and with four different distances between ship and bank. The second set contains ten tests and includes all measured forces, moments and motions. The results are obtained by tests carried out with the ship model C0U at different initially even keel conditions. The second subset consists of tests with a wide range of speeds, bank geometries, drift angles and propeller rates.

11.6.1 First subset open data

Ship model C0U is towed at zero drift angle, zero rudder angle and zero propeller rate at four constant forward speeds along bank SP_8_4.030_0 and at four lateral positions between ship and bank. The water depth h is 0.243 m or 1.35 times the ship model's draft.

The resulting running sinkages at the fore z_{VF} and aft z_{VA} perpendicular are made available.

11.6.2 Second subset of open data

The data in this subset is obtained with model tests carried out with C0U initially even keel ballasted but at different original drafts. This set contains a wide variation of the input parameters of the elaborated test program carried out at Flanders Hydraulics Research. The input parameters of ten tests (named A to J), as well as the test results, are also made available. For the tests B, C, E, F, I and J a registration of the water surface is published based upon three wave gauges at a fixed position in the towing tank.

Digital information of the open data including a mesh of the hull, propeller, rudder and drawings of the test set up and wave gauges can be obtained via the authors.

11.7 Weight distribution

11.7.1 Trapezoidal cross section

Next solved integrals are only valid for cross sections with a constant slope but the integral itself remains valid for all types of bank.

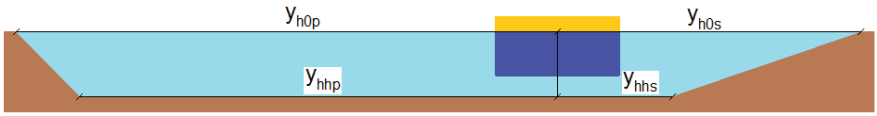

Figure 11.14 definition of the distances to calculate analytically a trapezoidal cross section

Figure 11.15 a graphical representation of the weight of a right triangle

The weight of a (right) triangle with coordinates $(y_1,z_1)(y_2,z_1)(y_1,z_2)$ (Figure 11.15) with $|y_1| < |y_2|$ and $|z_1| < |z_2|$ is:

$$\chi_{tria} = \int_{z_1}^{z_2} \int_{y_1}^{\left(y_2 - \frac{y_2 - y_1}{z_2 - z_1}(z - z_1)\right)} e^{-\left(\xi_y \frac{|y|}{y_{infl}} + \xi_z \frac{|z|}{T}\right)} dy\, dz \qquad (11.1)$$

For a surface piercing bank this integral is the summation of the weight of a rectangle and a triangle:

$$\chi_{SP} = \int_0^h \int_0^{y_{hhs}} e^{-\left(\xi_y \frac{|y|}{y_{infl}} + \xi_z \frac{|z|}{T}\right)} dy\, dz + \int_0^h \int_{y_{hhs}}^{\left(y_{h0s} - z\frac{y_{h0s} - y_{hhs}}{T}\right)} e^{-\left(\xi_y \frac{|y|}{y_{infl}} + \xi_z \frac{|z|}{T}\right)} dy\, dz \qquad (11.2)$$

Surface piercing rectangle:

$$\int_0^h \int_0^{y_{hhs}} e^{-\left(\xi_y \frac{|y|}{y_{infl}} + \xi_z \frac{|z|}{T}\right)} dy\, dz = -\frac{y_{infl} T}{\xi_y \xi_z} \left(-e^{-\xi_z \frac{h}{T}} + e^{\xi_y \frac{y_{hhs}}{y_{infl}} - \xi_z \frac{h}{T}} - e^{\xi_y \frac{y_{hhs}}{y_{infl}}} + 1\right) e^{-\xi_y \frac{y_{hhs}}{y_{infl}}} \qquad (11.3)$$

$$\int_0^h \int_0^{y_{hhs}} e^{-\left(\xi_y \frac{|y|}{y_{infl}} + \xi_z \frac{|z|}{T}\right)} dy\, dz = \frac{y_{infl} T}{\xi_y \xi_z} \left(e^{-\xi_z \frac{h}{T}} - e^{\xi_y \frac{y_{hhs}}{y_{infl}} - \xi_z \frac{h}{T}} + e^{\xi_y \frac{y_{hhs}}{y_{infl}}} - 1\right) e^{-\xi_y \frac{y_{hhs}}{y_{infl}}} \qquad (11.4)$$

$$\int_0^h \int_0^{y_{hhs}} e^{-\left(\xi_y \frac{|y|}{y_{infl}} + \xi_z \frac{|z|}{T}\right)} dy\, dz = \frac{y_{infl} T}{\xi_y \xi_z} \left(1 - e^{-\xi_y \frac{y_{hhs}}{y_{infl}}}\right) \left(1 - e^{-\xi_z \frac{h}{T}}\right) \quad (11.5)$$

$$\int_0^h \int_0^{y_{hhs}} e^{-\left(\xi_y \frac{|y|}{y_{infl}} + \xi_z \frac{|z|}{T}\right)} dy\, dz = \frac{y_{infl} T}{\xi_y \xi_z} \left(1 - e^{-\xi_y \frac{y_{hhs}}{y_{infl}}}\right) \left(1 - e^{-\xi_z \frac{h}{T}}\right) \quad (11.6)$$

Surface piercing right triangle

$$\int_0^h \int_{y_{hhs}}^{\left(y_{h0s} - z \frac{y_{h0s} - y_{hhs}}{h}\right)} e^{-\left(\xi_y \frac{|y|}{y_{infl}} + \xi_z \frac{|z|}{T}\right)} dy\, dz =$$

$$y_{infl} T \frac{e^{-\left(\xi_z + \frac{\xi_y}{y_{infl}}(y_{h0s} + y_{hTs})\right)} \left(\frac{\xi_y}{y_{infl}}(y_{h0s} - y_{hTs}) e^{\xi_z + \frac{\xi_y}{y_{infl}} y_{h0s}} + \xi_z e^{\frac{\xi_y}{y_{infl}} y_{hTs}} - \left(\xi_z + \frac{\xi_y}{y_{infl}}(y_{h0s} - y_{hTs})\right) e^{\frac{\xi_y}{y_{infl}} y_{h0s}}\right)}{\xi_y \xi_z \left(\xi_z + \frac{\xi_y}{y_{infl}}(y_{h0s} - y_{hTs})\right)} \quad (11.7)$$

$$= \frac{y_{infl} T e^{-\left(\xi_z \frac{h}{T} + \xi_y \frac{y_{h0s} + y_{hhs}}{y_{infl}}\right)} \left(\xi_z \frac{h}{T} e^{\xi_z \frac{h}{T} + \xi_y \frac{y_{hhs}}{y_{infl}}} - \left(\xi_y \frac{y_{h0s} - y_{hhs}}{y_{infl}}\right) e^{\xi_y \frac{y_{h0s}}{y_{infl}}} - \left(\xi_y \frac{y_{hhs} - y_{h0s}}{y_{infl}} + \xi_z \frac{h}{T}\right) e^{\xi_z \frac{h}{T} + \xi_y \frac{y_{h0s}}{y_{infl}}}\right)}{\xi_y \xi_z \left(\xi_y \left(\frac{y_{h0s} - y_{hhs}}{y_{infl}}\right) - \xi_z \frac{h}{T}\right)} \quad (11.8)$$

Surface piercing bank

$$\chi_{SP} = \chi_{triangle} + \chi_{rectangle} \quad (11.9)$$

$$\chi_{SP} = \frac{y_{infl} T}{\xi_y \xi_z} \left(\left(1 - e^{-\xi_y \frac{y_{hhs}}{y_{infl}}}\right) \left(1 - e^{-\xi_z \frac{h}{T}}\right) + \frac{e^{-\left(\xi_z \frac{h}{T} + \xi_y \frac{y_{h0s} + y_{hhs}}{y_{infl}}\right)} \left(\xi_z \frac{h}{T} e^{\xi_z \frac{h}{T} + \xi_y \frac{y_{hhs}}{y_{infl}}} - \left(\xi_y \frac{y_{h0s} - y_{hhs}}{y_{infl}}\right) e^{\xi_y \frac{y_{h0s}}{y_{infl}}} - \left(\xi_y \frac{y_{hhs} - y_{h0s}}{y_{infl}} + \xi_z \frac{h}{T}\right) e^{\xi_z \frac{h}{T} + \xi_y \frac{y_{h0s}}{y_{infl}}}\right)}{\left(\xi_y \left(\frac{y_{h0s} - y_{hhs}}{y_{infl}}\right) - \xi_z \frac{h}{T}\right)} \right) \quad (11.10)$$

11.7.2 Semi submerged cross section

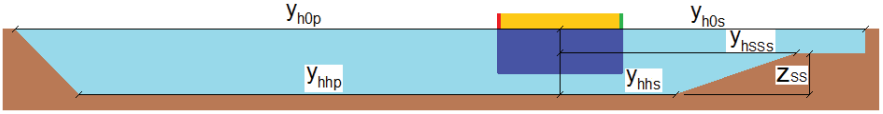

Figure 11.16 definition of the discrete lateral positions of importance

The starboard weighted area χ_s can be split into two parts:

$$\chi_s = \int_0^{h-z_{SS}} \int_0^{y_{h0s}} e^{-\left(\xi_y \frac{|y|}{y_{infl}} + \xi_z \frac{|z|}{T}\right)} dy\, dz$$

$$+ \int_{h-z_{SS}}^{h} \int_0^{y_{hSSs} - \frac{y_{hSSs}-y_{hhs}}{z_{SS}}(z-(h-z_{SS}))} e^{-\left(\xi_y \frac{|y|}{y_{infl}} + \xi_z \frac{|z|}{T}\right)} dy\, dz \qquad (11.11)$$

$$\chi_s = \int_0^{h-z_{SS}} \int_0^{y_{h0s}} e^{-\left(\xi_y \frac{|y|}{y_{infl}} + \xi_z \frac{|z|}{T}\right)} dy\, dz + \int_{h-z_{SS}}^{h} \int_0^{y_{hSSs} - (z-h+z_{SS})\frac{y_{hSSs}-y_{hhs}}{z_{SS}}} e^{-\left(\xi_y \frac{|y|}{y_{infl}} + \xi_z \frac{|z|}{T}\right)} dy\, dz$$

(11.12)

$$\frac{y_{hSSs}-y_{hhs}}{z_{SS}} = slope \qquad (11.13)$$

These equations 11.11 and 11.12 are only valid when the centre of the vessel is not located over the sloped bank.

11.8 Derivation of the water depth dependent Tuck Number

$$\boldsymbol{Tu_m(V)} = \frac{\left(\frac{Fr_h}{Fr_{crit,lim}}\right)^2}{\sqrt{1-\left(\frac{Fr_h}{Fr_{crit,lim}}\right)^2}} \tag{11.14}$$

$$\boldsymbol{Tu_m(V)} = \frac{\left(\frac{\frac{V}{\sqrt{gh_{ship}}}}{\left(2\sin\left(\frac{Arcsin(1-m_{lim})}{3}\right)\right)^{\frac{3}{2}}}\right)^2}{\sqrt{1-\left(\frac{\frac{V}{\sqrt{gh_{ship}}}}{\left(2\sin\left(\frac{Arcsin(1-m_{lim})}{3}\right)\right)^{\frac{3}{2}}}\right)^2}} \tag{11.15}$$

$$\boldsymbol{Tu_m(V)} = \frac{\left(\frac{\frac{V}{\sqrt{gh_{ship}}}}{\frac{V_{crit,lim}}{\sqrt{gh_{avg}}}}\right)^2}{\sqrt{1-\left(\frac{\frac{V}{\sqrt{gh_{ship}}}}{\frac{V_{crit,lim}}{\sqrt{gh_{avg}}}}\right)^2}} \tag{11.16}$$

$$\boldsymbol{Tu_m(V)} = \frac{\frac{h_{avg}}{h_{ship}}\frac{V^2}{V_{crit,lim}^2}}{\sqrt{1-\frac{h_{avg}}{h_{ship}}\frac{V^2}{V_{crit,lim}^2}}} \tag{11.17}$$

$$\frac{\sqrt{h_{avg}}}{\sqrt{h_{ship}}}\frac{V}{V_{crit,lim}} = \frac{\sqrt{gh_{avg}}}{\sqrt{gh_{ship}}}\frac{V}{\sqrt{gh_{avg}}\left(2\sin\left(\frac{Arcsin(1-m_{lim})}{3}\right)\right)^{\frac{3}{2}}} \tag{11.18}$$

$$\frac{\sqrt{h_{avg}}}{\sqrt{h_{ship}}}\frac{V}{V_{crit,lim}} = \frac{\sqrt{gh_{avg}}}{\sqrt{gh_{ship}}}\frac{V}{\sqrt{gh_{avg}}\left(2\sin\left(\frac{Arcsin(1-m_{lim})}{3}\right)\right)^{\frac{3}{2}}} = \frac{V}{\sqrt{gh_{ship}}\left(2\sin\left(\frac{Arcsin(1-m_{lim})}{3}\right)\right)^{\frac{3}{2}}} \tag{11.19}$$

11.9 Derivation of the simplified hyperbolic function

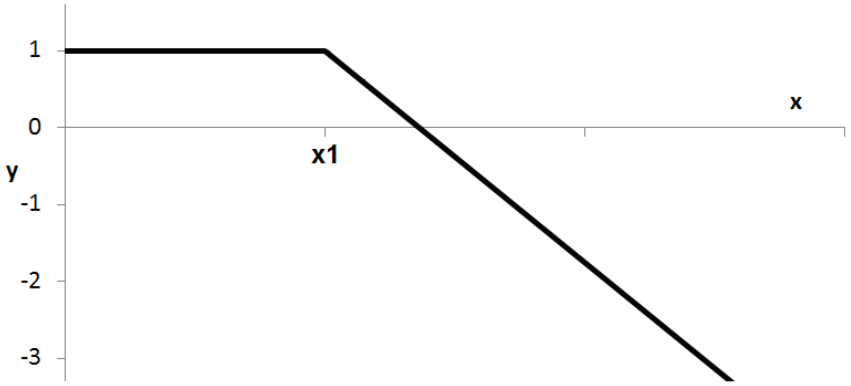

Figure 11.17 simplified hyperbolic function: two half open line segments with joint endpoint (x1, 1)

With s is the slope of the second line segment and the positive coefficient ξ:

$$y = 1 - \frac{-\sqrt{((-\xi)x1-(-\xi)x)^2-4.-\xi s}-(-\xi)x1-\xi x}{-2.\xi s} \tag{11.20}$$

$$y = \lim_{\xi\to\infty}\left(1 - \frac{-\sqrt{((-\xi)x1-(-\xi)x)^2-4.-\xi s}-(-\xi)x1-\xi x}{-2.\xi s}\right) \tag{11.21}$$

$$y = \lim_{\xi\to\infty}\left(1 - \frac{\sqrt{(x-x1)^2+4.\xi^{-1}s}+(x-x1)}{2\,s}\right) = 1 - \frac{|x-x1|+(x-x1)}{2\,s} \tag{11.22}$$

11.10 Zero crossing of the mathematical model for Y_F

The value $\frac{T}{h-T}$ is sought for when the mathematical model for the lateral force at the forward perpendicular is always zero.

$$\boldsymbol{Fr}^2 \frac{\left(\frac{T}{h-T}\right)^2 - \xi_{hT}{}^2}{\xi_h{}^2} = \mathbf{1} \tag{11.23}$$

$$\frac{\boldsymbol{T}}{\boldsymbol{h-T}} = \sqrt{\frac{\xi_h{}^2}{Fr^2} + \boldsymbol{\xi}_{hT}{}^2} \tag{11.24}$$

List of Figures

List of Tables

Bear in mind the past and the future
but don't ever let them rob you of the present
because it's all you've got.

Quote from the short film "The Runners"
by Matan Rochlitz & Ivo Gormley


MARITIME TECHNOLOGY
GHENT UNIVERSITY